Imperial College London

Department of Chemical Engineering

Development of Poly (ether ether ketone) Nanofiltration Membranes for Organic Solvent Nanofiltration in Continuous Flow Systems

By

João Porfírio da Silva Burgal

Supervisor: Prof. Andrew G. Livingston

A thesis submitted for the degree of Doctor of Philosophy of Imperial College London and the Diploma of Imperial College London.

2016

DECLARATION OF ORIGINALITY

I hereby declare that this thesis and the work reported herein was composed by and originated entirely from me. Information derived from the published and unpublished work of others has been acknowledged in the text and referenced appropriately.

Joao Porfirio da Silva Burgal
Imperial College London, 2016

Abstract

Organic solvent nanofiltration (OSN) is an energy saving technology that can replace more energy demanding separation technologies, such as evaporation and distillation. Nevertheless, OSN membranes that can withstand high temperature conditions as well as acidic or basic conditions are lacking on the market. In this thesis a poly(ether ether ketone) (PEEK) membrane is investigated for its suitability for OSN applications using polar aprotic solvents, such as DMF and THF, high temperatures, and basic/acidic conditions. By studying four grades of PEEK polymer powder from two different brands (VESTAKEEP® and VICTREX®), the VESTAKEEP® 4000P was selected for the subsequent studies. The post-phase inversion drying process of membrane fabrication was also studied and the drying step was shown to be crucial in obtaining separation performance in the nanofiltration (NF) range. The degree of sulphonation (DS) was also important and had to be maintained at low levels in order to retain the chemical and thermal stability of PEEK membranes. Subsequently, the scaling-up of PEEK membranes to spiral-wound modules was successfully achieved. In order to further manipulate the performance of PEEK NF membranes, two ways of controlling the molecular weight cut-off (MWCO) of PEEK membranes prepared via phase inversion and subsequent drying were studied. The two methods explored were the change of polymer concentration in the dope solution – 8 wt. %, 10 wt. % and 12 wt. % - and the variation of solvent filling the pores prior to drying – e.g. water, methanol, acetone, tetrahydrofuran and n-heptane. For each solvent, the drying temperature was proved to have an effect on the membrane performance - the higher the drying temperature, the higher the rejection and the lower the permeance. Following the drying treatment results, the negligible aging of PEEK membranes was demonstrated; a comparison with crosslinked polybenzimidazole (PBI) and polyimide (PI) membranes was also performed. The results showed a structural change for PBI and PI membranes due to a non-equilibrium glassy state, in contrast with PEEK membranes which were in quasi-equilibrium glassy state. High temperature filtrations were also performed in DMF up to 140 °C for the three polymeric membranes. PEEK was the most robust membrane with a stable performance after 4 filtration cycles whereas PBI and PI were stable for 2 and 1 cycles respectively. Due to their stability at high temperatures, and also their compatibility with catalysts, PEEK membranes were used in two different continuous Heck coupling reactions combined with OSN separation of the catalyst *in situ*. Two reactor configurations were investigated: a continuous single stirred tank reactor/membrane separator (m-CSTR); and a plug flow reactor (PFR) followed by m-CSTR (PFR-m-CSTR). It was possible to decrease the catalyst leaching to the product stream and to increase the overall turnover number (TON) of the Heck reactions.

Acknowledgments

In the course of these three (almost four) years, my PhD was some sort of an emotional rollercoaster sprinkled with a lot of self-doubt but luckily I had great people by my side to finish this ride.

First and foremost, this PhD was only possible because Prof. Livingston gave me the opportunity to be part of his research group. I would like to thank him for this great and intense experience that will stay with me forever. During these years I cannot thank him enough for all the intellectual effort that he has stimulated in me even when I thought it was already enough. Today I understand better what it means to perform good quality work and to have a higher attention to details. I have grown so much as a researcher and professional and I have to thank Prof. Livingston for this (even when at times it was a painful process).

I have also to thank to Dr. Ludmila Peeva who helped me a lot (really a lot!) during this PhD on a daily basis. Her guidance and advice were of utmost importance. I have to thank her for all the help in building the high temperature rig used in the experimental part of this thesis (I will never look at an HPLC pump the same way again). For all the time she spent correcting my manuscripts and giving me ideas (including for this thesis) I could not be more thankful. I have learned so much from her during these years; I can only hope to be as good of a Chemical Engineer as she is one day.

I have to thank Irina Valtcheva, James Campbell, Ana Gil, Nur Hidayati Othman, Maria Jimenez and Jeong F. Kim for being such great colleagues but above all, good friends. Thanks to all of you my days were brighter at Imperial (and it was sad to see you all going away). To Farah, Nilay and Mahmood, thank you for being such good office colleagues that later became friends as well.

To my research group I would like to express my gratitude for the good work environment and intellectual discussions. A big thank you to my students Carlos, Susana, Florian and Florine for all the great work they performed and for helping me during my PhD.

A big thank you to all the support staff in the Department of Chemical Engineering, in particular to Mrs. Raluca Reynolds for being so efficient in getting my POs processed so quickly (and for all the talks while waiting for meetings).

A big thank you as well to the Portuguese and Greek friends that I have met in London (if you are reading this you know who you are).

A todo o *gang* do Técnico, Joana Baltazar, Marta Santos, Gui Oliveira, Joana Carmelo, Joana Félix e Rita Cruz um muito obrigado pelos momentos na esplanada de Civil, por todas as conversas (quase) diárias no *whatsapp* e por continuarmos amigos mesmo estando em sítios diferentes do globo.

Quero também agradecer à D. Lurdes e ao Sr. Fernando por me terem acolhido na sua casa quando vim para Londres e que me fizeram sentir tão bem recebido que não poderia ter desejado melhor começo. Um muito obrigado por terem sido como uns pais numa altura de grande mudança na minha vida.

Para as minhas amigas de longa data, Rita Santos e Rita Elias, queria agradecer-vos do fundo do coração por todo o carinho que me deram em forma de abraços ou em forma de comida deliciosa (que só vocês sabem fazer tão bem). Obrigado também por irem dar um beijinho à minha mãe quando ela mais tinha saudades minhas.

À Joana Guedes e à Inês Lapa por terem sido as melhores amigas e companheiras de casa. Um obrigado também por terem ouvido todos os desabafos e frustrações mas acima de tudo por terem sobrevivido à tortura que vos causei com aquelas músicas pop que nem sequer sei a letra mas que trauteio de qualquer forma.

To Vagelis who came into my life when I least expected it and gave me so much love and support that I don’t even know how to thank him properly. Σε αγαπώ, αυτό είναι το μόνο πράγμα που μπορώ να πω. Είναι καταπληκτικό να γιορτάζω αυτές τις στιγμές έχοντάς σε στο πλευρό μου. Σε ευχαριστώ Βαγγέλη μου.

À minha família um obrigado por todo o apoio ao longo de todos estes anos, em especial para a minha mãe por ter sido tão presente e motivadora em todos os momentos da minha vida. Agradeço-lhe em especial por todas as torradas deliciosas que comia antes de ir para a escola e por todos os Bollycaos que me deu - e claro, por todo o amor e carinho!

List of Publications

Ludmila Peeva, Joao da Silva Burgal, Shankul Vartak, Andrew G. Livingston, Experimental strategies for increasing the catalyst turnover number in a continuous Heck coupling reaction, Journal of Catalysis, Volume 306, October 2013, Pages 190-201, ISSN 0021-9517, http://dx.doi.org/10.1016/j.jcat.2013.06.020.

Ludmila Peeva, Joao da Silva Burgal, Irina Valtcheva, Andrew G. Livingston, Continuous purification of active pharmaceutical ingredients using multistage organic solvent nanofiltration membrane cascade, Chemical Engineering Science, Volume 116, 6 September 2014, Pages 183-194, ISSN 0009-2509, http://dx.doi.org/10.1016/j.ces.2014.04.022.

João da Silva Burgal, Ludmila G. Peeva, Santosh Kumbharkar, Andrew Livingston, Organic solvent resistant poly(ether-ether-ketone) nanofiltration membranes, Journal of Membrane Science, Volume 479, 1 April 2015, Pages 105-116, ISSN 0376-7388, http://dx.doi.org/10.1016/j.memsci.2014.12.035.

João da Silva Burgal, Ludmila Peeva, Patrizia Marchetti, Andrew Livingston, Controlling molecular weight cut-off of PEEK nanofiltration membranes using a drying method, Journal of Membrane Science, Volume 493, 1 November 2015, Pages 524-538, ISSN 0376-7388, http://dx.doi.org/10.1016/j.memsci.2015.07.012.

James Campbell, Joao Da Silva Burgal, Gyorgy Szekely, R.P. Davies, D. Christopher Braddock, Andrew Livingston, Hybrid Polymer/MOF membranes for Organic Solvent Nanofiltration (OSN): Chemical Modification and the Quest for Perfection, Journal of Membrane Science, Available online 15 January 2016, ISSN 0376-7388, http://dx.doi.org/10.1016/j.memsci.2016.01.024.

João da Silva Burgal, Ludmila Peeva, and Andrew Livingston, Towards improved membrane production: using low-toxicity solvents for the preparation of PEEK nanofiltration membranes. Green Chemistry, 2016, DOI: 10.1039/C5GC02546J.

Table of contents

List of Figures

List of Tables

List of abbreviations

Abbreviation	Description
[EMIM]OAc	1-ethyl-3-methylimidazolium acetate
AFM	Atomic force microscopy
ATR-FTIR	Attenuated total reflectance Fourier Transform Infrared Spectroscopy
BPPM	chiral ligand (2S,4S)-1-tert-butoxycarbonyl-4-diphenylphosphino-2-(diphenylphosphinometyl)-pyrrolidine
CA	Cellulose acetate
CTA	Cellulose triacetate
DCM	Dichloromethane or methylene chloride
DI Water	Deionised water
DMA	Dynamic mechanical analysis
DMAc	N, N – dimethylacetamide
DMF	N,N-Dimethylformamide
DMFC	Direct methanol fuel cell
DMI	Dimethyl itaconate
DMSO	Dimethyl sulphoxide
DS	Degree of sulphonation
DSC	Dynamic scanning calorimetry
DTA	Differential thermal analysis
EDA	2-ethylenediamine
EE	Ethylether
Et_2O	Diethylether
EtOH	Ethanol
EVAL	Poly(ethylene-co-vinyl alcohol)
HCl	Hydrochloric acid
HDA	1,6-hexanediamine
HPLC	High pressure liquid chromatography
IB	Iodobenzene
IP	Interfacial polymerization
IPA	Isopropanol
KOH	Potassium hydroxide
MA	Maleic acid
MAE	Mean Absolute Error
MAPE	Mean Absolute Percentage Error
MEA	Monoethanolamine
MeOH	Methanol
MEUF	Micellar enhanced ultrafiltration
MF	Microfiltration
MIR	Middle infrared
MIR	Middle infrared
MMM	Mixed matrix membranes
MSA	Methane sulphonic acid
MSE	Mean Square Error
MW	Molecular weight
MWCO	Molecular weight cut-off
MWE	Molecular weight enlargement
NaOH	Sodium hydroxide
NEt_3	Triethylamine
NF	Nanofiltration
NG	Nucleation and growth
N-NMP	N-Methyl-2-pyrrolidone
ODA	1,8-octanediamine
OSN	Organic solvent nanofiltration
PA	Polyamide
PAEK	Poly(aryl ether ketone)
PAH	Poly(amide-hidrazide)
PAN	Polyacrylonitrile
PBI	Polybenzimidazole

Abbreviation	Description
PDA	1,3-propanediamine
PDMS	Poly(dimethylsiloxane)
PEEK	Poly(ether ether ketone)
PEEK-WC	poly(oxa-p-phenylene-3,3-phtalido-p-phenylenxoxa-p-phenylenoxoxy-p-phenylene) with Cardo group
PEG	Polyethylene glycol
PEK	Poly(ether ketone)
PEMFC	Polymer electrolyte membrane fuel cells
PI	Polyimide
PINs	Interpenetrating polymer networks
PPh_3	Triphenylphosphine
PS	Polystyrene
PSf	Polysulphone
PVP	Polyvinylpyrrolidone
RH	Relative humidity
RMSE	Root Mean Square Error
RO	Reverse osmosis
SA	Sulphuric acid
SD	Spinodal demixing
SDM	Standard deviation of the mean
SEM	Scanning electron microscopy
S-PEEK	Sulphonated poly(ether ether ketone)
SPEEK-WC	Sulphonated poly(oxa-p-phenylene-3,3-phtalido-p-phenylenxoxa-p-phenylenoxoxy-p-phenylene) with Cardo group
SW	Spiral-wound
TBPEEK	Modified PEEK with tertiarybutylhydroquinone (TBHQ) (instead of hydroquinone)
TEP	Triethylphosphate
TFC	Thin film composite
TGA	Thermal gravimetric analysis
TGS	Triglycine sulfate
THF	Tetrahydrofuran
TMCs	Transition metal catalysts
TMS	Thermomorphic multicomponent solvent
TON	Turnover number
TPPTS	Tris(3-sulfophenyl)phosphine trisodium salt
UF	Ultrafiltration
UV/Vis	Ultraviolet/visible detector
VAPEEK	Modified PEEK with diphenolic acid
XPS	X-ray photoelectron spectroscopy

List of symbols

Symbol	Description	Units
$p\ or\ \Delta p$	Applied pressure	Pa or bar
A	Area	m^2
F_c	Capillary forces	N
L	Coefficient of proportionality between flux and driving force	$mol.s.kg^{-1}$
C	Concentration	$mol.m^{-3}$
$K_{i,c}$	Convective hindrance factor	(-)
X	Conversion, dimensionless	(-)
D	Diameter	m
$D_{i,\infty}$	Diffusion coefficient	$m^2.s^{-1}$
$K_{i,d}$	Diffusion hindrance factor	(-)
x	Distance from membrane surface	m
S	Entropy	$J.K^{-1}$
F	Faraday constant	$C.mol^{-1}$
R	Ideal gas constant	$J.mol^{-1}.K^{-1}$
L	Length	cm
D_i	Liquid phase diffusion coefficient	$m^2.s^{-1}$
k	Mass transfer coefficient	$m.s^{-1}$
r_p	Membrane pore size	m
ℓ	Membrane thickness	m
c_i	Molar concentration	$mol.m^{-3}$
ṁ	Molar flow rate	(mol.min-1)
Pe	Peclet number	(-)
k	Permeability coefficient	$m.s^{-1}$
L_P	Permeance	$L.h^{-1}.m^{-2}.bar^{-1}$
K	pre-exponential factor/kinetic rate constant	min-1
n	reaction order, dimensionless	(-)
r	Reaction rate	$mol.L^{-1}.min^{-1}$
V	Reactor volume	mL
R_i	Rejection of solute *i*	(-) or %
t_r	Residence time	min
Re	Reynolds number	(-)
J_i	Solute molar flux	$mol.m^{-2}.s^{-1}$
z_i	Solute valence	(-)
K_i	Sorption coefficient	(-)
T	Temperature	K or °C
E	Tensile modulus of the polymer material	$N.m^{-2}$
t	Time	s or h
v	Velocity of the fluid	$m.s^{-1}$
Q	Volumetric flow rate	$mL.min^{-1}$
J	Volumetric flux	$L.h^{-1}.m^{-2}$

Greek symbols	Description	Units
γ_i	Activity coefficient	(-)
θ	Contact angle between the liquid and the membrane material	°
ρ	Density	$kg.m^{-3}$
Ψ	Electrical potential	V
v_i	Molar volume of species i	$m^3.mol^{-1}$
$\Delta\pi$	Osmotic pressure	Pa or bar
Φ_i	Partition coefficient	(-)
ε	Surface porosity	(-)
γ	Surface tension of the gas/liquid interface	$N.m^{-2}$
τ	Tortuosity	(-)
μ_i	Total chemical potential of species i	$J.mol^{-1}$
μ	Viscosity	Pa.s

Subscripts	Description
i	Any general system component
gen	Generated in the CSTR
in	System inlet stream
out	CSTR outlet stream
P	Product
perm	Permeate
PFR	Plug flow reactor
ref.	reference
ret	Retentate
S	Substrate

Chapter 1. Introduction

1.1 Research motivation

Conventional molecular separation processes such as evaporation and distillation require high amounts of energy due to the latent heat of vaporization of liquids [1]. As an alternative, membrane technology has lower energy consumption than conventional separation processes, requiring only one-tenth of energy to process an equivalent volume of liquid [2]. Organic solvent nanofiltration (OSN) is a novel technology that could be used for the separation of products with high added value from organic solvents using selective solvent stable membranes [2]. Nowadays, most nanofiltration (NF) membranes are produced from polymeric materials such as polyimide or polyamide membranes, which cannot be used at high temperatures due to lack of thermal stability [3]. Polyimides are unstable in some amines and have generally poor stability and performance in polar aprotic solvents. Therefore, crosslinking of PI is necessary to increase their solvent resistance and the DuraMem® (crosslinked PI, Evonik MET, UK) series offer long term stability in most polar aprotic solvents (acetone, tetrahydrofuran, dimethylformamide) [4-6]. Polyamide NF membranes are usually constituted by a thin active layer (TAL) fabricated by interfacial polymerization (DL, Osmonics and TFC NF, Koch Fluid Systems). In general, the PA layer is cross-linked to induce porosity and stabilize the structure [7]. Nevertheless, despite crosslinking both materials suffer chemical degradation under acidic/basic conditions [8, 9]. Consequently, OSN polymeric membranes that can withstand high temperature conditions as well as acidic or basic conditions are lacking on the market.

An alternative polymer that can be used in OSN is poly(ether ether ketone) (PEEK). This polymer exhibits strong chemical resistance in harsh solvents, and PEEK membranes require neither crosslinking due to their inherent chemical resistance, nor pore preserving agents [10]. In addition, the solvents used to dissolve PEEK are methane sulphonic acid (MSA) and sulphuric acid (SA), which can be simply neutralized in water by adding a base. In this work, non-modified and non-sulphonated PEEK NF membranes are explored as a viable “green” alternative to crosslinked PI and PA membranes. Given the intrinsic chemical and thermal resistance the usage of these membranes is explored in continuous catalytic reactions with reaction and separation *in situ* (2-in-1 process).

1.2 Thesis structure

The thesis starts with a literature review (Chapter 2) covering membrane technology and organic solvent nanofiltration to introduce and familiarize the reader with the topic. After this, the project objectives are defined and explained (Chapter 3). The subsequent chapters are experimental and focused on the fabrication of PEEK nanofiltration membranes as well as

on the understanding of the transport properties of PEEK NF membranes. In Chapter 4, the production of PEEK NF membranes with low degree of sulphonation using PEEK polymer powders from different brands, VICTREX® and VESTAKEEP®, is presented and explained. The drying of PEEK NF membranes from water without conditioning agent is shown to be the reason for the nanofiltration properties of PEEK membranes. The membranes are characterized with parameters such as contact angle, degree of sulphonation and degree of crystallinity. Using the results obtained in the previous chapter, the membranes are scaled-up to spiral wound modules (Chapter 5). In this chapter, the casting speed of PEEK membranes in continuous mode is studied and so is the drying temperature of the membranes in order to understand the influence of these parameters on the final spiral wound module performance. Chapter 6 is a discussion of the "greenness" of PEEK production when compared with three ways of producing alternative PI based membranes. The environmental burden is assessed using green metrics, E-factor and solvent intensity, at both bench and industrial scales. In Chapter 7, PEEK NF membranes are further manipulated by drying from different solvents at different temperatures and the effects of these factors are studied in terms of membrane performance. In this chapter three different polymer dope concentrations are also studied. A statistical model is applied to understand how some solvents parameters, such as vapour pressure, viscosity and surface tension, influence the final performance of PEEK NF membranes when drying them at 120 °C. In Chapter 8, the negligible aging of PEEK membranes is demonstrated and compared with PBI and PI membranes under similar annealing conditions. In addition, different solvents are filtered at temperatures below their corresponding boiling point in order to assess the stability and performance of PEEK membranes at different filtration temperatures and understand the transport mechanism under conditions other than ambient temperature. The final experimental chapter, Chapter 9, is a proof-of-concept of PEEK nanofiltration membranes in two continuous catalytic Heck reactions (2-in-1 process). Chapter 10 encompasses the overall conclusions and recommendations for future work in this research topic.

Chapter 2. Literature review

2.1 Membranes: the basics

In a very simple way a membrane is a discrete interface that moderates the permeation of chemical species (liquid or gas) in contact with it; the membrane acts as a permselective barrier between two phases, the retentate and the permeate, when filtering a feed stream through it using a driving force (concentration, pressure, temperature gradient and electrochemical potential). This definition describes a number of different structures which can be from biological or synthetic origins. Synthetic membranes are divided into organic (polymeric), inorganic (ceramic) and hybrids of these two (mixed matrix membranes)[11, 12].

Regarding the average pore diameter of the membrane filter (whether it is an organic, inorganic or mixed matrix membrane) the separation processes can be classified as reverse osmosis, nanofiltration (particles and dissolved molecules smaller than about 2 nm are rejected), ultrafiltration (particles and dissolved macromolecules smaller than 0.1 μm and larger than about 2 nm are rejected), microfiltration (particles and dissolved macromolecules larger than 0.1 μm are rejected) and conventional filtration. Reverse osmosis membranes are so dense that discrete pores do not exist (transport occurs via statistically distributed free volume areas) [12, 13].

2.1.1 Ceramic membranes

Ceramic membranes usually present an asymmetric structure composed of at least two porous layers of one or more different materials. The membranes generally possess a macroporous support, one or two mesoporous intermediate layers and a microporous (or a dense) top layer. The inorganic support provides mechanical stability and defines the external shape of the membrane. The intermediate layers link the pore size differences between the support layer and the top layer (active layer). The separation performance of ceramic membranes is directly associated with the overall membrane morphology. For porous ceramic membranes, separation properties are directly determined by characteristics of the porous structure such as pore size, shape, connectivity, particle size, etc. whereas for dense ceramic membranes, the gas tightness, crystal structures and microstructure, etc. are important parameters. The most common materials used to produce ceramic membranes are metal oxides such as Al_2O_3, TiO_2, ZrO_2, SiO_2, etc. or combinations of them. However, these materials are not the most suitable for mixed conducting properties. Mixed ionic-electronic conducting (MIEC) materials such as perovskite or perovskite-related structures are used for dense oxygen transport membranes due to the significant mixed conducting capabilities [14]. In order to prepare ceramic membranes several methods such as slip casting, tape casting, extrusion and pressing are usually employed. For multi-layer

membranes a coating step on a membrane support can be further applied using dip-coating, sol-gel, chemical vapour deposition or electrochemical vapour deposition. Nevertheless, the final membrane product or membrane support can only be obtained through firing [15].

Inorganic membranes are more expensive than organic polymeric membranes but they possess advantages such as temperature and wear resistance, well-defined stable pore structure and chemically inertness [16]. The main obstacle for them to be used more widely is the expensive production cost, complicated synthesis and process scale-up as well as their brittleness and handling difficulties [17, 18].

2.1.2 Polymeric membranes

Depending on their morphology, polymeric membranes can be divided into two types – symmetrical (isotropic) membranes and anisotropic (asymmetric) membranes. Symmetrical membranes can be further divided into symmetric porous membranes and nonporous dense membranes whereas anisotropic membranes can be further divided into anisotropic porous membranes and thin-film composite anisotropic membranes. A further explanation of the different types of polymeric membranes is presented below.

2.1.2.1 Symmetrical porous membranes

This type of membranes has a rigid, highly voided structure with randomly distributed, interconnected pores; the pore size is in the order of 0.01 to 10 μm in diameter which makes it suitable for ultra- and microfiltration. The separation of solutes by porous membranes is mainly a function of pore size distribution and molecular size [12].

2.1.2.2 Nonporous/dense membranes

Nonporous, dense membranes are made of a dense film and are mostly used in pervaporation, gas separation, and reverse osmosis. The driving forces governing the transport in this type of membranes are pressure, concentration, or electrical potential gradient. The separation occurs because of the differences in diffusivity and solubility in the membrane material for each of the components. Given the low flux in dense films it is common to use an anisotropic structure to improve it [12].

2.1.2.3 Asymmetric porous membranes

These membranes (also called integrally skinned asymmetric membranes) consist of a very thin and dense skin layer (0.1–1 μm) on top of a thick and highly porous sub-layer (100–200 μm with an average void size ranging from 0.01 to 1 μm), where both layers are composed of the same material and formed in a single operation. The skin (top layer) acts as the actual selective barrier, whereas the sublayer provides the mechanical support and prevents the membrane from breaking. The skin layer allows for higher selectivity and

permeability when compared to the previous mentioned membrane types [12, 16]. The phase inversion technique method by which such membranes are prepared was first introduced by Loeb and Sourirajan in the sixties [19]. The term “phase inversion” refers to the controlled transformation of a cast polymeric solution from a liquid state to a solid state. This process is a controlled liquid-liquid demixing that starts with a thermodynamically stable polymer solution. Different techniques can be used to induce the phase inversion process such as immersion in a non-solvent bath (‘immersion precipitation’), evaporation of the volatile solvent from a polymer that was dissolved in a solvent/non-solvent mixture (‘controlled evaporation’), lowering the temperature (‘thermal precipitation’) and placing the cast film in a vapour phase which consists of a non-solvent saturated with a solvent (‘precipitation from vapour phase’) [20]. More details will be given on ‘immersion precipitation’ in section 2.4.

2.1.2.4 Thin film composite (TFC) membranes

TFC membranes are composed of two layers, an ultra-thin skin (active layer) and a porous support layer (usually an asymmetric membrane prepared via phase inversion), which are formed in a two-step process. Usually the layers are different from one another in terms of chemical composition; different polymer materials can be used, thus enabling the optimization to maximise the overall membrane performance. TFC membranes have experienced tremendous development since the concept of interfacial polymerization (IP) was first introduced by Mogan in 1965 [21]. Apart from the IP technique other coating techniques are also available, such as casting an ultrathin film separately, then laminating it to a support; dip-coating/solvent casting a solution of a polymer onto a support; dip-coating a solution of a reactive monomer or prepolymer onto a support, followed by a post-curing with heat or irradiation; and depositing a barrier film directly from a gaseous phase monomer plasma [22].

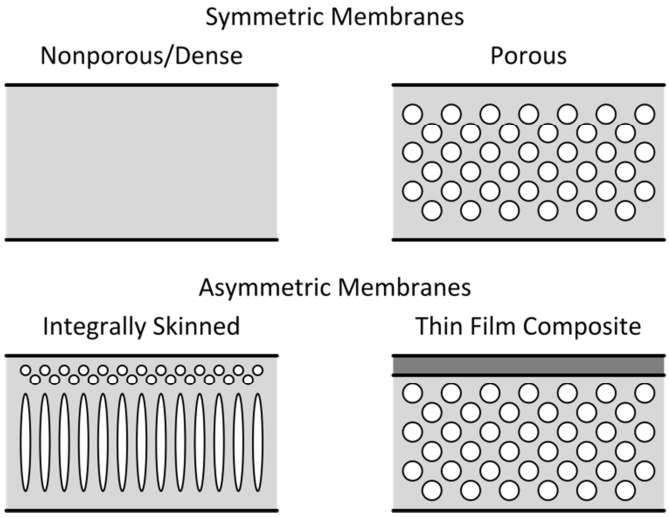

Figure 2.1 – Schematic representation of the four basic polymeric membrane types: nonporous/dense, symmetric porous, asymmetric porous and thin film composite.

2.1.3 Mixed matrix membranes (MMM)

This type of membrane is a hybrid of organic and inorganic membranes in which the tailoring of new membranes combines properties of both types [22]. Inorganic materials, such as nanotubes, zeolites, nanoparticles, clay and fullerene, are used as the dispersed phase in mixed matrix membranes; such materials possess a unique structure and mechanical strength and when added to the polymer matrix they are expected to improve regular polymer membranes. However, fabrication of MMM usually involves some problems like weak contact of particles in the polymer matrix and poor distribution of the dispersed phase in the continuous polymer matrix phase. In addition other factors such as particle size, particle pore size, dispersed phase load and polymer type and properties can also affect the mixed matrix properties [23].

2.2 Membrane characterization

Membrane science studies performed in a systematic way started in the eighteenth century with philosopher scientists. During the nineteenth and early twentieth centuries there were no industrial or commercial uses of membranes; mainly they were used as laboratory tools to develop physical/chemical theories [12].

In order to assess its suitability in a certain separation or class of separations membranes need to be characterised; the characterization is necessary to relate structural membrane properties such as pore size, pore size distribution, free volume and cristallinity to membrane separation processes. Given that membranes range from porous to nonporous depending on the type of separation problem involved, completely different characterization techniques will be employed in each case.

For nonporous membranes common methods used are permeability, physical methods such as differential scanning calorimetry (DSC)/differential thermal analysis (DTA), plasma etching and surface analysis such as X-ray photoelectron spectroscopy (XPS) and Auger electron spectroscopy.

For porous membranes two different types of characterization methods can be used:

- Structure-related parameters: determination of pore size, pore size distribution, top layer thickness and surface porosity; common techniques used are electron microscopy (EM), atomic force microscopy (AFM), bubble point method, mercury intrusion method for example.

- Permeation-related parameters: determination of the actual separation parameters using solutes that are more or less retained by the membrane [11] ("cut-off" determination); filtration experiments either in dead-end mode or cross-flow mode are the standard technique to obtain the molecular weight "cut-off" (MWCO), defined as the lowest molecular weight solute that is 90% retained by the membrane. During filtration two features are obtained, the permeability and the separation ability of the membrane (MWCO). The permeance, B, is defined as the flow rate of solution per unit membrane area per unit pressure drop. In general, the flux, J, (Equation 2.1) is measured at a given pressure Δp and hence, B (Equation 2.2) can be calculated by dividing J per Δp [5].

$$J[L.T^{-1}] = \frac{Flow\ rate\ [L^3.T^{-1}]}{Membrane\ area\ [L^2]} \qquad \text{Equation 2.1}$$

$$B[L^2.M^{-1}.T] = \frac{J[L.T^{-1}]}{\Delta p[M.L^{-1}.T^{-2}]} \qquad \text{Equation 2.2}$$

The rejection (R) of a solute *i* will determine the membrane separation ability and is described by the following equation (Equation 2.3):

$$R_i[\%] = \left(1 - \frac{C_{P,i}}{C_{F,i}}\right) \times 100 \qquad \text{Equation 2.3}$$

If a homologous series of solutes is used for filtration purposes, the rejection of each component can be calculated and plotted against its corresponding molecular weight yielding in a rejection profile for the membrane (Figure 2.2).

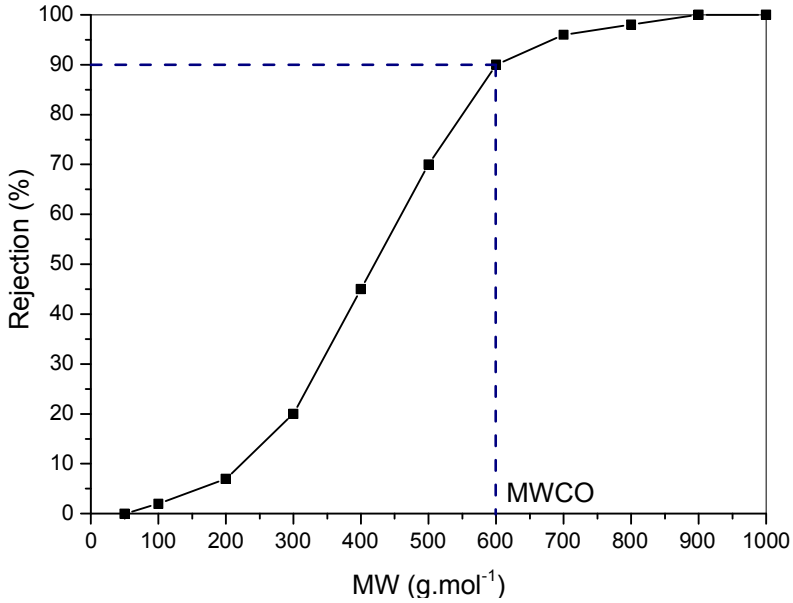

Figure 2.2 – Schematic representation of rejection profile for nanofiltration membranes with indication of the MWCO.

2.3 Membrane transport models

In terms of developing a new process model there are three levels to take into account: a) transport through the membrane; b) fluid dynamics and mass transfer (module level); and c) process scale.

Transport models are a useful tool to understand and possibly predict fluxes and rejections for a certain membrane [17]. Three types of models have been identified to describe transport through a membrane. The first type has its origin from irreversible thermodynamics and considers the membrane as a black box, not considering any membrane property. The other two types, pore-flow model and solution-diffusion model, consider the membrane properties and describe the transport of solutes as function of structural and physicochemical parameters [17, 22].

2.3.1 Irreversible thermodynamics

In the irreversible thermodynamics model transport is considered as an irreversible process during which free energy is dissipated continuously and entropy is produced. This increase of entropy (S) can be calculated from the dissipation function ϕ (Equation 2.4)

$$\phi = \frac{TdS}{dt} = \sum_i J_i X_i \qquad \text{Equation 2.4}$$

where J_i and X_i represent the conjugated fluxes and forces, respectively, T the temperature and t the time. A linear relationship between fluxes and forces can be assumed when the system is close to equilibrium, as shown in Equation 2.5,

$$J_i = \sum_j L_{ij} X_j \qquad \text{Equation 2.5}$$

where the sum includes all forces X_j acting on the system, while L_{ij} represent the phenomenological coefficients [17].

2.3.2 Pore-flow model and solution-diffusion models

In the class of models that account for membrane properties, the overall driving force producing movement of a permeant is the gradient in its chemical potential. Consequently, the flux, J_i, of the component i, becomes:

$$J_i = -L \frac{d\mu_i}{dx} \qquad \text{Equation 2.6}$$

where L is the coefficient of proportionality (not necessarily constant) between flux and driving force and μ_i is the total chemical potential of species i; μ_i can be subdivided into a chemical potential depending on pressure, temperature and concentration gradients and an electrochemical potential depending on electromotive force. This unifying approach is quite useful for processes that involve more than one driving force, for example, pressure and concentration in RO and NF. Simplifying the chemical potential to the driving forces generated by concentration and pressure gradients:

$$d\mu_i = RTdln(\gamma_i c_i) + v_i dp \qquad \text{Equation 2.7}$$

where c_i is the molar concentration, γ_i the activity coefficient, v_i the molar volume of species i, and p the pressure [22].

2.3.2.1 Pore-flow model

Pore-flow model models assume that the concentrations of solvent and solute within a membrane are uniform and that the chemical potential gradient across the membrane is expressed only as a pressure gradient [17]. The transport through porous membranes in the absence of a concentration gradient, based on a pure hydrodynamic analysis, can be described by Darcy's law (Equation 2.8)

$$j_i = k \frac{(p_0 - p_l)}{l} \qquad \text{Equation 2.8}$$

k is the permeability coefficient which is a function of structural factors, such as membrane pore size, r_p, surface porosity, ε, and tortuosity, τ; l is the membrane thickness.

In the case of pure solvent flux, for which no significant concentration gradient is present across the membrane, the flux equation becomes the well-known Hagen-Poiseuille model:

$$V = \frac{\varepsilon r_p^2 \Delta p}{8\mu\tau l} \qquad \text{Equation 2.9}$$

According to this model, the viscosity, μ, is the only solvent parameter affecting permeation. The influence of the membrane is represented by the pore size, r_p, the porosity, ε, the tortuosity, τ, and the membrane thickness, l. No solvent-membrane interaction parameters are used to describe the flow [22].

2.3.2.2 The solution-diffusion model

The solution-diffusion model was proposed in the nineteenth century but did not have many supporters until the 1940s; it was used to explain transport of gases through polymeric films. Using the solution-diffusion model for gas transport was relatively uncontroversial, but the transport mechanism in reverse osmosis membranes was a dividing issue in the 1960s and early 1970s. However, by 1980, the solution-diffusion model became accepted and currently the pore-flow model is not commonly used to describe reverse osmosis.

This model is usually adopted for transport through dense membranes. In this kind of membrane, free volume elements are present as statistical fluctuations that appear and disappear at about the same time scale as the motions of permeants through the membrane. These free-volume elements are different from the pores, which are fixed in time and space. Because no pressure gradient exists across the membrane, Equation 2.7 for the solute flux becomes:

$$J_i = -\frac{RTL}{c_i}\frac{dc_i}{dx} = -D_i\frac{dc_i}{dx} \qquad \text{Equation 2.10}$$

This equation has the same form as Fick's law, where the term is RTL/c_i is replaced by the diffusion coefficient, D_i.

The final equation for the solution-diffusion model, after integration over the membrane thickness, is:

$$J_i = \frac{K_i D_i^{SD} c_{i,0}}{l}\left(1 - e^{-\frac{v_i(\Delta p - \Delta\pi)}{RT}}\right) \qquad \text{Equation 2.11}$$

Equation 2.11 is valid for both solute and solvent fluxes across the membrane in terms of the pressure and concentration difference across the membrane. Therefore, the solution

diffusion model does not require the distinction between solute and solvent, and can easily be extended to multicomponent mixtures.

2.4 Organic solvent nanofiltration (OSN)

In this research work the main focus is on integrally skinned polymeric OSN membranes produced via 'immersion precipitation' (section 2.1.2.3), a common method used for nanofiltration/reverse osmosis membrane synthesis. The most common polymers used for OSN membranes preparation via this technique are polyacrylonitrile (PAN), polyimide (PI), polyamide (PA) and polybenzimidazole (PBI) for example; as supports it is common to use PAN, poly(vinylidene fluoride) (PVDF) and blends of polysulphone/sulphonated poly(ether ether ketone) (S-PEEK). Usually the solvent stability is related to the chemical structure of the polymer and the presence of certain structural elements, such as aromatic groups, imide bonds or fluorine-atoms [17, 19].

In order to simplify the thermodynamic aspects of 'immersion precipitation' it is fairly standard to use a three component (solvent; non-solvent; polymer) phase diagram. The initial casting solution is situated in the stable region, outside the binodal; between the binodal and spinodal the polymer solution is metastable; and inside the spinodal the solution is in the unstable region. There are two possible ways to phase separate: one most common denominated 'binodal demixing' (BD), and one less frequent designated as 'spinodal demixing' (SD). In the 'binodal demixing' the polymer solution phase separates into a polymer lean and a polymer rich phase according to the nucleation and growth (NG) mechanism. Ideally, the nuclei would just grow and mostly progress to a phase coalescence. In the SD the polymer solution crosses the critical point directly into the unstable region. In contrast to BD two co-continuous phases will be formed instead of well-defined nuclei. Another important thing to take into account besides the mechanism that initiates the phase separation is the moment at which the developing structure gets fixed. This means that if the binodal gets crossed already at time t demixing will start immediately (instantaneous demixing); otherwise it is necessary that more non-solvent enters the film so that the binodal can be crossed and demixing can start (delayed demixing).

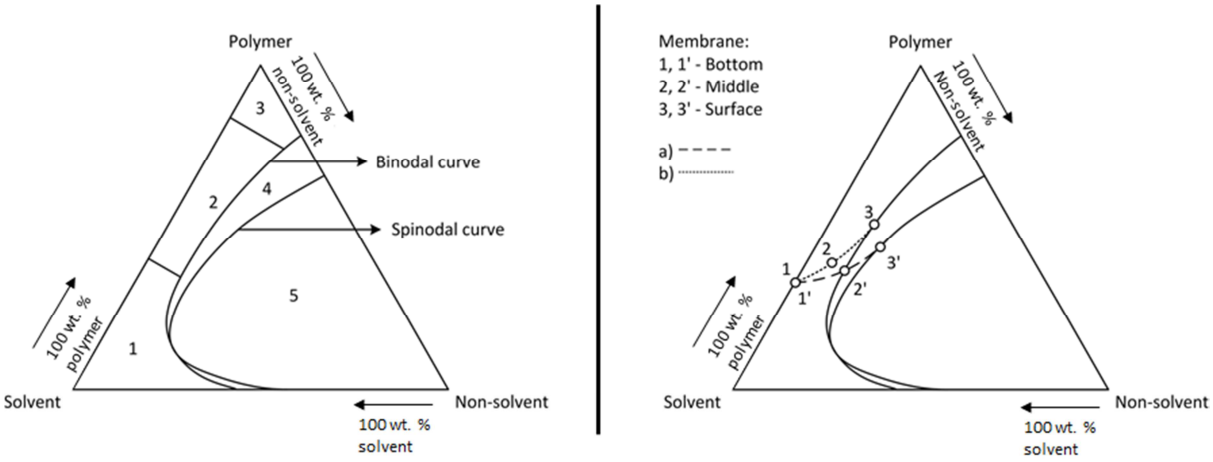

Figure 2.3 – Left image: Schematic example of a three component phase diagram used to describe membrane formation during phase separation in non-solvent. Right image: Composition across the polymer film at time t almost immediately after contacting with non-solvent for a) instantaneous and b) delayed demixing (adapted from [20]).

Other parameters besides thermodynamics characteristics of the polymer solution and kinetics aspects of diffusion determine as well the morphology [17, 20]. These are described below:

2.4.1 Type of polymer

The type of polymer will influence the performance of the membrane. For instance, the polymer structure, linear or non-linear, can have an impact on the flux given the fact that membranes prepared from non-linear polymers, which possess higher interchain-distance, will lead to higher fluxes. In addition, the hydrophilicity/hydrophobicity balance can lead to a more or less water permeable membrane and the charge density can determine salt rejection [17, 20].

2.4.2 Composition of the casting solution

In terms of casting solution it is necessary to take into account the polymer concentration, addition of volatile solvents, addition of non-solvents or 'bad' solvents and pore forming additives. For polymer concentration it is known that by increasing the initial polymer concentration a denser skin with increased thickness, sublayers with lower porosities and lower fluxes are obtained, mainly due to the delayed demixing. Volatile solvents such as ethylether (EE) and tetrahydrofuran (THF), are added in order to produce integrally skinned asymmetric membranes with the dry/wet method (where the evaporation step is essential). As for addition of non-solvent or 'bad solvents' their usage is mainly focused in order to control the porosity of the membranes. Pore forming additives can be used to increase permeability and porosity with or without compromising the selectivity. For example addition of LiCl or $LiNO_3$ to poly(amide-hidrazide) (PAH) casting solutions result in a higher

permeability without lowering selectivity. Besides inorganic additives it is also common to add organic additives such as glycerol, polyethylene glycol (PEG), polyvinylpyrrolidone (PVP), etc.; for example, adding maleic acid (MA) to cellulose triacetate (CTA) increases the porosity and permeability [17, 20, 24].

2.4.3 Post-casting treatment

In the post-casting treatment several factors such as temperature and time of evaporation, relative humidity of the air and air velocity (if a convective flow is applied) can play a role. In terms of evaporation time there seems to be two contradictory effects. For membranes prepared from PA, PAH and CA the flux decreases and the rejection increases with increasing evaporation time. However, Soroko et al. [25] and See-Toh et al. [26] have concluded that increasing evaporation time reduces the flux but has no effect on rejection for PI membranes. In terms of temperature of evaporation, Young et al. [27] found that for poly(ethylene-co-vinyl alcohol) (EVAL) - although not used for OSN – a membrane structure with a particulate morphology was obtained at low temperatures after all the casting solution evaporated. Nevertheless, the rise in the evaporation temperature changed EVAL membrane structure from a particulate to a dense morphology. In addition, for PAH it was observed that with increasing temperature lower fluxes and higher rejections were obtained reaching a plateau at 100 °C; above this temperature the inverse behaviour occurred in terms of solute rejection (probably due to polymer degradation) [18, 20].

2.4.4 Coagulation bath

The choice of non-solvent (coagulation bath) will influence the membrane morphology as well. As mentioned before in ‘immersion precipitation’, the higher the rate of exchange between solvent and non-solvent the higher the porosity of the membrane; this is true for example for NMP/water (solvent/non-solvent) pair. It is also common to use additives like alcohols or DMF (N, N – dimethylformamide) to vary the exchange rate of solvent/non-solvent as well. Another factor to take into account in the coagulation bath is the temperature. In general, an increase in the temperature of the coagulation bath leads to a higher exchange rate and consequently to a more porous structure [20, 24].

2.4.5 Post-treatment

In order to stabilise and improve the membrane performance there are several post-treatments that can be used including annealing in water or under dry conditions, exposure to concentrated mineral acids, drying with the solvent exchange technique and treatment with conditioning agents.

Crosslinking is used to enhance chemical stability and rejection properties of integrally skinned membranes. Different crosslinking methods have been used for polymeric

membranes, including thermal crosslinking, ultraviolet (UV) crosslinking and chemical crosslinking [22]. PI is by far the most common organic polymer used for synthesis of membranes for gas separation and organic solvent nanofiltration given its excellent thermal stability combined with good chemical stability and mechanical strength. PIs are characterized by the presence of the imide group in the polymer backbone and several PI types have been developed for gas separation processes, pervaporation and OSN throughout the years. In terms of OSN, for a long time the P84 based Starmem® membranes were the only commercially available PI based OSN on the market. Other PI OSN membranes appeared in the market more recently such as Solsep (the Netherlands), Puramem™ (uncrosslinked, Evonik, UK) and DuraMem® (crosslinked, Evonik, UK) [4, 6]. Nevertheless, the above mentioned commercial PI OSN membranes have been shown to give good performances in several organic solvents (e.g. toluene, methanol, ethyl acetate, etc.), but polyimides are unstable in some amines and have generally poor stability and performance in polar aprotic solvents and chlorinated solvents such as methylene chloride (DCM), tetrahydrofuran (THF), dimethyl formamide (DMF) and n-methyl pyrrolidone (NMP), in which most polyimides are soluble. The reason for crosslinking PI is related to the suppression of plasticization in gas separation and pervaporation processes, to the increased hydrophilicity of the PI for aqueous pervaporation and the improved solvent resistance which make it a good membrane for pervaporation, OSN and fuel cell applications. See Toh et al. [6] showed that post-casting crosslinking of P84® membranes with aliphatic diamines (1,2-ethylenediamine (EDA), 1,3-propanediamine (PDA), 1,6-hexanediamine (HDA) and 1,8-octanediamine (ODA)) resulted in membranes resistant to DMAc (N, N – dimethylacetamide), DMSO (Dimethyl sulfoxide), NMP (N – methyl - 2 – pyrrolidone) and DMF. The EDA crosslinked membrane presented the highest flux in DMF (8 $L.m^{-2}.h^{-1}.bar^{-1}$) and a good stability in DMF even after 120 h of testing. Nevertheless, it was observed that the toluene flux decreased with crosslinking and thermal annealing, probably due to a densification of the separation layer. See Toh et al. [28] further developed these membranes by tuning the MWCO between 200 and 1000 Da when changing the ratio of solvent to co-solvent in the casting solution. They verified that with the increasing DMF to dioxane ratio the membranes became more open and presented higher fluxes. Vandezande, et al. filed a patent based on a study they performed using Matrimid® PI membranes. In this patent they claim to prepare PI membranes via phase inversion or by an adapted method called ‘Solidification of Emulsified Polymer dope by Phase Inversion’ (containing nanozeolite precursors) and crosslink them with p-xylylenediamine (XDA). The resulting membranes are stable in DMAc, DMSO, NMP, THF and DMF [29, 30].

Linder, et al. patented a synthesis procedure for TFC OSN-membranes with a crosslinked PAN support. Crosslinking was performed by immersing the PAN membranes in an organic

or inorganic base, followed by heat treatment at elevated temperatures (110–130 °C); the membrane may (optimally) be further insolubilized or crosslinked by heating (e.g., in air) in the region of about 250 °C for a time period of several minutes up to several hours (although compaction must be avoided) [17, 31, 32]. Although PAN shows good solvent resistance, the PDMS separating layer swells appreciably in many solvents resulting in limited solvent stability [6].

More recently polybenzimidazole (PBI) has gained much attention for applications in gas separation, aqueous NF, fuel cells and OSN due to thermal, mechanical and chemical stability in corrosive environments [33]. PBI dissolves in polar aprotic solvents, such as DMAc, NMP and DMSO, from which solutions can be prepared and cast. For filtration in these solvents the polymer needs to be crosslinked with aliphatic dihalogenes or xylene dihalogenes [34, 35]. Valtcheva et al. [36] reported crosslinked PBI with 1,4 – dibromobutane (DBB) and α,α'-dibromo-p-xylene (DBX). The authors verified that the PBI membrane crosslinked with DBX maintained its performance in DMF before and after addition of piperidine as a solute. The permeance was between 5 and 9 $L.h^{-1}.m^{-2}.bar^{-1}$ for PBI crosslinked with DBX (before and after piperidine addition) whereas for PBI crosslinked with DBB the permeance decreased from 3 to 1 $L.h^{-1}.m^{-2}.bar^{-1}$. It is also important to mention that PEG 400, 2000 and 8000 were never fully rejected for PBI crosslinked with DBB (even before piperidine addition) while for PBI crosslinked with DBX PEG 2000 and 8000 were 100 % rejected by the membrane (before and after piperidine addition).

For most membranes prepared by wet phase inversion it is common to be stored under wet conditions because the structure of the membrane changes ("collapses") when the membrane is subjected to a drying process. In the case of ultrafiltration membranes (and nanofiltration as well) drying almost without exceptions induces irreversible loss of solvent permeance which is thought to be related to the collapse of the nodular structure [37]. In fact, using a multiple solvent exchange procedure can minimize the risk of nodule collapse upon drying. In this procedure, the residual non-solvent present in the membrane after immersion is replaced by a first solvent, which is miscible with the non-solvent; this solvent is then replaced by a more volatile solvent, which can be removed easily by evaporation to obtain a dry membrane [38-40]. One way to describe this nodular collapse is by using the theory introduced by Brown [41] for polymer latex particles during film formation. Beerlage [37] used this theory for polyimide ultrafiltration membranes and related the capillary forces (F_c) with the resistance of the matrix to deformation (F_r) developed by Brown. F_c is given by Equation 2.12 where γ ($N.m^{-2}$) is the surface tension of the gas/liquid interface inside the pores, r_p (m) is the pore radius, θ (°) is the contact angle between the liquid and the membrane material and A (m^2) is the pore cross sectional area. F_r is given by Equation 2.13

where E ($N.m^{-2}$) is the tensile modulus of the polymer material and is a measure of the pore wall elasticity. According to this approach if $F_c > F_r$ then collapse of the nodular structure will occur (Equation 2.14).

$$F_c = \frac{2\gamma}{r_p}.cos\theta.A \quad \text{Equation 2.12}$$

$$F_r = 0.37\ E.A \quad \text{Equation 2.13}$$

Thus for any given pore size the pore will collapse if:

$$\frac{2\gamma.cos\theta}{r_p} > 0.37 \times E \quad \text{Equation 2.14}$$

Based on the decrease of surface tension (for example via solvent exchange) it is possible to maintain the pore structure of a membrane (i.e. to minimise the capillary force) if the strength of the matrix is high enough [37, 39-42].

2.5 Poly(ether ether ketone) (PEEK) membranes

In this work a non-sulphonated and non-modified PEEK membrane is investigated as novel solvent resistant nanofiltration membrane. As mentioned before there is the possibility of crosslinking a polymer in order to make it more resistant to organic solvents (specifically polar aprotic solvents). An alternative approach is to use an intrinsically resistant material such as PEEK or poly(ether ketone) (PEK).

PEEK or poly(oxy-1,4-phenylene-oxy-1,4-phenylenecarbonyl-1,4-phenylene) was developed in 1979 as a result of extending ICI's "VICTREX" range of aromatic polymers with a crystalline material. The first application area for the polymer was as extruded insulation for high performance wires and cables, but there is now a wide spread of applications including injection moulded parts, chemically resistant surface coatings, monofilament for industrial belts and filters and as the matrix in carbon fibre composites for aerospace components [43]. PEEK is a semi-crystalline high performance thermoplastic with a rigid aromatic backbone structure constituted of a hydroquinone and a benzophenone segment. It possesses good thermal - melt and glass transition temperatures of 340 °C and 143 °C respectively - and mechanical properties, broad chemical resistance, oxidation stability and passive biocompatibility [44-47].

PEEK membranes are only resistant to strong polar organic solvents such as DMF, DMAc, DMSO and pyridine when the degree of sulphonation (DS) is low (DS around 4 mol %) [48]. At room temperature PEEK is only soluble in sulphuric acid (SA) and methanesulphonic acid (MSA), while at temperatures close to the melting point, PEEK dissolves in high boiling point esters, benzophenone or diphenyl sulphone [49]. On the one

hand the high chemical resistance of PEEK makes it an excellent material for OSN membranes, but on the other hand this resistance reduces its processability. When dissolved in SA, PEEK undergoes a sulphonation reaction (Figure 2.4) which modifies its chemical structure, reducing crystallinity and consequently increasing solubility.

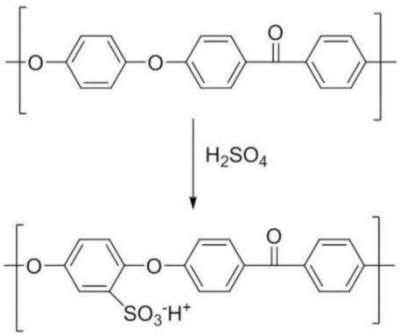

Figure 2.4 – Schematic principle for the sulphonation of poly(ether ether ketones).

Thus it is necessary to strictly control the degree of sulphonation (DS) because it will strongly influence the stability of the membrane in solvents such as DMF, DMSO or DMAc. PEEK membranes are only resistant to strong polar organic solvents such as DMF, DMAc, DMSO and pyridine when DS is low (DS around 4 mole %) [48]. In fact, above 30 mole % DS PEEK is soluble in hot DMF, DMSO and DMAc; above 40 mole %, in the same solvents at room temperature; above 70 mole % in MeOH and at 100 mole % in hot water [50].

PEEK membranes have been reported in literature for different applications such as continuous catalysis, gas separation, fuel cells, MF, UF, NF and RO [51]. PEEK membranes can be in non-sulphonated form, PEEK, or in sulphonated form, S-PEEK; both sulphonated and non-sulphonated forms can be modified.

In terms of non-sulphonated PEEK membranes not much has been reported in literature besides a few patents, mainly in the field of micro- and ultrafiltration using PEEK as membranes or as supports [24, 52, 53]. In fact, Shimoda and Hachiya [24] claimed a method for preparing non-sulphonated PEEK for microfiltration or ultrafiltration at high temperatures. In their method they leave the dope solution at 15 °C until membrane formation (casting) after dissolving it in concentrated sulphuric acid. In addition, the authors use as post-treatment a heat treatment for raising the cristallinity of the membrane by using a heat stabilizing solvent at a wet condition in order to obtain a heat resistant membrane durable even in water at 130 °C or higher. U.S. Patent numbers 4,992,485 [52] and 5,089,192 [54] disclose preparation of PEEK membranes from non-sulphonating acid solvents that include methane sulfonic acid and trifluoromethane sulfonic acid. European Patent Specification EP 0737506 [55] discloses preparation of improved polymeric membranes based on PEEK mixtures with polyethylene terephthalate. The membranes are formed by the solution casting

process from a methane sulphonic acid/sulphuric acid solvent mixture. Yuan [53] presents a process for the preparation of porous poly (aryl ether ketone) (PAEK) articles from PAEK/polyimide blends by a melt extrusion process followed by the removal of the polyimide phase. Porous PAEK articles exhibit a uniform pore size distribution and can be used as a porous media for a broad range of applications, including porous membranes for fluid separations, such as microfiltration, nanofiltration, and ultrafiltration, and as a sorption media. Sulphonated PEEK, S-PEEK, is mainly reported in literature as being used in gas separation [56, 57], polymer electrolyte membrane fuel cells (PEMFCs) and direct methanol fuel cells (DMFCs), posing an alternative to Nafion membranes [58]. S-PEEK can be obtained via post-sulphonation [59] or via sulphonated monomers [56]. In the first case, concentrated sulphuric acid is used at room temperature for long reaction times; the sulphonation reaction is initially a heterogeneous process and, as a consequence, it produces different fractions of polymer with a variable degree of sulphonation (DS) [58, 59].

Modifying PEEK is also a common technique to solubilize it in order to prepare membranes via the immersion technique. PEEK-WC [poly(oxa-p-phenylene-3,3-phtalido-p-phenylene-oxa-p-phenylene-oxy-p-phenylene) with Cardo group] is a modified PEEK that is amorphous and soluble in many organic solvents with medium polarity (e.g. chloroform, dichloromethane, dimethylsulfoxide, dimethylacetamide (DMAc), dimethylformamide, 1-methyl-2-pyrrolidinone, etc.), whereas it is not soluble in water and alcohols. PEEK-WC has a lactonic group, called Cardo group (WC in the polymer name means With Cardo), which prevents the crystalline organization of the polymer chain; hence it is suitable for the preparation of membranes by casting [59]. PEEK-WC can also be in its sulphonated form as SPEEK-WC. Applications for these membranes are focused mainly in gas separation, pervaporation, biomedical applications and – in its sulphonated form – in fuel cells [51].

Another recent approach for modifying PEEK was reported by Hendrix et al [60, 61]. This research group proposes two ways of modifying PEEK either by adding a different monomer [61] or by crosslinking PEEK [60]. The idea behind the addition of a different monomer is related to the fact that available polymers were not developed explicitly as membrane materials. These polymers may contain various additives such as stabilizers and flame retardants that can influence the phase inversion process. Therefore, they opted to produce their own polymer by selecting a different monomer to synthesize a soluble PEEK, namely tertiarybutylhydroquinone (TBHQ) (instead of hydroquinone). The produced TBPEEK was fully soluble in polar aprotic solvents, such as NMP and THF, allowing the preparation of phase inversion membranes; the produced membranes were stable in hexane, acetonitrile, methanol and IPA. As for crosslinking PEEK, this research group used a similar approach as reported for modification. Diphenolic acid was used as a monomer (to make it soluble in polar aprotic solvents) and after activation of the carboxylic acid in the polymer casting

solution the cast polymer film could be crosslinked by diamines (which were dissolved in the coagulation bath). The resulting membrane, VAPEEK, was stable in acetone and IPA showing retentions of around 90 % for Rose Bengal (MW = 973.67 $g.mol^{-1}$). All modifications for PEEK polymer are summarized in Table 2.1.

Table 2.1 – List of PEEK polymers reported in literature.

Polymer	Abbreviation	Molecular structure	Modified
Poly(ether ether ketone)	PEEK	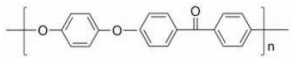	No
Sulphonated poly(ether ether ketone)	S-PEEK	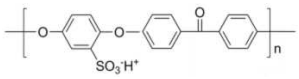	Yes
poly(oxa-p-phenylene-3,3-phtalido-p-phenylenxoxa-p-phenylenoxoxy-p-phenylene) with Cardo group	PEEK-WC	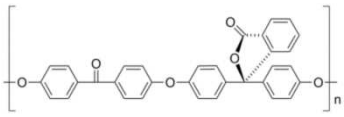	Yes
Sulphonated poly(oxa-p-phenylene-3,3-phtalido-p-phenylenxoxa-p-phenylenoxoxy-p-phenylene) with Cardo group	S-PEEK-WC	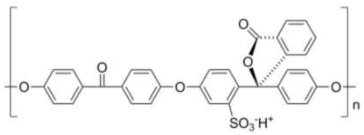	Yes
Modified PEEK with tertiarybutylhydroquinone (TBHQ) (instead of hydroquinone)	TBPEEK	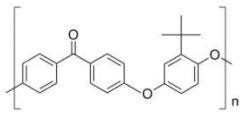	Yes
Modified PEEK with diphenolic acid	VAPEEK	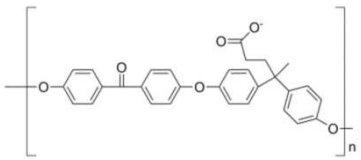	Yes

Chapter 3. Project objectives

The overall objective of this thesis is to develop and investigate a membrane in the nanofiltration range resistant to high temperatures and basic/acidic conditions. PEEK polymer is a suitable candidate for producing such membranes as it possesses good thermal - melt and glass transition temperatures of 340 °C and 143 °C respectively - and mechanical properties, broad chemical resistance, oxidation stability and passive biocompatibility [44-47]. A possible application for the developed membrane is in continuous catalytic reactions with separation in situ (2-in-1 process). To achieve the overall aim of this thesis, the following objectives were addressed:

3.1.1 Objective 1: Gain control over PEEK membranes in terms of performance and stability

The influence of the crystallinity, molecular weight (MW) and degree of polymerisation of PEEK polymer is one of the factors that will influence the membrane structure. Since PEEK polymer will not be synthesized it is necessary to test different PEEK polymers from different brands such as VESTAKEEP® and VICTREX®. The grades to be used are VESTAKEEP 2000P and 4000P from EVONIK and VICTREX® 150P and 450P from VICTREX®. Since the PEEK polymer powders will be dissolved in mixtures of methane sulphonic acid (MSA) and sulphuric acid (SA) the DS should be studied in order to control membrane fabrication and avoid the disadvantages that come with high DS. The effect of different ratios of these two acids on the DS will be monitored. Additionally, the effect of temperature and time of dissolution will be investigated, since it is known that these are two very important parameters. The formed membranes will be tested in terms of performance (flux and rejection) and in terms of solvent, acid and base resistance.

3.1.2 Objective 2: Scaling-up of PEEK nanofiltration membranes

PEEK membranes will be prepared at larger scale and rolled into 1.8’’x 12’’ modules for proof of concept at kilogram scale. The membrane modules will be tested over a long period to evaluate their performance in a large scale and compare them with laboratory scale performance.

3.1.3 Objective 2: Controlling MWCO of PEEK nanofiltration membranes

In terms of molecular-weight cut-off (MWCO) it is well known that there is always a trade-off between rejection and flux in terms of membrane performance. In order to manipulate membrane performance it is possible to vary the composition of the dope solution or vary the conditions either during the phase inversion step or via a post-treatment step (drying, conditioning or crosslinking) [3,4]. Changes in the composition of the dope solution and

different post-treatments will be evaluated in order to tune the MWCO. The two methods explored were the change of polymer concentration in the dope solution – 8 wt. %, 10 wt. % and 12 wt. % - and the variation of solvent filling the pores prior to drying. Volatile solvents such as water, methanol and tetrahydrofuran will be used as well as non-volatile solvents, e.g., PEG200 and PEG400.

3.1.4 Objective 3: Testing PEEK membranes for high-temperature filtrations

Most RO and NF membranes are usually applied in processes that operate at ambient temperature such as desalination and purification and recovery of valuable compounds [7, 62]. However, in several industrial applications, operating conditions can require working temperatures higher than 90 °C [7, 63, 64]. In order to prove the intrinsic resistance of PEEK membranes and their applicability at high temperatures, different solvents will be filtered through PEEK membranes at high temperatures and pressure.

3.1.5 Objective 4: PEEK membranes for challenging applications

The final objective of this research work is to apply PEEK membranes for retaining the catalyst in a high temperature continuous catalytic reaction. Based on the results obtained in the previous objectives, a suitable membrane will be chosen and used for the challenging conditions of a catalytic reaction.

Chapter 4. Organic solvent resistant poly(ether-ether-ketone) nanofiltration membranes

The work described in this chapter has been published in the following paper:

João da Silva Burgal, Ludmila G. Peeva, Santosh Kumbharkar, Andrew Livingston, Organic solvent resistant poly(ether-ether-ketone) nanofiltration membranes, Journal of Membrane Science, Volume 479, 1 April 2015, Pages 105-116, ISSN 0376-7388, http://dx.doi.org/10.1016/j.memsci.2014.12.035.

Abstract

In this chapter four grades of PEEK polymer, VESTAKEEP® 2000P and 4000P and VICTREX® 150P and 450P, were tested and it was verified that different grades produced membranes with different performances; the post-phase inversion drying process of membrane fabrication was shown to be crucial in obtaining separation performance in the nanofiltration range. The DS was also important and was controlled to be in the range 3.7 wt. % to 6.7 wt. %. The tightest membrane, produced from VESTAKEEP® 4000P and obtained after drying at 20 °C from water, presented a permeance of 0.22 $L.h^{-1}.m^{-2}.bar^{-1}$ and molecular weight cut-off (MWCO) of 400 $g.mol^{-1}$ in THF, and a permeance of 0.07 $L.h^{-1}.m^{-2}.bar^{-1}$ and a MWCO of around 470 $g.mol^{-1}$ in DMF. These are the first reported non-sulphonated and non-modified PEEK membranes capable of separations in the nanofiltration range and resistant to DMF and THF and to basic and acidic aqueous solutions.

4.1 Introduction

Despite the fact that first research publications on organic solvent nanofiltration membranes can be dated back to the 80s, there is still a limited number of commercial membranes available on the market and most of them are based on polyimide (PI) or polyacrylonitrile (PAN) polymers. However, polyimides are unstable in some amines and have generally poor stability and performance in polar aprotic solvents (tetrahydrofuran (THF), dimethyl formamide (DMF) and n-methyl pyrrolidone (NMP)) and chlorinated solvents such as methylene chloride (DCM), in which most polyimides are soluble. Crosslinking of PI OSN membranes increases their solvent resistance and the DuraMem® (crosslinked PI, Evonik MET, UK) series offer long term stability in most polar aprotic solvents (acetone, tetrahydrofuran, dimethylformamide), but are still not recommended in the presence of chlorinated solvents, strong amines and strong acids and bases [65].

One approach to making a polymeric membrane more resistant to organic solvents is to crosslink the polymer. This approach has been shown for PI [5] (most commercial OSN membranes) and polybenzimidazole (PBI) [66] (see section 2.4.5). Another approach is to use an intrinsically resistant material such as polyether ether ketone (PEEK) or poly(ether ketone) (PEK). PEEK membranes have been reported in literature for different applications such as continuous catalysis, gas separation, fuel cells, MF, UF, NF and RO [51]. Most PEEK membranes presented in the literature are modified. Modifying PEEK is a common technique to solubilise it in order to prepare membranes via the phase inversion technique. However, by modifying the polymer (or the membrane) the inherent chemical resistance can be lost. For a more detailed description of PEEK modifications please see section 2.5.

This chapter makes a detailed investigation into the production of non-sulphonated PEEK nanofiltration (MWCO around 350 – 500 $g.mol^{-1}$) membrane resistant to polar aprotic solvents (such as DMF) and acids and bases. Different factors affecting membrane separation performance are studied including degree of suphonation and membrane post-treatment procedures. It is shown that the post-manufacturing membrane drying step is of vital importance for the nanofiltration performance.

4.2 Experimental design

The methodology used in this study was based on the comparison of PEEK membranes produced from four different polymer grades (coded PM-A, PM-B, PM-C and PM-D) in terms of performance (permeance and rejection). For each of the different membranes (PM-A to PM-D) four replications were performed in order to have a statistically robust sample. All the results were analysed using F-tests. For the permeance data the F-test was used for permeance values obtained after 24 hours. For rejection data the F-test was applied to each individual polystyrene (PS), i.e. for each solute size (different MW) the four different membranes were compared with each other. Statistical significance was considered at $p<0.05$. Data are presented as means ± standard deviation of the mean (SDM).

4.3 Methods

4.3.1 Materials

2,4-Diphenyl-4-methyl-1-pentene (α-methylstyrene dimer), methanesulphonic acid (MSA), sulphuric acid (SA) 95 vol.%, sodium hydroxide (NaOH), potassium hydroxide (KOH) and monoethanolamine (MEA) were obtained from Sigma-Aldrich. N,N-Dimethylformamide (DMF), tetrahydrofuran (THF) and hydrochloric acid (HCl) 37 vol. % were obtained from VWR UK. VESTAKEEP® 2000P and 4000P were kindly donated by Evonik Industries;

VICTREX® 150P and 450P were obtained from VICTREX®. Styrene oligomer standards with a molecular weight distribution of 580 (PS580) and 1300 (PS1300) were obtained from Agilent Technologies Deutschland GmbH, Germany. All reagents were used as received without any further purification.

4.3.2 Membrane preparation

PEEK powder from two commercial brands was selected: VESTAKEEP® and VICTREX®. Two grades from VESTAKEEP®, 2000P and 4000P, and two grades from VICTREX®, 150P and 450P were used. Polymer powder was dissolved at a concentration of 12 wt. % in a mixture of 3:1 wt. % methanesulfonic acid (MSA) and sulphuric acid (SA) by mechanical stirring (IKA RW 20 digital) at 20 °C, until complete homogenisation of the polymer solution. For each of the polymer grades two polymer dope solutions were prepared. Prior to casting the polymer solution was left 72-96 hours at 20 °C until complete removal of air bubbles. The membranes were cast using a bench top laboratory casting machine (Elcometer 4340 Automatic Film Applicator) with a blade film applicator (Elcometer 3700) set at 250 µm thickness. The polymer dope solution obtained was poured into the blade and cast on a polypropylene support (Novatex 2471, Freudenberg Filtration Technologies Germany) with a transverse speed of 0.5 $cm.s^{-1}$. Following this, the membranes were immersed in deionised (DI) water in a precipitation bath at 20 °C; the water bath was changed several times until pH 6-7. Finally, the membranes were left to dry at 20 °C in the open laboratory except when specified otherwise.

The viscosity of the dope solution was measured immediately after casting using a rotary viscometer (LV-2020 Rotary Viscometer Cannon instruments, S16 spindle) and all values were recorded at 1 rpm spindle speed and 20 °C.

All the membrane formation steps were performed in an air conditioned room with temperature set at 20 °C and with a relative humidity (RH) in the range of 30-40%.

4.3.3 Membrane characterisation

4.3.3.1 Solubility test

4.3.3.1.1 Solubility in pure solvents

In order to test the solubility of PEEK membranes in different solvents, two pieces of membranes from two batches with the same composition were immersed in DMF, THF, EtOH, acetone, DCM and n-hexane. The membranes were left immersed in the solvents for 168 h (7 days) and their solubility was checked visually (no weight loss measurement was performed).

4.3.3.1.2 Solubility in acidic and basic solutions

PEEK membranes were immersed in the following aqueous (DI water) solutions: 2 M H_2SO_4, 2 M HCl, 2 M KOH, 25 M NaOH and 16.4 M monoethanolamine (MEA). The membranes were left immersed in the solutions for 2880 h (4 months) and their solubility was checked by performing a weight loss measurement.

4.3.3.2 Molecular weight determination

The M_W of the four PEEK polymer grades was estimated from viscosity measurements with an Ubbelohde viscometer following the same procedure as Devaux et al. [49]. The concentrations of the solutions (PEEK in sulphuric acid 95 v/v %) were 5 $g.L^{-1}$, 2.5 $g.L^{-1}$ and 1.0 $g.L^{-1}$.

4.3.3.3 Elemental microanalysis

PEEK powder and PEEK membranes without the polypropylene support were sent to elemental microanalysis in order to determine the content of C, H, N and S. For C, H, N analysis a CE440 analyser (Exeter Analytical) was used whereas a titration using barium perchlorate was used for determination of S content.

From the sulphur content, the degree of sulphonation (DS) was calculated according to the following equation,

$$DS\ (\%) = \frac{S_E\ (wt\%)}{S_T\ (wt\ \%)} \times 100 \qquad \text{Equation 4.1}$$

where, S_E represents experimental ratio of sulphur to carbon and S_T represents theoretical ratio of sulphur to carbon in SPEEK (wt %) for 100 % sulphonation. According to [67], sulphonation occurs only on a phenyl ring flanked by two ether groups (A-ring) of the PEEK repeat unit, as shown in Figure 2.4. Further sulphonation (more than one) on the A-ring does not occur under this condition because the acid group exerts an electron-withdrawing effect [67].

4.3.3.4 Attenuated total reflectance Fourier Transform Infrared Spectroscopy (ATR-FT-IR)

ATR-FT-IR spectra were recorded on a Perkin-Elmer Spectrum 100 spectrometer equipped with a Universal ATR sampling accessory (diamond crystal), a red laser excitation source (633 nm), and middle infrared (MIR) triglycine sulfate (TGS) detector operating at room temperature. The scans were collected for each sample in the spectral range of 4000-600 cm^{-1}. To improve the signal-to-noise ratios, spectra were recorded with an incident laser power of 1 mW and a resolution of 4 cm^{-1}.

4.3.3.5 Contact angle

Contact angle measurements were performed with an EasyDrop Instrument (manufactured by Kruess) at room temperature using the drop method. This method consists of depositing a drop of water on the surface of a piece of membrane using a micropipette. The contact angle was measured automatically by a video camera in the instrument using drop shape analysis software. At least five independent measurements on different membrane pieces were performed.

4.3.3.6 Differential scanning calorimetry (DSC)

Changes in the degrees of crystallinities of the membranes produced from different grades were observed by differential scanning calorimetry (DSC) (TA INSTRUMENTS Q 2000 DSC). Samples were heated from 20 to 400 °C at a constant ramp rate of 10°C.min^{-1} in DSC aluminium pans (heating cycle 1). After cool down at a rate of 10°C.min^{-1} to 20 °C the samples were heated using the same method as the one used in heating cycle 1 (heating cycle 2). A sharp peak at about 330 – 340 °C is characteristic of PEEK crystal melting. The area under the melting curve was used to calculate the heat required for the melting process. The heat of melting for a 100% crystalline PEEK sample is 130 J.g^{-1} [68]. Thus, the ratio of the two heats of melting was calculated to obtain the degree of crystallinity of the sample.

4.3.3.7 Atomic force microscopy (AFM)

Atomic force microscopy was carried out using Multimode 4 (Bruker, CA, USA) atomic force microscope (AFM) equipped with E – type or J – type piezo scanner. Samples were attached on a microscope glass slide using double sided tape. The images were captured under tapping mode using a silicon probe (PPP - NCH, Nanosensors TM, Switzerland) having nominal tip radius of 7 nm with cantilever resonance frequency range of 204 – 497 kHz and spring constant of 42 N.m^{-1}. Scan size of 5 µm for standard images (analysis of roughness) was captured. A sampling resolution of 512 points per line and a speed of 1 Hz were used. Surface roughness is presented as average roughness (R_a), root-mean-square roughness (R_{rms}), and kurtosis.

4.3.3.8 Scanning Electron Microscopy (SEM)

For cross-section imaging a membrane sample was broken in liquid nitrogen and pasted vertically onto SEM stubs covered with carbon tape. For surface imaging a membrane sample was cut and pasted horizontally onto SEM stubs covered with carbon tape. The samples were then coated with a chromium-layer in an Emitech K575X peltier under an argon atmosphere to reduce sample charging under the electron beam. SEM pictures of the surface and cross section of membrane samples were recorded using a Scanning Electron

Microscope of low resolution (JEOL 6400) at 20KV and under dry conditions at room temperature.

4.3.3.9 Membrane performance and analysis

In order to test the membranes, a rig with 8 membrane cross-flow cells was used (see Figure 4.1). PEEK membranes were initially conditioned by passing pure solvent through at 30 °C and 30 bar (for 1 h). Polystyrene standard solution was then poured into the feed reservoir, and the system was pressurized again up to 30 bar and the temperature set at 30 °C. The polystyrene standard solution was prepared by dissolving 2,4-Diphenyl-4-methyl-1-pentene (dimer, M_W = 236 g.mol^{-1}) and Polystyrene Standards with a M_W ranging from 295 to 1995 g.mol^{-1} (homologous series of styrene oligomers (PS)) in DMF or THF at a concentration of 1 g.L^{-1}. Permeate and retentate samples were collected at different time intervals for rejection determination. Concentrations of PS in permeate and retentate samples were analysed using an Agilent HPLC system with a UV/Vis detector set at a wavelength of 264 nm. Separation was accomplished using an ACE 5-C18-300 column (Advanced Chromatography Technologies, ACT, UK). A mobile phase comprising 35 vol.% analytical grade water and 65 vol.% tetrahydrofuran (THF) both containing 0.1 vol. % trifluoroacetic acid was used [5].

The flux (J) and permeance (B) were determined using Equation 2.1 and Equation 2.2 and the rejection (R_i) of PS was evaluated applying Equation 2.3. The corresponding MWCO curves were obtained from a plot of the rejection of PS versus their molecular weight.

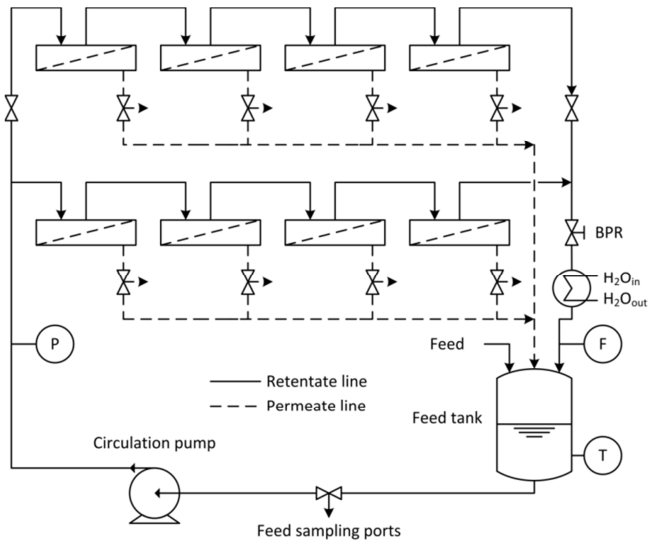

Figure 4.1 – Schematic representation of the 8 cells cross-flow rig used in this study. Legend: P – pressure gauge; T – thermocouple; F – flow meter; BPR – back pressure regulator.

4.4 Results and discussion

4.4.1 Testing different PEEK grades

The viscosity, spindle speed and the M_W of each of the polymer grades are presented in Table 4.1. For both brands the higher grade polymers have higher M_W and result in more viscous dope solutions (Table 4.1). It is expected that grades with higher M_W will form tighter membranes because of the lower mobility in the polymer chains (higher terminal relaxation time) [69].

Table 4.1 – Summary of PEEK membranes prepared from two different polymer brands, VESTAKEEP® and VICTREX®, and different polymer grades, 2000P and 4000P for VESTAKEEP®, and 150P and 450P for VICTREX®. The membranes listed below were prepared with the same dope composition: 12 wt. % PEEK polymer, 66 wt. % MSA and 22 wt. % SA. The M_W (kDa) and the viscosity (Pa.s) of the membrane dope solution as well as the spindle speed (rpm) used are presented in this table. The Mw is estimated from intrinsic viscosity measurements as described in [49].

Membrane code	Polymer brand	Polymer grade	Estimated M_W (kDa)	Viscosity (Pa.s)	Spindle speed (rpm)
PM-A	VESTAKEEP®	2000P	32.10	35.28	1.5
PM-B	VESTAKEEP®	4000P	39.05	56.60	1.0
PM-C	VICTREX®	150P	38.15	14.19	4.0
PM-D	VICTREX®	450P	53.33	36.88	1.5

4.4.1.1 Performance in THF

The separation performance of the membranes listed in Table 4.1 was tested in THF with PS, before and after drying at 20 °C, in order to determine the permeance and the MWCO. The results showed that PEEK membranes with nanofiltration properties can only be obtained after drying the wet membranes. This phenomenon can be attributed to a secondary reorganisation of the polymeric chains and collapse of the porous structure [37, 39, 70, 71]. On the negative side the drying process almost without exception induces irreversible loss of solvent permeance. It can be seen from Figure 4.2 that the permeance values for membranes PM-A, PM-B, PM-C and PM-D were much higher before drying. On average a decrease of permeance around 36 times was observed for membranes PM-A and PM-C whereas for membranes PM-B and PM-D there was a decrease of permeance of 121 and 82 times respectively. All wet membranes showed low rejection of the PS markers (Figure 4.2 A2) and apparently have separation performance within the ultrafiltration range. Upon drying (Figure 4.2 B2) the same membranes retain much smaller molecules and exhibit nanofiltration performance. These results show how important the drying process is in formation of a nanofiltration membrane.

PM-C, the lowest grade of VICTREX®, presented the highest permeance with a value around 0.7 $L.h^{-1}.m^{-2}.bar^{-1}$ but had a MWCO around 600 $g.mol^{-1}$. PM-B, the membrane with the lowest permeance, 0.22 $L.h^{-1}.m^{-2}.bar^{-1}$, had a MWCO of 400 $g.mol^{-1}$. Both PM-A and PM-D had similar permeances, 0.33 $L.h^{-1}.m^{-2}.bar^{-1}$ and 0.38 $L.h^{-1}.m^{-2}.bar^{-1}$ respectively but

slightly different MWCOs of around 420 g.mol^{-1} and 460 g.mol^{-1}. To evaluate how significant these differences were, an F-test test of the results was performed which suggested that the membranes produced from different grades were in fact different from each other. Applying an F-Test (degree of freedom (DF) = 3) to the permeance data at 24 hours an F value of ~ 16.6 was obtained which is higher than the critical F (rejection region), 3.5. As a result the membrane permeances were in fact different for each type of membrane. For the rejection data an F-test was also used (DF = 3) and data for F-values is shown in Table 4.2. The F-test clearly shows that membranes are statistically different for the range of MW from 295 g.mol^{-1} to 995 g.mol^{-1} thus proving that the differences in MWCO obtained for each membrane were in fact statistically significant.

Table 4.2 – F-values obtained from the comparison of the four types of membrane for each PS ranging from 236 g.mol^{-1} to 1095 g.mol^{-1}. The F-critical is equal to 3.49 given the fact that the sampling has the same size for all PS considered (N=4).

MW (g.mol^{-1})	236	295	395	495	595	695	795	895	995	1095
F-value	0.80	4.36	8.38	8.08	7.70	5.07	5.34	3.95	3.50	2.91

As mentioned above it was expected that the higher the polymer M_W, the tighter the membrane formed. VICTREX® 450P was the grade with higher M_W, 53.33 kDa, but the membrane produced from it (PM-D) was not the tightest; and the membrane produced from VICTREX® 150P, PM-C, was the loosest membrane but the M_W, 38.15 kDa, was not the lowest. The M_W values obtained for the VICTREX® grades were higher than the expected because Shibuya and Porter [67] reported a M_W for an ICI (now VICTREX®) PEEK grade 380P of 38.6 kDa (apparently provided by the supplier). The accuracy of this type of measurement is arguable because the viscosity measurements were performed by dissolving the polymer powder in H_2SO_4 95 % v/v, which is very hygroscopic and any water uptake could increase the viscosity of H_2SO_4 resulting in a considerable error for M_W determination. Regardless of this source of variation, the values obtained for the polymer grades were within the range reported in literature [72, 73]. However, when looking at the viscosity of the dope solutions (Table 4.1) one can observe that the performance of the different membranes followed a trend: the higher the viscosity the tighter the membrane. In fact, it was expected that polymers with higher M_W should result in membrane dope solutions with higher viscosity. Nevertheless, it is important to state that the viscosity of the dope was measured at high polymer concentration (12 wt. %), which means that the dilute solution viscosity theory no longer applies, and at different spindle speeds. It was expected that viscosity of the dope solution could explain the results obtained because higher casting solution viscosities slow down non-solvent in-diffusion, resulting in membranes with thicker and denser skin-layers and sublayers with lower porosities. However, the membranes

present macrovoids in the sublayer (porous structure) a phenomenon that is associated mostly with instantaneous precipitation [17]. The acid used as solvent may also induce thermal precipitation in contact with water, which makes understanding the phase inversion even more difficult. It should be also noted that the actual composition of the polymer powder is not known and even small amounts of additives present may alter the solution viscosities.

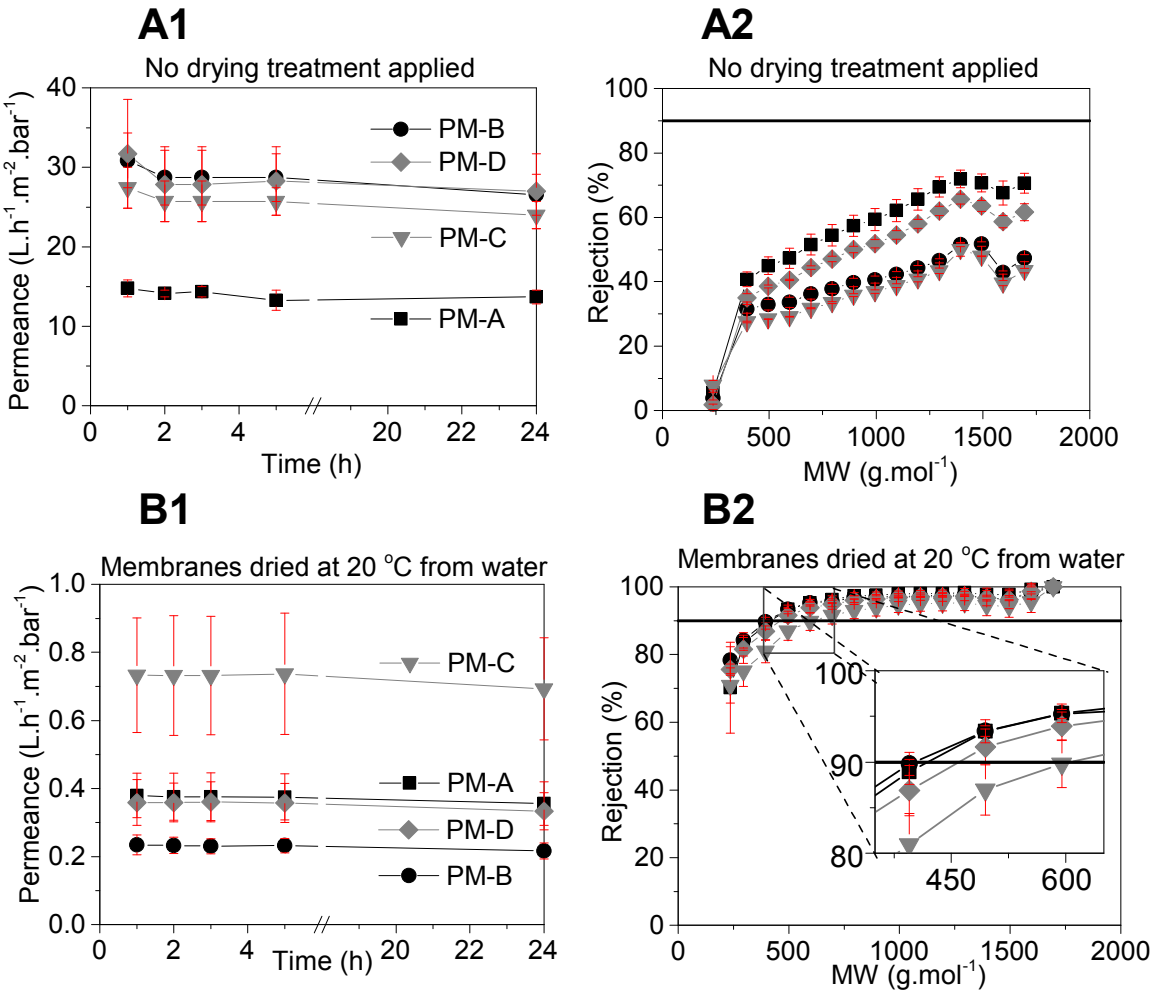

Figure 4.2 – A1 and B1: Permeance values (L.h^{-1}.m^{-2}.bar^{-1}) over a period of 24 h for the different membranes under study using THF as solvent. B1 and B2: Rejection values of the different PEEK membranes under study as a function of the molecular weight (M_W, g.mol^{-1}) of different polystyrenes after 24 hours. Membranes under study: PM-A, PM-B, PM-C and PM-D. All the membranes presented in A1 and A2 were directly removed from the water bath and inserted in the cross-flow cells (no drying treatment was applied). All the membranes presented in B1 and B2 were dried at 20 °C prior to their insertion in the cross-flow cells. The flow-rate, temperature and pressure were set at 100 L.h^{-1}, 30 °C and 30 bar, respectively. The red bars represent the standard deviation of the mean. The membranes from different grades are significantly different ($p \leq 0.05$, F-test).

4.4.1.2 Performance in DMF

After testing the membranes listed in Table 4.1 (dried at 20 °C) in THF, they were also tested in DMF with PS in order to determine the permeance and the MWCO. By testing in a harsh solvent such as DMF the stability of PEEK was demonstrated. The permeance results

can be seen in Figure 4.3. Comparing with the results from THF, the permeance of all studied membranes decreased because of the higher viscosity of DMF, 0.802 mPa.s, when compared with THF, 0.46 mPa.s [74]. The decrease in permeance was on average 2.3, 3.6, 3.3 and 3.7 times for membranes PM-A, PM-B, PM-C and PM-D, respectively. This result is within agreement with the predictions of the pore flow model where the flux should be inversely proportional to the viscosity of the solvent [17]. PM-C, the lowest grade of VICTREX®, presented the highest permeance with a value around 0.21 $L.h^{-1}.m^{-2}.bar^{-1}$ but had a MWCO around 700 $g.mol^{-1}$; PM-A and PM-D had the same MWCO of around 600 $g.mol^{-1}$ but different permeances of 0.15 $L.h^{-1}.m^{-2}.bar^{-1}$ and 0.09 $L.h^{-1}.m^{-2}.bar^{-1}$ respectively. PM-B, the tightest membrane presented a permeance of 0.07 $L.h^{-1}.m^{-2}.bar^{-1}$ and a MWCO of around 470 $g.mol^{-1}$.

Apparently the rejection of PS in DMF is lower than that in THF. It is now interesting to evaluate whether this is again in agreement with the pore flow model. According to the pore flow model [75, 76] the rejection could be described by the following equation:

$$R_i = 1 - \frac{\phi(k_c + Y)}{1 - [1 - \phi(k_c + Y)]e^{-Pe}} \qquad \text{Equation 4.2}$$

Where $K_{i,c}$ is the convective hindrance factor, $\Phi_i$is the partition coefficient and Pe is the Peclet number which is defined as follows:

$$Pe = \frac{\mathrm{K}_{i,c} V \Delta x}{\mathrm{K}_{i,d} D_{i,\infty}} = \frac{\mathrm{K}_{i,c}}{\mathrm{K}_{i,d} D_{i,\infty}} \left(\frac{r_p^2 \Delta P}{8\mu} \right) \qquad \text{Equation 4.3}$$

Where $K_{i,d}$ and $K_{i,c}$ are the diffusion and convective hindrance factors, respectively, V is the solvent flux, $D_{i,\infty}$ is the solute diffusion coefficient and Δx is the membrane thickness. According to this model, the viscosity, μ, is the only solvent parameter affecting permeation. The influence of the membrane is represented by the pore size, r_p.

From the rejection equation (Equation 4.2) the higher the Peclet number the smaller the exponential term and therefore the bigger the denominator is, hence higher rejection. Assuming that there are no significant changes in the membrane pore size and solute diameter associated with different solvents the rejection will be determined by the Peclet number value in a given solvent and more specifically by the solute diffusion coefficient and the solvent viscosity. Thus from the Peclet number ratios for the two solvents one can obtain

$$\frac{Pe_{DMF}}{Pe_{THF}} = \frac{D_{THF,\infty}}{D_{DMF,\infty}} \frac{\mu_{THF}}{\mu_{DMF}} \qquad \text{Equation 4.4}$$

Solvent viscosity in fact contributes twice to the Peclet number, once via the flux equation and again via the diffusion coefficient of the solute. If the diffusion coefficient of the solute is

inversely proportional to the viscosity (e.g. Wilke-Chang correlation) than these effects will cancel each-other and the solute rejection will be independent of the viscosity. But even than if we substitute the diffusion coefficients from the Wilke-Chang correlation [77] in the above equation one could obtain

$$\frac{Pe_{DMF}}{Pe_{THF}} = \left(\frac{M_{THF}}{M_{DMF}}\right)^{1/2} = 0.993 \qquad \text{Equation 4.5}$$

Where, M is the molecular mass of the solvent. The above ratio suggests higher rejection should be expected for equivalent species dissolved in THF than if dissolved in DMF. An extensive empirical study performed by Siddiqi and Lucas [78] has shown that the diffusion coefficient in organic solvents could be described by an empirical correlation where the viscosity is on a power of 0.907. Thus for the Peclet number ratios one can obtain

$$\frac{Pe_{DMF}}{Pe_{THF}} = \left(\frac{v_{THF}}{v_{DMF}}\right)^{0.265}\left(\frac{\mu_{THF}}{\mu_{DMF}}\right)^{0.093} = 0.964 \qquad \text{Equation 4.6}$$

Where, μ and v are the viscosity and molecular volume of the solvent respectively. Again the result suggests that higher rejection in THF should be expected and the effect would be even more pronounced. Of course this simplification does not account for the solute-solvent-membrane interactions that may be far more important in certain cases, but the result is in agreement with the experimental results and is an interesting calculation.

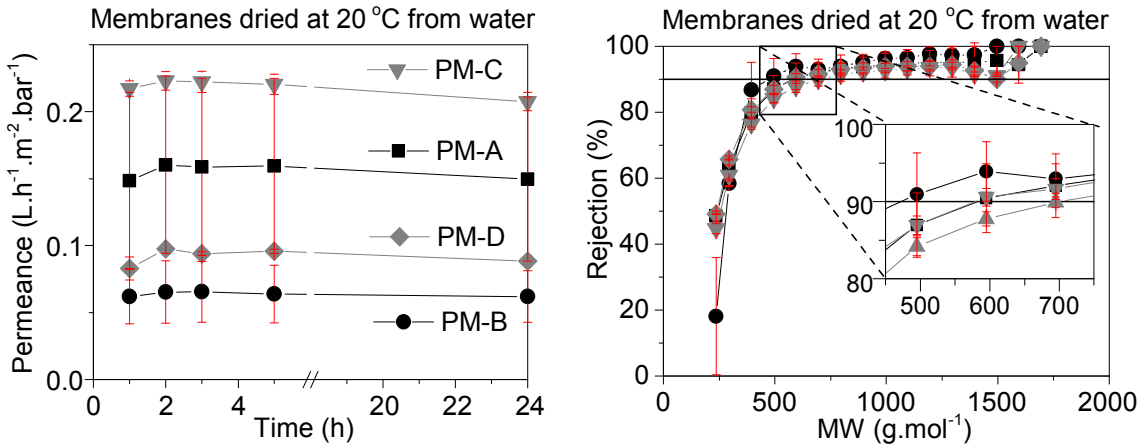

Figure 4.3 – Left: Permeance values (L.h^{-1}.m^{-2}.bar^{-1}) over a period of 24 h for the different membranes under study using DMF as solvent. Right: Rejection values of the different PEEK membranes under study as a function of the molecular weight (M_W, g.mol^{-1}) of different polystyrenes after 24 hours. Membranes under study: PM-A, PM-B, PM-C and PM-D. All the membranes presented were dried at 20 °C prior to their insertion in the cross-flow cells. The flow-rate, temperature and pressure were set at 100 L.h^{-1}, 30 °C and 30 bar, respectively. The red bars represent the standard deviation of the mean.

A summary of the performance (permeance and MWCO) of PEEK membranes PM-A, PM-B, PM-C and PM-D filtered with THF or DMF as solvents and using PS as solutes is presented in Table 4.3.

Although the different membranes under study gave slightly different performances in terms of permeance and MWCO a comparison of the cross-sections did not seem to show any obvious differences (Figure 4.4): the membranes all presented an asymmetric structure with finger-like macrovoids. However, when observed at higher magnification the differences in terms of performance could be related to the top layer (separating layer) differences. Membranes PM-A, PM-C and PM-D presented (on average) a separation layer with a thickness of 1.5 µm, 1.67 µm and 1.82 µm respectively whereas PM-B presented a separation layer (on average) with a thickness of 3.87 µm. This much thicker separation layer could be the reason for PM-B to being the tightest membrane.

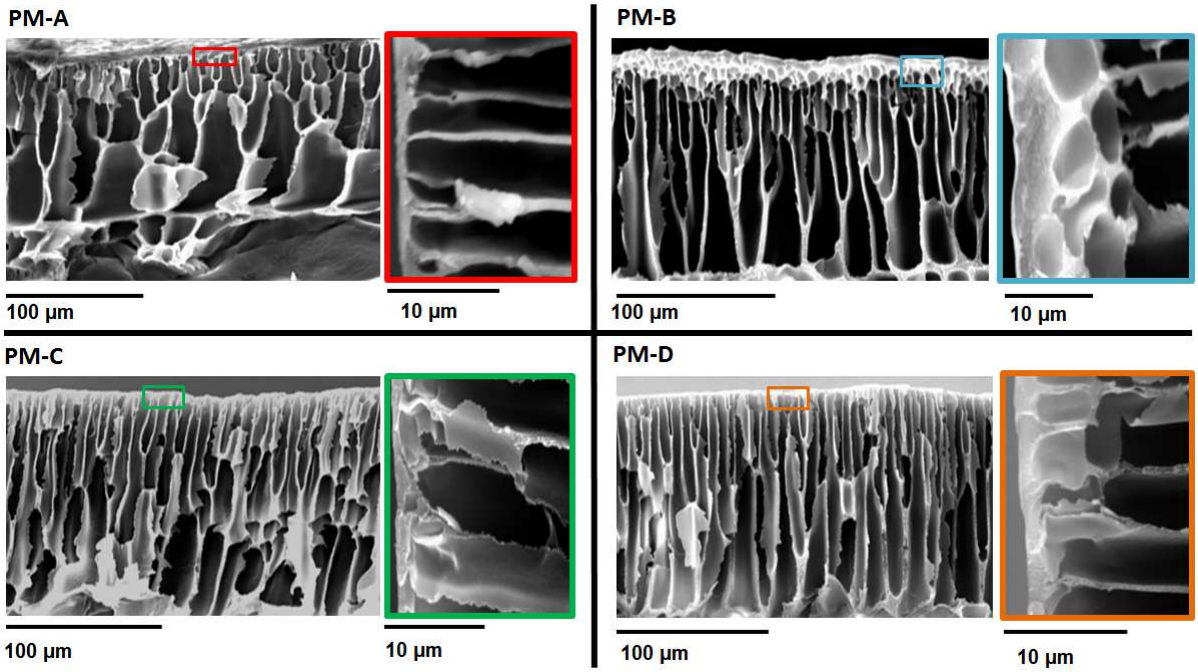

Figure 4.4 – Cross-section SEM images (magnification 300 ×) and a detail of the separating layer (magnification 3,300 ×) of the different membranes under study: PM-A, PM-B, PM-C, PM-D.

Table 4.3 – Permeance ($L.h^{-1}.m^{-2}.bar^{-1}$) and MWCO ($g.mol^{-1}$) of PEEK membranes PM-A, PM-B, PM-C and PM-D filtered with THF or DMF as solvent and using PS as solutes.

Membrane code	Polymer brand	Polymer grade	Permeance in THF/DMF ($L.h^{-1}.m^{-2}.bar^{-1}$)	MWCO in THF/DMF ($g.mol^{-1}$)
PM-A	VESTAKEEP®	2000P	0.33/0.15	420/600
PM-B	VESTAKEEP®	4000P	0.22 /0.07	400/470
PM-C	VICTREX®	150P	0.70/0.21	600/700
PM-D	VICTREX®	450P	0.38/0.09	460/600

4.4.2 The effect of DS on the performance of PEEK membranes

As mentioned in the introduction when using sulphuric acid as a solvent for PEEK it is important that the DS of the polymer is closely monitored. In order to prove the low-sulphonation level of the PEEK membranes developed in this research work, and hence their stability, it was necessary to determine the DS using elemental microanalysis. Initially the use of FTIR was attempted as a simpler and faster method for DS analysis as suggested by Loy and Sinha [79]. These authors [79], used FTIR to establish a correlation between the ratio of 1492 cm^{-1}:1472 cm^{-1} absorption peaks and the DS (%). However, no visible split in the peak around the 1490-1470 cm^{-1} region was observed in the samples making it impossible to use the same correlation (see Figure A1 in the Appendix). In addition, it is also important to mention that the above correlation was obtained for DS in the range of 50 to 80 % (which would narrow its extrapolation for lower or higher DS). As a comparative term the polymeric powder was also analysed in terms of sulphur content in order to verify the extent of sulphonation from the raw powder. The polymer powder for the different grades showed similar DS of around 2.71 % except PEEK VESTAKEEP® 4000P which presented a DS of 0.74 %. This very low DS for the different PEEK polymer grades might be residual sulphur of diphenyl sulphone used as solvent in polymerization [80]. All produced membranes had a DS in the range of 3.7 to 6.7 %, PM-B had the lowest at 3.74 % (Figure 4.5); for membranes PM-A, PM-C and PM-D the DS doubled, whereas for PM-B the increase in the DS was around five times (as compared to the original polymer powder). The low DS for the membranes in the study was in accordance with their stability in THF and DMF.

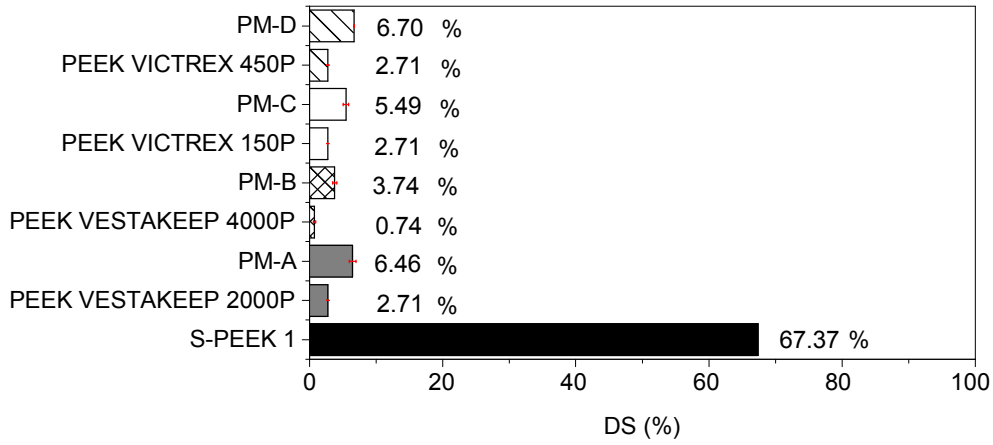

Figure 4.5 – Degree of sulphonation (%) per mass of polymer determined according to the method described in section 4.3.3.2 for the different PEEK polymer grades and for the PEEK nanofiltration membranes under study: PM-A, PM-B, PM-C and PM-D. The red bars represent the standard deviation of the mean (from two independent samples). S-PEEK 1 is a membrane reported in literature [56] for CO_2 separation from gas mixtures containing N_2 or CH_4 and is presented in this figure to emphasise the low DS of the membranes in the current study.

As presented before, the DS for the different membranes under study was very low (between 3-6 %) and it did not affect the membrane stability in DMF and THF. However, it seems to partially change the crystallinity of PEEK as can be seen from the XRD spectra in Figure 4.6. PEEK in its native form is semi-crystalline, with an orthorhombic structure (for the crystal structure) and four main diffraction peaks in the XRD patterns, i.e. (110), (111), (200) and (211) [81, 82]. Comparing the XRD patterns between the PEEK polymer grades and the corresponding membranes, the four distinct peaks present initially in the powder somewhat disappeared in the corresponding membrane. This fact is related to a decrease in crystallinity and means that even though the DS was very low for all membranes a loss of crystallinity was observed due to the polymer processing - solubilisation in a 3:1 wt. % mixture of MSA and SA, casting and drying. Although a change in the degree of crystallinity (DC) was visible from the XRD patterns it was not possible to quantify it. Therefore, DSC was chosen as an alternative technique to determine the DC. In this technique, and as described in 4.3.3.6, the ratio of the two heats of melting (of the sample and of the 100 % crystalline PEEK) was calculated to obtain the DC of the sample (Figure 4.7). From the results obtained one can verify that there is a decrease in the DC from the powder, and the membrane produced from the corresponding powder regardless of the heating cycle. Considering heating cycle 1, VESTAKEEP® 2000P showed the highest DC, 65.63 %, whereas VESTAKEEP® 4000P showed the lowest with a value of 48.11 %. This fact is in agreement with PEEK being a semi-crystalline polymer. Nevertheless, PM-B was the membrane with the highest DC, 44.78%, and therefore the one where the decrease in DC was less pronounced (6.92 % decrease); in contrast, PM-D showed a decrease in the DC of 44.93 %. When looking at heating cycle 2, the DCs obtained are different because the first heating and cooling down of the samples changed its properties, namely its heat of fusion. The DC calculated from heating cycle 2 was only considered to prove the trend in DC.

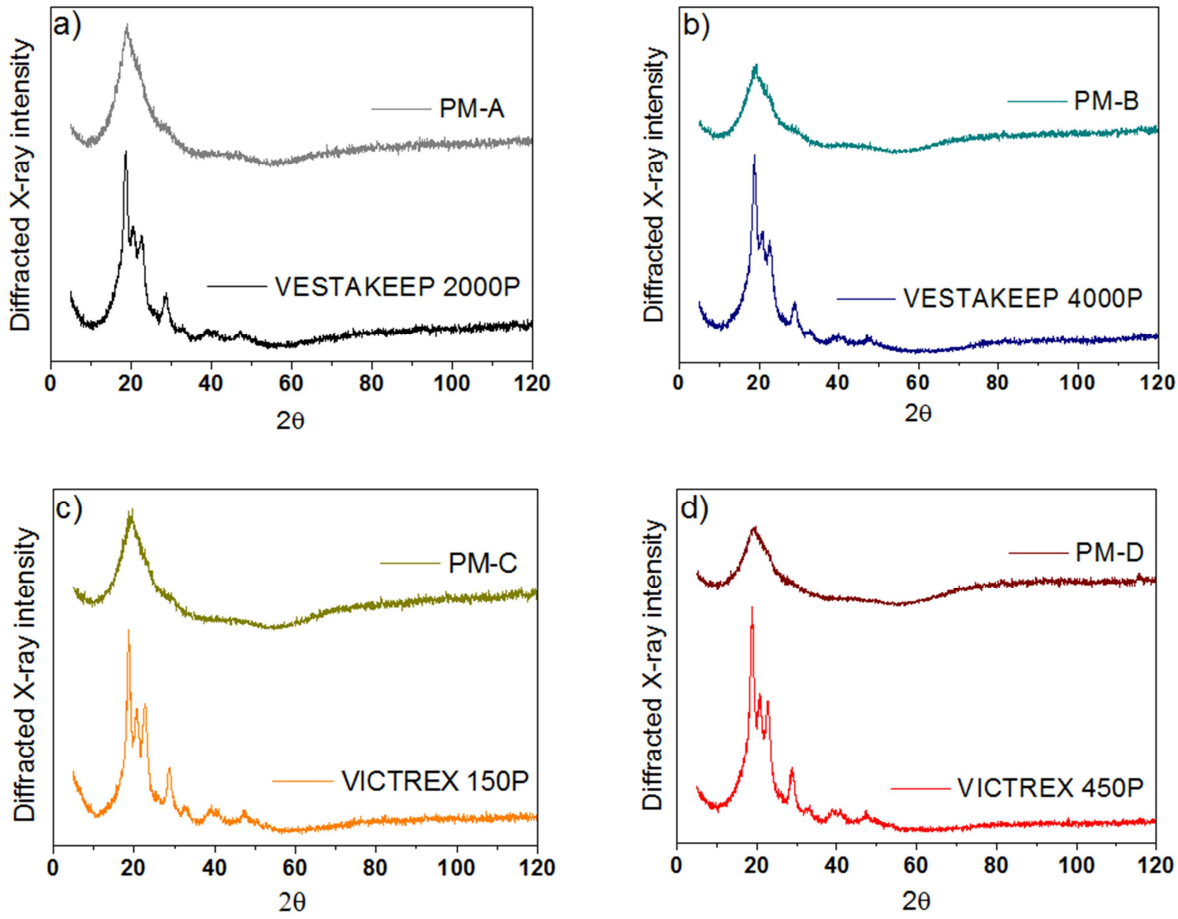

Figure 4.6 – XRD spectra of the different PEEK polymer grades and the corresponding membranes produced from them: a) – VESTAKEEP 2000P and PM-A; b) – VESTAKEEP 4000P and PM-B; c) – VICTREX 150P and PM-C; d) – VICTREX 450P and PM-D.

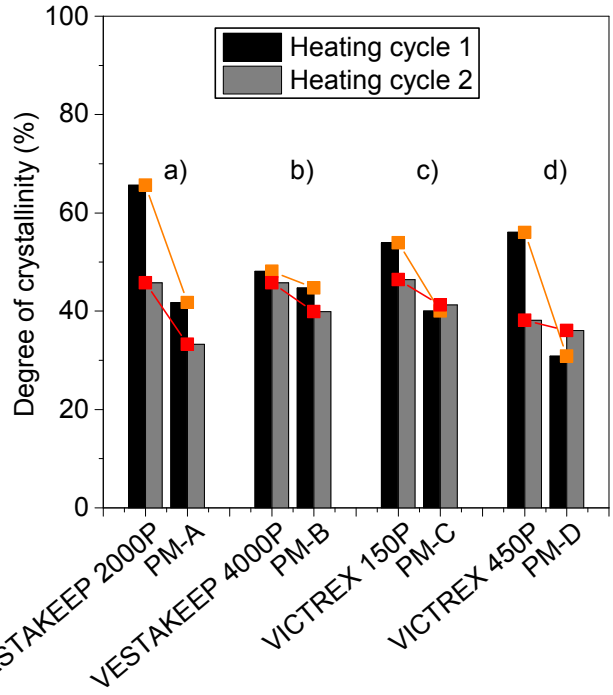

Figure 4.7 – Degree of crystallinity (%) obtained from DSC for the different PEEK polymer grades and the corresponding membranes produced from them: a) – VESTAKEEP 2000P and PM-A; b) – VESTAKEEP 4000P and PM-B; c) – VICTREX 150P and PM-C; d) – VICTREX 450P and PM-D. The degree of crystallinity was calculated for the first heating cycle and for the second heating cycle.

Another change observed was the difference in contact angle when comparing PEEK membranes under study and the original PEEK material. The VICTREX® membranes PM-C and PM-D had higher contact angles, both around 75°, than the VESTAKEEP® membranes, 60° (Figure 4.8). PEEK material in its native form has a contact angle of around 80° [83]. This decrease in the contact angle from the original material to the membrane could be related to the DS which despite being very low could slightly change the membrane contact angle; the higher the DS the more hydrophilic the membrane becomes. However this may not be the only factor affecting contact angle, since PM-A and PM-D have similar DS but different contact angles.

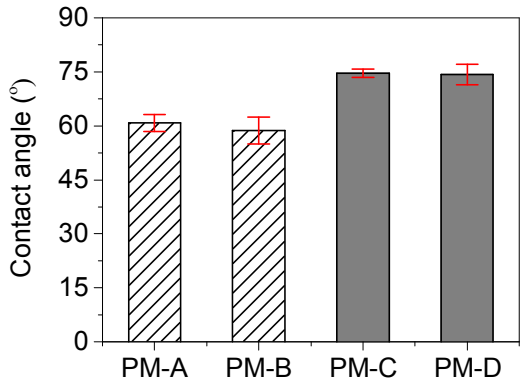

Figure 4.8 – Contact angle (˚) of polymer/water interface obtained for the PEEK nanofiltration membranes under study (PM-A, PM-B, PM-C and PM-D) according to the method described in 4.3.3.5. The red bars represent the standard deviation of the mean (from five independent measurements). All the membranes presented were dried at 20 °C.

The target is to develop PEEK membranes capable of separations in the nanofiltration range. Since PM-B was the tightest membrane produced, further investigations were carried out on this membrane only, in an attempt to optimise its production and manipulate separation performance. Firstly it was decided to start by investigating the effect of MSA and SA on DS of the produced PEEK membranes. PM-B dope solutions were prepared in three different ways: i) using MSA:SA 3:1 (as described before); ii) using methane sulfonic acid (MSA) and dichloromethane (DCM) (to help dissolution of the polymer), designated by PM-B LS (low sulphonation); and iii) using only SA, designated by PM-B HS (high sulphonation) (vide Table 4.4 for detailed concentrations of polymer and solvents). All membranes were cast twice; once from a dope solution kept for 3 days at 20 °C (denoted with index 3) and second time from a dope kept for 30 days at 20 °C (denoted with index 30) in order to test the influence of reaction time on the DS.

It was assumed that the DS should increase from PM-B LS to PM-B HS and that DS of PM-B should be similar to the one of PM-B LS. The results from ATR-FTIR for the prepared membranes are shown in Figure A1Figure A and from the spectra one can see that PM-B and PM-B LS (30) had very similar spectra whereas PM-B HS (30) had a less defined spectrum in the range of 400-1200 cm^{-1}. The results of DS (%) from elemental analysis can be seen in Figure 4.9. PM-B LS (3) (cast after 3 days) and PM-B LS (30) (cast after 30 days), which represent two different pieces of membranes prepared from different dopes, showed DS of 5.76 % and 3.36 %, respectively, which suggests that in the presence of MSA there may be some sulphonation reaction; this result is not in strict accordance with what has been described in literature, as MSA is not considered a sulphonating agent [50]. In addition, it was expected that the DS should be higher for PM-B LS (30) but results presented seem to indicate otherwise. This might be related to the fact that not all MSA was

removed completely from the smallest nodules while washing the membrane with DI water. PM-B (3) and PM-B (30), had a similar DS of 3.74 % and 5.00 %, respectively; this small increase of 1.3 % in the DS is in accordance with previous studies where temperature has far more pronounced effect on the DS when compared with the time of reaction [41]. In addition, the range of DS values for the ratio SA:MSA of 1:3 is in accordance with the values obtained by MacKnight et al. for the same ratio [50]. PM-B HS (3) and PM-B HS (30), which were prepared with sulphuric acid as solvent (vide Table 4.4) had a higher difference in terms of DS, 53.19 % versus 84.06 %. This increase in the DS is related to the reactivity of SA over time with PEEK since SA is considered to be a strong sulphonating agent.

Table 4.4 – Summary of PEEK membranes prepared from three different dopes and with different compositions. These membranes were used for studying the degree of sulphonation.

	Polymer dope composition (wt. %)			
Membrane code	**PEEK**	**MSA**	**SA**	**DCM**
PM-B	12	66	22	0
PM-B LS	12	86	0	2
PM-B HS	12	0	88	0

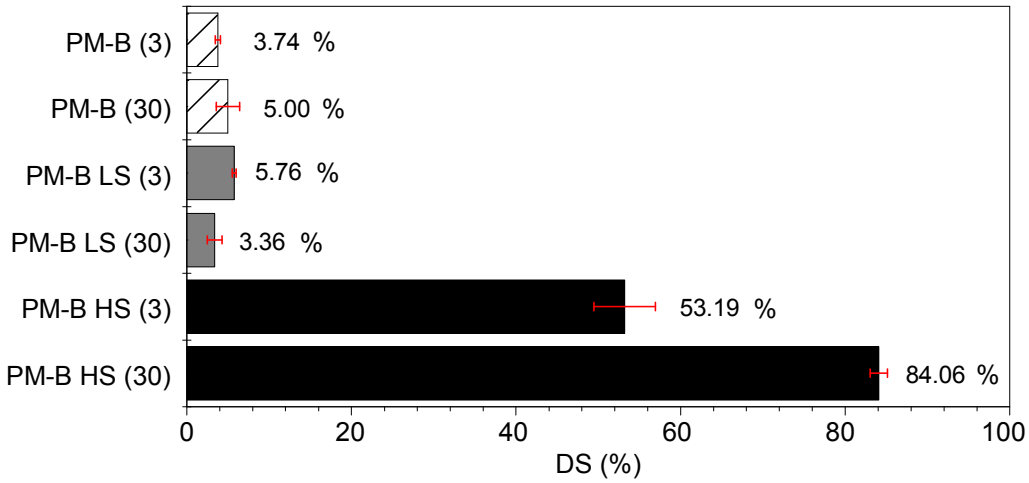

Figure 4.9 - Degree of sulphonation (%) per mass of polymer determined according to the method described in section 4.3.3.2 for the PEEK nanofiltration membranes under study: PM-B, PM-B LS and PM-B HS. The numbers in brackets indicate two different pieces of membranes from different dopes kept at 20 °C that were cast after 3 days (3) and 30 days (30). The red bars represent the standard deviation of the mean (from two independent samples).

As mentioned before, the DS affects the performance of PEEK membranes in terms of solubility characteristics in different solvents. A solubility test was then performed in order to verify the solubility of the three different membranes in six solvents (see Table 4.5). Both PM-B and PM-B LS showed the same behaviour regardless of the time of casting (3 or 30 days) being insoluble in all solvents tested which is expected given the similarity of DS values for both membranes. As for PM-B HS, the high DS greatly affected its stability. For PM-B HS (30) which presented the highest DS, 84.06 %, the membrane was completely degraded in DMF, THF and EtOH. In acetone the membrane showed some swelling before

complete disintegration and in DCM and n-hexane it proved to be stable. As for PM-B HS (3) the membrane was insoluble in all solvents except for DMF where it immediately dissolved.

The membranes PM-B LS and PM-B HS were not tested in terms of performance (permeance and rejection) because PM-B LS (3) and PM-B LS (30) were not a uniform dope solution and consequently a uniform membrane was not produced - DCM is not miscible with water and some irregularities could be observed on the membrane surface - and PM-B HS (3) and PM-B HS (30) after drying became very brittle; in addition, and as mentioned before, they were not resistant in DMF.

PM-B (3) was also tested in terms of solubility in acidic and basic solutions with different concentrations (vide Table 4.6). Over a period of 2880 h (4 months) negligible weight loss (< 1 %) was observed. Even in a 2 M H_2SO_4 (one of the acids used as solvent for dissolving the polymer) the membrane presented great resistance with only a weight loss of 0.65 %.

Consequently, PM-B was the chosen membrane for further performance studies.

Table 4.5 – Solubility of PEEK films (at 20 °C for 168 h) in different solvents

Solvent	PM-B (3) PM-B (30)	PM-B LS (3) PM-B LS (30)	PM-B HS (3)	PM-B HS (30)
DMF	Insoluble	Insoluble	Soluble	Soluble
THF	Insoluble	Insoluble	Insoluble	Soluble
EtOH	Insoluble	Insoluble	Insoluble	Soluble
Acetone	Insoluble	Insoluble	Insoluble	Swollen/Soluble
n-hexane	Insoluble	Insoluble	Insoluble	Insoluble
DCM	Insoluble	Insoluble	Insoluble	Insoluble

Table 4.6 – Weight loss (%) of PM-B (3) for a period of 2880 h (at 20 °C) in different acidic and basic solutions.

Acid/Base	Concentration (M)	Mass loss (%)
H_2SO_4	2	0.65
HCl	2	0.28
KOH	2	0.68
NaOH	25	0.21
MEA	16.4	0.00

4.5 Conclusions

This chapter demonstrated that it is possible to produce nanofiltration membranes from highly resistant native PEEK material. The membranes had a low degree of sulfonation and exhibited excellent resistance toward polar aprotic solvents, acids and bases. Membrane separation performance was tested in THF and DMF. Permeance of THF ranged from 0.2 to 0.8 $L.h^{-1}.m^{-2}.bar^{-1}$ and the MWCO varied from 400 to 600 $g.mol^{-1}$. The permeance of DMF was lower, as expected from the increase in solvent viscosity (DMF is 1.7 times more

viscous than THF), and ranged from 0.07 to 0.21 $L.h^{-1}.m^{-2}.bar^{-1}$, while the MWCO varied from 470 to 700 $g.mol^{-1}$. The post-phase inversion drying process of the membranes was shown to be the reason for change in the separation performance from ultra to nanofiltration range. Some correlation between MW of the PEEK polymer and membrane performance was also established: higher MW PEEK polymer produces tighter membranes with lower permeances.

Chapter 5. Scaling-up of PEEK nanofiltration membranes to spiral-wound membrane modules

The work described in this chapter has been published in the following paper:

João da Silva Burgal, Ludmila Peeva, and Andrew Livingston, Towards improved membrane production: using low-toxicity solvents for the preparation of PEEK nanofiltration membranes. Green Chemistry, 2016.

Abstract

In this chapter, PEEK NF membranes were successfully scaled-up to spiral-wound modules. Two different casting speeds were used for continuous casting of PEEK membranes, 0.01 $m.s^{-1}$ and 0.06 $m.s^{-1}$. The modules produced from each of the continuous sheets presented different permeances but similar rejection profiles. Module 1 (lower casting speed) presented a THF permeance of 0.47 $L.h^{-1}.m^{-2}.bar^{-1}$ and Module 2 (higher casting speed) a permeance of 0.26 $L.h^{-1}.m^{-2}.bar^{-1}$. Module 1 was reused after drying and the permeance decreased only to 0.41 $L.h^{-1}.m^{-2}.bar^{-1}$ showing that no wet storage was required for these modules. A difference in the thickness of the separating layer was also observed under SEM for Modules 1 and 2, 176 nm and 230 nm respectively.

5.1 Introduction

Scaling-up of membranes to membrane modules is important in industrial separation processes because of their high membrane area per volume ratio [84]. In terms of commercial modules there are four major types: plate-and-frame, tubular, hollow fibre and spiral-wound (SW) modules (Figure 5.1). The plate-and-frame modules consist of layering together the membrane, the feed spacers and the product spacers between two end plates. The feed mixture is then permeated through the membrane surface and enters the permeate channel making its way to the permeation collection manifold. Usually used for small scale applications they are used nowadays in electrodialysis and pervaporation systems. Tubular modules consist of a porous paper or fiberglass support with the membrane formed on the inside of the tubes. They are constructed in a way that a large number of tubes are manifolded in series and the permeate is collected from each tube and sent to a permeate collection header. Hollow fibres can have two well-established configurations. The first one is the shell-side feed design where the system is pressurized from the shell side and the permeate passes through the fibre wall exiting through the open fibre ends. The other configuration is the bore-side feed where the fibres are open at both ends, and the feed fluid is circulated through the bore of the fibres. SW modules have a simple design with one

membrane envelope (small laboratory scale) to several membrane envelopes (industrial scale) wound around a perforated central collection tube. Each membrane envelope consists of membrane and permeate and feed spacers and the SW module is placed inside a tubular pressure vessel. SW modules are preferred over hollow fibre modules - that have a higher packing density than the SW modules – due to the trade-off between ease of operation and more control for fouling and permeation rates. SW modules can be used in a wide range of applications from RO to UF such as desalination, water treatment, treatment of industrial waste water and recovery of valuable products in the pharmaceutical industry [85]. In terms of OSN there are some commercially available spiral-wound modules made from polymeric membranes including Koch® membrane series [86], the SolSep membranes [87] and the DuraMem® and PuraMem® membrane series [88, 89]. PEEK membranes possess advantages over other polymeric membranes as stated in the previous chapter and their manufacture is simple in terms of no need of crosslinking and conditioning agent decreasing its environmental burden as will be shown in the next chapter.

In this chapter PEEK membranes are scaled-up to SW modules and cast with two different casting speeds. More optimization studies are required in order to understand in-depth the factors affecting membrane performance in a larger scale.

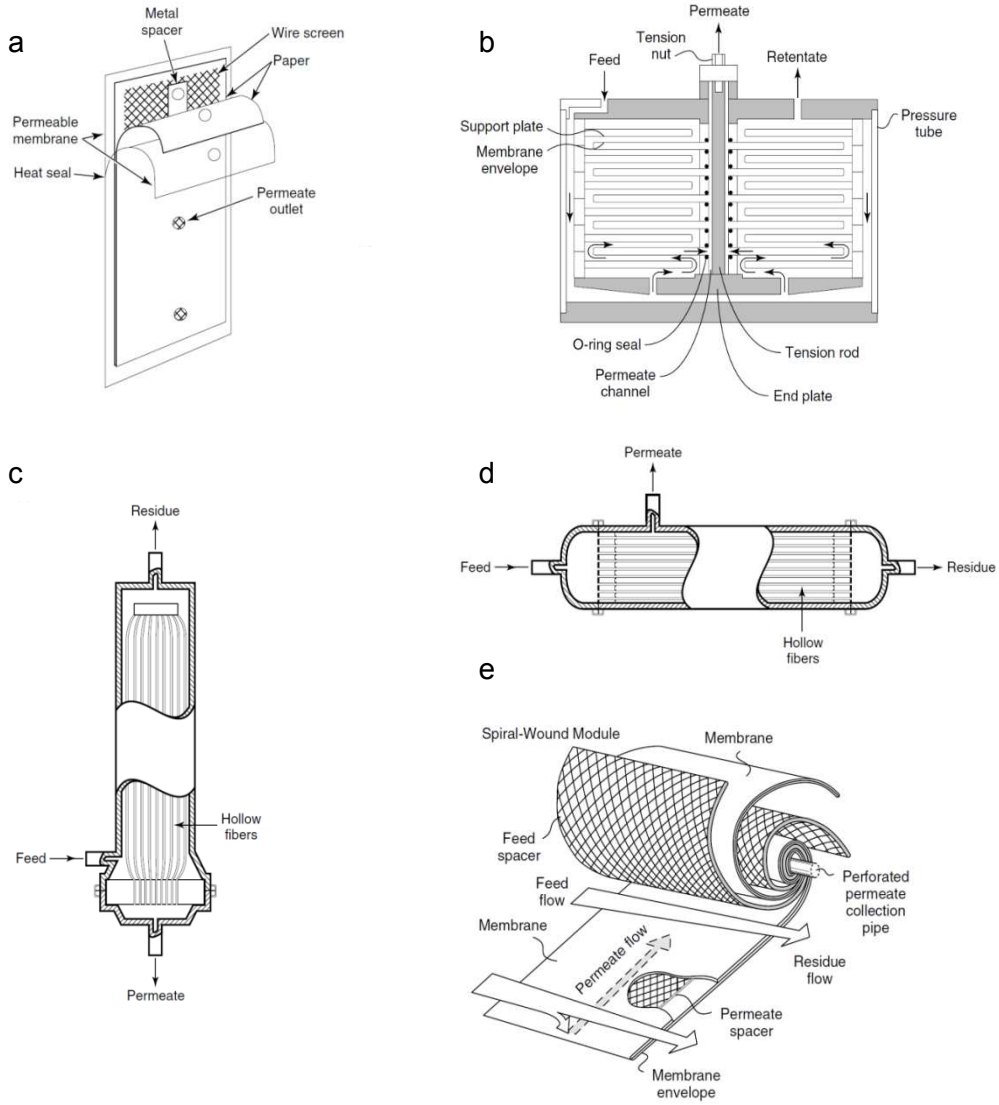

Figure 5.1 – Different types of membrane modules. a) Early plate-and-frame design developed by Stern et al. [90] for the separation of helium from natural gas. b) Schematic of a plate-and-frame module. c) and d) Two types of hollow-fiber modules used for gas separation, reverse osmosis, and ultrafiltration applications. c) Shell-side feed d) Bore-side feed. e) Exploded view of a spiral-wound module with single envelope. Adapted from Baker [85]. Reprinted with permission from John Wiley and Sons: License Number: 3798700810008; date: Jan 30, 2016; publication: Wiley Books; title: Membrane Technology and Applications, 3rd Edition.

5.2 Methods

5.2.1 Materials

2,4-Diphenyl-4-methyl-1-pentene (α-methylstyrene dimer) and methanesulphonic acid (MSA) were obtained from Sigma-Aldrich. Tetrahydrofuran (THF) and sulphuric acid (SA) 95 vol.% was obtained from VWR UK. VESTAKEEP® 4000P was kindly obtained from Evonik Industries. The styrene oligomer standards with a molecular weight distribution of 580

(PS580) and 1300 (PS1300) were obtained from Agilent Technologies Deutschland GmbH, Germany. All reagents were used as received, without any further purification.

5.2.2 Membrane preparation

PEEK powder VESTAKEEP® 4000P was dissolved at a concentration of 12 wt. % using the same procedure described in 4.3.2 (Chapter 4).

5.2.2.1 Bench-scale membranes

At bench scale the membranes were cast using a bench top laboratory casting machine (Elcometer 4340 Automatic Film Applicator) with a blade film applicator (Elcometer 3700) set at 250 µm thickness. The polymer dope solution obtained was poured into the blade and cast on a polypropylene support (Novatex 2430, Freudenberg Filtration Technologies Germany) with a transverse speed of 0.005 $m.s^{-1}$ (lowest controllable speed in the bench casting machine). Immediately after, the membranes were phase inverted by immersion in DI water at 20 °C; the water in the bath was then changed several times until it reached pH 6-7. Finally, the membranes were left to dry at 20 °C or 70 °C (membrane M1). The reason for drying the membranes at 70 °C was because the spiral-wound modules were inserted in the oven to cure the adhesive used for sealing the membranes.

5.2.2.2 Spiral-wound modules

For scaling-up to spiral-wound modules the membranes were cast using a continuous casting machine with a blade film applicator set at 250 µm thickness. The polymer dope solution was poured into the blade and cast on a polypropylene support (Novatex 2430, Freudenberg Filtration Technologies Germany) with transverse speeds of 0.01 $m.s^{-1}$ (lowest controllable speed in the continuous casting machine; membrane M2) and 0.06 $m.s^{-1}$ (membrane M3). The membranes were dried at 20 °C, cut into 1.5 m length sheets, rolled around a perforated central collection tube and sealed at 70 °C with an adhesive (supplied by Evonik Industries). The final rolled modules were approximately 0.0457 m in diameter and 0.3048 m long (1.8”x12”). Each module was made up of one membrane leaf (~0.4 m^2, ~1.5 m x ~0.25 m) resulting in an effective area of ~0.2 m^2. The material for the feed spacer was polypropylene (Naltex N02015_90PP-NAT, Delstar technology Inc) whereas polyester was used for the permeate spacer (T 3410 Ea, Hornwood Inc.). The thickness of the feed spacer was 0.51 mm and 0.28 mm for the permeate spacer. The overall thickness of the membrane was 0.30 mm. The finished spiral wound module was then inserted into a pressure vessel for testing (see Figure 5.2 B). The feed solution passes in the axial direction through the feed channel across the membrane surface. The filtrate is moved along the permeate channel and is collected in a perforated tube in the centre of the module. The degree of sulphonation

(DS) for PEEK NF membranes is comprised between 3.7 and 5 % [10]. A summary of membranes produced can be found in Table 5.1.

Table 5.1 – Summary of membranes produced in bench and continuous scales. Casting speed ($m.s^{-1}$) and total membrane length (m) are presented in this table.

Membrane code	Casting scale	Casting speed ($m.s^{-1}$)	Total length (m)
M1	Bench	0.005	0.3
M2	Continuous	0.01	5
M3	Continuous	0.06	5

5.2.3 Polystyrene markers solution and analysis

The polystyrene standard solution was prepared according to the method described in 4.3.3.9. Concentrations of PS in permeate and retentate samples were analysed using the method described in 4.3.3.9 (Chapter 4) and [6].

5.2.4 Membrane performance

The flux (J) and permeance (L_P) were determined using Equation 2.1 and Equation 2.2 and the rejection (R_i) of PS was evaluated applying Equation 2.3. The corresponding MWCO curves were obtained from a plot of the rejection of PS versus their molecular weight.

In order to test the membranes a rig with 8 cross-flow membrane cells (effective membrane area = 14 cm^2 per cell) was used (see Figure 5.2). A polystyrene standard solution was poured into the feed reservoir and the system was pressurized to 30 bar and the temperature set at 30 °C. In order to test the spiral-wound module the same system was used by simply disconnecting the 8 cross-flow cells from the whole system and connecting the module instead.

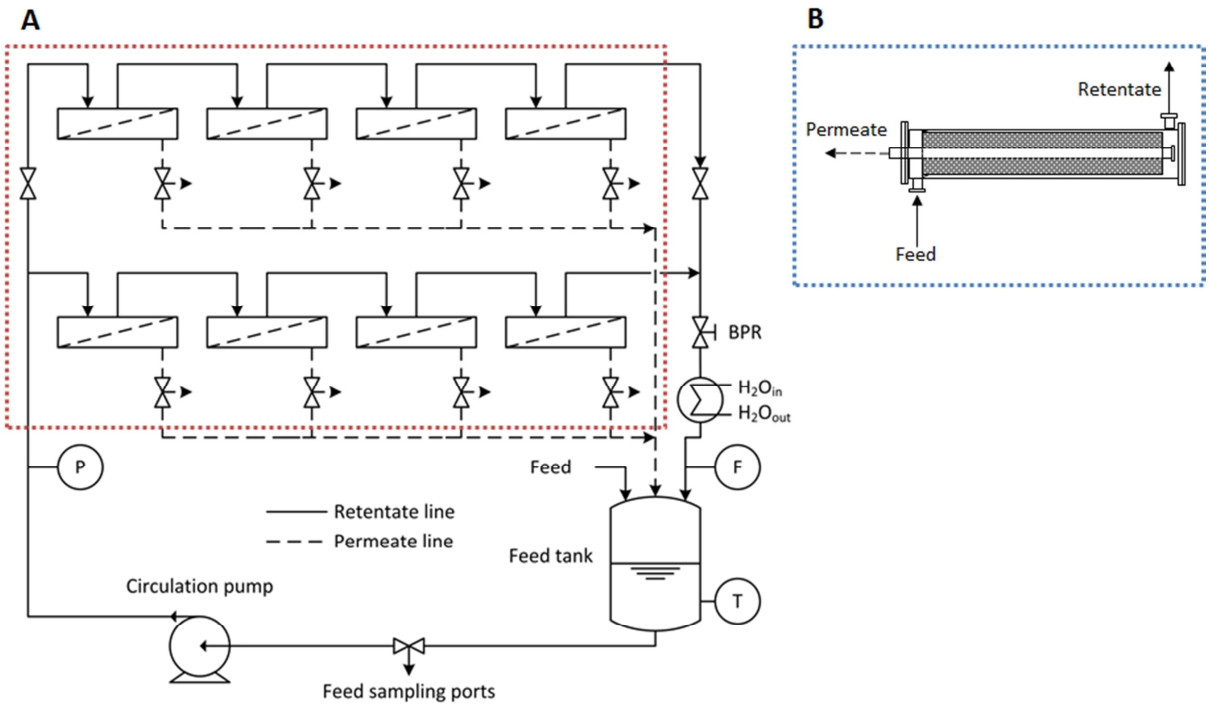

Figure 5.2 – Schematic representation of the two configurations used in this study for testing membrane discs (configuration A) and membrane spiral wound modules (configuration B, flow diagram not depicted but similar to the one in configuration A). Legend: P – pressure gauge; T – thermocouple; F – flow meter; BPR – back pressure regulator.

5.2.5 Membrane characterization

5.2.5.1 Atomic force microscopy (AFM)

Atomic force microscopy was carried out using the method described in 4.3.3.7 (Chapter 4). Surface roughness is presented as average roughness (R_a) and root-mean-square roughness (R_{rms}).

5.2.5.2 Scanning Electron Microscopy (SEM)

For cross-section imaging a membrane sample was broken in liquid nitrogen and pasted vertically onto SEM stubs covered with carbon tape. For surface imaging a membrane sample was cut and pasted horizontally onto SEM stubs covered with carbon tape. The samples were then coated with a chromium-layer in a Q150T turbo - pumped sputter coater (Quorum Technologies Ltd.). SEM pictures of the surface and cross section of membrane samples were recorded using a high resolution SEM, LEO 1525, Karl Zeiss with an accelerating voltage of 5 kV and under dry conditions at room temperature.

5.2.6 Experimental design

Each experiment was repeated in parallel using membrane coupons obtained from different locations on the membrane sheet. For the module data two continuous membrane sheets were produced from two different polymer dopes cast at different speeds (see section 2.2.2). Data are presented as means ± standard deviation of the mean (SDM).

5.3 Results and discussion

A proof of concept for scaling up PEEK membranes to spiral-wound module was performed in this work. The first step was to assess the stability and performance of PEEK membranes produced at bench and continuous scales and then subjected to drying at 20 °C and 70 °C (see Table 5.1 for a summary of membranes prepared). The membranes were tested in the 8-cell rig (membrane discs with an area of 14 cm^2) using THF as solvent and PS as solute markers. The membranes produced at bench scale had similar performances (20 °C drying, M1.1 and 70 °C drying, M1.2): MWCO of ~ 395 $g.mol^{-1}$ and permeance of ~ 0.20 $L.h^{-1}.m^{-2}.bar^{-1}$ (Figure 5 left). This can be explained by their similar average separating layer thickness of ~ 180 nm (see Figure 5.4).

For the membranes produced continuously, M2 and M3, the rejection was similar irrespective of the drying temperature. The permeance difference between M2.1 and M2.2 was + 0.17 $L.h^{-1}.m^{-2}.bar^{-1}$ and the permeance difference between M3.1 and M3.2 was - 0.30 $L.h^{-1}.m^{-2}.bar^{-1}$. Comparing the membranes from different batches but dried at the same temperature also showed a considerable difference (M2.1 vs. M3.1 and M2.2 vs. 3.2). These differences in permeance could be explained by the spatial variation of the membranes and indicates that a better controlled process may be required (Figure 5.4). However, the average permeance of the four samples from continuous manufacture – M2.1, M2.2, M3.1 and M3.2 – is 0.235 $L.h^{-1}.m^{-2}.bar^{-1}$, which is close to the bench scale manufacture. The reason for using two different casting speeds in continuous manufacturing was to avoid the creases obtained in M2 (see Figure 5.5 D) attributed to the lower casting speed used for producing that membrane.

Table 5.2 – Summary of membranes tested in the 8-cell rig. Membrane batch, casting scale and drying temperature (°C) are presented.

Membrane code	Membrane batch	Casting scale	Drying temperature (°C)
M1.1	M1	Bench	20
M1.2	M1	Bench	70
M2.1	M2	Continuous	20
M2.2	M2	Continuous	70
M3.1	M3	Continuous	20
M3.2	M3	Continuous	70

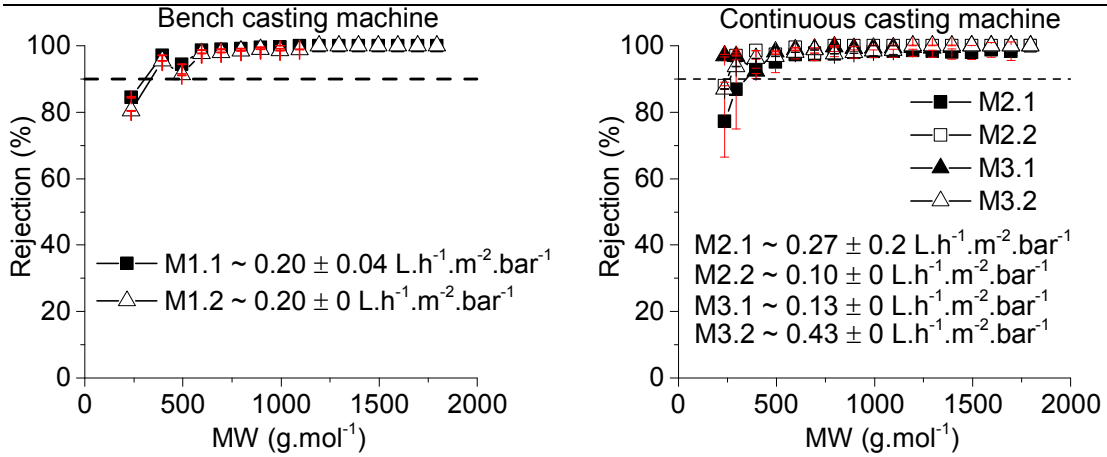

Figure 5.3 – Left: Rejection values and permeance of PEEK membranes cast using bench casting machine and dried at 20 °C (M1.1) and at 70 °C (M1.2) as a function of the molecular weight (MW, g.mol^{-1}) of different polystyrenes over time. Right: Rejection values and permeance of PEEK membranes cast continuous and dried at 20 °C (M2.1 and M3.1) and at 70 °C (M2.2 and M3.2) as a function of the molecular weight (MW, g.mol^{-1}) of different polystyrenes over time. The membranes were tested in the 8 cross-flow cells with a solution of THF and PS (1 g.L^{-1}) for 24 hours.

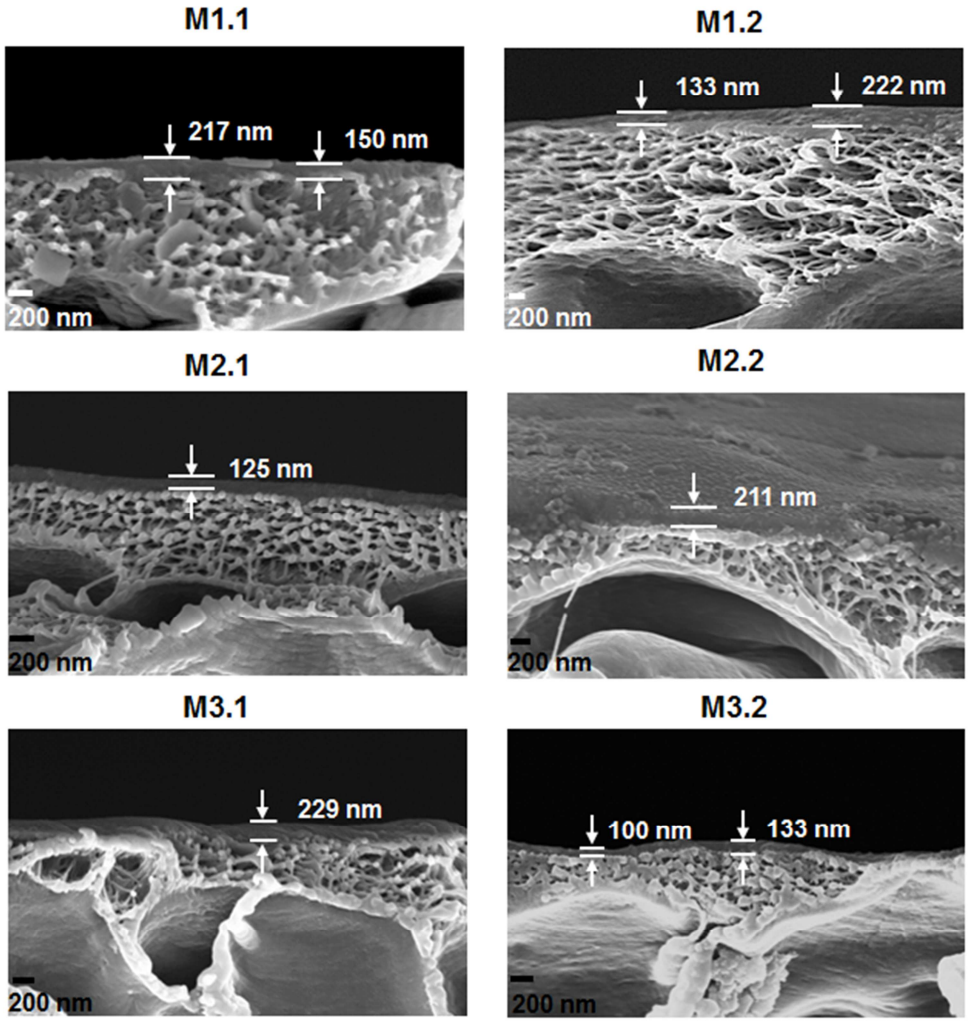

Figure 5.4 – SEM cross-sectional images of membranes M1.1, M1.2, M2.1, M2.2, M3.1 and M3.2.

The modules tested, Modules 1 and 2, presented similar rejection values as the flat sheet membranes which were used to produce them, M2 and M3 respectively. However, the modules had different values of permeance when compared with the flat sheet membranes (Figure 5.5). Module 1 had a permeance of 0.47 $L.h^{-1}.m^{-2}.bar^{-1}$ whereas M2.1 (dried at 20 °C) and M2.2 (dried at 70 °C) had permeances of 0.27 and 0.1 $L.h^{-1}.m^{-2}.bar^{-1}$, respectively. Module 2 presented a permeance of 0.26 $L.h^{-1}.m^{-2}.bar^{-1}$ while M3.1 (dried at 20 °C) and M3.2 (dried at 70 °C) had permeances of 0.13 and 0.43 $L.h^{-1}.m^{-2}.bar^{-1}$, respectively. From the data obtained from the 8-cell rig for membrane discs, a non-uniformity of the separating layer across the 5 m length of the continuous membranes (M2 and M3) was hypothesized. These differences in thickness of the separating layer could explain the discrepancies in permeance. From the SEM images, on an average of 4 samples (separated by 30 cm in longitudinal direction, 3 measurements for each sample separated by 500 nm) thicker separating layers for Module 2 can be seen when compared with Module 1, 230 nm and 176 nm respectively (Figure 5.6 and Table 5.3), thus explaining the higher permeance value for Module 1. In addition, some rather thin areas were observed in the separating layer of Module 1 as opposed to Module 2 where unusually thick areas were present (Figure 5.6). It should be noted that the total area of membrane under test in a module (0.2 m^2) is much higher than a disc (0.0014 m^2), and so the module represents an integrated permeance over a much larger sample. Another hypothesis postulated by Karan et al., 2015 [1] was to check changes in roughness before and after filtration. Using AFM images it was possible to verify an increase in roughness from the flat sheet membranes (before filtration) to the modules (after filtration).

The non-uniformity of the module separating layer suggests that up-scaling of the PEEK membrane is not a straightforward procedure and further research and optimisation is required. Nevertheless, these results successfully proved the scalability of PEEK OSN membranes. In addition the PEEK membrane modules proved to be quite robust. In general to stay reusable, polymeric membrane modules have to be stored in a solvent. However, Module 1 was deliberately left to dry out after the first filtration and then used again (Figure 5.5 B) showing only a slight decrease in permeance, 0.41 $L.h^{-1}.m^{-2}.bar^{-1}$ vs. 0.47 $L.h^{-1}.m^{-2}.bar^{-1}$ (before drying, Figure 5.5 A).

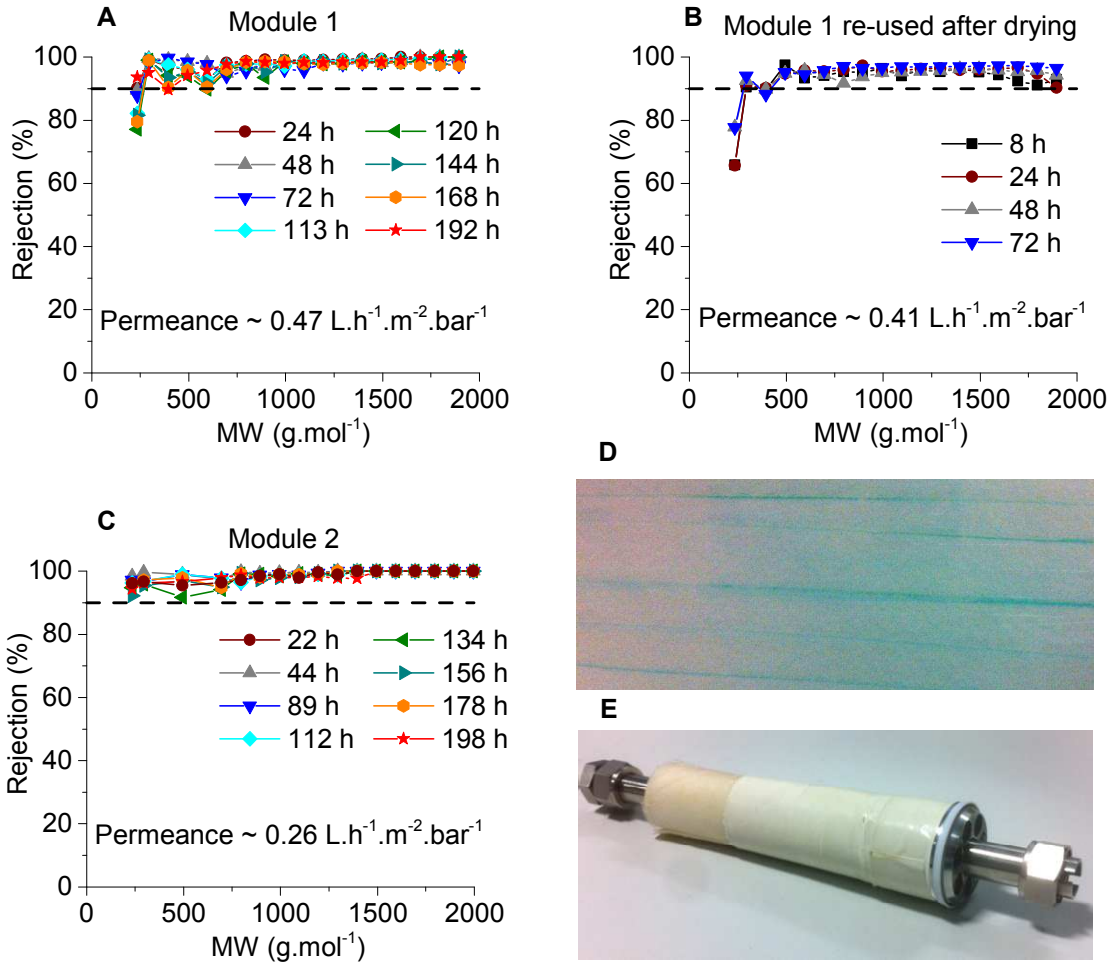

Figure 5.5 – Rejection values and permeance of PEEK spiral wound module as a function of the molecular weight (MW, g.mol^{-1}) of different polystyrenes over time. The membranes were used to filterwith a solution of THF and PS (1 g.L^{-1}). A: Filtration run performed over a period of 192 hours with Module 1 (membrane from M2 batch). B: Filtration run performed over a period of 72 hours re-using Module 1 after drying it from THF. C: Filtration run performed over a period of 198 hours with Module 2 (membrane from M3 batch). D: Membrane surface of membrane from M2 batch depicting creases. E: Module 2.

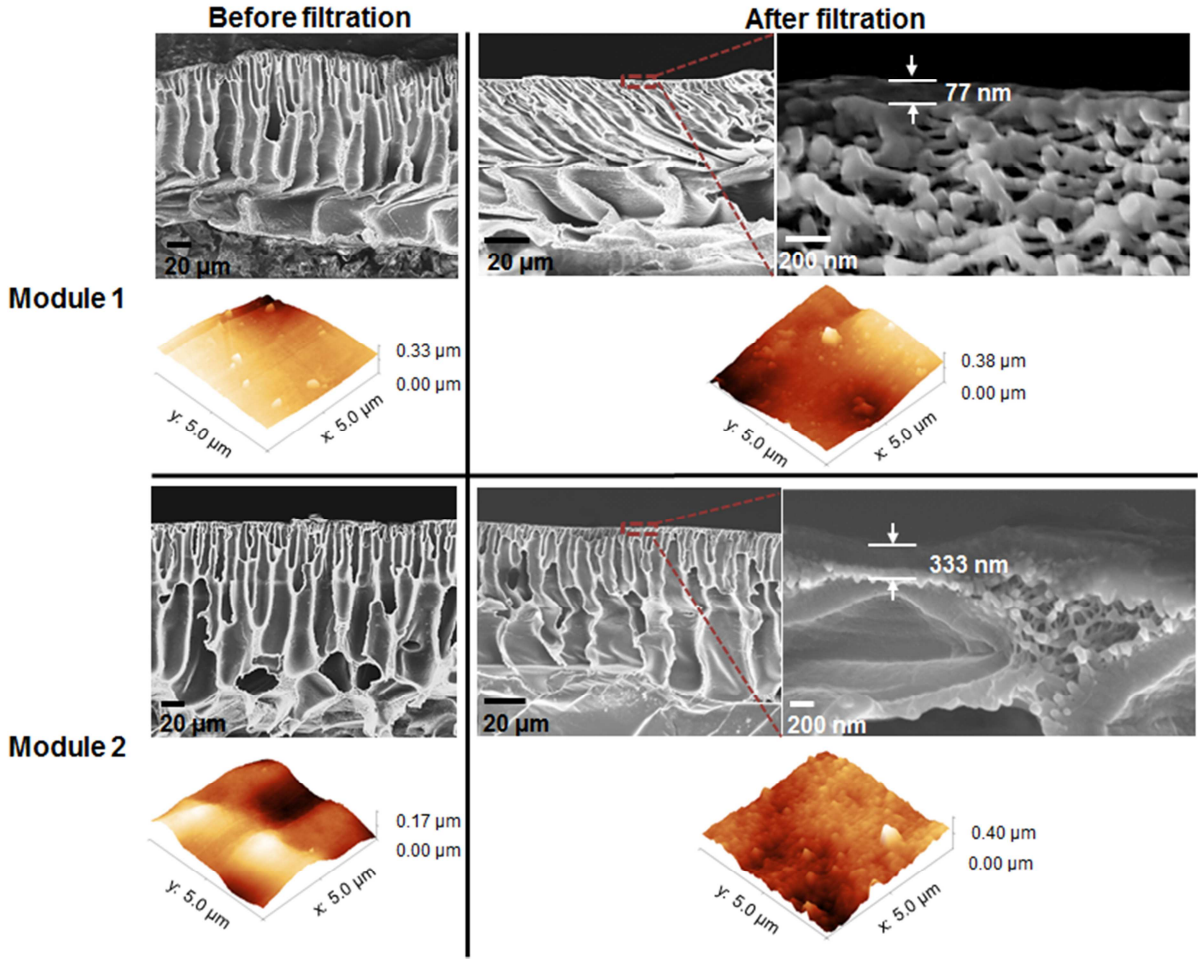

Figure 5.6 – Cross-sectional SEM images and AFM topographical images of membranes M2 (used to produce Module 1) and M3 (used to produce Module 2) before and after module testing revealing changes in overall membrane thickness, surface roughness and different separating layer thicknesses.

Table 5.3 – Quantitative summary of membrane overall thickness, separating layer thickness and surface roughness obtained from AFM topographical images.

Membrane code	Overall thickness (µm)	Separating layer thickness (nm)	Average roughness (R_a) (nm)	Root-mean-square roughness (R_{rms}) (nm)
M2 before filtration	**128 ± 10**	**-**	**40.9**	**54.6**
M2 after filtration	**80 ± 4**	**176 ± 50**	**47.8**	**63.4**
M3 before filtration	**150 ± 24**	**-**	**30.1**	**37.3**
M3 after filtration	**80 ± 5**	**230 ± 68**	**44.1**	**54.8**

5.4 Conclusions

Scaling up of the PEEK membrane to spiral-wound modules was successfully completed and data for performance of two modules is presented. Module 1 showed permeance of 0.47 $L.h^{-1}.m^{-2}.bar^{-1}$ and Module 2 permeance of 0.26 $L.h^{-1}.m^{-2}.bar^{-1}$ but the rejection was similar for both modules, with MWCO of ~ 300 $g.mol^{-1}$. These differences in permeance were attributed to the different thicknesses of the separating layer and surface area originating from the different casting speeds used for casting membranes for Module 1 and Module 2, 0.01 $m.s^{-1}$ and 0.06 $m.s^{-1}$ respectively. Module 1 showed an average thickness of the separating layer of 176 nm and Module 2 an average thickness of 230 nm. Module 1 was reused after drying and presented a similar rejection profile but slightly lower permeance, 0.41 $L.h^{-1}.m^{-2}.bar^{-1}$. This result showed that PEEK modules did not need to be stored in a wet state in order to retain their performance properties.

Chapter 6. Assessment of environmental burden of PEEK nanofiltration membranes

The work described in this chapter has been published in the following paper:

João da Silva Burgal, Ludmila Peeva, and Andrew Livingston, Towards improved membrane production: using low-toxicity solvents for the preparation of PEEK nanofiltration membranes. Green Chemistry, 2016.

Abstract

In this chapter it is shown that PEEK membranes are “green” from the production point of view when compared with commercial polyimide (PI) based OSN membranes. Green metrics (E-factor and solvent intensity) and waste cost were used in order to assess the environmental burden of PEEK membranes: the solvent intensity of PEEK membranes is 8.3 vs. 35-224 for PI based membranes, and the waste cost for PEEK membranes is 46 £.kg^{-1} of polymer vs. 1019 £.kg^{-1} of polymer (bench scale) and 189 £.kg^{-1} of polymer (industrial scale) for PI based membranes. As a final assessment, the solvent intensity and environmental burden associated with permeating a THF flow of 100 L.h^{-1} using PEEK membranes was also assessed. The results showed a waste cost of 1.4 £.m^{-2} of membrane, significantly lower than PI based membranes.

6.1 Introduction

Organic solvents are widely used in industry and pose a problem due to their high volatility, environmental persistence and high toxicity. Furthermore, these solvents will become waste solvent as they cannot be reused in the original process due to residual contaminations and quality and regulatory guidelines [91, 92]. Consequently, the demand for greener chemicals is increasing due to concerns from regulatory bodies when assessing environmental impacts, and to the tightening of discharge regulations [93]. Following the 12 principles of green chemistry [94], membrane science could play an important role in the usage of safer solvents and auxiliaries, and in improving the energy efficiency of industrial processes. This is because membrane processes have low energy consumption, are simple to scale-up, operate and maintain [95-97].

Whilst membranes are green in terms of industrial processes, major environmental impact can be caused by their production and one cannot separate this from the industrial process application. OSN is emerging as a “green” separation technology in various industries, particularly as an alternative for pharmaceutical processes [2]. Various

publications evaluate the greenness of OSN processes, and compare them with conventional separations [95, 97-99]. However, very few publications consider the environmental impact of membrane production itself [96]. Main focus is given to polymeric membranes as ceramic membranes require high temperature and pressures, limiting the improvement of these processes in terms of environmental burden [100]. Nevertheless, in terms of bionanocomposites and/or hybrid materials there seems to be more flexibility to design “greener” routes [101, 102].

Nowadays, most integrally skinned asymmetric (ISA) OSN polymeric membranes are made from polymers such as polyimide (PI), polyacrylonitrile (PAN) and polyibenzimidazole (PBI). All of these polymers need to be dissolved in solvents such as N,N-dimethylformamide (DMF), N,N-dimethylacetamide (DMA), N-methyl-2-pyrrolidone (NMP), and tetrahydrofuran (THF) [4-6, 103]. These solvents are considered harmful (see for e.g. GSK's Solvent Selection Guide for Medicinal Chemistry) and industry has been trying to avoid them in order to implement safer processes [104, 105]. In addition to this, membranes prepared from the above polymers are only resistant in most polar aprotic solvents after chemical crosslinking of the polymer, and the membrane structure is only maintained through the addition of a preserving agent such as PEG or silicone oil. Polyimide (the most commonly used polymer for OSN membranes) is usually crosslinked with difunctional amines that might not react fully (usually they are present in excess), which will further create an environmental burden in terms of waste generation [106, 107]. Some “greener” alternatives for preparing PI OSN membranes have been proposed. For instance, Soroko et al. [108] proposed a method where the original solvents are replaced by DMSO and acetone (which are considered “greener” solvents when compared to DMF and 1,4- dioxane), and the crosslinking step is performed using water as a solvent (instead of IPA). The authors reported that membranes prepared using this method have similar performance in terms of rejection compared to PI OSN membranes prepared from DMF/1,4-dioxane, with the advantage of eliminating toxic organic solvents in the membrane formation step. Another method for PI membrane preparation was proposed by Vanherck et al. [109] and consists of simultaneous phase inversion and coagulation (SIM) of the polymer dope solution. In this method the crosslinker is dissolved in the coagulation bath (a 2 in 1 approach) at lower concentrations, 0.5 % to 5 % (w/v), thus generating less waste. This method was further developed in research work by Hendrix et al. where three different difunctional amines were studied in concentrations ranging from 3 % to 9 % (w/v) [110].

Safer solvents such as methyl and ethyl lactate [111, 112], triethylphosphate (TEP) [113], dimethyl sulfoxide (DMSO) [108], γ-Butyrolactone (γ-BL), and ionic liquids (ILs) have been proposed for replacing the “classic” solvents in the phase inversion technique [93]. For example, Xing et al. [114] presented a method of preparing PBI using the ionic liquid 1-ethyl-

3-methylimidazolium acetate ([EMIM]OAc) as an alternative to DMAc as a solvent. Most of these solvents are used for dissolving polymers that are either not stable in organic solvents (such as cellulose acetate for example) or stable in a limited number of solvents like PBI or PI and require further chemical crosslinking in order to be resistant to harsh solvents (see Figure 6.1).

In this chapter, a comparison between the manufacturing process of OSN PEEK membranes and three ways of manufacturing PI based membranes (one of the widely used OSN ISA membranes on the market) was performed in terms of green metrics. The evaluation is implemented for both lab scale and postulated industrial scale production. In addition, a comparison between PEEK modules and PI modules manufacturing was assessed in terms of environmental burden for permeating 100 $L.h^{-1}$ of THF.

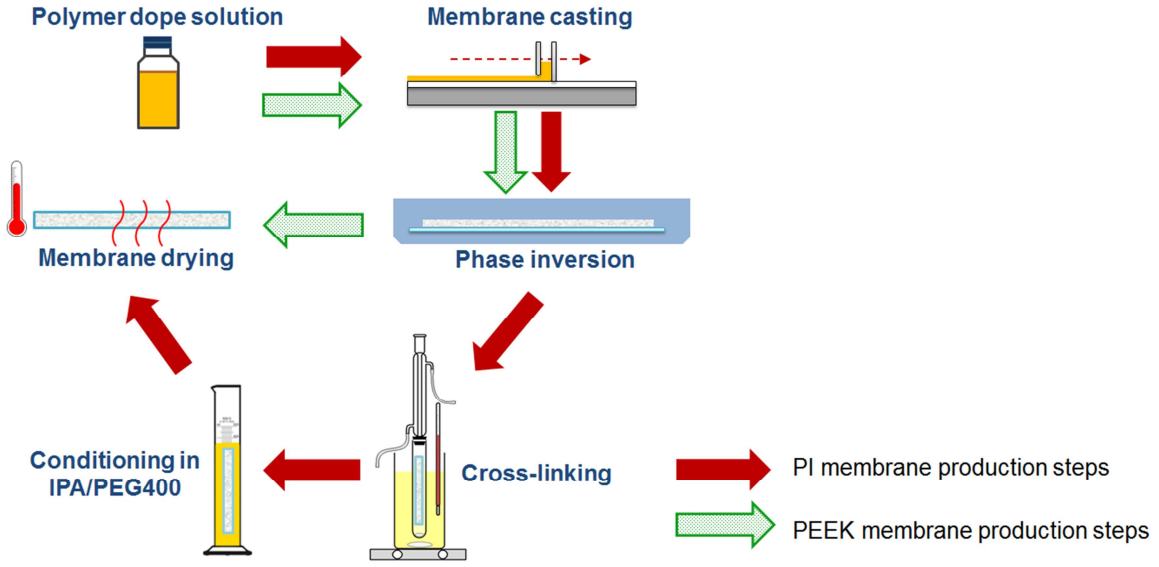

Figure 6.1 – Schematic representation of the steps involved in the PI and PEEK membrane preparation.

6.2 Results and discussion

6.2.1 Evaluating the "greenness" of PEEK membrane production

Green metrics for the production of PEEK membranes were calculated and compared with P84 polyimide (PI) membranes manufactured in three different ways. The first method considers P84 membranes produced by dissolving the polymer in DMF and 1,4 – dioxane, carrying out phase inversion in water and crosslinking with diamine in IPA. This is a well-established procedure widely reported in literature [4, 6]. The other two methods introduce some modifications to the original procedure. The second method is P84 production using DMSO and acetone in place of DMF and 1,4 – dioxane, and was proposed by Soroko et al.

[108]; the third method is P84 production through simultaneous phase inversion and crosslinking (SIM) and was reported by Hendrix et al. [110].

For fairness of comparison the PEEK and P84 PI based membranes presented in this study have similar separation properties, i.e. molecular weight cut-offs (MWCOs) in the range of ~ 300 $g.mol^{-1}$. The experimental procedures for the production of P84 PI membranes and PEEK membranes are summarized in Table 6.1.

Table 6.1 – Comparison of the experimental procedure for producing PEEK, P84 standard method, P84 green method and P84 SIM method. The crosslinking used for the different methods of producing P84 is presented as mass of crosslinker per water bath volume (w/v %).

	PEEK	P84 standard method	P84 green method	P84 SIM method
Polymer (wt. %)	12 %	22 %	22 %	22 %
Solvents (wt. %)	MSA: 66 % SA:12 %	DMF: 58.5 % 1,4 –dioxane: 19.5 %	DMSO: 58.5 % acetone: 19.5 %	NMP: 44 % THF: 29 % IPA: 5 %
Phase inversion in water	Yes	Yes	Yes	Yes
Solvent exchange (e.g.: IPA)	No	Yes	No	No
Crosslinking	No	Yes (0.1 w/v % of water bath)	Yes (0.1 w/v % of water bath)	Yes (3 w/v % of water bath)
Conditioning in PEG/IPA or IPA	No	Yes	Yes	Yes

*Please note that crosslinking in the standard method is performed in IPA (4.8 wt.% crosslinker), the concentration is recalculated for the water bath to simplify the comparison with the other methods.

A comparison between bench and industrial scales was also performed for each of the membranes studied. For a bench scale membrane, usually 30 g of dope solution are cast onto a non-woven backing and immersed in a 20 L water bath (10 L of water for PEEK membranes). The membranes are then washed with 1.5 L water and subsequently P84 membranes are washed with IPA. For industrial scale the following assumption was made: 83.3 kg of polymer dope solution is cast on a non-woven backing material and immersed in a 10 m^3 water bath (7 m^3 of water for PEEK membranes). The membranes are then rinsed for 3 h in 0.5 m^3 of water and P84 membranes are later washed with IPA. For P84 membranes there is also the chemical crosslinking step which generates liquid waste. Usually a 40 wt. % excess of diamine (e.g. 1,6-hexamethylenediamine, HDA) is dissolved in a solvent (0.8 kg HDA. kg^{-1} of dope and 7 kg of crosslinking medium per 1 kg of dope). The density for PEEK and P84 membrane films is 212 $kg.m^{-3}$ and 464 $kg.m^{-3}$ respectively and the thickness of the membrane films is 140 µm (values obtained experimentally). In this study, and for reasons of simplicity, it was considered that the solvents, crosslinking reagent, IPA and PEG were

disposed with the water bath (see Figure 6.2). All solvents and reagents except acetone and IPA have high boiling points and cannot easily be removed from water by evaporation. In addition to this, the levels of organic solvents present in waste water are high (see Figure 6.3 C) and they need to be further treated in order to reduce toxicity levels. Note that DMSO and acetone are less toxic when compared with DMF and 1,4 – dioxane, but they still need to be removed from the waste water before disposal in order to comply with environmental regulations. The price for disposing liquid waste is assumed to be £7.50 per 25 L of chlorinated or non-chlorinated solvent [96]. Although PEEK does not generate organic solvent waste it does generate an acidic (pH < 1) waste water rich in sulphates and sulphites that has to be neutralized with a solution of NaOH (price 12.12 £. kg^{-1}, VWR). In this study the amount of NaOH (solution of 0.5 M) necessary to fully neutralize the H^+ ions present in the waste water was taken into account for calculating the waste cost; this acid-base reaction leads to the formation of sodium sulphate and sodium sulphite in solution.

It is important to point out that solvent waste is a complex subject and should be incorporated when designing an environmentally friendly process [115]. For example, Amelio et al. [92] compared incineration of waste solvents with distillation using Eco-indicator 99, UBP-97, global warming potential, cumulative energy demand and CO_2-balance. These metrics can be used when performing a lifecycle assessment (from the polymer production to the membrane process) to which is not the aim of this chapter. In this study, the Green metrics used, E-factor and Solvent Intensity, are presented below (Equation 6.1 and Equation 6.2). These metrics were chosen to be comparable with previously reported results [96].

$$E-factor = \frac{mass\ of\ waste\ produced\ (kg)(including\ water)}{mass\ of\ product\ (kg)} \qquad \text{Equation 6.1}$$

$$Solvent\ intensity = \frac{mass\ of\ all\ solvents\ used\ (kg)(excluding\ water)}{mass\ of\ product\ (kg)} \qquad \text{Equation 6.2}$$

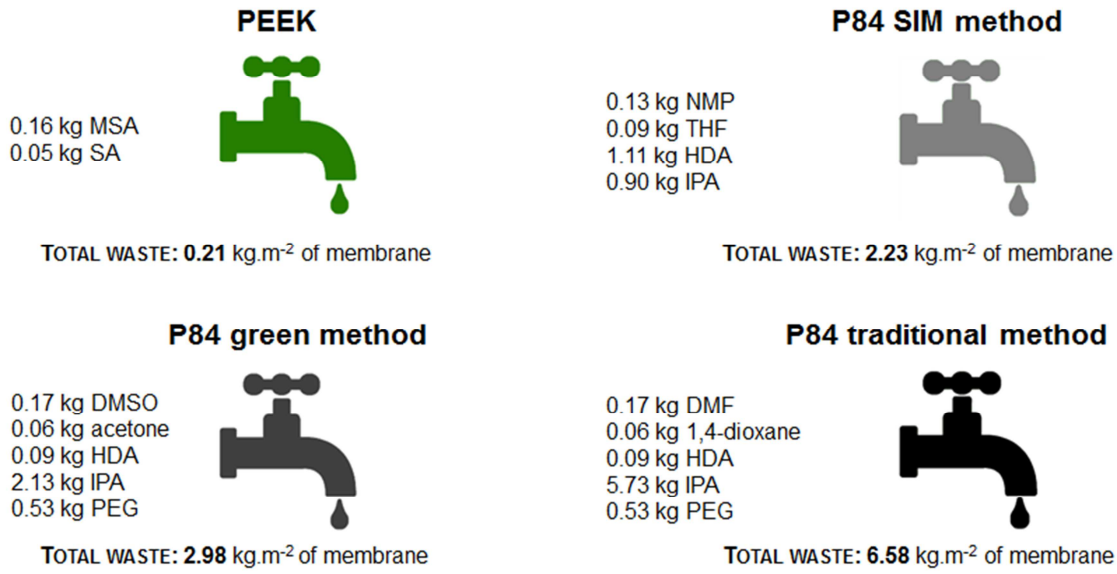

Figure 6.2 – Comparison of the composition of the waste stream and the total waste generated per m^2 of membrane at industrial scale.

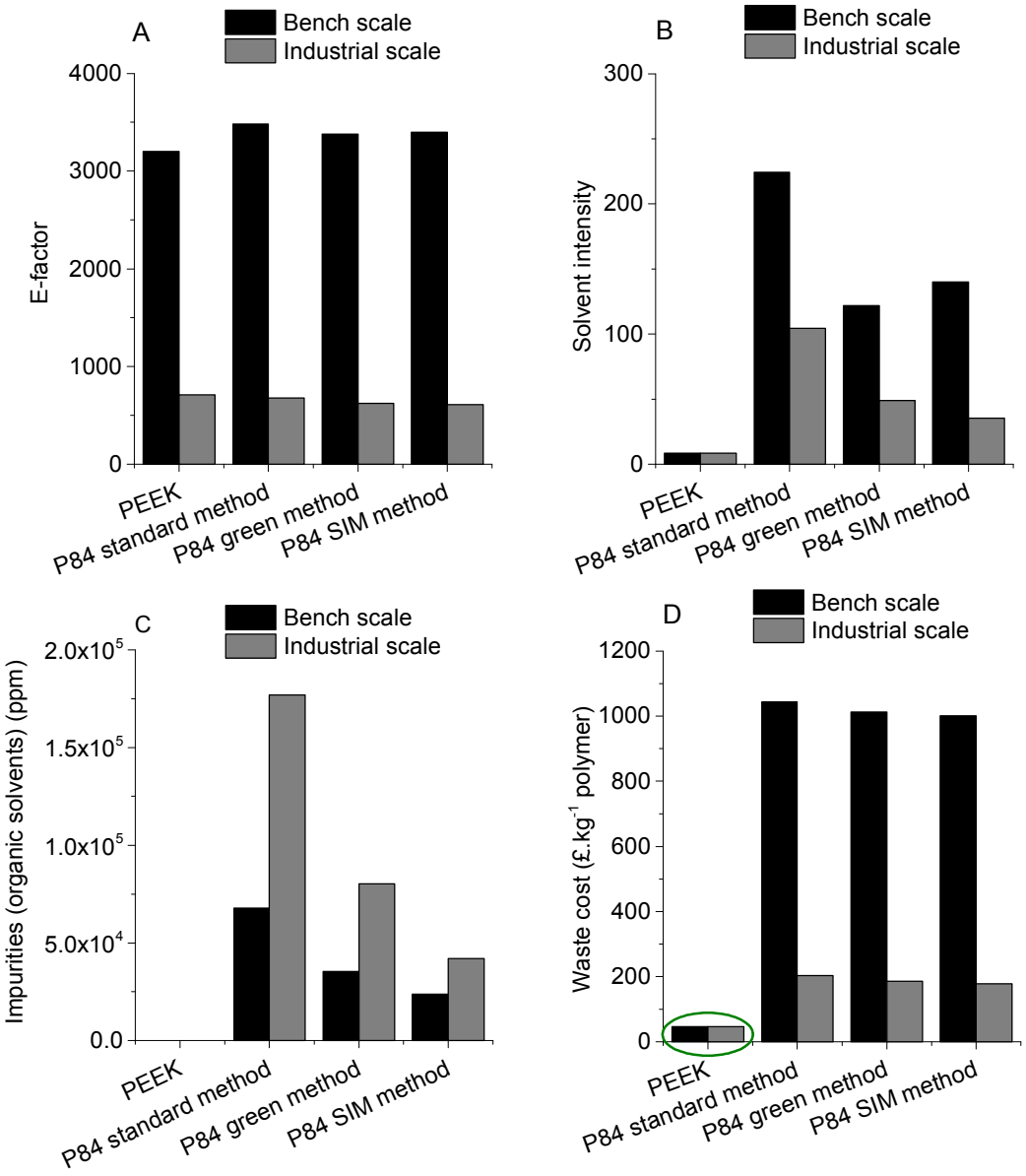

Figure 6.3 – E-factor, solvent intensity, organic solvent impurities in aqueous waste stream and waste cost treatment for PEEK membranes and P84 membranes produced in bench and industrial scale.

The E-factor (Figure 6.3 A) for all membranes is lower when producing at industrial scale than at bench scale because per kg of polymer less water is used at industrial scale. Nevertheless, the E-factor is very similar for all membranes at the respective scale which is a result of the high usage of water for phase inversion. Analyzing the solvent intensity (Figure 6.3 B) it can also be seen that the industrial scale is more efficient and less IPA is consumed. For both scales (bench and industrial) producing P84 membranes using the standard method has the highest solvent intensity, followed by the green method and SIM method (the P84 production method that consumes the least solvents of the three at industrial scale). PEEK membranes have the lowest solvent intensity with a value of 8.3 (for both scales) due to the usage of only MSA and SA as solvents throughout the whole

production process. This is the reason why there are no organic solvents present in the waste water stream originating from the production of PEEK membranes (Figure 6.3 C). Production of P84 via the standard method generates the highest concentration of organic solvents at both industrial (~ 1.8×10^5 ppm) and bench scale (~ 6.8×10^4 ppm) due to the usage of high boiling point solvents in the dope preparation and the usage of IPA for crosslinking and/or conditioning. The other two methods of producing P84 generate lower amounts of impurities in the waste stream but are still in the order of magnitude of 10^4 to 10^5 ppm.

The fact that no organic solvent waste is generated during PEEK production makes the waste cost treatment at industrial scale 4.1 times lower (in average) when compared with the P84 industrial scale production methods, and 22.2 times lower (in average) at bench scale.

6.2.2 The overall "greenness" of PEEK membranes

Although PEEK membranes are apparently a greener alternative from the production point of view, it is also important to assess environmental impact from the application point of view. In this section a comparison between the module area of PEEK and P84 required for permeating 100L.h^{-1} of THF at 30 bar is performed in terms of its environmental burden. Only solvent permeation has been considered for this exercise but in fairness it should have been also considered the separation of two species with different MWs and its separation using a diafiltration. The permeance of PEEK modules considered was 0.47 L.h^{-1}.m^{-2}.bar^{-1} (Module 1) and 0.26 L.h^{-1}.m^{-2}.bar^{-1} (Module 2) (data from Chapter 5), and the permeance of P84 standard method (vide Table 6.1) was 0.22 L.h^{-1}.m^{-2}.bar^{-1} (data obtained from crosslinked P84 flat sheet membranes with a MWCO of 300 g.mol^{-1}). However, a value of 2.33 L.h^{-1}.m^{-2}.bar^{-1} was found in literature for DuraMem® 300 modules [116] (PI based membranes). For fairness of comparison both permeances were considered in computing the total waste generated and the total waste cost. The area required for PEEK Module 1 to permeate 100 L.h^{-1} at 30 bar is 7.09 m^2, for PEEK Module 2 is 12.82 m^2, for P84 low permeance is 15.15 m^2 and for P84 high permeance is 1.43 m^2. In order to calculate the mass of membrane required (and therefore the corresponding waste composition excluding water) for permeating 100L.h^{-1} of THF, the area of membrane is multiplied by the thickness and film density. The results are presented in Figure 6.4. As expected PEEK has on average 13 times lower total waste than the average total waste of P84 membranes (both low and high permeance), 2.2 kg vs. 29 kg. This difference is mainly because in the production of PEEK membranes only MSA and SA will be present in the waste water stream. In the production of P84 membranes besides DMF and 1,4-dioxane there will be crosslinker and IPA (impregnating solvent) in the waste water stream, thus increasing the total waste generated. Analysing the total waste cost PEEK is presented as a viable green option with

an average total waste cost 5.6 times lower than the average total waste cost of P84 membranes, 13.5 vs. 76.

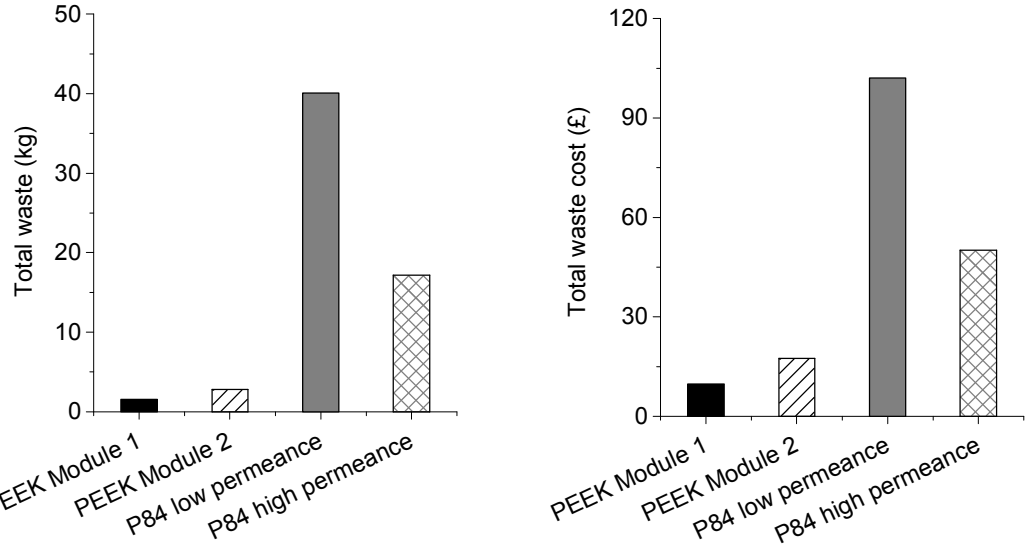

Figure 6.4 – Total waste generated (left), kg, and total waste cost treatment (right), £, for PEEK membranes and P84 membranes (standard method) calculated using the membrane area required to permeate 100 L.h^{-1} of THF at 30 bar pressure.

6.3 Conclusions

In terms of their manufacturing process and waste-treatment cost PEEK membranes are an environmentally friendly choice when compared with other common OSN membranes such as polyimide based membranes. In this chapter a comparison was performed at bench and industrial scales with three methods of producing polyimide P84 crosslinked membranes: the "traditional" method; the green method and the SIM method. Calculating the E-factor and the solvent intensity in order to compare the different membrane production it was possible to conclude that PEEK membrane manufacturing has a much lower environmental burden. PEEK had a solvent intensity of 8.3 whereas P84 production methods had values in the range of 35 to 224. For the total waste generated per m^2 of membrane area (industrial scale) PEEK is by far the greenest with a total waste produced of 0.21 kg.m^{-2} of membrane whereas P84 traditional method generated 6.58 kg.m^{-2} of membrane; the SIM method and the green method had similar values of 2.23 and 2.98 kg.m^{-2} of membrane, respectively. As a result, PEEK had a low waste cost per kg of polymer of around 46 £.kg^{-1} of polymer, 22.2 and 4.1 times lower (in average) than P84 methods at bench and industrial scales, respectively. Finally, the overall greenness of PEEK was determined in order to assess the environmental burden of permeating 100 L.h^{-1} of THF. As a comparison P84 module data were obtained and total waste (kg) and total waste cost (£) were calculated. The solvent intensity was 13 times lower, in average, than P84 modules, 2.2 vs. 29, and the total waste cost 5.6 times lower, in average, than P84 modules (low and high permeance).

PEEK can be a greener alternative than conventional PI modules in the OSN field although optimization work in scaling-up is required to obtain more consistent membrane performances.

Chapter 7. Controlling molecular weight cut-off of PEEK nanofiltration membranes using membrane drying

The work described in this chapter has been published in the following paper:

João da Silva Burgal, Ludmila Peeva, Patrizia Marchetti, Andrew Livingston, Controlling molecular weight cut-off of PEEK nanofiltration membranes using a drying method, Journal of Membrane Science, Volume 493, 1 November 2015, Pages 524-538, ISSN 0376-7388, http://dx.doi.org/10.1016/j.memsci.2015.07.012.

The modelling of the post-phase inversion drying process of PEEK nanofiltration membranes was performed in MATLAB with a code kindly provided by Dr. Patrizia Marchetti.

Abstract

In this research paper we report investigations into controlling the molecular weight cut-off (MWCO) of PEEK membranes prepared via phase inversion and subsequent drying. The two methods explored were change of polymer concentration in the dope solution – 8 wt. %, 10 wt. % and 12 wt. % - and the variation of solvent filling the pores prior to drying – e.g. water, methanol, acetone, tetrahydrofuran and n-heptane. The results show that it is possible to vary the MWCO from 295 $g.mol^{-1}$ to 1400 $g.mol^{-1}$ by varying these parameters. A statistical analysis based on a genetic algorithm showed that the Hansen solubility parameter, polarity and their interactions with molar volume were likely to be the most important parameters influencing the performance of PEEK membranes when drying from different solvents. In addition, the drying temperature also proved to have an effect on the membrane performance - the higher the temperature the higher the rejection and the lower the permeance.

7.1 Introduction

OSN membranes can be used for separation in the chemical and pharmaceutical industry to perform concentration and purification and solvent recovery. Recently, it was shown how OSN could be used for catalytic reactions with reaction and separation occurring in situ under high temperature and basic conditions [117]. One of the main challenges of fabricating suitable OSN membranes is to have the right MWCO to perform the separation of interest. The most widely used method for manufacturing polymeric membranes is the phase inversion method. This method involves four main steps: dissolving a polymer in an appropriate solvent (dope solution); membrane casting; phase inversion (wet or dry); and membrane post-treatment [118].

It is known that it is possible to manipulate the membrane performance by varying the composition of the dope solution (e.g. polymer concentration), varying the conditions during the phase inversion step or via a post-treatment step (drying, conditioning or crosslinking) [28].

As mentioned in section 2.4.5 most membranes prepared by wet phase inversion are stored under wet conditions because the structure of the membrane changes ("collapses") when the membrane is subjected to drying. In the case of ultrafiltration membranes (and nanofiltration as well) drying almost without exceptions induces irreversible loss of solvent permeance which is thought to be related to the collapse of the nodular structure [37]. Using a multiple solvent exchange procedure can minimize the risk of nodule collapse upon drying. The theory of nodular collapse was introduced by Brown [41] for polymer latex particles during film formation. Beerlage [37] used this theory for PI ultrafiltration membranes and related the capillary forces (F_c) with the resistance of the matrix to deformation (F_r) developed by Brown (see section 2.4.5 for a full description of Brown's theory).

Based on the decrease of surface tension (for example via solvent exchange) it is possible to maintain the pore structure of a membrane (i.e. to minimise the capillary force) if the strength of the matrix is high enough [37, 39-42].

In the previous chapter, the excellent stability and performance of native PEEK nanofiltration membranes has been described [10]. This chapter focuses on a detailed investigation of how to manipulate the separation properties (MWCO) of non-sulphonated nanofiltration PEEK membrane in a range of 350 – 500 g.mol^{-1}. Different factors affecting membrane separation performance are studied including polymer concentration in the dope solution and membrane post-treatment procedures (solvent exchange). It is shown that the post-manufacturing membrane drying step is of vital importance for the membrane nanofiltration performance.

7.2 Methods

7.2.1 Materials

2,4-Diphenyl-4-methyl-1-pentene (α-methylstyrene dimer) and methanesulphonic acid (MSA) were obtained from Sigma-Aldrich. N,N-Dimethylformamide (DMF), tetrahydrofuran (THF), propanone (acetone), 2-propanol (IPA), methanol (MeOH), ethanol (EtOH), n-hexane, heptane, acetonitrile and sulphuric acid (SA) 95 vol.% were obtained from VWR UK. VESTAKEEP® 4000P was kindly obtained from Evonik Industries. The styrene oligomers

standards with a molecular weight distribution of 580 (PS580) and 1300 (PS1300) were obtained from Agilent Technologies Deutschland GmbH, Germany. All reagents were used as received without any further purification.

7.2.2 Membrane preparation

The same dope preparation procedure used in 4.3.2 (Chapter 4) was used with some modifications. PEEK powder VESTAKEEP® 4000P was dissolved at concentrations of 8 wt. %, 10 wt. % and 12 wt. % in a mixture of 3:1 wt. % methanesulfonic acid (MSA) and sulphuric acid (SA). The membranes were cast according to the procedure described in 4.3.2. For the membranes produced with a 12 wt. % polymer concentration a solvent exchange from water to IPA, MeOH, n-hexane, EtOH, acetone, THF, heptane or acetonitrile was performed. Finally, the membranes were left to dry at either 20 °C, 40 °C, 80 °C, 120 °C or 140 °C[1] (reported as the glass transition temperature for PEEK) [44, 68]. Membrane preparation steps are represented in Figure 7.1. The viscosity of the dope solution was measured immediately after casting using a rotary viscometer (LV-2020 Rotary Viscometer Cannon instruments, S16 spindle) and all values were recorded at 1 rpm spindle speed and 20 °C.

All the membrane formation steps were performed in an air conditioned room set at 20 °C and with a relative humidity (RH) in the range of 30-40%.

Figure 7.1 – Schematic representation of the steps involved in the PEEK membrane preparation.

7.2.3 Membrane characterization

7.2.3.1 Thermal gravimetric analysis (TGA)

TGA measurements of PEEK samples were performed using a TGA Q500 (TA Instruments) and 100 µL platinum pans. The measurements were done under nitrogen and oxygen atmosphere and a gas flow of 40 mL·min^{-1} for nitrogen and 60 mL·min^{-1} for air. The heating rates varied between 10 K·min^{-1} and 40 K·min^{-1} and each sample was maintained at the target temperature – 20 °C, 40 °C, 80 °C, 100 °C and 120 ° - for 400 min (isothermal step).

[1] The drying temperature of 140 °C was only used for membranes dried from water.

7.2.3.2 Dynamic mechanical analysis (DMA)

Rectangular specimens of water "wet" membranes having a size of 35 mm × 6 mm × 0.2 mm (L × W × H) were used for the dynamic mechanical experiments. Dynamic mechanical thermal analyser (Tritec 2000DMA, TA Instruments) was used for the evaluation of the dynamic modulus (stiffness) and mechanical damping (tan δ). Membrane properties were measured over the temperature range from 25 to 120 °C at a heating rate of 2 $K.min^{-1}$. The tests were carried out at 1 Hz with a displacement of 0.05 mm.

7.2.3.3 Differential scanning calorimetry (DSC)

Changes in the degree of crystallinity of the samples during drying were observed by differential scanning calorimetry (DSC) (DSC Q200, TA Instruments). Samples were heated from 20 to 400 °C at a constant ramp rate of 10°$C.min^{-1}$ in DSC aluminium pans (heating cycle 1). After cooling down at a rate of 10°$C.min^{-1}$ to 20 °C the samples were heated using the same method as the one used in heating cycle 1 (heating cycle 2). A sharp peak at about 330 – 340 °C is characteristic of PEEK crystal melting. The area under the melting curve was used to calculate the heat required for the melting process. The heat of melting for a 100% crystalline PEEK sample is 130 $J.g^{-1}$ [68]. Thus, the ratio of the two heats of melting was calculated to obtain the degree of crystallinity of the sample.

7.2.3.4 Scanning Electron Microscopy (SEM)

The same method used in 4.3.3.8 was applied in order to obtain cross-sectional and surface pictures of the membranes.

7.2.3.5 Membrane performance and analysis

In order to test the membranes a rig with 8 membrane cross-flow cells was used (effective membrane area = 14 cm^2 at each cell, see Figure 4.1 in section 4.3.3.9). PEEK membranes were initially conditioned by passing pure solvent through at 30 °C and 30 bar (for 1 hour). Polystyrene standard solution was then poured into the feed reservoir and the system was pressurized again up to 30 bar and the temperature set at 30 °C.

The polystyrene standard solution was prepared according to the method described in 4.3.3.9.

The flux (J) and permeance (L_P) were determined using Equation 2.1 and Equation 2.2 and the rejection (R_i) of PS was evaluated applying Equation 2.3 (all equations in section 2.2). The corresponding MWCO curves were obtained from a plot of the rejection of PS versus their molecular weight. To eliminate the effect of compaction typically observed over the first 2-5 hours of experiment, for membrane performance comparison purposes only the steady state flux (after 24 hours) was considered (steady state flux was considered achieved

when two flux (permeance) measurements within a 1 h interval showed the same value within ± 0.02 L. m^{-2} .h^{-1}.bar^{-1}).

7.2.4 Experimental design

The methodology used in this study was based on the comparison of PEEK membranes dried at 120 °C and produced either with different polymer concentration (8 wt. %, 10 wt. % and 12 wt. %) or dried from different solvents (solvent exchange) in terms of performance (permeance and rejection). For each of the different membranes four replicates were performed in order to have a statistically robust sample. All the results were analysed using F-test. For the permeance data the F-test was used for permeance values obtained after 24 hours. For rejection data the F-test was applied to each individual polystyrene (PS), i.e. for each solute size (different MW) the four different membranes were compared with each other. Statistical significance was considered at $p<0.05$. Data are presented as means ± standard deviation of the mean (SDM).

7.2.5 Design of Experiments

The impregnation of PEEK membranes was analysed using statistically designed experiments to allow the variation of more than one parameter at a time. Design of Experiment (DoE) is a systematic approach for evaluating cause and effect relationships, with the final aim of understanding and optimising a given process [119]. Design Expert® version 8 from Stat-Ease Inc. (USA) was used to obtain the values for each parameter for each set of PEEK membranes. A linear 2-level factorial design was chosen as this type of design enables screening through a set of parameters and finding the significant ones. The design was made for five parameters: molecular weight of poly ethylene glycol (PEG), concentration (wt. %), drying temperature (°C), time of impregnation (h) and solvent which membranes are dried from (water or IPA). These parameters were varied over two levels, a minimum and a maximum, which are presented in Table 7.1. The responses for the DoE software, permeance and rejection of the dimer, were obtained using acetone as solvent and polystyrene oligomers as markers. The PEEK membranes were produced with a polymer concentration of 12 wt. % following the method described in 7.2.2 with the exception that the membranes were impregnated with different MW poly ethylene glycols (PEGs) after phase inversion. All membranes produced were characterized using the method described in 7.2.3.5.

Table 7.1 - Summary of the parameters (molecular weight (MW), PEG concentration (% w/w), time of impregnation (h), drying temperature (°C) and solvent (water or IPA)), their coding and the minimum and maximum values used to evaluate the influence of PEG impregnation in permeance and rejection.

Factor	Name (unit)	Minimum	Centre point	Maximum
A	MW ($g.mol^{-1}$)	200	400	600
B	Concentration (% w/w)	2	51	100
C	Time (h)	6	15	24
D	Temperature (°C)	20	60	100
E	Solvent	IPA	N/A	Water

7.3 Results and discussion

7.3.1 Control of pore collapsing for tuning MWCO using volatile solvents

7.3.1.1 The effect of polymer concentration and drying temperature

As reported previously, the nanofiltration properties of PEEK membranes are correlated to the drying of the membranes [10]. Nevertheless, the permeance values reported were relatively low. In order to improve the permeance - without compromising the MWCO - a study on polymer concentration (8 wt. % to 12 wt. %) and drying temperatures (20 °C, 40 °C, 80 °C and 120 °C) was performed in order to determine their influence on membrane performance (Table 7.2).

Table 7.2 – Summary of PEEK membranes PM-B prepared from dopes with different polymer concentrations (8 wt.%, 10 wt.% and 12 wt.%) and dried from water at different temperatures. The viscosity (Pa.s) of the membrane dope solution as well as the spindle speed (rpm) used are presented in this table. These membranes were used to test the influence of polymer concentration and drying temperature on permeance and rejection.

Membrane code	Polymer concentration (wt. %)	Viscosity (Pa.s)	Spindle speed (rpm)	Drying temperature (°C)
PM-B 8 wt% 20 °C	8	7.72 ± 0.04	10	20 °C
PM-B 8 wt% 40 °C				40 °C
PM-B 8 wt% 80 °C				80 °C
PM-B 8 wt% 120 °C				120 °C
PM-B 10 wt% 20 °C	10	25.46 ± 1.86	3	20 °C
PM-B 10 wt% 40 °C				40 °C
PM-B 10 wt% 80 °C				80 °C
PM-B 10 wt% 120 °C				120 °C
PM-B 12 wt% 20 °C	12	58.03 ± 1.58	1	20 °C
PM-B 12 wt% 40 °C				40 °C
PM-B 12 wt% 80 °C				80 °C
PM-B 12 wt% 120 °C				120 °C

As expected, the membranes with lower polymer concentration (8 wt. %) presented higher permeance values, in the range of 1.25 $L.h^{-1}.m^{-2}.bar^{-1}$ to 2.30 $L.h^{-1}.m^{-2}.bar^{-1}$, and a MWCO in the range of 795 $g.mol^{-1}$ to 1295 $g.mol^{-1}$ (Figure 7.2). Interestingly, the membranes dried at 20 °C and 120 °C were the tightest ones and with lower permeance whereas the ones dried at 40 °C and 80 °C presented a higher MWCO and higher permeance, i.e., there was no trend as a function of the temperature. Both higher polymer concentrations – 10 wt. % and 12 wt. % - presented lower permeances and lower MWCO (tighter membranes). The permeance of the membranes prepared with 10 wt. % of polymer was in the range of 0.42 $L.h^{-1}.m^{-2}.bar^{-1}$ to 0.52 $L.h^{-1}.m^{-2}.bar^{-1}$ and the MWCO was in the range of 395 $g.mol^{-1}$ to 495 $g.mol^{-1}$. As for the 12 wt. % membranes, the permeance was in the range of 0.18 $L.h^{-1}.m^{-2}.bar^{-1}$ to 0.40 $L.h^{-1}.m^{-2}.bar^{-1}$ and the MWCO was in the range of 295 $g.mol^{-1}$ to 395 $g.mol^{-1}$. It can be seen from the different membranes dried at 120 °C (Figure 7.3) that the polymer concentration had a greater influence on membrane performance than drying temperature (Figure 7.2). The difference was more noticeable between the 8 wt. % and the 10 wt. % than between the 10 wt. % and the 12 wt. %. The difference in performance for different polymer concentrations could be explained by the viscosity of the dope solution, because the 8 wt. % polymer dope solution had 3.30 times and 7.51 times lower viscosity than the 10 wt. % polymer dope and 12 wt. % polymer dope respectively. In contrast, the difference in viscosity between 10 wt. % polymer dope solution and 12 wt. % polymer dope solution was only 2.28 times. The viscosity of the dope solution (Table 7.2) could explain the results obtained because higher casting solution viscosities slow down non-solvent in-diffusion and demixing is delayed, resulting in membranes with thicker and denser skin-layers and sublayers with lower porosities. From the SEM images (Figure 7.3 bottom) it was found that membranes PM-B 8 wt.% 120°C had a thinner active layer of approximately 2.0 μm whereas for membranes with higher polymer concentration the active layer had a thickness of approximately 2.9 μm.

There is no sharp border line between MWCO of the different membrane separation processes, however in general nanofiltration is considered to cover separations of molecules within the 200 – 2000 Da range [28]. As such all PEEK membranes reported in this study are nanofiltration membranes. However, currently the organic solvent nanofiltration membranes market suffers a lack of “tight” membranes with MWCO at the lowest range of nanofiltration, ~200 Da, that can be used for example for solvent recovery. According to the literature search performed, there is only one OSN membrane on the market claiming MWCO of 150Da – DuraMem®150 manufactured by Evonik Industries. Therefore, it was chosen to investigate further the tightest membrane from the PEEK series in an attempt to manipulate its MWCO and eventually make it tighter. Given the fact that the membranes with a polymer

concentration of 12 wt. % presented the lowest MWCO, all subsequent studies in this research work were performed using this polymer concentration.

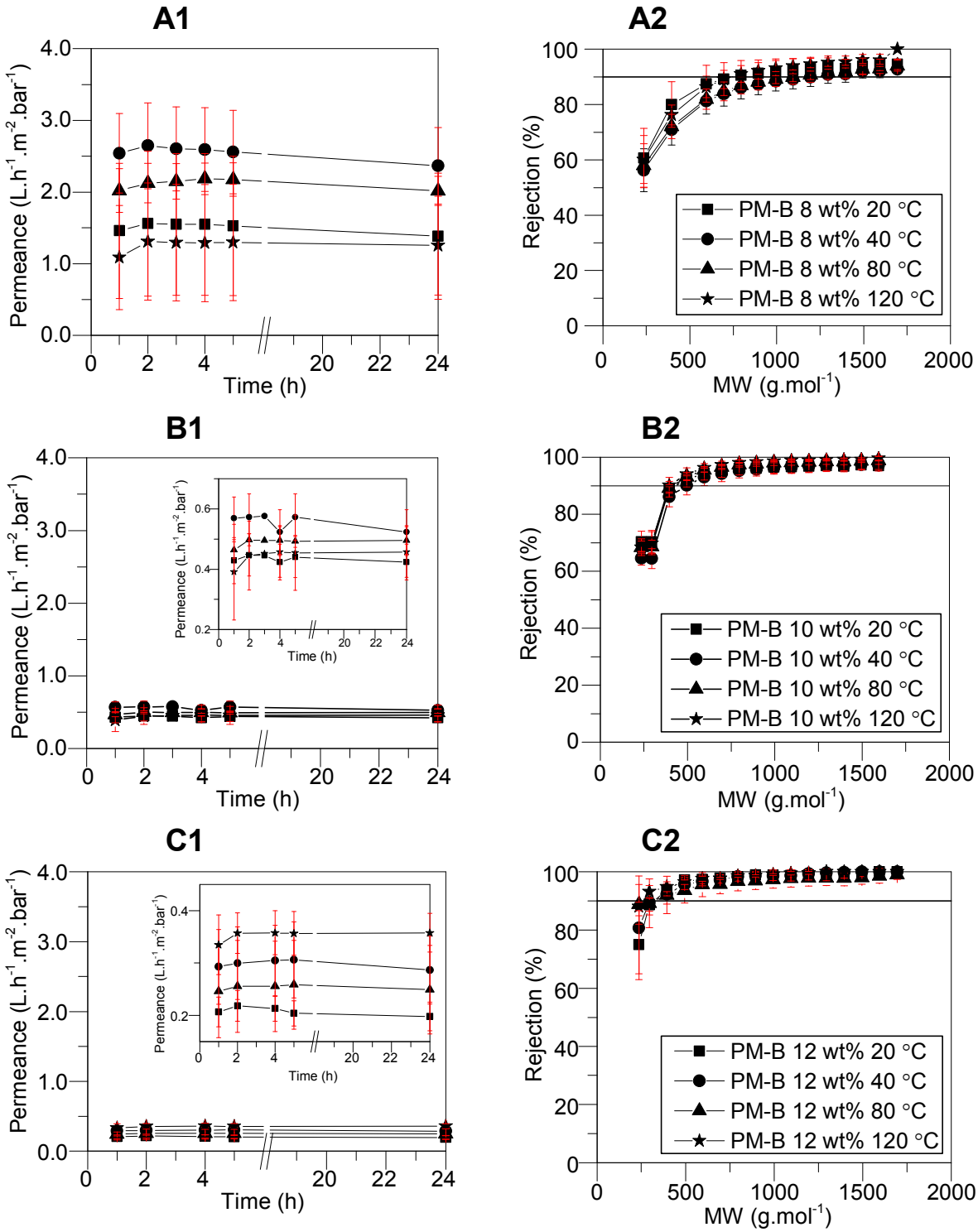

Figure 7.2 – A1, B1 and C1: Permeance values ($L.h^{-1}.m^{-2}.bar^{-1}$) over a period of 24 h for the different membranes under study. A2, B2 and C2: Rejection values of the different PEEK membranes under study as a function of the molecular weight (M_W, $g.mol^{-1}$) of different polystyrenes after 24 hours. All the membranes presented were dried from water at different temperatures (20 °C, 40 °C, 80 °C and 120 °C) prior to their insertion in the cross-flow cells. The membranes were used to filter with a solution of THF and PS (1 $g.L^{-1}$). The flow-rate, temperature and pressure were set at 100 $L.h^{-1}$, 30 °C and 30 bar, respectively. The red bars represent the standard deviation of the mean.

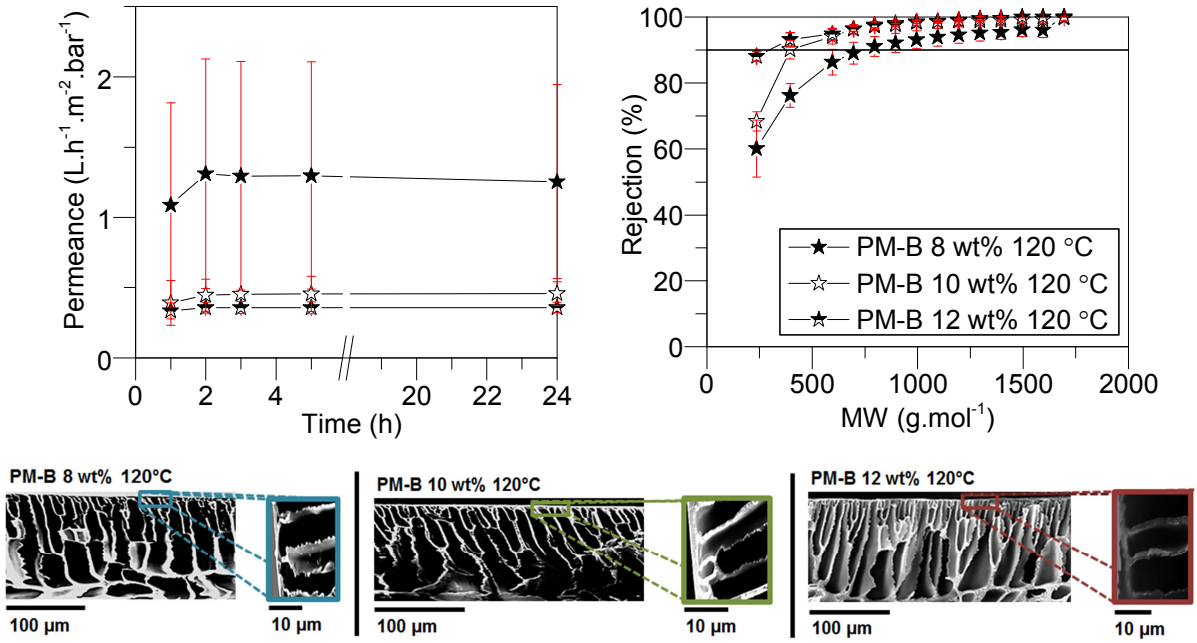

Figure 7.3 – Top left: Permeance values (L.h^{-1}.m^{-2}.bar^{-1}) over a period of 24 h for the different membranes under study. Top right: Rejection values of the different PEEK membranes under study as a function of the molecular weight (M_W, g.mol^{-1}) of different polystyrenes after 24 hours. All the membranes presented were dried from water at 120 °C prior to their insertion in the cross-flow cells. The membranes were used to filter with a solution of THF and PS (1 g.L^{-1}). The flow-rate, temperature and pressure were set at 100 L.h^{-1}, 30 °C and 30 bar, respectively. The red bars represent the standard deviation of the mean. The membranes dried from water at 120 °C are significantly different ($p \leq 0.05$, F-test). Bottom: Cross-section SEM images (magnification 300 ×) of the different membranes under study: PM-B 8wt% 120 °C, PM-B 10wt% 120 °C and PM-B 12wt% 120 °C.

7.3.1.2 The effect of drying solvent

As already mentioned in 2.4.5 and according to the literature [37, 41], the final membrane pore size is greatly influenced by the surface tension of the solvent filling membrane pores prior to drying. To investigate this effect on the PEEK membranes a solvent exchange from water to IPA, MeOH, EtOH, n-hexane, acetone or THF was performed after the phase inversion process in order to change the surface tension and possibly achieve different extents of collapsing in the polymer nodular structure. Water has a surface tension of 72.8 mN.m^{-1} while the remaining solvents have similar (and much lower) values of surface tension in the range of 18.4 mN.m^{-1} to 26.4 mN.m^{-1} (Table 7.3).

The contact angle water/PEEK was measured to be 60°. It was not possible to measure contact angles for the other solvents, since the droplet spread instantaneously, thus these contact angles were assumed as 0°. Therefore, and according to the theory presented by Brown (Equation 2.14) [41], membranes immersed in IPA, MeOH, EtOH should give similar MWCO because of the similarity in surface tension; n-hexane should present higher MWCO (looser membranes) because it has the lowest surface tension and acetone and THF should give tighter membranes (excluding the ones dried from water). According to this method F_c

should be higher for water at any given pore radius and therefore, pore collapse in water is expected to occur to a much higher extent. As a result, membranes dried from all the other solvents should be looser than membranes dried from water with the following order (from lower MWCO to higher MWCO membrane): water < THF < acetone < MeOH < EtOH < IPA < n-hexane. Together with the solvent type the effect of drying temperature on the permeance and on the MWCO was also studied. The membranes produced are presented in Table 7.3.

Table 7.3 – Summary of PEEK membranes PM-B 12 wt % prepared from different dopes and with different post-treatments. These membranes were used to test the influence of solvent exchange and drying temperature on permeance and rejection. In addition, properties of the solvents used for the solvent exchange: surface tension (mN.m^{-1}), MW (g.mol^{-1}), boiling point (°C), vapour pressure (kPa) and molar volume (cm^3.mol^{-1}). All properties listed were obtained from [120] at 20 °C and 1 bar.

			Solvent properties			
Membrane code	Drying solvent	Drying temperature (°C)	Surface tension (mN.m^{-1})	Boiling point (°C)	Vapour pressure (kPa)	Molar volume (cm^3.mol^{-1})
PM-B1.1	Water	20 °C	72.8	100	2.33	18.0
PM-B1.2	Water	40 °C				
PM-B1.3	Water	80 °C				
PM-B1.4	Water	120 °C				
PM-B2.1	MeOH	20 °C	22.6	64	16.93	40.6
PM-B2.2	MeOH	40 °C				
PM-B2.3	MeOH	80 °C				
PM-B2.4	MeOH	120 °C				
PM-B3.1	EtOH	20 °C	22.3	78	5.95	58.6
PM-B3.2	EtOH	40 °C				
PM-B3.3	EtOH	80 °C				
PM-B3.4	EtOH	120 °C				
PM-B4.1	IPA	20 °C	21.7	82	4.10	76.9
PM-B4.2	IPA	40 °C				
PM-B4.3	IPA	80 °C				
PM-B4.4	IPA	120 °C				
PM-B5.1	Acetone	20 °C	23.3	56	30.80	73.8
PM-B5.2	Acetone	40 °C				
PM-B5.3	Acetone	80 °C				
PM-B5.4	Acetone	120 °C				
PM-B6.1	THF	20 °C	26.4	66	21.60	81.9
PM-B6.2	THF	40 °C				
PM-B6.3	THF	80 °C				
PM-B6.4	THF	120 °C				
PM-B7.1	n-hexane	20 °C	18.4	69	20.17	131.4
PM-B7.2	n-hexane	40 °C				
PM-B7.3	n-hexane	80 °C				
PM-B7.4	n-hexane	120 °C				

As mentioned before in Section 7.3.1.1, the permeance for all membranes dried from water at different temperatures had permeance values in the range of 0.20 to 0.36 $L.h^{-1}.m^{-2}.bar^{-1}$. The membranes dried from water at 120 °C had almost double the permeance of membranes dried at 20 °C. This fact could be attributed to residual water that may have been retained in the smallest pores (thus obstructing solvent permeance), whilst above 100 °C (boiling point of water at 1 bar) all residual water may have been completely removed (hence higher permeance). Another interesting result was to determine the effect of temperature on the degree of crystallinity of the membranes dried from water (Figure A3 in the Appendix). It can been seen that from PM-B1.1 (dried at 20 °C) to PM-B1.4 (dried at 120 °C) there were no changes in the membrane crystallinity. A membrane dried at 140 °C was also prepared. It showed THF permeance of 0.04 $L.h^{-1}.m^{-2}.bar^{-1}$ but no rejection in the NF range (data not shown), possibly due to defects originating from the partial melting of the backing material, and was not further investigated. Thus, all subsequent drying experiments were limited to 120°C.

As for membranes dried from the alcohols, it can be observed that for MeOH (Figure 7.4 A1 and A2) the permeance values varied more with the temperature ranging from 1.07 $L.h^{-1}.m^{-2}.bar^{-1}$ (PM-B2.4) to 2.3 $L.h^{-1}.m^{-2}.bar^{-1}$ (PM-B2.3). From the rejection data (Figure 7.4 A2) it can be observed that the drying temperature has a greater effect on the MWCO, i.e, the higher the drying temperature the tighter the membrane. For the temperatures of 40 °C and 80 °C the rejection values were in fact quite similar, although the variability of the membranes PM-B2.2 and PM-B2.3 makes it difficult to confirm this result. The loosest membrane, PM-B2.1, had a MWCO beyond the NF range. Membranes PM-B2.2 and PM-B2.3 presented a MWCO of around 1300 $g.mol^{-1}$, but the standard deviation was not narrow enough to validate the result. The tightest membrane, PM-B2.4, had a MWCO around 600 $g.mol^{-1}$.

For the membranes dried from EtOH (Figure 7.4 B1 and B2) the permeance varied from 1.07 $L.h^{-1}.m^{-2}.bar^{-1}$ (PM-B3.1) to 2.1 $L.h^{-1}.m^{-2}.bar^{-1}$ (PM-B3.3). From the rejection data (Figure 7.4 B2) one can observe that for the temperatures of 40 °C and 80 °C the rejection values were quite similar and both had a MWCO beyond the NF range; membrane PM-B3.1 presented a MWCO of around 1595 $g.mol^{-1}$; and the tightest membrane, PM-B3.4, had a MWCO around 795 $g.mol^{-1}$.

For the membranes dried from IPA (Figure 7.4 C1 and C2) the permeance was on average 3.5 times higher than the membranes dried from water. In fact, the values of permeance ranged from 0.81 $L.h^{-1}.m^{-2}.bar^{-1}$ (PM-B4.2, dried at 40 °C) to 1.36 $L.h^{-1}.m^{-2}.bar^{-1}$ (PM-B4.4 dried at 20 °C). Analysing the rejection data it can be seen that the higher the drying temperature, the tighter the membrane, with the exception of PM-B4.2 (dried at 40

°C). For temperatures of 40 °C and 80 °C the rejection values were quite similar, although slightly higher for PM-B4.2 (as mentioned above). The membrane with the lowest permeance (PM-B4.4) presented the lowest MWCO and its value was around 500 $g.mol^{-1}$. For membrane PM-B4.1 (membrane with a high permeance) the MWCO was in the upper range of NF with a value around 1400 $g.mol^{-1}$.

In the case of alcohols, it was speculated that the boiling points of each of the alcohols are lower than the boiling point of water (Table 7.3) which allows for more solvent to be removed from the membrane pores at a faster rate; therefore, the drying temperature had more pronounced effect on the properties of the membrane when compared with water.

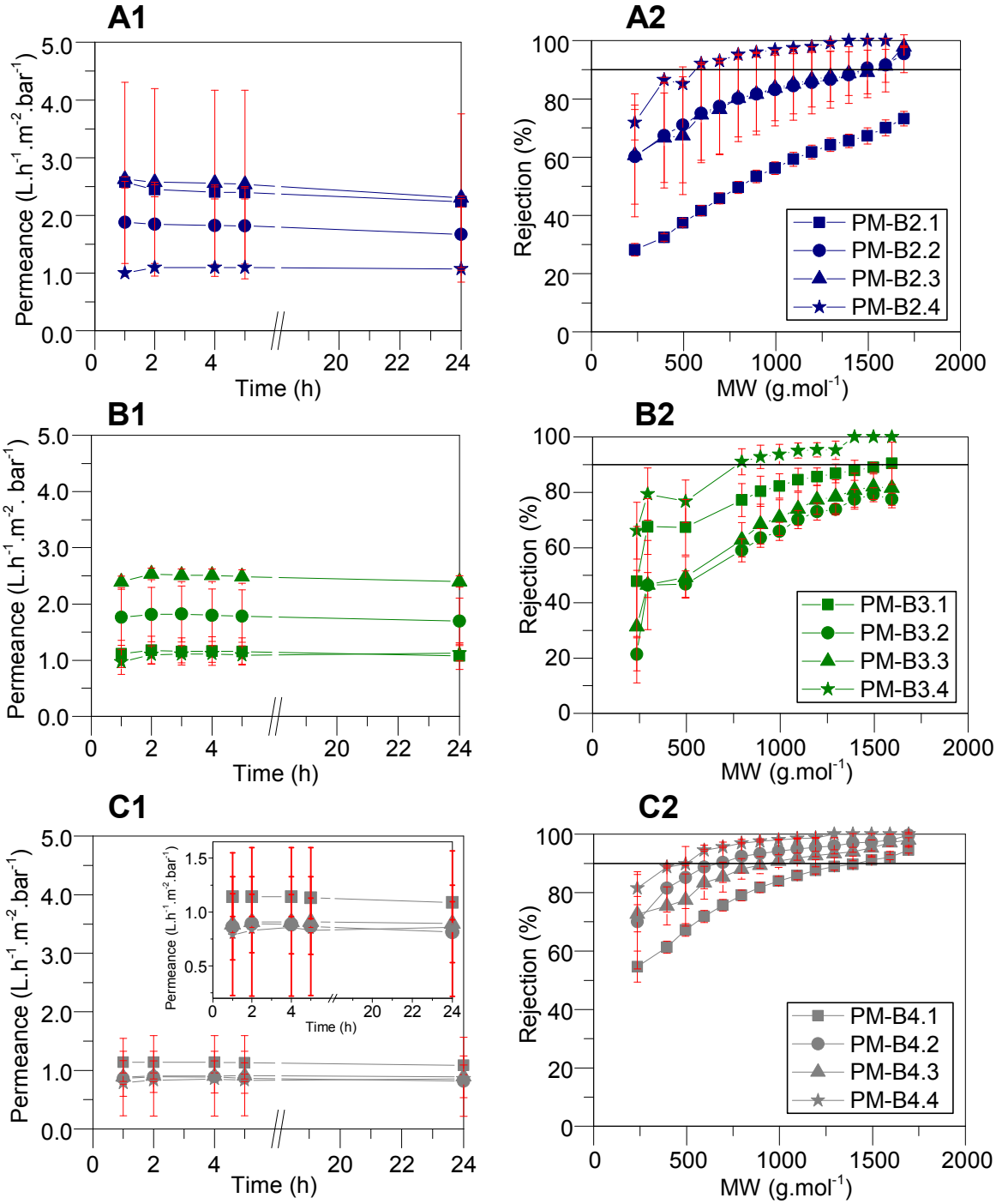

Figure 7.4 – A1, B1 and C1: Permeance values ($L.h^{-1}.m^{-2}.bar^{-1}$) over a period of 24 h for the different membranes under study. A2, B2 and C2: Rejection values of the different PEEK membranes under study as a function of the molecular weight (M_W, $g.mol^{-1}$) of different polystyrenes after 24 hours. Membranes PM-B2.x, PM-B3.x and PM-B4.x (x= 1,2,3 and 4) were dried from MeOH, EtOH and IPA respectively at different temperatures (20 °C, 40 °C, 80 °C and 120 °C) prior to their insertion in the cross-flow cells. The membranes were used to filter with a solution of THF and PS (1 $g.L^{-1}$). The flow-rate, temperature and pressure were set at 100 $L.h^{-1}$, 30 °C and 30 bar, respectively. The red bars represent the standard deviation of the mean.

Figure 7.5 D and E show that membranes dried from acetone and THF were affected to a greater extent by the temperature. For both solvents (acetone and THF), the membranes

had similar performances at 20 °C to 80 °C, but a substantial difference arose when dried at 120 °C (Figure 7.5 D2 and E2). In the case of acetone, the membranes dried at 120 °C had a permeance of 2.15 $L.h^{-1}.m^{-2}.bar^{-1}$ which was on average 4.5 times lower than for any other drying temperature considered; the MWCO was 895 $g.mol^{-1}$ while for the other drying temperatures the membranes produced were not in the NF range. For the membranes dried from THF over the temperature range of 20 °C to 80 °C the standard deviations made it difficult to assess within a confidence interval either permeance and rejection. Nevertheless, for a temperature of 120 °C the membranes presented a permeance of 2.72 $L.h^{-1}.m^{-2}.bar^{-1}$ which was on average 28 times lower than PMB-6.1 and 12 times lower than PMB-6.2 and PMB-6.3. This membrane did not present a MWCO in the NF range, but nevertheless from Figure 7.5 E2 one can observe that a shift occurred in terms of rejection when comparing PM-B6.4 with the other membranes, presumably due to tightening of the membrane matrix by increasing drying temperature.

For membranes dried from n-hexane the temperature effect was not that pronounced but nevertheless the membranes dried at 120 °C were tighter (MWCO = 595 $g.mol^{-1}$) than the ones dried at other temperatures which had similar performances (MWCO around 1400 $g.mol^{-1}$). The permeance ranged from 1.06 $L.h^{-1}.m^{-2}.bar^{-1}$ to 1.49 $L.h^{-1}.m^{-2}.bar^{-1}$. It is also important to point out that membranes dried from n-hexane had two solvent exchanges from water to IPA and then to n-hexane. In this particular case water and IPA could still be present in the smaller pores and the drying solvent might not have been pure n-hexane but a mixture of the three (although IPA and water should be present in very small amounts).

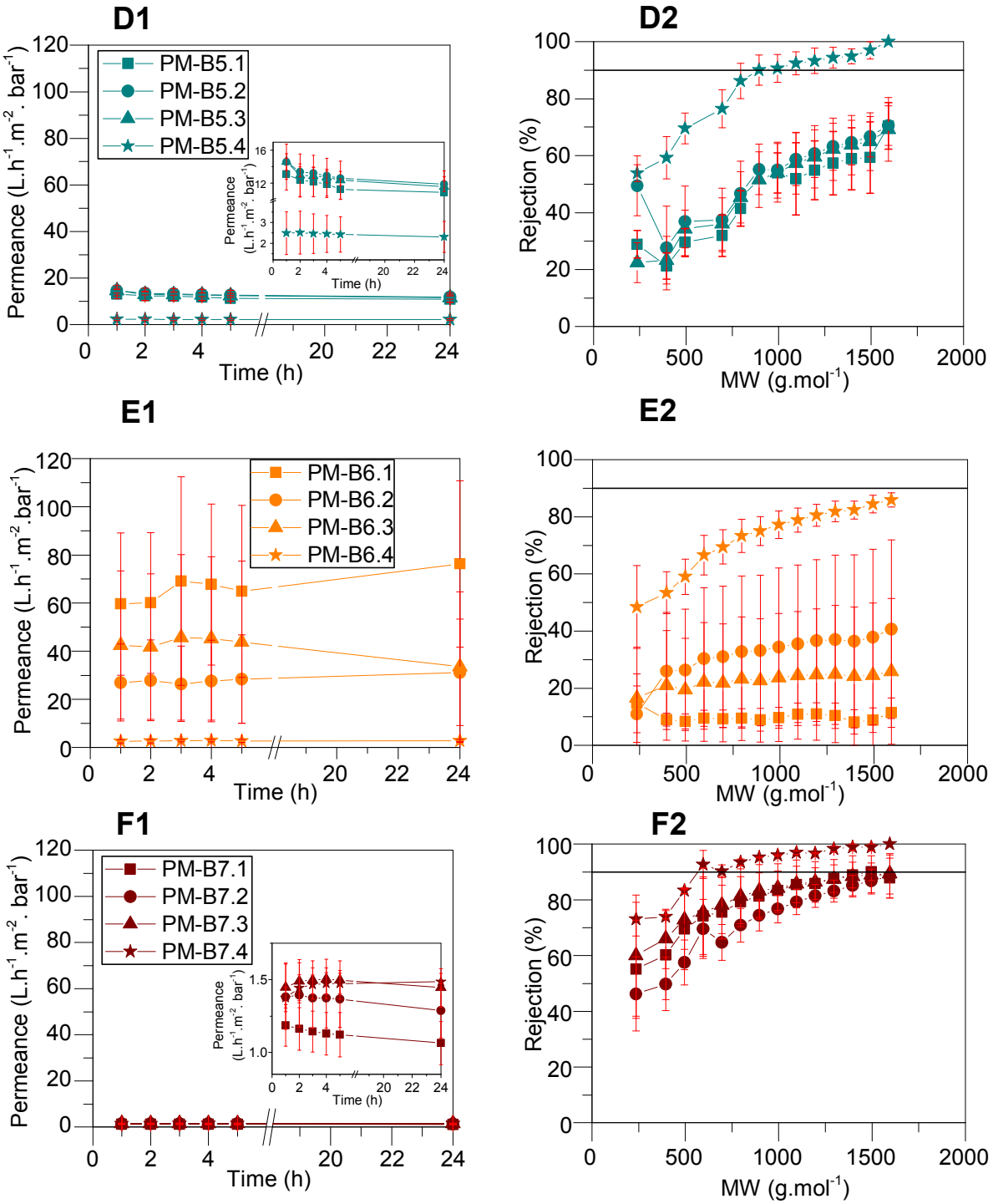

Figure 7.5 – D1, E1 and F1: Permeance values ($L.h^{-1}.m^{-2}.bar^{-1}$) over a period of 24 h for the different membranes under study. D2, E2 and F2: Rejection values of the different PEEK membranes under study as a function of the molecular weight (M_W, $g.mol^{-1}$) of different polystyrenes after 24 hours. Membranes PM-B5.x, PM-B6.x and PM-B7.x (x= 1,2,3 and 4) were dried from acetone, THF and n-hexane respectively at different temperatures (20 °C, 40 °C, 80 °C and 120 °C) prior to their insertion in the cross-flow cells. The membranes were used to filter with a solution of THF and PS (1 $g.L^{-1}$). The flow-rate, temperature and pressure were set at 100 $L.h^{-1}$, 30 °C and 30 bar, respectively. The red bars represent the standard deviation of the mean.

In order to investigate whether the solvent was completely removed after 24 h at 20 °C and 120 °C membranes PM-B1.4, PM-B3.4 and PM-B6.4 were further dried using a vacuum oven at 120 °C. From Figure 7.6 one can observe that the membranes PM-B1.4 and PM-B3.4 did not change in terms of rejection performance once vacuum drying was applied. Only a slight increase of the permeance was observed, suggesting some residual solvent may still be present in the smallest pores, but this does not significantly affect the separation properties. However, for membrane PM-B6.4 there was a decrease in permeance of about two times and the membrane was tighter after vacuum oven was applied (MWCO ~ 1395 $g.mol^{-1}$). This shows that for looser membranes there might be rearrangement of the polymeric structure and further nodule collapse from vacuum treatment. Nevertheless, there seems to be a physical limit in the collapse; the membrane did not collapse completely to, for example, the same degree as water dried membrane.

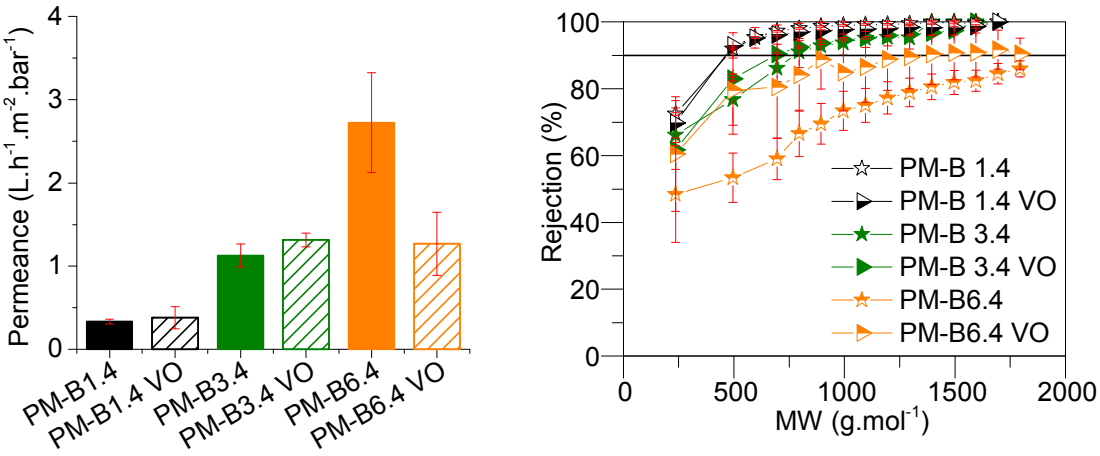

Figure 7.6 – Left: Permeance values ($L.h^{-1}.m^{-2}.bar^{-1}$) at 24 h for the different membranes under study. Right: Rejection values of the different PEEK membranes under study as a function of the molecular weight (M_W, $g.mol^{-1}$) of different polystyrenes after 24 hours. All the membranes presented were at least dried from water, EtOH, acetone and THF at 120 °C and some were further dried in a vacuum oven (code VO) at 120 °C for 24 h prior to their insertion in the cross-flow cells. The membranes were used to filter with a solution of THF and PS (1 $g.L^{-1}$). The flow-rate, temperature and pressure were set at 100 $L.h^{-1}$, 30 °C and 30 bar, respectively. The red bars represent the standard deviation of the mean.

The influence of drying time and cool-down rate were also evaluated (Table 7.4). Experimental data showed that regardless of the drying time, 0.5 h or 24 h, the membrane performance does not change (Figure 7.7). This means that an air-drying treatment at 120 °C for 0.5 h was sufficient to provide the same performance when 24 h was applied which constitutes considerable energy savings from a process point of view. In terms of cooling-down rate, there was no difference between instantaneous cool-down (∞) or 40 $°C.h^{-1}$ cool-down rate, further indicating that the membrane reaches a “frozen” and stable state once it is heated at 120 °C.

Table 7.4 – Summary of PEEK membranes PM-B prepared from different dopes and with different post-treatments. These membranes were used to test the influence of drying time and cool-down rate on permeance and rejection.

Membrane code	Drying solvent	Drying temperature (°C)	Drying time (h)	Cool-down rate (°C.h^{-1})
PM-B1.4A1	Water	120 °C	0.5	40
PM-B1.4A2	Water	120 °C	0.5	∞ (Instantaneous)
PM-B1.4B1	Water	120 °C	24	40
PM-B1.4B2	Water	120 °C	24	∞ (Instantaneous)

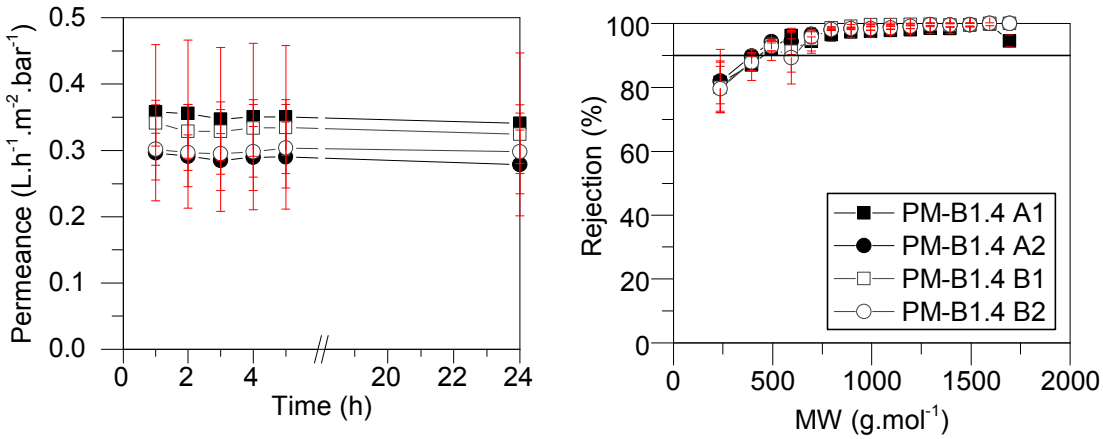

Figure 7.7 – Left: Permeance values (L.h^{-1}.m^{-2}.bar^{-1}) over a period of 24 h for the different membranes under study. Right: Rejection values of the different PEEK membranes under study as a function of the molecular weight (MW, g.mol-1) of different polystyrenes after 24 hours. All the membranes presented were dried from water at 120 °C for 0.5 h (A) or for 24 h (B) and cool downed slowly (1) or fast (2) prior to their insertion in the cross-flow cells. The membranes were used to filter with a solution of THF and PS (1 g.L^{-1}). The flow-rate, temperature and pressure were set at 100 L.h^{-1}, 30 °C and 30 bar, respectively. The red bars represent the standard deviation of the mean.

Apparently the correlation proposed by Brown and adopted by Beerlage [37] and by Gevers et al. [121], can explain only to a limited extent the results obtained. This correlation accounts for surface tension, but not for other solvent properties, which may be important during membrane drying, such as boiling point, vapour pressure, Hansen solubility parameter, viscosity and molar volume. Brown's correlation is also based on the assumption that a complete solvent exchange has taken place in all of the membrane pores. However this may not be the case if some residual water is retained in the smallest membrane pores, or some of the pores are filled with solvent mixtures with properties (specifically surface tension) different from the pure solvent.

These findings are in agreement with literature studies. Matsuyama et al. [122] performed extensive study on the effect of drying on the structure of microporous polyethylene membranes. They observed that polymer film contraction can be attributed to a

combination of two physical phenomena: densification of the amorphous regions of the film and collapse of pores due to capillary forces (Figure 7.8). They investigated 11 different solvents and concluded that membrane porosity is inversely proportional to the solvent surface tension and the boiling point of the solvent. These authors hypothesized that pore collapse involves rearrangement of the amorphous polymer molecules within the matrix phase. Since such a rearrangement requires time, it is hypothesized that the longer the capillary force is in effect, the greater the time for rearrangement of polymer chains in the matrix phase and the greater the extent of pore collapse. This rather logical hypothesis explains the experimental results well and the difference between the membranes dried from the different solvents. Having a lower boiling point and higher vapour pressure, acetone and THF disappear much faster from the membrane pores, shortening the action time of capillary force applied and the degree of pore collapse. However it somewhat contradicts the general trend for decrease of the membrane MWCO with the increase of the drying temperature observed with all solvents. The latter effect may be attributed to a larger contribution of the second phenomenon – densification of the amorphous regions due to polymer chain relaxation. In any case it is clear that the change from ultrafiltration to nanofiltration in the PEEK membranes is due to a secondary rearrangement of the polymeric chains during the drying-heating-cooling post-manufacturing treatment.

Other studies also pointed out similar effects of the solvent boiling point [123] and the drying temperature [124] on the membrane permeance and MWCO. Interestingly a few studies [38, 123, 124] present a correlation between the polymer-drying solvent affinity (expressed in terms of the Hansen solubility parameter) and the dried membrane properties. For this case study the solubility parameter for PEEK at 20 °C is reported as 9.5 $(cal.cm^{-3})^{0.5}$ vs. water - 25.5 $(cal.cm^{-3})^{0.5}$, methanol - 14.5 $(cal.cm^{-3})^{0.5}$, IPA - 11.5 $(cal.cm^{-3})^{0.5}$, EtOH – 13.4 $(cal.cm^{-3})^{0.5}$, n-hexane – 6.9 $(cal.cm^{-3})^{0.5}$, acetone – 10 $(cal.cm^{-3})^{0.5}$ and THF – 9.1 $(cal.cm^{-3})^{0.5}$ [6, 125]. Therefore THF and acetone have the highest affinity to PEEK and should be more difficult to remove from the pores, resulting on them being more open. This seems to be the case since these membranes presented the highest MWCO. However, when considering IPA, which has higher affinity to PEEK than MeOH and should be therefore more difficult to remove from the pores, the opposite is observed: the IPA-dried membrane is tighter than the MeOH one. Again it seems that the contribution of the solvent – polymer affinity factor is not the primary driver and that other factors are dominant during the membrane drying.

It should be also noted that none of the parameters in Equation 2.14 is independent of the temperature. In fact both the solvent surface tension and the tensile modulus decrease with the increase of the drying temperature [126, 127]. The rate of this decrease in both terms of

Equation 2.14 may actually change the inequality for a given pore radius, and thus alter the degree of pore collapse. This effect may also contribute to the fact that for temperatures between 40 °C and 80 °C the rejection values were quite similar and they did not follow a specific order. It has been shown however that close to the glass-transition temperature PEEK undergoes a sharp decline in the tensile strength (Figure A5 in the Appendix). Therefore between 120 °C and 140 °C the effect of the surface tension should be more pronounced. In other words, a fair comparison between different drying solvents can be made for a drying temperature of 120 °C, where all solvents were presumably completely evaporated and pore collapse was predominantly due to the surface tension effect. This comparison is shown in Figure 7.9. As expected, membranes dried from water had a higher extent of pore collapse when compared with membranes dried from other solvents. This is in accordance with predictions from Brown's theory, but does not explain the results obtained for the other solvents.

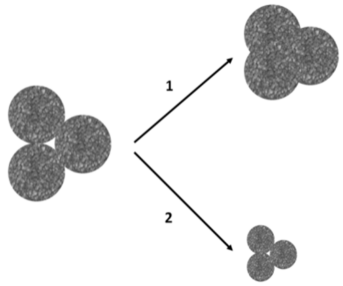

Figure 7.8 – Schematic representation of the two physical phenomena methods proposed by Matsuyama et al.[122]: 1 - collapse of pores due to capillary forces; 2 - densification of the amorphous regions of the film.

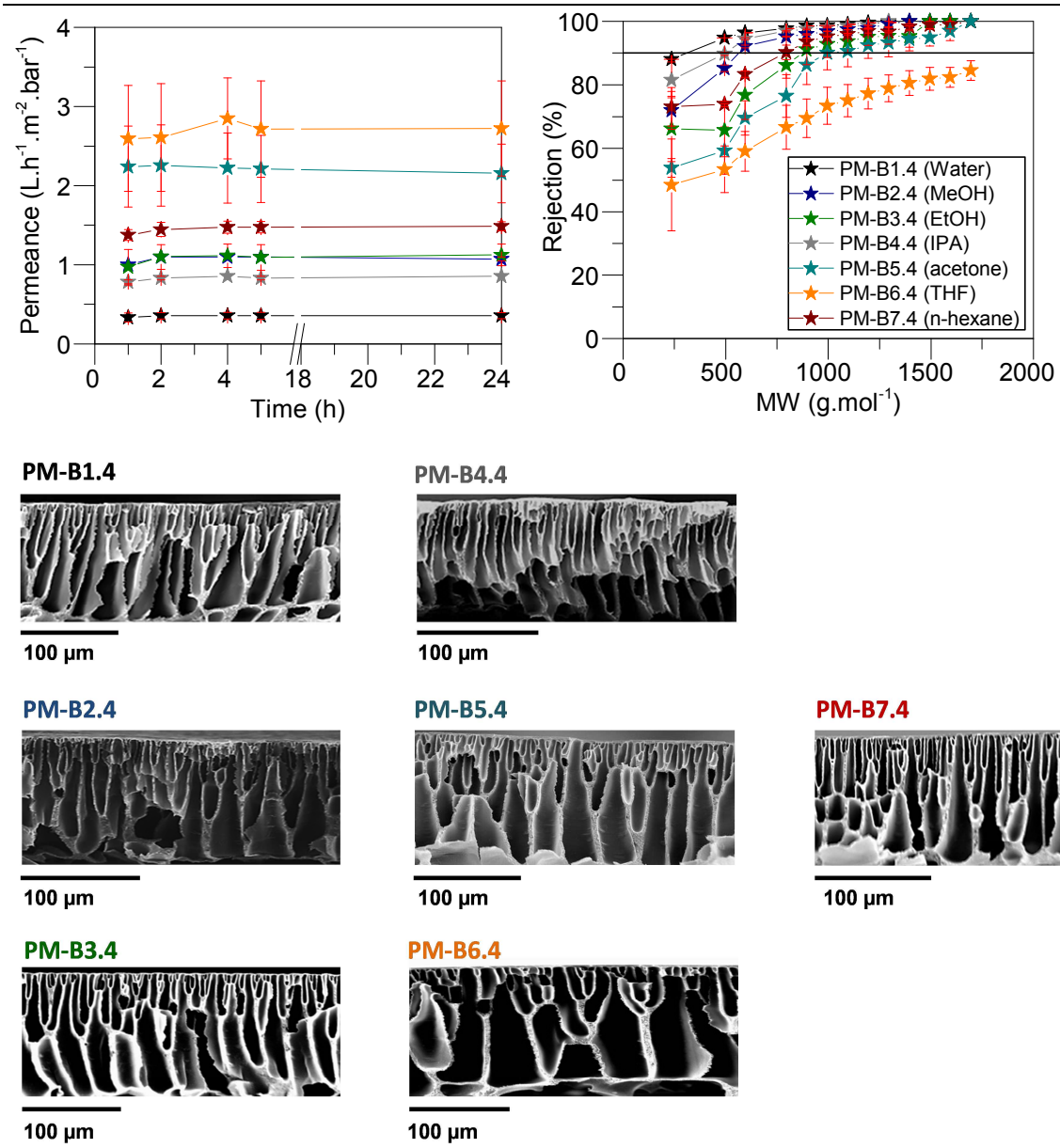

Figure 7.9 – Top left: Permeance values ($L.h^{-1}.m^{-2}.bar^{-1}$) over a period of 24 h for the different membranes under study. Top right: Rejection values of the different PEEK membranes under study as a function of the molecular weight (M_W, $g.mol^{-1}$) of different polystyrenes after 24 hours. Membranes PM-B1.4, PM-B2.4, PM-B3.4, PM-B4.4, PM-B5.4, PM-B6.4 and PM-B7.4 were dried at 120 °C prior to their insertion in the cross-flow cells from water, MeOH, EtOH, IPA, acetone, THF and n-hexane, respectively. The membranes were used to filter with a solution of THF and PS (1 $g.L^{-1}$). The flow-rate, temperature and pressure were set at 100 $L.h^{-1}$, 30 °C and 30 bar, respectively. The red bars represent the standard deviation of the mean. The membranes dried from water, MeOH, EtOH, IPA, acetone, THF and n-hexane at 120 °C are significantly different ($p \leq 0.05$, F-test). Bottom: Cross-section SEM images (magnification 300 ×) of the different membranes under study: PM-B1.4, PM-B2.4, PM-B3.4, PM-B4.4, PM-B5.4, PM-B6.4 and PM-B7.4.

7.3.2 Modelling the post-phase inversion drying process of PEEK nanofiltration membranes

As mentioned before, the drying of PEEK membranes is a very complex phenomenon involving interactions between the solvent and the polymeric membrane as well as mass and

heat transfer mechanisms combined with capillary forces. To date a satisfying phenomenological theory to describe such phenomenon has not been developed.

In order to understand which are the most important solvent properties that affect the drying process, a genetic algorithm was used in this research work to correlate solvent properties with membrane performance (the solvent permeance and the α-methyl styrene dimer flux were used as performance descriptors). The "weight" of each property was computed in order to assess the relevance of the parameters. The membrane performance at 120 °C was chosen for each solvent, since this was characterised by a more pronounced variation of permeance and MWCO (see Figure 7.9). The solvent properties were obtained from literature for 20 °C and no correction of the solvent properties with temperature was implemented. As not all the properties can be easily correlated with temperature, the choice of using all the properties at 20 °C was made to avoid introduction of further sources of error. However, in all fairness, by fixing the temperature to 120 °C the heat transfer contribution might be negligible when computing the model.

The solvent properties were chosen in order to account for heat transfer contribution (vapour pressure), mass transfer contribution (viscosity), capillary forces (surface tension), steric effects (molar volume) and interactions between solvent and polymeric material (Hansen solubility parameter and polarity parameter). Initially, a linear model was used to describe the experimental flux data, with and without constant factor (Equation 2.1). In order to have an overdetermined system, a total of nine solvents was used. In addition to the seven solvents reported in the previous sections, acetonitrile and n-heptane were introduced. Properties and performance results for all these solvents can be found in Table A2 in the Appendix. The regression system is overdetermined, as seven model parameters are regressed from performance data of nine different solvents. In order to evaluate the regression performance of the algorithm certain statistical measures have been proposed. The main measures used in literature are the Mean Absolute Error (MAE), the Mean Absolute Percentage Error (MAPE), the Mean Square Error (MSE) and the Root Mean Square Error (RMSE) [128]. In this work the MAPE (defined below, Equation 7.2) was chosen as a measure of the error.

$$Y_{model}^{S_j} = b_0 + \sum_{i=1}^{n} b_i X_i^{S_j} \qquad \text{Equation 7.1}$$

$$MAPE\ (\%) = \frac{1}{n}\sum_{j=1}^{n}\left|\frac{Y_{exp}^{S_j} - Y_{model}^{S_j}}{Y_{exp}^{S_j}}\right| \times 100 \qquad \text{Equation 7.2}$$

Where $Y_{model}^{S_j}$ is the model prediction for performance (solute flux or permeance) in respect to a given solvent j (j = 1,…,9), $X_i^{S_j}$ the solvent property (i = 1,…,6), b_0 the constant factor, b_i the coefficient associated with each $X_i^{S_j}$ (model coefficient), n the number of solvents studied and $Y_{exp}^{S_j}$ the experimental result for performance (solute flux or permeance) in respect to a given solvent j (j = 1,…,9). In this work, the values of MAPE correspond to the sum of the contribution from permeance and solute flux, i.e., $MAPE_{Total} = MAPE_{permeance} + MAPE_{rejection}$. The coefficients associated with solvent property (b_i) for both solute flux and permeance are presented in Table 7.5 and the experimental data and model fitting are presented in Figure 7.10.

Table 7.5 – Solute flux model coefficients associated with solvent properties.

Coefficient associated with solvent property ($\mathbf{b_i}$)					
		Solute flux		Permeance	
Solvent property	**Symbol**	**Linear model with constant factor**	**Linear model without constant factor**	**Linear model with constant factor**	**Linear model without constant factor**
Constant factor	b_0	123	Not applicable	16.8	Not applicable
Vapour pressure ($\boldsymbol{X_1}$)	b_1	-3.86×10^{-1}	-3.95×10^{-1}	7.47×10^{-3}	3.04×10^{-3}
Surface tension ($\boldsymbol{X_2}$)	b_2	7.31×10^{-1}	2.08	-6.88×10^{-2}	1.16×10^{-1}
Hansen solubility parameter($\boldsymbol{X_3}$)	b_3	-5.00	-12.7	3.55×10^{-1}	-7.14×10^{-1}
Polarity parameter ($\boldsymbol{X_4}$)	b_4	-4.89×10^{-1}	3.06	-3.16×10^{-1}	1.71×10^{-1}
Molar volume ($\boldsymbol{X_5}$)	b_5	-4.76×10^{-1}	-1.45×10^{-1}	-5.18×10^{-2}	4.10×10^{-1}
Viscosity ($\boldsymbol{X_6}$)	b_6	-7.48	-14.4	3.72×10^{-1}	-5.79×10^{-1}

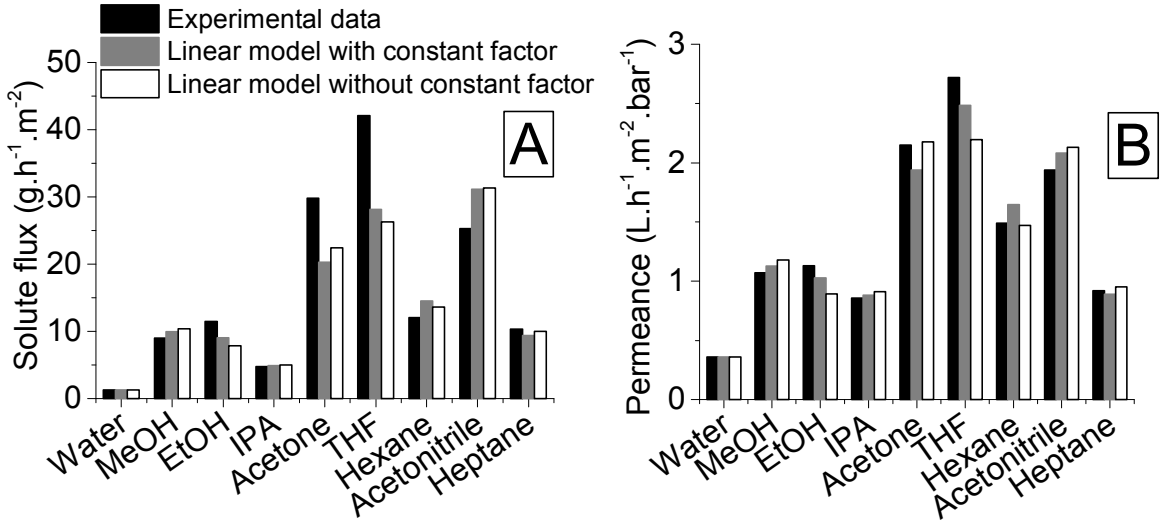

Figure 7.10 – A: Experimental data for solute flux and prediction of solute flux values using linear model with and without constant factor. B: Experimental data for permeance and prediction of permeance values using linear model with and without constant factor.

The MAPE values for linear model with and without constant factor were 9.58 % and 9.80 % respectively. Based on this result, the linear model with constant factor showed the best fitting and it was chosen for assessing the parameter weight (%). The parameter weight (%) was calculated using the equation below and the results are shown in Table 7.6.

$$Parameter\ weight\ (\%) = \frac{\left|b_i X_i^{S_j}\right|}{\sum_{i=0}^{n}\left|b_i X_i^{S_j}\right|}, i = 0, \ldots, 9;\ X_0^{S_j} = 1 \qquad \text{Equation 7.3}$$

Table 7.6 – Parameter weight (%) for both solute flux and permeance using the linear model with constant factor. The sign in brackets indicates if a given solvent property had a negative or positive effect on the overall response.

	Parameter weight (%)	
Solvent property	**Solute flux**	**Permeance**
Vapour pressure	1.91 (-)	0.19 (+)
Surface tension	7.32 (+)	4.54 (-)
Hansen solubility parameter	21.80 (-)	10.14 (+)
Polarity parameter	8.02 (-)	33.89 (-)
Molar volume	13.57 (-)	9.85 (-)
Viscosity	1.96 (-)	0.64 (+)
Constant factor	45.41 (+)	40.70 (+)

The most important parameters are polarity, Hansen solubility parameter and molar volume for both permeance and solute flux. For the solute flux model, all these parameters had a negative effect whereas for the permeance model the Hansen solubilty parameter had a positive effect and both polarity and molar volume had a negative effect. Nevertheless, the constant factor showed higher importance for both models. By carrying on with the three

most important parameters, it was possible to develop a linear model which accounts for single effects as well as interaction effects (Equation 7.4).

$$Y_{model}^{S_j} = b_0 + b_3 X_3^{S_j} + b_4 X_4^{S_j} + b_5 X_5^{S_j} + c_1 X_3^{S_j} X_4^{S_j} + c_2 X_3^{S_j} X_5^{S_j} + c_3 X_4^{S_j} X_5^{S_j} \quad \text{Equation 7.4}$$

c_i denotes coefficients associated with solvent property interactions. The coefficients associated with solvent property (b_i) or with solvent property interactions (c_i) for both solute flux and permeance are presented in Table 7.7 and the experimental data and model fitting are presented in Figure 7.11.

Table 7.7 – Solute flux model coefficients associated with solvent properties and solvent property interactions.

		Coefficient associated with solvent property/ solvent property interaction (b_i or c_i)	
Solvent property/ solvent property interaction	**Symbol**	**Solute flux**	**Permeance**
Constant factor	b_0	473.7	30.4
Hansen solubility parameter($\boldsymbol{X_3}$)	b_3	-3.02×10^{1}	-2.02
Polarity parameter ($\boldsymbol{X_4}$)	b_4	-6.44	-3.99×10^{-1}
Molar volume ($\boldsymbol{X_5}$)	b_5	-1.76	-1.09×10^{-1}
$\boldsymbol{X_3 \times X_4}$	c_1	4.05×10^{-1}	2.76×10^{-2}
$\boldsymbol{X_3 \times X_5}$	c_2	2.83×10^{-1}	1.28×10^{-2}
$\boldsymbol{X_4 \times X_5}$	c_3	-4.02×10^{-2}	-1.42×10^{-3}

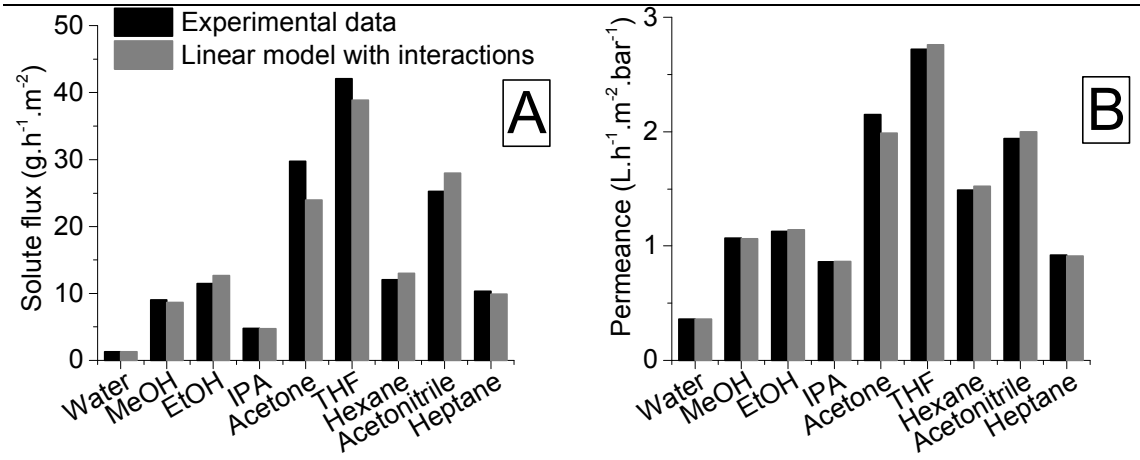

Figure 7.11 – A: Experimental data for solute flux and prediction of solute flux values using linear model with interactions. B: Experimental data for permeance and prediction of permeance values using linear model with interactions.

The regression improved significantly with respect to the model that accounted for single effects only. The MAPE value for linear model with interactions was 1.41 % which was much lower than the one obtained for the linear models without property interactions. This result showed that taking into account the three most important parameters and their interactions improves the fitting, suggesting that the properties were not completely independent of each other. The parameter weight/ solvent property interaction (%) was calculated using Equation 7.3 and the results are shown in Table 7.8.

Table 7.8 – Parameter weight (%) for both solute flux and permeance using the linear model with interactions. The sign in brackets indicates if a given solvent property/ solvent property interaction had a negative or positive effect on the overall response.

	Parameter weight / solvent property interaction (%)	
Solvent property/ solvent property interaction	**Solute flux**	**Permeance**
Constant factor ($\boldsymbol{b_0}$)	26.06 (+)	27.80 (+)
Hansen solubility parameter($\boldsymbol{X_3}$)	19.38 (-)	15.38 (-)
Polarity parameter ($\boldsymbol{X_4}$)	15.62 (-)	15.99 (-)
Molar volume ($\boldsymbol{X_5}$)	7.64 (-)	7.92 (-)
$\boldsymbol{X_3 \times X_4}$	12.40 (+)	13.79 (+)
$\boldsymbol{X_3 \times X_5}$	12.00 (+)	9.09 (+)
$\boldsymbol{X_4 \times X_5}$	6.91 (-)	4.09 (-)

Polarity and Hansen solubility parameter were still the most important parameters but molar volume was surpassed by the interaction between the Hansen solubility parameter and polarity and by the interaction between Hansen solubility parameter and molar volume. The signs of the parameters – which indicates positive or negative effect - were the same for

both solute flux and permeance (sovent flux). This means that both solute and solvent flux were affected in the same way by the solvent properties/ solvent property interaction. These results showed again how important the interactions between solvent properties were in terms of model fitting.

Overall polymer drying is a very complex and not well understood phenomena. Further extensive investigation is required to elucidate and gain a better control over the PEEK nanofiltration membrane properties.

7.3.3 Control of pore collapsing for tuning MWCO using non-volatile solvents

The concept of molecularly imprinted membranes (MIM) studied by Székely *et al*. [129] consists of combining molecular imprinting technology and membrane technology. In this study the authors imprinted PBI membranes with 2-aminopyrimidine by the phase inversion method. Using a similar concept of molecular imprinting, PEEK membranes were impregnated with poly ethylene glycols (PEGs) as non-volatile solvents. This procedure allows for the PEG to remain in the pores and further manipulate the final membrane performance. In order to identify which parameters and their interactions are relevant, a statistical analysis based on Design of Experiments (DoE) was performed. The parameters are presented in Table 7.1. As responses both permeance and dimer rejection were measured.

From analysis of the data (Table A3, Figure A6 and Figure A7 in the Appendix) using the DoE software, it was possible to verify that the most important parameters were the concentration of PEG, the drying temperature and the interactions between these two parameters (for both permeance and rejection of the dimer) (Figure 7.12). Interestingly, the molecular weight of the PEGs did not have a huge impact on the membrane performance. Therefore, a study of PEEK membranes impregnated with different concentrations of PEG 400 (MW = 400 g.mol^{-1}) using IPA as a solvent was performed. All membranes were dried at 20 °C.

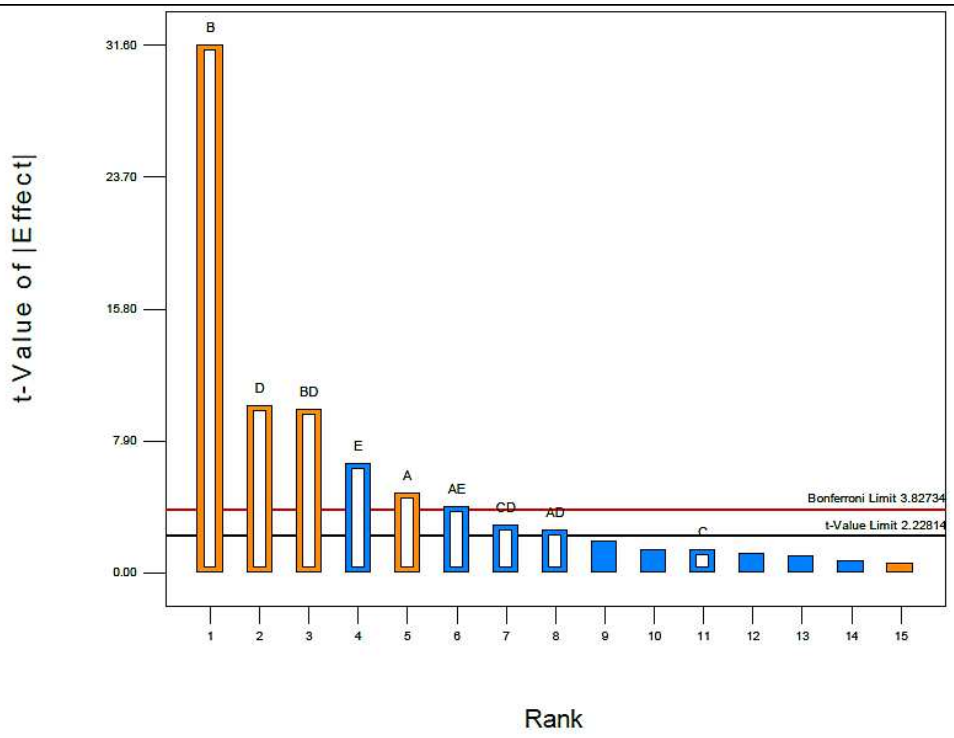

Figure 7.12 – Pareto chart obtained using the Design Expert® software for the five parameters studied in the DoE.

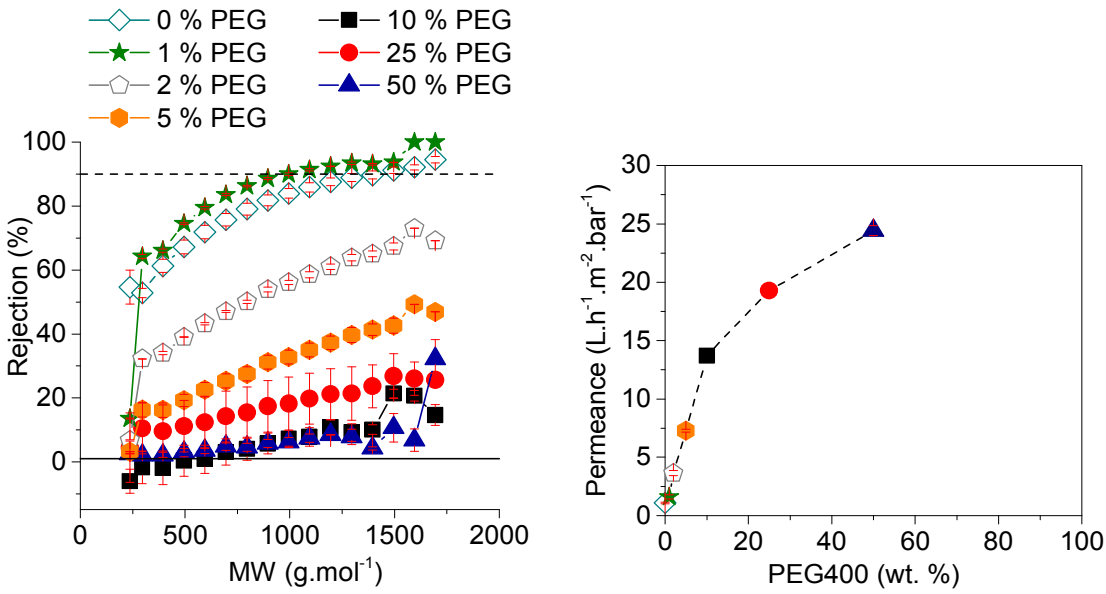

Figure 7.13 – Rejection values (%) (left) and permeance values ($L.h^{-1}.m^{-2}.bar^{-1}$) (right) over a period of 24 h for the PEEK membranes impregnated with different concentrations of PEG 400 (wt. %). The membranes were used to filter with a solution of THF and PS (1 $g.L^{-1}$). The flow-rate, temperature and pressure were set at 100 $L.h^{-1}$, 30 °C and 30 bar, respectively. The red bars represent the standard deviation of the mean.

From Figure 7.13 it was possible to verify that the permeance increased with PEG400 concentration (wt. %). PEEK membranes dried without PEG400 (0 wt. %) had a permeance of 1.09 $L.h^{-1}.m^{-2}.bar^{-1}$ whereas PEEK membranes dried from a 50 wt. % PEG400 had a permeance of 24.4 $L.h^{-1}.m^{-2}.bar^{-1}$ (22 times increase in permeance). Accordingly, the

rejection decreased with the increase in the PEG concentration. The membranes with 10 wt. % PEG400, 20 wt. % PEG400 and 50 wt. % PEG400 had similar rejection which can be explained by the fact that after 10 wt. % the membranes might have similar rejections (close to 0 %) in the nanofiltration range. This short study shows that it is also possible to further manipulate the membrane properties after phase inversion by impregnating with a non-volatile solvent like PEG.

7.4 Conclusions

The post-fabrication drying process of PEEK membranes was found to be the reason for variation in the separation performance from the ultra to nanofiltration range. Two factors were investigated in an attempt to manipulate membrane MWCO: the concentration of polymer in the dope solution and the solvent filling the pores prior to drying. When varying the polymer dope concentration from 8 wt. % to 12 wt. % a shift from more open membranes (8 wt. %) to tighter membranes (10 wt. % and 12 wt. %) was observed. A parallel between dope solution viscosity and membrane performance was drawn in order to explain the difference in performance for different polymer concentrations: the higher the viscosity the tighter the membranes produced. The type of solvent filling the membrane pores prior to drying had a pronounced effect on the separation performance. It was possible to vary the MWCO from 295 $g.mol^{-1}$ to 1400 $g.mol^{-1}$ (in terms of nanofiltration range). Another parameter studied for both factors (polymer concentration and solvent filling prior to drying) was the effect of drying temperature. For membranes dried from water the effect of drying temperature was negligible whereas for membranes dried from other solvents the effect was more pronounced (e.g. acetone and THF). In summary, by increasing the temperature from 20 °C to 120 °C it was possible to further manipulate the MWCO when drying from the same solvent. In addition, it was also shown that it is possible to further manipulate the PEEK membranes by impregnating them with non-volatile solvents like PEG. In order to set some guidance (and understanding) for a phenomenological study of membrane drying a statistical analysis of the presented data was performed in order to assess the relevant solvent properties involved. The Hansen solubility parameter, polarity and their interactions with molar volume were found to be the most important parameters influencing membrane MWCO. Nevertheless, this is just the beginning of a very complex phenomenon that needs to be further pursued in order to be fully understood.

Chapter 8. PEEK nanofiltration membranes under extreme conditions

The work described in this chapter has been submitted for publication in Journal of Membrane Science.

Abstract

The aging of polymeric membranes is still a problem nowadays in industrial applications with a flux decline over time. In this study, the negligible aging of poly(ether-ether-ketone) (PEEK) membranes was shown and compared with crosslinked polybenzimidazole (PBI) and polyimide (PI) membranes. PBI and PI membranes after annealing at 120 °C became brittle and lost all permeance in THF. Annealing PEEK membranes at 20 °C or 120 °C increased the Young's Modulus of elasticity from 61 MPa to 108 MPa and PEEK membranes annealed at 120 °C presented a permeance of ~ 0.2 $L.h^{-1}.m^{-2}.bar^{-1}$ in THF (after 6 h and 24 h of annealing). This result showed a structural change for PBI and PI membranes due to a non-equilibrium glassy state in contrast with PEEK membranes which were in quasi-equilibrium glassy state. High temperature filtrations were also performed in DMF up to 140 °C for the three polymeric membranes. PEEK was the most robust membrane with a stable performance after 4 filtration cycles whereas PBI and PI were stable for 2 and 1 cycles respectively.

8.1 Introduction

Conventional molecular separation processes such as evaporation and distillation require high amounts of energy due to the latent heat of vaporization of liquids [1]. As an alternative, membrane technology has lower energy consumption than conventional separation processes requiring only one-tenth of energy to process an equivalent volume of liquid [2]. On the negative side there are still outstanding issues with membranes performance stability overtime. Most commercially available nanofiltration (NF) (and reverse osmosis (RO)) membranes are either integrally skinned asymmetric (ISA) membranes or thin film composite (TFC) membranes made from glassy polymeric materials that undergo gradual alterations of their characteristics over time, aging, leading to changes in membrane performance [17, 130, 131].

This aging phenomenon occurs from a non-equilibrium excess state towards a stabilized equilibrium state in a time-dependent manner via structural relaxation [132-134]. Usually, aging can be characterized by a gradual decrease in sample volume (densification), which leads to increased brittleness, decreased gas permeability, decreased enthalpy, and

alterations in other properties [134]. Most commercial NF ISA membranes for Organic Solvent Nanofiltration (OSN) exhibit more than 30 % permeance decline over time and the intrinsic solvent permeance of ISA polyimide based membranes is negligible because solvent cast and annealed films of polyimide typically have low or no flux [26].

Since glassy polymers constitute an important group of materials in several high performance applications that operate below (or close to) the glass transition temperature, Tg, materials that show negligible or inexistent aging are therefore required [135]. Microporous polymers with a rigid backbone structure that have poor molecular packing have been proposed [136]. TFC membranes of polyacetylenes and polymers of intrinsic microporosity (PIMs) have been proposed for OSN and given their high free volume high permeance and selectivity are expected. Previous studies have demonstrated polyacetylene poly(1-(trimethylsilyl)-1-propyne) (PTMSP) TFC membranes usability for solvents such as methanol, ethanol and acetone with permeances of 7.7, 4.8 and 17 $L.h^{-1}.m^{-2}.bar^{-1}$, respectively [137, 138]. PIM-1 TFC membranes reported in literature were used for toluene and acetone with low rejection of polyethylene glycols (PEGs) and for n-heptane with rejection of hexaphenylbenzene (HPB) above 90% [139-142]. The highest reported PIM-1 permeance is 18 $L.h^{-1}.m^{-2}.bar^{-1}$ for a 140 nm thick membrane [142].

Even though PIM TFC membranes present higher permeances compared with ISA membranes they are still susceptible to physical aging [143]. To date, stability as well as permeance and rejection data for polar aprotic solvents for PIMs has not been reported. In addition, most filtration data published in literature for both PIM and ISA membranes is performed at room temperature [3]. However, in several industrial applications operating conditions can require working temperatures higher than 90 °C [7, 63, 64].

Although NF membranes are widely used the factors governing their separation, i.e, the physicochemical mechanisms governing solvent and solute transport at the molecular level have not yet been comprehensively elucidated even at ambient temperature [62, 63]. The effect of temperature on permeance and rejection has been studied before but most experimental studies available in literature are performed in aqueous solutions. One of the first studies was performed by Londsdale et al. In this experimental work the authors verified that in the range of 32-50 °C pure water flux increased with the increase of temperature in cellulose acetate membranes [144]. Amar et al. [63] studied the effect of temperature (ranging from 22 to 50 °C) in the transport of water and neutral solutes (glycerin, arabinose, glucose and sucrose) in Desal5DK membranes. The authors verified a decrease in solute rejection and an increase in water flux with the increase in temperature. Sharma et al. performed three studies [145-147] using two commercially available polyamide thin-film composite membranes designated as “DL” (Osmonics) and “TFCS” (Koch Fluid Systems) to investigate changes in water permeability and sieving capabilities of polymeric NF

membranes with temperature in the range of 5–41 °C. For neutral solutes and using a log-normal distribution the authors calculated an increase in the average pore size with temperature, 21% for DL membrane and 12 % for the TFCS membrane. The temperature dependence of neutral solutes for both membranes showed that the rejection of highest and lowest molecular weight solutes was independent of permeate flux at all temperatures. For electrolytes the authors verified an increase in electrolyte permeability as a function of temperature but no rejection data as a function of temperature is presented. Jin et al [148] studied the rejection of humic acid and sodium chloride observing a decrease in rejection in both components when increasing the temperature from 15 to 35 °C. Other studies also demonstrate the same trend for flux and for rejection [149, 150].

The increase in water flux cannot be solely attributed to a decrease in bulk and intrapore viscosity but is connected to membrane structural changes – higher temperature expands the diameter of diffusion pore - and some authors considered it an activated permeation process [63, 146, 151]. Inorganic membranes have the same trend as polymeric membranes and it is known that increased pore sizes cannot be the reason for the decreased rejection with increasing temperature because inorganic membranes show a negligible thermal expansion in the temperature range of 30 – 70 °C [62] [3]. In the study performed by Tsuru et al. titania nanofiltration membranes were used and the rejection of neutral solutes decreased with temperature. However, for electrolytes, the authors verified that rejection was constant in the range of 30-70 °C because the filtration solutions were at pH 3.5 where TiO_2 was positively charged. Other factors such as increase in diffusivity of solutes and higher mass transfer coefficients can also explain this trend in rejection for both inorganic and polymeric membranes.

As mentioned above, the usual tendency for NF is an increase in flux and decrease in rejection with increasing temperature; however, other studies have shown otherwise. Goosen et al. [152] studied the effect of feed temperature on the permeate flux in a spiral-wound module and verified an increase in flux from 20 to 40 °C; nevertheless, at 30 °C the permeate flux went through a minimum. Schaep et al. [153] observed a slight increase of rejection for divalent ions (sulphate, calcium and magnesium) with temperature but a decrease in rejection for monovalent ions (chloride, potassium and sodium) for UTC20 membranes (Toray Industries). Mänttäri et al. [154] found that in general the retention of glucose decreased with the increase of temperature except for the non-temperature resistant membranes (XN40 and NF200) where the retention increased. In the same study, these authors verified that for NF200 membranes the total dissolved carbon (TDC) retention decreased with temperature but rejection of inorganic compounds (such as salts) were temperature-independent. Jian et al. also reported no influence of temperature (< 1 %) in the rejection of dyes (MW 600 – 900 Da) for poly (phthalazine ether sulfone ketone) (PPESK)

membranes in the temperature range of 20-70 °C [155]. In another study, Han et al. [156] observed an increase in water flux while the rejection for 1000 $mg.L^{-1}$ Na_2SO_4 solution only had a slight decrease when increasing the temperature from 20 to 90 °C (the authors used sulphonated poly(phthalazinone ether sulphone)/poly(phthalazinone ether sulphone) (SPPES/PPES) membranes).

In terms of OSN, Siddique et al. [8] performed filtrations at different temperatures (30 °C, 50 °C, 80 °C and 100 °C) using DMF as the solvent and polystyrene (PS) as the markers for a period of 6 hours at 30 bar using an APTMS (3-Aminopropyl trimethoxysilane) crosslinked P-84 polyimide (PI). In this study the authors found no difference in rejection for the different temperatures studied but an increase in permeance with the temperature from 0.02 $L.h^{-1}.m^{-2}.bar^{-1}$ to 0.17 $L.h^{-1}.m^{-2}.bar^{-1}$.

PEEK can fill the gap for both non-aging membranes and for high-temperature resistant OSN membranes. Membranes produced from this material possess inherent intrinsic permeance i.e. the membranes do not collapse completely when dried in air and do not become brittle (hence no need for pore preserving agent) [10, 157]. In contrast the intrinsic solvent permeance of ISA polyimide based membranes is negligible because solvent cast and annealed films of polyimide typically have low or no flux [26]. PEEK membranes also exhibit strong chemical resistance to bases and stability at 85-90 °C [44, 45, 47, 117, 158] without requiring crosslinking [157] and they are chemically inert towards catalysts [9].

In this chapter, the negligible aging of PEEK NF membranes annealed at 120 °C for different time periods using THF permeance measurements is presented. The performance of PEEK NF membranes is also shown for filtrations with N,N-dimethylformamide (DMF) up to a maximum temperature of 140 °C. PEEK showed a high stability when filtered with DMF at 140 °C (close to its glass transition temperature) for a period of four heating cycles. As a comparison, commercial crosslinked PI based membrane Duramem® 300 and crosslinked polybenzimidazole (PBI) 22 wt. % membrane were also filtered with DMF but their stability proved to be inferior as that of PEEK.

8.2 Methods

8.2.1 Materials

2,4-Diphenyl-4-methyl-1-pentene (α-methylstyrene dimer), methanesulphonic acid (MSA) and α,α'-dibromo-p-xylene (DBX) and 2-methyltetrahydrofuran were obtained from Sigma-Aldrich. N,N-Dimethylformamide (DMF), N-Methyl-2-pyrrolidone (NMP), Dimethylacetamide (DMAc), toluene, tetrahydrofuran (THF), propan-2-ol (IPA), sulphuric acid (SA) 95 vol.% and polyethylene glycol (PEG) 400 were obtained from VWR UK. VESTAKEEP® 4000P was kindly obtained from Evonik Industries UK. Celazole® S26 polybenzimidazole (PBI, MW=27,000 g mol^{-1}) solution was purchased from PBI Performance Products Inc. (USA).

The styrene oligomers standards with a molecular weight distribution of 580 (PS580) and 1300 (PS1300) were obtained from Agilent Technologies Deutschland GmbH, Germany. All reagents were used as received without any further purification.

8.2.2 Membranes

Two commercially available polyimide-based membranes, Puramem 280 (non-crosslinked) and DuraMem® 300 (crosslinked), were obtained from Evonik. PEEK membranes 12 wt. % dried from water at 120 °C were prepared according to the method described in 7.2.2 and [10]. Polybenzimidazole (PBI) membranes 22 wt. % crosslinked with dibromoxylene (DBX) were prepared according to the protocol described in [103].

8.2.3 Polystyrene markers solution and analysis

The polystyrene standard solution was prepared using the method described in section 4.3.3.9 (Chapter 4). Permeate and retentate samples were collected at different time intervals for rejection determination. Concentrations of PS in permeate and retentate samples were analysed using the method described in section 4.3.3.9 (Chapter 4) and [6].

8.2.4 Membrane performance

The flux (J) and permeance (L_P) were determined using Equation 2.1 and Equation 2.2 and the rejection (R_i) of PS was evaluated applying Equation 2.3. The corresponding MWCO curves were obtained from a plot of the rejection of PS versus their molecular weight.

To study the effect of annealing temperature, a rig with an effective membrane area of 0.07 cm^2 was used. A Gilson HPLC pump (Model 305) provided the flow, set at 5 $mL.min^{-1}$. The pressure of the filtration unit, 30 bar, was controlled using a back-pressure regulator. The feed tank volume was 20 mL, and the volume of the filtration unit plus the associated tubing was approximately 5 mL.

The oxygen permeation was performed with a simple system where an oxygen cylinder is connected to a one-way valve and followed by a pressure gauge and the membrane chamber (Chamber total volume = 1.622×10^{-4} m^3 and effective membrane area = 2.5×10^{-4} m^2). Initially, the whole system was pressurized to ~ 4.1 bar and the one-way valve was disconnected thereafter (passive pressure). From this point onwards the pressure drop is recorded over time using LabView.

For the high temperature filtrations, a rig consisting of two cross-flow cells (effective membrane area = 51 cm^2 each) in parallel was used (see Figure 8.1). In both cross-flow cells, a Gilson HPLC pump (Model 305) provided the flow, set at 9 $mL.min^{-1}$. The pressure of each cell was controlled using a back-pressure regulator, and a magnetic stirrer was placed inside each cell (stirred at 500 rpm) to maintain a constant hydrodynamic profile. The feed

tank volume was 200 mL, and the volume of each cell plus the associated tubing was approximately 100 mL.

Polystyrene standard in THF solution was poured into the feed reservoir and the system was pressurized to 30 bar and the temperature set at 30 °C. For each of the solvents the maximum operating temperature was set to be at 10 degrees below the boiling point of the corresponding solvent. Each temperature was set constant for 24 h prior to change and at the end of the temperature cycle the system was cooled down to 30 °C (see Figure 8.1). Each experiment was repeated in parallel using membrane coupons obtained from different dope solutions. Data are presented as means ± standard deviation of the mean (SDM).

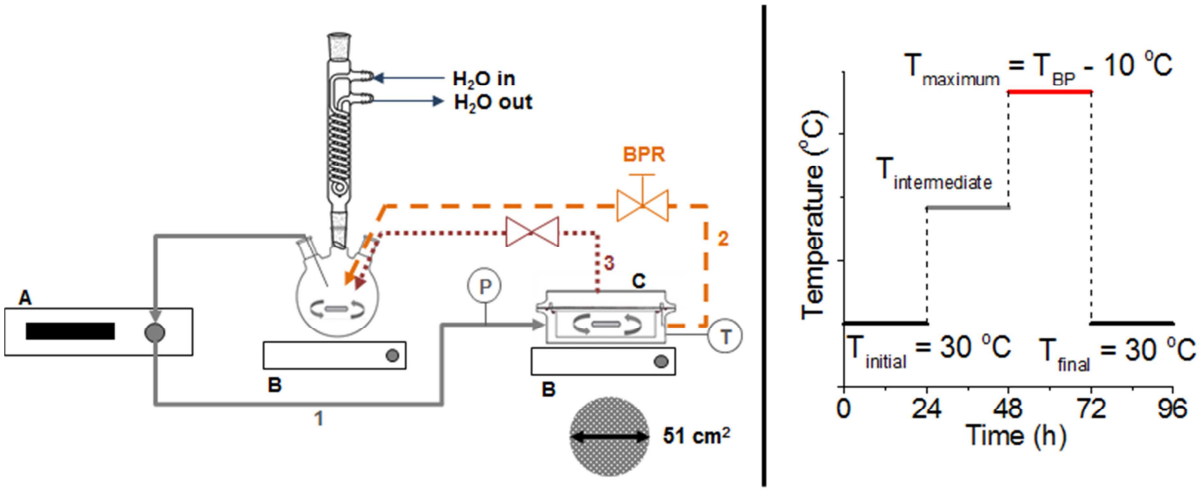

Figure 8.1 – Left: Schematic representation of the high temperature cross-flow rig used in this study. Legend: 1: Feed inlet stream; 2: retentate stream; 3: permeate stream; A: HPLC pump; B: hot stirring plate; C: cross-flow cell; P: pressure gauge; T: thermocouple; BPR: back pressure regulator. Note: only one cross-flow is depicted. Right - Schematic representation of the temperature cycles as a function of time.

8.3 Membrane characterization

8.3.1 Scanning Electron Microscopy SEM

For cross-section imaging a membrane sample without non-woven support was broken in liquid nitrogen and pasted vertically onto SEM stubs covered with carbon tape. For surface imaging a membrane sample was cut and pasted horizontally onto SEM stubs covered with carbon tape. The samples were then coated with a chromium-layer in a Q150T turbo - pumped sputter coater (Quorum Technologies Ltd.). SEM pictures of the surface and cross section of membrane samples were recorded using a high resolution SEM, LEO 1525, Karl Zeiss with an accelerating voltage of 5 kV and under dry conditions at room temperature.

8.3.2 Measurement of tensile strength

The mechanical properties of the prepared PEEK membranes annealed at 20 °C, 120 °C and 190 °C were measured by an EZ50 (LLOYD Instruments) at room temperature. Strips

20 mm wide and 50 mm long were cut from the prepared membranes for tensile tests. Tensile tests were performed at a speed of 5 mm.min^{-1} with a 1000 N sensor loaded. Tensile strength was calculated from the maximum recorded stress at the breaking point, and the tensile modulus was evaluated from the initial slope of the stress–strain curves. For all samples, the non-woven support material was removed prior any mechanical testing.

8.3.3 Differential scanning calorimetry (DSC)

A DSC TA Q2000 was used for DSC measurements. Heating scans were performed at 10 °C.min^{-1} from 30 °C to 500 °C but in order to detect the glass transition temperature slower heating rates of 2 °C.min^{-1} were used around that region. The samples were analysed under 50 mL nitrogen and 50 mL helium gas flow. The temperature and fusion heat were calibrated using indium and tin standards. For all samples, the non-woven support material was removed prior any mechanical testing.

8.3.4 Measurement of Brunauer–Emmett–Teller (BET) surface area

N_2 adsorption measurements were carried out in a 3Flex Surface Characterization Analyzer (Micromeritics Instrument Corporation) to determine BET surface area of PEEK, PBI and PI membranes annealed at 120 °C for 24 h and degassed under vacuum. For all samples, the non-woven support material was removed prior any mechanical testing.

8.4 Theoretical analysis of results (pore size probability function)

In line with what has been used by other authors in this field it was adopted the log-normal probability density function. The density function has an advantage over the Gaussian distribution, being only defined for positive values of the pore diameter ($0<d_p<\infty$) [75]. Most authors use the definition proposed by Belfort et al. [159] and latter reviewed and recommended by Zydney et al.[160]. The log-normal distribution is as follows:

$$f_R(d_p) = \frac{1}{d_p\sqrt{2\pi b}} exp\left[-\frac{\left(\left[\log\frac{d_p}{\bar{d}_p}\right]+\frac{b}{2}\right)^2}{2b}\right] \qquad \text{Equation 8.1}$$

$$b = log\left[1+\left(\frac{\sigma}{\bar{d}_p}\right)^2\right] \qquad \text{Equation 8.2}$$

In order to estimate mean pore size $(\bar{d}_p)$ and standard deviation (σ) a fitting of experimental rejection data to the log normal distribution is performed. However, given that this approach lacks a physical basis, more recent research considers the underlying phenomena and utilises the hydrodynamic model of hindered solute transport in pores in estimating $\bar{d}_p$and σ. In this work this approached is adopted. The starting point for this model

is the extended Nernst–Planck equation for the transport of charged solutes but for the scope of this paper the formulas will not be deduced. From the Nernst-Planck equation an expression for rejection as a function of pore size can be obtained and is as follows:

$$R_i = 1 - \frac{\phi(k_c + Y)}{1 - [1 - \phi(k_c + Y)]e^{-Pe}} \qquad \text{Equation 8.3}$$

The terms Y and Pe are, respectively, a dimensionless solute function (independent of solute concentration) and the Peclet number and can be calculated according to Equation 8.4 and Equation 8.5.

$$Y = \frac{32\mu k_d D_{i,\infty} \upsilon}{RT d_p^2} \qquad \text{Equation 8.4}$$

$$Pe = \frac{(k_c + Y) d_p^2}{32\mu k_d D_{i,\infty}} \qquad \text{Equation 8.5}$$

Where μ is viscosity, $D_{i,\infty}$is the diffusion coefficients of the solutes in the bulk solvent, υ the molar volume of the solvent and d_p is the pore diameter. The convective and diffusive hindrance factors (k_c and k_d) can be defined as:

$$k_c = \frac{u}{u_w} \qquad \text{Equation 8.6}$$

$$k_d = \frac{D_p}{D_{i,\infty}} \qquad \text{Equation 8.7}$$

Where u is the solute speed in the pore, u_w average solvent speed and D_p the solute diffusion coefficient in the pore. These hydrodynamic drag coefficients can be correlated with the solute to pore radii fraction, λ (Equation 8.8 to Equation 8.10).

$$\lambda = \frac{d_i}{d_p} \qquad \text{Equation 8.8}$$

$$k_c = A + B\lambda + C\lambda^2 + D\lambda^3 \qquad \text{Equation 8.9}$$

$$k_d = E + F\lambda + G\lambda^2 + H\lambda^3 \qquad \text{Equation 8.10}$$

The values of the constants are presented in Table 8.1 [161] and are a result of detailed studies from Deen [162] and Bowen et al. [163] and [164].

Table 8.1 – Values of the constants for Equation 8.9and Equation 8.10 for λ between 0 and 0.8 and λ between 0.8 and 1 [161].

Constant	0<λ≤0.8	0.8<λ≤1
A	1.0	−6.830
B	0.054	19.348
C	−0.988	−12.518
D	0.441	0
E	1.0	−0.105
F	−2.30	0.318
G	1.154	−0.213
H	0.224	0

These equations are valid for cylindrical pores with velocity profiles not completely developed. When the pores are relatively narrow and long, these profiles should in fact be totally developed and k_c should be multiplied by $(2 - \Phi)$ with Φ corresponding to the solubility equilibrium at the interfaces (Equation 8.11).

$$\phi = (1 - \lambda)^2 \qquad \text{Equation 8.11}$$

The solute diameters (d_i) were determined by the Stokes–Einstein equation:

$$d_i = \frac{kT}{3\pi\mu_0 D_{i,\infty}} \qquad \text{Equation 8.12}$$

The diffusion coefficients of the solutes in the bulk solvent were determined by the Wilke–Chang equation [77] (Equation 8.13), where the solute molar volume (V_i) at the boiling point was determined using a group contribution method as presented by Zhao et al. [165]. In cases where the pore diameters are significantly small and similar to the solvent diameter ($d_p \approx d_{solv}$), pore viscosities need to be corrected since they are significantly higher than the bulk values (μ_0) [76] (Equation 8.14). This variation of viscosity was subject to the condition that $\eta = 10\eta_0$ when $d_p < 0.46\ nm$ [75].

$$D_{i,\infty} = \frac{1.173 \times 10^{-16}(\varphi M_i)^{0.5} T}{\mu_0 V_i^{0.6}} \qquad \text{Equation 8.13}$$

$$\frac{\mu}{\mu_0} = 1 + 18\left(\frac{d_{solv}}{d_p}\right) - 9\left(\frac{d_{solv}}{d_p}\right)^2 \qquad \text{Equation 8.14}$$

For certain broad pore size distributions, it is expected that the 'tail' of large pores will affect the overall rejection due to the d_p^4 averaging of porewise rejection, $R_i^{calc}(d_p)$. It is suggested in literature that the distribution has to be truncated to neglect the effect of the 'tail' of large pores [75]. However, it is still desirable for the new distribution to be shaped like

the log-normal distribution for those pores which contribute the overwhelming majority of the distribution. The total area under the predicted curve is computed using the trapezium rule. The new distribution function (f_R') is defined in Equation 8.15 and it is subject to the limiting case that $f_R' = f_R'$ as $r_{max} \to \infty$. The overall rejection is then calculated using the new distribution (Equation 8.16).

$$\frac{f_R'}{f_R} = \frac{1}{\int_0^{d_{pmax}} f_R d(d_p)} \qquad \text{Equation 8.15}$$

$$R_i^{calc} = \frac{\int_0^{d_{pmax}} \frac{f_R' d_p^4 R_i}{\mu} d(d_p)}{\int_0^{d_{pmax}} \frac{f_R' d_p^4}{\mu} d(d_p)} \qquad \text{Equation 8.16}$$

By introducing a truncated distribution a new parameter is required in any calculation, namely $d_{p_{max}}$. Since there is limited available data on pore size distributions for NF membranes and current evidence suggests that pore diameter greater than twice the mean are uncommon, the upper limit set for the calculations was $d_{p_{max}} = 2\bar{d}_p$.

8.5 Results and discussion

8.5.1 Non-aging of PEEK NF membranes

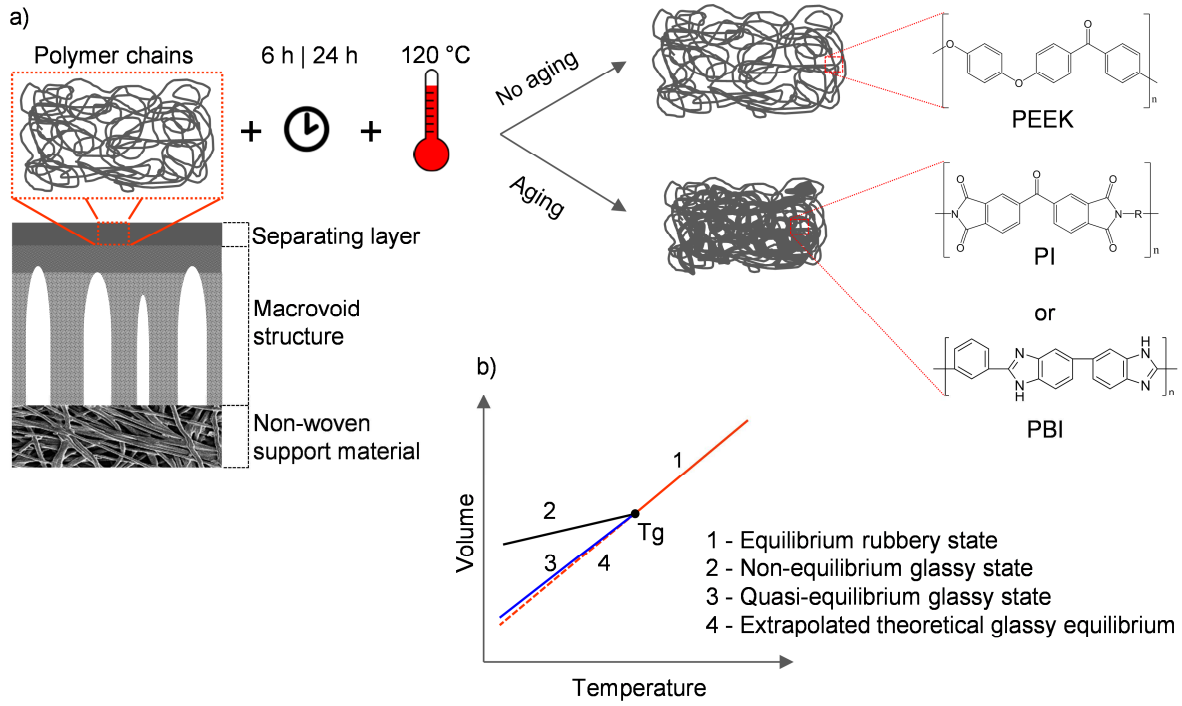

Figure 8.2 – a) Schematic of the effect of time and temperature in the polymer chains of ISA membranes. PEEK polymer chains show no signs of aging, in contrast with PI and PBI which undergo significant aging. b) Qualitative volume vs. temperature diagram for a glass-forming polymer depicting the equilibrium rubbery and glassy states as well as the quasi and no-equilibrium glassy states.

Typically polymer aging below the glass transition temperature (Tg) is a slow process and equilibrium might not be achieved on experimentally-accessible timescales [166]. One way to accelerate this process is to increase the temperature (thermal annealing). Figure 8.2 a) sketches the procedure adopted to test the aging of PEEK membranes. In addition to PEEK membranes, PBI 22 wt. % and PI (DuraMem® 300) based membranes were also tested for comparison. All membranes were immersed in water without addition of impregnating agents (such as PEG). The procedure simply consisted in annealing (air drying) at 120 °C for a period of 6 h or 24 h. It is hypothesised that PEEK membranes are in a quasi-equilibrium glassy state whereas PBI and PI membranes are in a non-equilibrium state (Figure 8.2 b)). This means that with time there is a tendency of the polymeric material towards the theoretical glassy equilibrium and as a consequence a decrease in free volume. However, aging can be a slow process and equilibrium might not be achieved on experimentally-accessible timescales [166]. One way to accelerate this process is to increase the temperature. The chosen temperature of 120 °C for annealing was a compromise between the glass transition temperature (Tg) of PEEK (146 °C [167]) and the melting point of the polypropylene, ~ 160 °C [168]. Both PI and PBI have much higher Tg of 330 °C and 427 °C,

respectively [2, 97]. It is important to mention that PBI, PEEK and PI membranes were in different initial states in terms of membrane structure and pore size. Ideally, a comparison between these membranes should have been performed with the same symmetric structure and with similar initial pore size. Dynamic scanning calorimetry (DSC) was performed for the different membranes annealed for 6 h, 24 h and 48 h hours in an attempt to verify the existence of physical aging according to the enthalpy recovery method [169] (see Figures A8 to A10 in the Appendix). The results are somewhat inconclusive. For PEEK and PI there seems to be a slight shift of Tg to higher values when increasing the annealing time, as may be expected but no enthalpy recovery peak can be observed. This could be due to the fact that the DSC analysis measures the bulk properties of the material while the aging may be occurring only in the thin separating layer of the membrane and its thermal contribution is diminished. A typical cold crystallisation peak was observed on all PEEK thermograms at ~ 160 °C associated with reorganisation of the crystalline regions. The area of the peak is getting smaller with the annealing time suggesting crystal relaxation to a more stable configuration [170]. For PBI even the Tg was difficult to determine due to its high value.

Once dried, the PBI and PI membranes undergo a molecular rearrangement that macroscopically manifests itself in brittleness. On the contrary, the PEEK membranes can be dried at temperatures up to 120 °C without any preserving agent and still maintain their structural integrity. Figure 8.3 a) shows the fractures produced in PI and PBI after annealing due to densification of the polymer matrix which leads to reduced mobility of the polymer chains. This reduced mobility causes the amorphous regions to behave more like crystalline regions thus decreasing the permeance of the membrane. In the case of PEEK membranes it is known that PEEK does not pack efficiently and it is manifested in a maximum achievable crystallinity of less than 50 % [171]. Therefore, its free volume does not decrease in the same extent as PI and PBI. In other words PEEK is less prone to physical aging. One reason for this could be the unusual uniplanar growth of PEEK lamellae in thin films - single-crystal-like, uniplanar orientation of lamellae essentially on edge. This results in formation of “ordered” spherulites (see Figure 8.4) which would probably pack inefficiently. The amorphous phase trapped within these spherules would be rather immobilized and hardly susceptible to aging but still may serve as a permeation channels within the membrane structure. Reasons for this extraordinary growth of PEEK lamellae in thin films are possibly related to its chain conformation, which would impart an unusually anisometric cross section to its molecules [172]. Similar unusual "fibrillar" but very narrow lamellar crystals of 20-40 nm in width and 10-15 nm in thickness have been observed by other researchers [173].

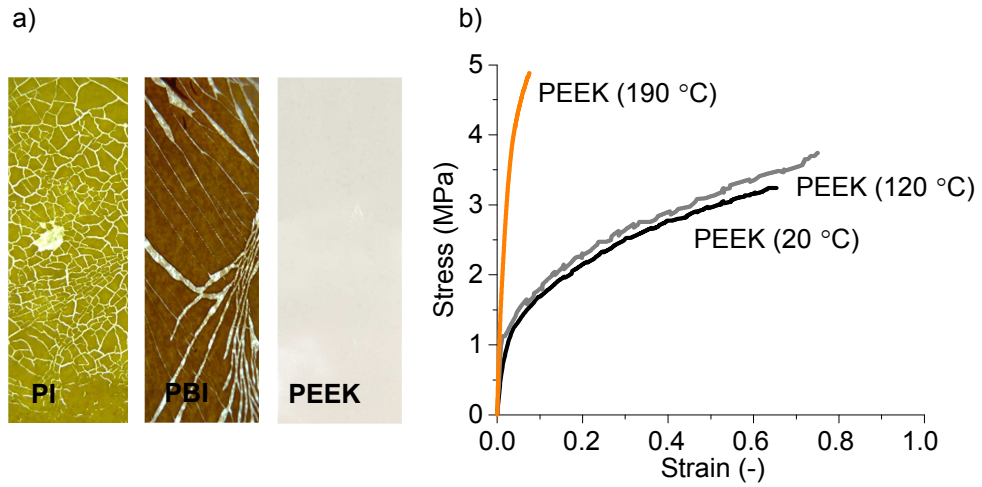

Figure 8.3 – a) Photographs of PI, PBI and PEEK membranes after annealing at 120 °C depicting the fractures for both PI and PBI membranes. b) Stress–strain curves of PEEK membranes obtained at 20 °C illustrating the effect of annealing temperature (20 °C, 120 °C and 190 °C) on the tensile properties of the membranes.

Other studies also suggest that for semirigid para-linked aromatic polymers such as poly(ether-ether-ketone) (PEEK, poly(oxy-1,4-phenyleneoxy- 1,4-phenylenecarbonyl-1,4-phenylene)) or poly- (ethylene terephthalate) (PET), there are indications for strong interactions between amorphous and crystalline regions. The presence of crystalline regions impacts dramatically the glass transition temperature (*T*g), the glass and subglass relaxation characteristics of amorphous regions, and the ability of amorphous regions to undergo physical aging. In this case, a majority of amorphous regions in the semicrystalline structure become perturbed, or constrained, upon crystallization a so-called “rigid amorphous phase”. Interestingly, a reverse influence of amorphous regions on some properties of crystalline regions, such as crystal thermal expansion can also be observed for these polymers [174].

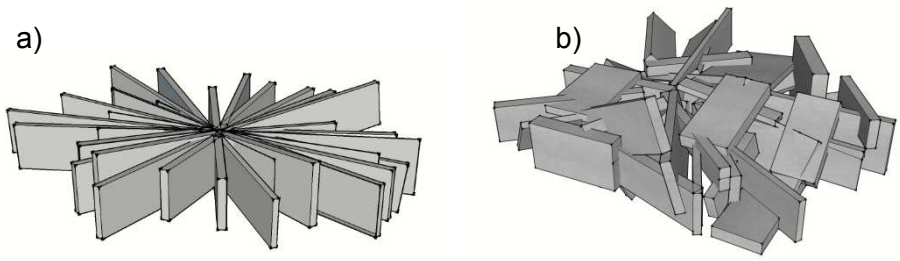

Figure 8.4 – Highly schematic representations of thin film spherulites in a) PEEK and b) more typical polymers. Adapted from Lovinger and Davis [172].

Positron annihilation studies of PEEK suggest that the average free volume size of the polymer is within the range 80 $Å^3$ (assuming spherical shape that is a diameter of 5.35 Å) and does not change substantially upon annealing (after annealing for 1h at 160 °C the average size of free volume decreased from 80 to 78 $Å^3$ and the reduction in the free-volume fraction was only 20 %). These results are in agreement with the hypothesis of negligible (or

very slow) aging of PEEK [175]. Slightly lower average free volume size 69.7± 2.2 $Å^3$ (5.10 ± 1.6 Å diameter) has been determined for PEEK samples prepared by melt extrusion at 370 °C [176].

In contrast, PALS studies of PBI films annealed at 200 °C for 12 h have revealed an average free volume size of 49.6 $Å^3$ (corresponding to diameter of 4.56 Å) suggesting tighter polymer packing than PEEK [177]. Other studies also suggest very tight chain packing in PBI that could be attributed to the presence of H-bonding in PBI that brings chains closer [178]. Although the produced PBI polymer is crosslinked the trend would still remain.

PEEK membranes were annealed at 20 °C, 120 °C (air dried) and 190 °C (dried under vacuum) in order to assess the effect of temperature on the tensile strength. PBI and PI were not tested in terms of tensile strength (stress-strain curve) because of their brittleness. The Young's Modulus of elasticity increased with temperature for PEEK membranes and values of 61 MPa, 108 MPa and 170 MPa were obtained for 20 °C, 120 °C and 190 °C respectively. The maximum strain attained at 190 °C is much lower, 7.5 %, than the strain values obtained at 20 and 120 °C, 65 % and 75 % respectively. The break point (maximum stress) is similar at 20 °C and 120 °C, 3.2 MPa and 3.7 MPa respectively, but increased at 190 °C to a value of 4.88 MPa. Even when annealing at 190 °C (above Tg in order to erase any thermal history of the polymer) it was possible to observe the mechanical integrity of the membrane although with lower strain than the one at 120 °C (the membrane was less elastic). This further enhances the fact that PEEK does not pack efficiently as the amorphous regions cannot move freely within the crystalline regions. Therefore, structural relaxation and consequent polymer matrix densification are phenomena that did not occur to such a great extent, as the polymer was close to its equilibrium packing once solvent was removed after annealing.

Although macroscopic properties have been assessed, it was necessary to understand the implications of this phenomenon at a molecular level. Given that membranes are used for separation of solutes, it is essential to investigate the changes occurring in the separating layer of the membranes which in general represents 0.1 % of the overall membrane volume (for ISA membranes). According to literature, the surface of a polymer film has enhanced mobility at the free surface (the separating layer) and attractive substrate-polymer interactions (reduced chain mobility is thought to happen near the substrate-polymer interface) [179, 180]. If a polymer is not in an equilibrium state it is more prone to have polymer rearrangements in the separating layer.

The membranes were tested in a filtration unit with an area of 0.07 cm^2 because only small areas could be obtained given the brittleness of PBI and PI membranes after annealing. For that reason it was necessary to handle the membrane coupons with extreme

care in order to test their performance in THF using polystyrene (PS) as solutes. After 24 h of annealing at 20 °C it was possible to verify that PI and PBI lost THF permeance and the same was observed for 6 h (data not shown) and 24 h of annealing at 120 °C. PEEK membranes retained the same THF permeance as expected from previous published data, ~ 0.2 $L.h^{-1}.m^{-2}.bar^{-1}$, after 24 h of annealing at 20 °C and after 6 h (data not shown) and 24 h of annealing at 120 °C (Table 8.2). The same trend was observed for oxygen permeation with negligible pressure drop (during a period of 18 hours) for PBI and PI membranes annealed at 120 °C for 24 h (see Figure A11). However, from the N_2 BET surface area it is evident that a correlation between membrane liquid permeance and gas adsorption cannot be established. The membranes with higher BET surface area were PBI and PI, 450 $m^2.g^{-1}$ and 93 $m^2.g^{-1}$ respectively whereas PEEK showed a low BET surface area of 42 $m^2.g^{-1}$ (Table 8.2). This result implies that a high BET surface area does not necessarily correspond to high liquid permeance (or even to any permeance at all). The N_2 BET surface area is a function of the amount of N_2 adsorbed and therefore is dependent on the diffusivity of N_2 in a specific material. N_2 has a very low diffusion coefficient in PEEK [181] and the measurement is performed at 77 K which means the polymer is in a frozen state where not all voids can be accessed. As mentioned before, the separating layer accounts for a very small percentage of the overall membrane and is expected to present minimal contribution toward the BET area. Therefore, molecular rearrangements in the separation layer would not be detected by BET measurement. BET isotherms of the membranes are shown in Figure S4.

Table 8.2 – Permeance ($L.h^{-1}.m^{-2}.bar^{-1}$) in THF with polystyrene (PS) standards (nominal Mp of 580 Da and 1.3 kDa) as solute markers (concentration = 1 $g.L^{-1}$) for PEEK, PBI and PI membranes annealed at 20 °C and 120 °C for 24 h. N_2 BET surface area (fitting performed for partial pressures between 0.05 and 0.35) for PEEK, PBI and PI membranes annealed at 120 °C for 24 h.

	THF permeance @ 30°C [$L.h^{-1}.m^{-2}.bar^{-1}$]		
Sample name	Annealing at 20 °C for 24 h	Annealing at 120 °C for 24 h	BET surface area [$m^2.g^{-1}$]
PBI 22 wt.% crosslinked DBX	n.m.	n.m.	450 ± 2
PEEK	0.2 ± 0.03	0.2 ± 0.04	42.3 ± 0.1
DuraMem® 300	n.m.	n.m.	93.4 ± 0.8

n.m. – Not measurable

8.5.2 High temperature performance for different OSN membranes

In this section it is described the performance of PEEK, PBI 22 wt. % crosslinked with dibromoxylene (DBX) and Duramem® 300 (PI based) membranes according to the operating temperature in terms of permeance and PS rejection. The experiments were conducted by performing consecutive temperature cycles. The maximum temperature (T_{max}) reached was 140 °C (10 °C below the boiling point of DMF) as shown in Figure 8.1.

For PEEK membranes an increase of permeance of 4.2 fold and 19.3 fold was observed for 85 °C and 140 °C respectively (initial 30 °C as reference). For PBI, the increase was less pronounced, 3 fold and 2.4 fold for 85 °C and 140 °C respectively. However, this fact cannot be explained solely by the decrease in viscosity as can be seen in Figure 8.5 e) when comparing experimental values of permeance with initial permeance corrected with viscosity using simple pore-flow model (Equation 8.17). This means that there were structural changes to the membrane active layer as strongly supported by the fact that the final performance at 30 °C is different from the initial performance at 30 °C. The large increase in PEEK membrane permeance at 140 °C could be expected since this is very close to the Tg of this polymer. However, it is important to emphasize that other factors are playing a role when filtering solvents at higher temperatures such as the real intrapore viscosity, changes in the membrane morphology and the sorption/desorption phenomenon associated with the transport mechanism [3, 7, 63, 145, 146, 182]. To understand the extent of the contribution of viscosity, Equation 8.17 calculates a permeance at temperature T (L_T) based on the permeance at 30 °C (L_{30}), and adjusting for the viscosity as shown below:

$$L_T = L_{30}.\frac{\mu_{30}}{\mu_T} \qquad \text{Equation 8.17}$$

The PI membranes permeance decreased by a factor of 5.7 at 85 °C and at 140 °C the membranes virtually degraded. This membrane degradation can be explained by the crosslinking chain scission at higher temperatures where the activation energy can be reached. After chain scission the membrane becomes soluble in DMF.

In order to test the PI membrane stability without crosslinking, a PuraMem® 280 was filtered using toluene as solvent. The membrane had a lower initial performance at 30 °C than what was expected but from the experiment performed it was possible to verify a decline in performance (decline in permeance) with the temperature (Figure A13). Possibly, the initial lower performance was related to trace amounts of DMF in the system (even though it was thoroughly clean). Therefore, it was not possible to assess if the PI membrane itself was temperature resistant; but nevertheless the permeance decline suggests membrane structure densification (aging).

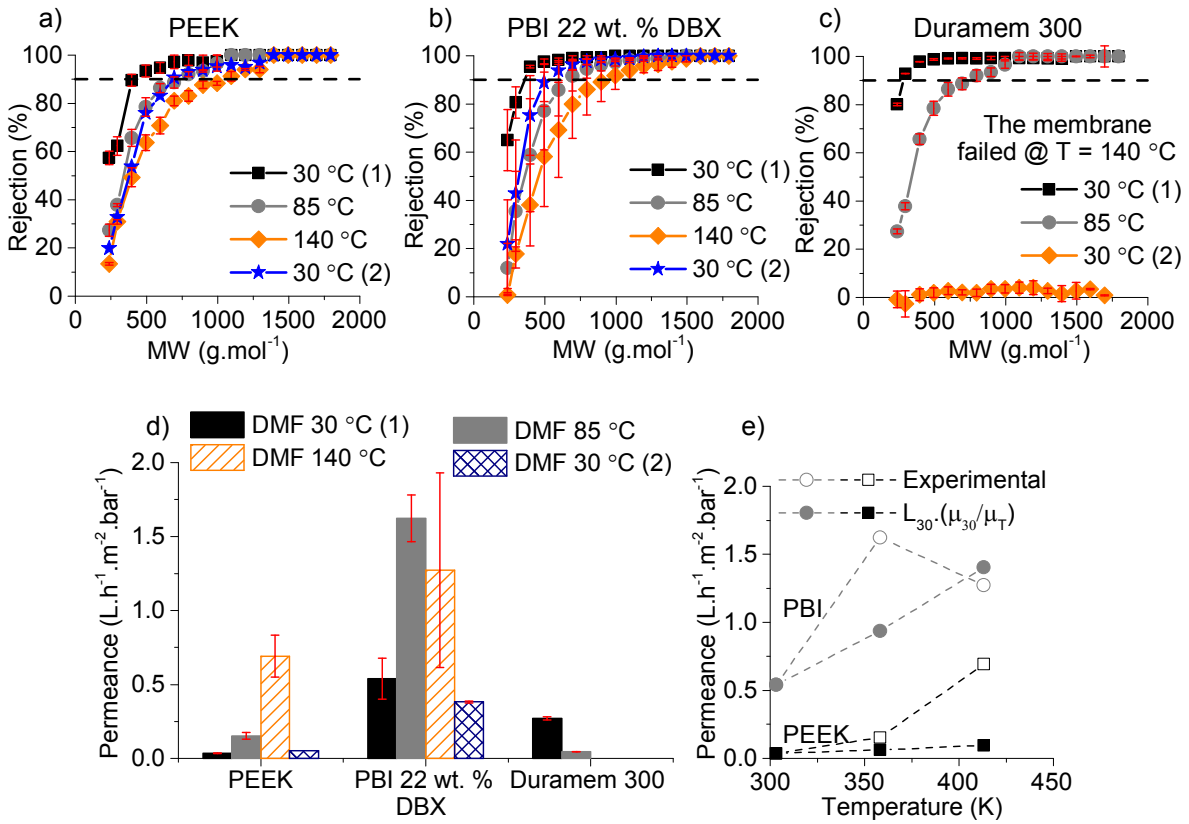

Figure 8.5 – (a), (b) and (c) Rejection values (%) as a function of temperature for PEEK, PBI 22 wt.% crosslinked with DBX and Duramem® 300 membranes, respectively. (d) Permeance values (L.h^{-1}.m^{-2}.bar^{-1}) as a function of temperature for PEEK, PBI 22 wt.% crosslinked with DBX and Duramem® 300 membranes. (e) Experimental values of permeance and $L_{p_0}.(\mu_0/\mu)$ values for PEEK and PBI membranes. The membranes were used to filter with a solution of DMF and PS (1 g.L^{-1}) at 30 bar and samples were taken at 30 °C, 85 °C, 140 °C and after cooling down to 30 °C.

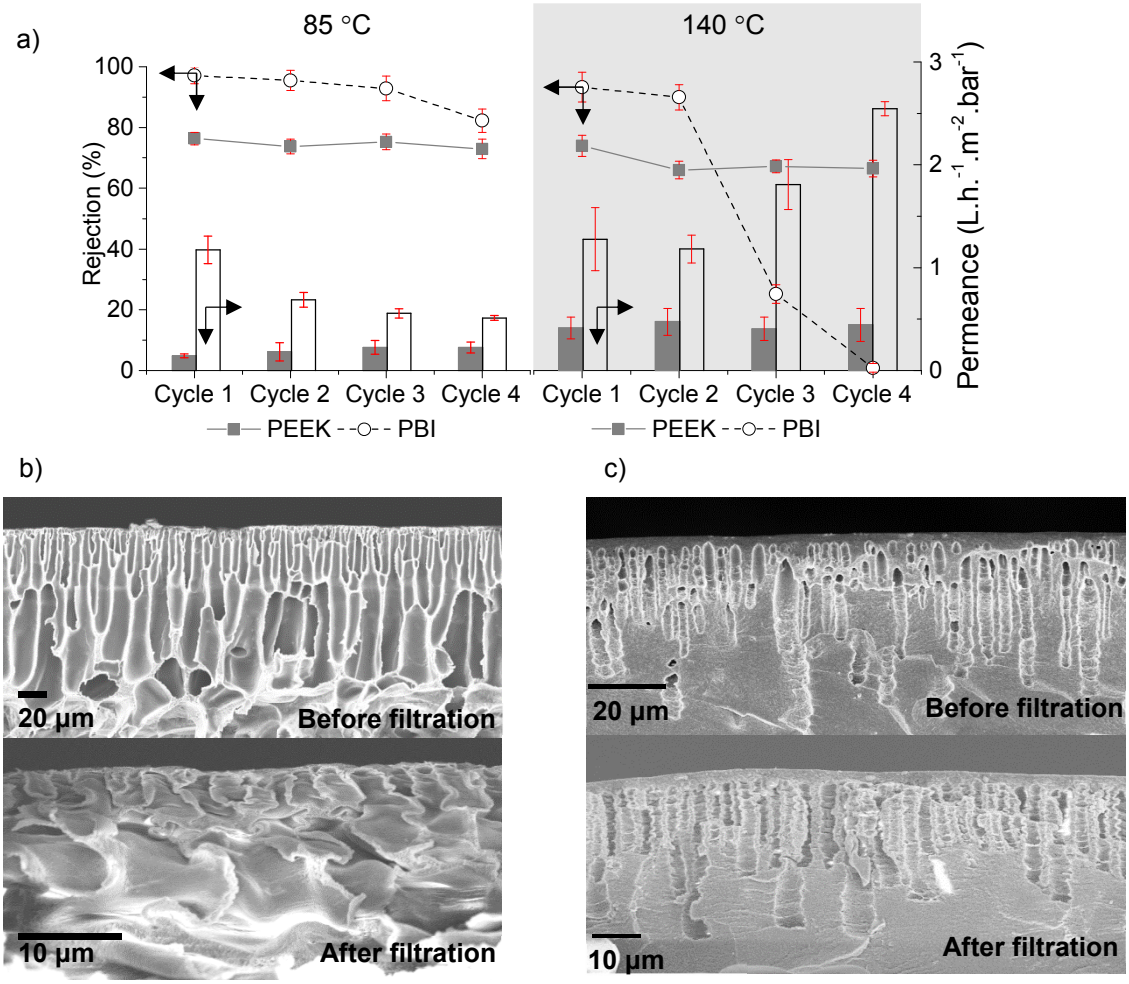

Figure 8.6 – Permeance ($L.h^{-1}.m^{-2}.bar^{-1}$) and rejection values (%) of the polystyrene with MW of 595 $g.mol^{-1}$ for PEEK and PBI membranes at 85 °C and 140 °C for four temperature cycles. b) SEM images (magnification 5000 x) of PEEK membrane before and after the four temperature cycles. c) SEM images (magnification 5000 x) of PBI 22 wt.% crosslinked with DBX membrane before and after the four temperature cycles.

PEEK and PBI membranes showed great stability in DMF after one temperature cycle and further stability tests were performed with both membranes. Using the same set-up, stability of PEEK and PBI was studied during four temperature cycles. PEEK revealed a great stability over time with similar performances at 85 °C and 140 °C with a rejection of the polystyrene with MW of 595 $g.mol^{-1}$ of 73% and 62% respectively (Figure 8.6 a)). The permeance was on average 0.2 and 0.4 $L.h^{-1}.m^{-2}.bar^{-1}$ at 85 °C and 140 °C respectively (Figure 8.6 a)). In cycle 1 the membrane had lower permeance at 85 °C compared with the other three cycles but no difference in rejection was observed for all cycles at the same temperature. PEEK membranes showed high structural compaction before and after filtration (Figure 8.6 b)).

PBI showed stability at 85 °C for all the four cycles although with a shift towards higher MWCO from cycle 1 to cycle 4 (which indicates an opening of the structure). The initial rejection of the polystyrene with MW of 595 $g.mol^{-1}$ (cycle 1) was 95 % and for cycle 4 it was

82 % (Figure 8.6 a)). At 140 °C, cycles 1 and 2 showed a small difference in terms of rejection but cycles 3 and 4 clearly showed a loss of the separation properties observed for the previous cycles at the same temperature with a rejection of 0 % for cycle 4 (Figure 8.6 a)). The permeance at 85 °C decreased from 1.19 to 0.52 $L.h^{-1}.m^{-2}.bar^{-1}$ for cycles 1 and 4 respectively and at 140 °C the opposite trend was observed with an increase from 1.28 to 2.54 $L.h^{-1}.m^{-2}.bar^{-1}$ for cycles 1 and 4 respectively. The increase of permeance at 140 °C was in agreement with the loss in rejection but at 85 °C the permeance decrease was not accompanied by an increase in rejection which might indicate signs of aging for PBI membranes. The membranes showed some swelling and compaction after filtration (Figure 8.6 c)). Even though PBI failed at 140 °C in cycle 4, it was possible to verify a closing of the polymeric structure at 30 °C (after cool-down). The same phenomenon was observed for PEEK membranes after cool-down. This implies that to a certain extent the polymer chains can rearrange themselves and tend towards a more closed structure that can be thermodynamically favourable. Permeance and rejection data for cycle 4 are shown in the supplementary information (Figure A14).

8.5.3 High temperature filtrations for PEEK membranes using other solvents

PEEK membranes were also filtered with tetrahydorfuran, 2-methyltetrahydrofuran and toluene in this study (see Figure 8.7) and the trend was a decrease in rejection with the increase of temperature except for toluene. The rejection for 2-methylTHF changed slightly with the increase of temperature to a value of ~ 500 $g.mol^{-1}$ at 70 °C. The permeance increased by a factor of 2.3 at 70 °C in comparison with the initial 30 °C. The initial and final 30 °C permeances were very similar, ~ 0.17 $L.h^{-1}.m^{-2}.bar^{-1}$ (Figure 8.7 a1) and a2)). With THF, and following the same trend for 2-methylTHF, the rejection was similar for all temperatures with an increase of MWCO at 65 °C to a value of ~ 595 $g.mol^{-1}$. The permeance at 65 °C and final 30 °C increased by a factor of ~ 2.1 and ~ 1.42, respectively, in comparison with the initial 30 °C (0.24 $L.h^{-1}.m^{-2}.bar^{-1}$).

As mentioned before, toluene was an exception from the higher MWCO (lower rejection) at higher temperature rule. The initial MWCO was ~ 500 $g.mol^{-1}$ and with the increase of temperature the membrane had rejections above 90 % for all PS studied. This can be related to previous studies by Wolf *et al*. that claims toluene is readily absorbed by amorphous PEEK, while crystalline PEEK is impenetrable to toluene [183]. The work also showed that toluene solubility decreases with temperature. Toluene absorption has also been shown to increase the crystallinity of PEEK via solvent-induced crystallization [184]. The permeance did not diminish as the temperature increased, probably because the reduction of solvent viscosity becomes the predominant effect. The permeance increased by

a factor of ~ 9.5 at 100 °C when compared with the initial 30 °C permeance, 0.08 $L.h^{-1}.m^{-2}.bar^{-1}$. The final 30 °C permeance was around 0.19 $L.h^{-1}.m^{-2}.bar^{-1}$, 2.5 times higher than the initial 30 °C permeance.

Using the same approached as before, the experimental values of permeance were compared with the initial permeance corrected with viscosity using simple pore-flow model (Equation 8.17). For all solvents studied it was possible to verify a discrepancy between the experimental and corrected values of permeance (Figure A15). DMF and toluene were the solvents with a greater difference because the maximum temperature reached for both solvents were much higher than for THF and 2-methylTHF. These results clearly indicated that as mentioned before the viscosity was not the only factor responsible for in the increase of permeance with temperature.

Therefore, and using the pore-flow model with a pore size probability function, it was possible to verify the changes in pore-size with temperature (correcting the viscosity for each temperature). In Table 8.3, the pore sizes calculated with the pore flow model for the different solvents are presented. For DMF and THF there was an increase in pore size and for toluene and 2-methylTHF a decrease in pore size for the PEEK membranes when comparing the initial and final 30 °C. PEEK membranes presented a calculated pore size of 0.656 nm at the initial 30 °C and reached a maximum at 140 °C with a value of 1.263 nm. The final 30 °C calculated pore size for this solvent was 0.976 nm. For the filtration with THF, the PEEK membranes presented similar values of calculated pore size with an initial and final value at 30 °C of 0.584 nm and 0.632 nm, respectively. For 2-methylTHF, the calculated initial pore size at 30 °C was 0.598 nm, reaching a maximum at 70 °C with a value of 0.649 nm and decreasing to 0.583 nm at the final 30 °C (after cool-down). As for toluene, the decrease in pore size was more pronounced, starting with a value of 0.737 nm (the initial 30 °C) and decreasing to a value of 0.533 nm. For the intermediate and maximum temperatures the pore size presented the same value of 0.583 nm. This model was applied just to demonstrate the differences in pore size for the different temperatures (and solvents) studied. The pore flow model just like any other mathematical model has some limitations, namely the assumption of cylindrical pores instead of molecular voids. Another assumption, is that the solutes are spherical and do not change conformation in different solvents, and with temperature.

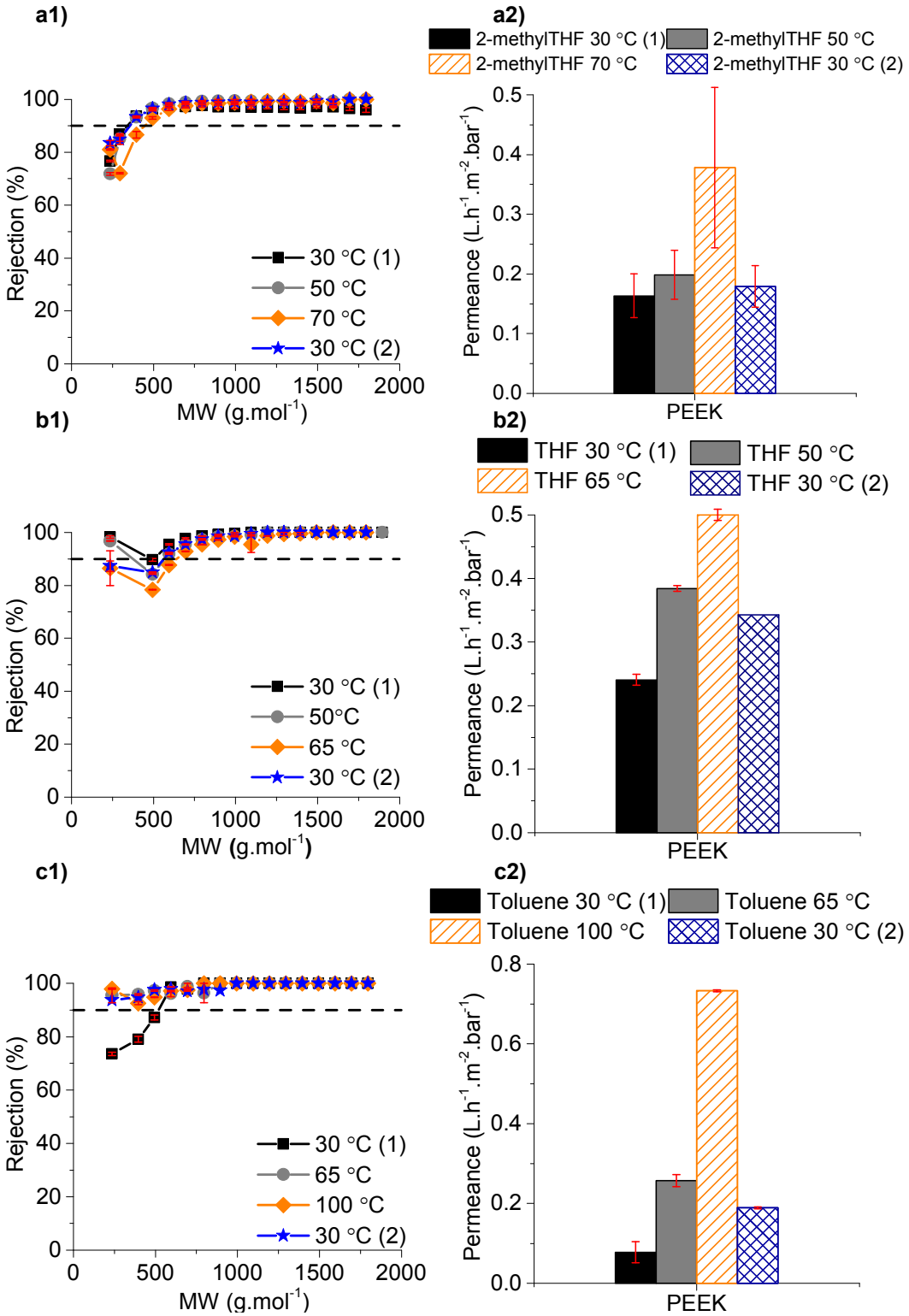

Figure 8.7 – a1) Rejection values (%) for PEEK membranes after 24h at 30 °C, 50 °C, 70 °C and cooling down to 30 °C. a2) Permeance values ($L.h^{-1}.m^{-2}.bar^{-1}$) for PEEK membranes after 24h at 30 °C, 85 °C, 140 °C and cooling down to 30 °C. b1) Rejection values (%) for PEEK membranes after 24h at 30 °C, 50 °C, 65 °C and cooling down to 30 °C. b2) Permeance values ($L.h^{-1}.m^{-2}.bar^{-1}$) for PEEK membranes after 24h at 30 °C, 50 °C, 65 °C and cooling down back to 30 °C. c1) Rejection values (%) for PEEK membranes after 24h at 30 °C, 85 °C, 140 °C and cooling down to 30 °C. c2) Permeance values ($L.h^{-1}.m^{-2}.bar^{-1}$) for PEEK membranes after 24h at 30 °C, 85 °C, 140 °C and cooling down to 30 °C. The membranes were used to filter with a solution of X solvent (X=2-methyltetrahydrofuran for a, THF for b and toluene for c) and PS (1 $g.L^{-1}$).

Table 8.3 – Theoretical mean pore size and standard deviation for PEEK membranes filtered with DMF, 2-methylTHF, THF or Toluene at different temperatures.

	30 °C (1)		$T_{intermediate}$		$T_{maximum}$		30 °C (2)	
Solvent	d_p (nm)	σ (nm)	d_p (nm)	σ (nm)	d_p (nm)	σ (nm)	d_p (nm)	σ (nm)
DMF	0.656	0.035	0.784	0.294	1.263	0.277	0.976	0.181
2-methylTHF	0.598	0.001	0.632	0.028	0.649	0.034	0.583	0.000
THF	0.584	0.000	0.583	0.000	0.670	0.000	0.632	0.027
Toluene	0.737	0.106	0.583	0.000	0.583	0.000	0.533	0.069

Given the positive results obtained with PEEK at 140 °C with DMF as a solvent, it was devised an experiment to further test the resistance of PEEK at high temperatures. For this experiment N-Methyl-2-pyrrolidone (NMP) was used as filtering solvent in order to achieve a maximum filtration temperature of 190 °C (10 degrees below the boiling point of NMP). However, to perform this experiment the PEEK could not have backing and it was necessary to assess the differences in performance of a membrane cast with and without polypropylene backing. The procedure adopted to cast a membrane is the same as described in 7.2.2 with the exception that the dope is directly cast on a glass plate. From Figure 8.8, one can observe that the membrane without backing had the same rejection profile as with backing but the permeance was slightly higher, 0.29 $L.h^{-1}.m^{-2}.bar^{-1}$ vs. 0.18 $L.h^{-1}.m^{-2}.bar^{-1}$.

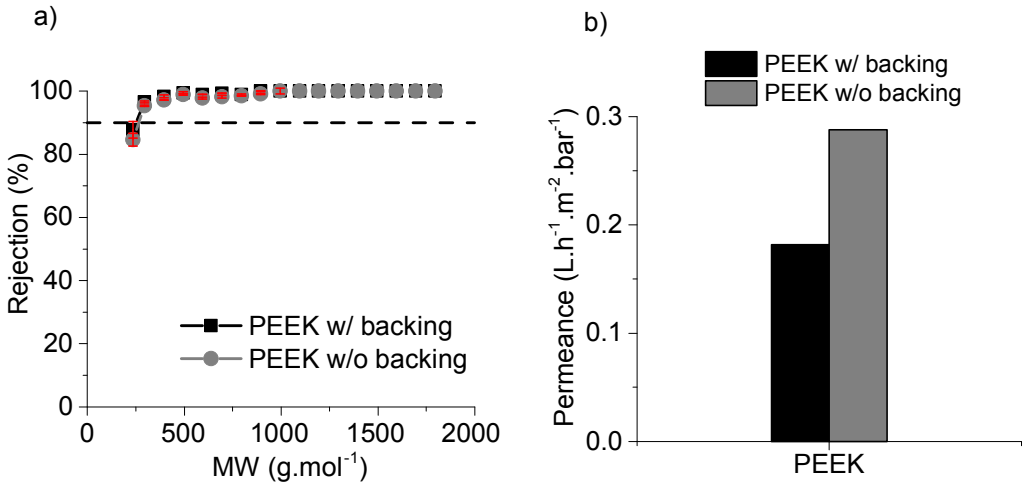

Figure 8.8 – a) Rejection values (%) for PEEK membranes dried at 120 °C with and without PP backing. b) Permeance values ($L.h^{-1}.m^{-2}.bar^{-1}$) for PEEK membranes dried at 120 °C with and without PP backing. The membranes were used to filter with a solution of tetrahydrofuran and PS (1 $g.L^{-1}$) using the cross-flow rig presented in Figure 4.1 (section 4.3.3.9).

The filtration with NMP is presented in Figure 8.9. As stated before all experiments are performed in parallel and the mean and standard deviation are presented. However, the two membranes studied, A and B, performed very differently and it was necessary to show the rejection data separately. Both membranes presented a performance at 30 °C that was very

different from the one presented in Figure 8.8. Membrane A lost all separation properties at 190 °C (with negative rejection) and even after cooling-down to 30 °C. On the contrary, Membrane B still retained some separation at 190 °C although not in the NF range. From these results, and after opening the membrane cells, it was possible to observe that the o-rings used for sealing were visibly showing signs of degradation. In fact, this degradation might have been present from the beginning (the o-rings used for this experiment have been used for the temperature cycles at 140 °C in DMF), thus explaining the lower rejection at the initial 30 °C. The permeance at 30 °C (without backing) was ~ 0.2 $L.h^{-1}.m^{-2}.bar^{-1}$ for both membranes and increased 17 and 14 times at 190 °C for Membranes A and B respectively.

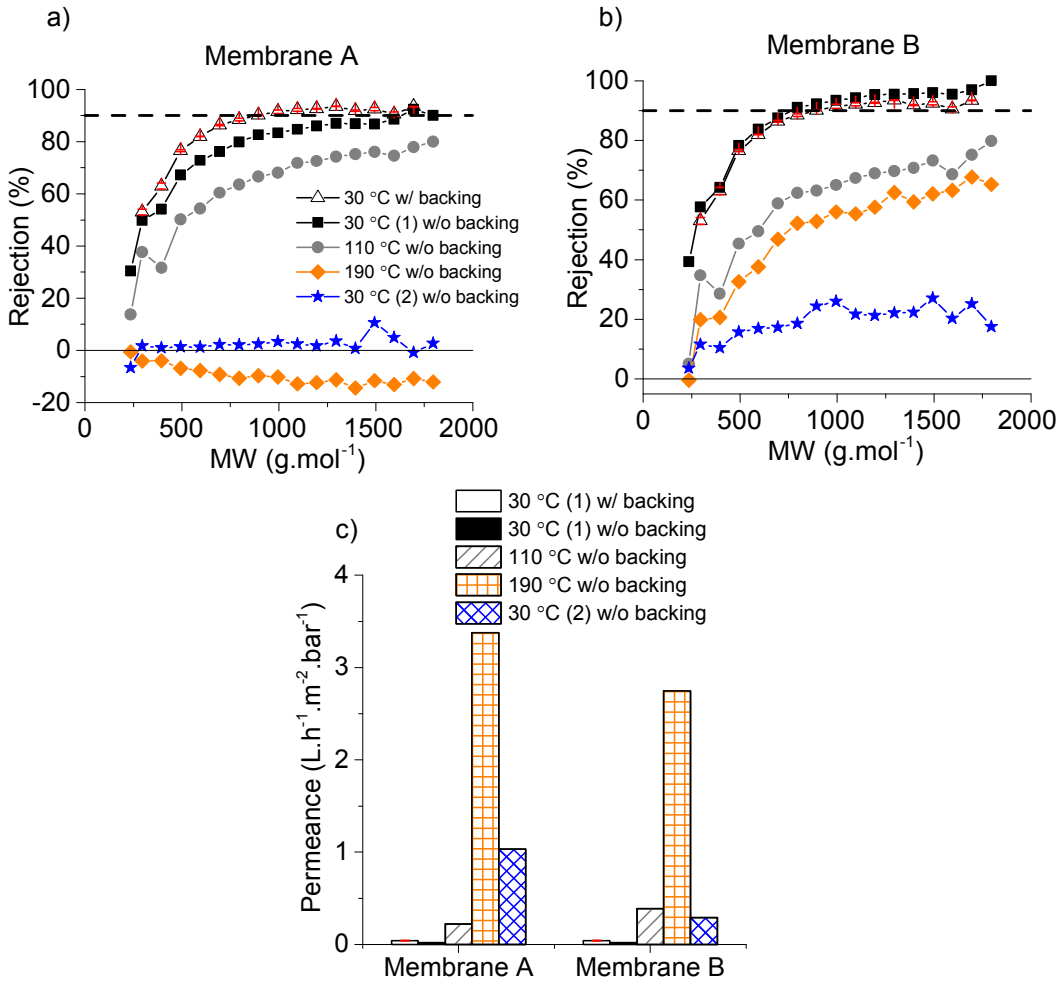

Figure 8.9 – a) Rejection values (%) for PEEK membrane A after 24h at 30 °C with (w/) and without (w/o) backing, 110 °C w/o backing, 190 °C w/o backing and cooling down to 30 °C w/o backing. b) Rejection values (%) for PEEK membrane B after 24h at 30 °C with (w/) and without (w/o) backing, 110 °C w/o backing, 190 °C w/o backing and cooling down to 30 °C w/o backing. c) Permeance values ($L.h^{-1}.m^{-2}.bar^{-1}$) for PEEK membranes A and B after 24h at 30 °C with (w/) and without (w/o) backing, 110 °C w/o backing, 190 °C w/o backing and cooling down to 30 °C w/o backing. The membranes were used to filter with a solution of NMP and PS (1 $g.L^{-1}$).

The results suggest that manufacturing membranes from polymers closer to their equilibrium glassy state may be the way to avoid physical aging over time while maintaining

a good overall performance (high permeance and high rejection of solutes). High temperature applications of OSN membranes are still highly unexplored area and the transport phenomena in these conditions are very complex and difficult to understand. There is a need for predictive models of the structural changes that membranes undergo at high temperatures and how to use these as advantage (for instance as a foul self-cleaning membrane) and the findings of this chapter are a tiny step in this direction.

8.6 Conclusions

The change in performance over time for most ISA membranes has been a major drawback due to loss in permeance (known as physical aging). In this study, PEEK NF membrane was reported as a non-aging membrane under drying conditions. The tensile strength was measured for PEEK membranes air-dried at 20 °C and 120 °C and for PEEK membranes vacuum dried at 190 °C. The results showed no difference between 20 °C and 120 °C but an increase of Young's Modulus of elasticity for 190 °C (the membrane was less elastic). For PBI and PI membranes that were annealed at 120 °C it was not possible to measure tensile strength due to the brittleness after drying. It was possible to verify that because of molecular rearrangement at a surface level PBI and PI presented no permeance after 6 h and 24 h of annealing even though both presented higher than PEEK N_2 BET surface area. PEEK maintained its permeance after 6 h and 24 h of annealing at 120 °C due to inefficient polymer packing that prevents major polymer rearrangements (negligible aging). For the high temperature filtrations PEEK was stable over a period of 4 weeks in DMF, withstanding temperatures up to 140 °C (around the glass transition temperature of PEEK) without loss of permeance and selectivity. This result indicates that PEEK membranes can be used in applications requiring heating cycles such as catalytic reactions in combination with thermomorphic multicomponent solvent (TMS). PI membranes could not resist one cycle of high temperature, and even though PBI membranes were robust for the first two filtration cycles their performance changed with a decrease in rejection for cycles 3 and 4. However the separation performance of PBI membranes was restored to nearly its original state once the membranes were cooled down. This is an important observation suggesting self-healing properties of these membranes. With the increase of temperature, the membranes presented a higher pore size (lower rejection, reversible at cool-down) which could be an advantage if this mechanism is used to clean the membrane in case any foul occurs on its surface or for developing "smart" membranes capable for fractionating different range of molecules by simply changing the operating temperature.

Chapter 9. PEEK nanofiltration membranes applied to continuous catalytic reactions

Part of the work described in this chapter has been published in the following paper:

Ludmila Peeva, Joao da Silva Burgal, Shankul Vartak, Andrew G. Livingston, Experimental strategies for increasing the catalyst turnover number in a continuous Heck coupling reaction, Journal of Catalysis, Volume 306, October 2013, Pages 190-201, ISSN 0021-9517, http://dx.doi.org/10.1016/j.jcat.2013.06.020.

Abstract

This chapter presents two different continuous Heck coupling reactions combined with organic solvent nanofiltration (OSN) separation of the catalyst *in situ*, using polymeric membranes at high temperature (> 80 °C) and high concentration of base (> 0.3 mol.L^{-1}). Two reactor configurations are investigated: a continuous single stirred tank reactor/membrane separator (m-CSTR); and a plug flow reactor (PFR) followed by m-CSTR (PFR-m-CSTR). For the first Heck reaction (Heck reaction 1) the combined PFR-m-CSTR configuration was found to be the most promising, achieving conversions above 98 % and high catalyst turn-over numbers (TONs, moles of product synthesised per mol catalyst added, see Equation 9.6) of ~20,000. In addition, low contamination of the product stream (~ 27 mg Pd per kg of product) makes this process configuration attractive for the pharmaceutical industry. For the second Heck reaction (Heck reaction 2), which was a more challenging reaction, the overall conversion was low for both the m-CSTR and PFR-m-CSTR configurations, 87 % and 79 % respectively. Therefore, these reactions exhibited low TONs: ~ 1273 (for the m-CSTR configuration) and ~ 81 (for the PFR-m-CSTR configuration). The product streams presented a Pd contamination around 33 mg Pd.kg of $product^{-1}$ for the m-CSTR configuration and 153 mg Pd.kg of $product^{-1}$ for the PFR-m-CSTR configuration.

9.1 Introduction

Many organic syntheses require expensive homogeneous transition metal catalysts (TMCs) to effect the reactions. Separation of these catalysts from the reaction products and solvents is difficult, requiring the use of energy intensive and waste-generating downstream processing [185, 186]. In addition, distillation, the most commonly used separation method, requires high temperatures (unless the product is very volatile) and most homogeneous catalysts are thermally labile (even at reduced pressure usually decomposition can occur).Other conventional processes such as chromatography or extraction also lead to catalyst loss [187].

Recovery of a (noble) metal catalyst is useful not only for obvious economic reasons but also because contamination of a product by heavy metal impurities is undesirable and must be limited to sub-ppm levels [186]. Considerable research has been undertaken to heterogenize TMCs with different techniques such as encapsulation, interphase chemistry, phase-tagging for biphasic catalysis on ionic liquids and various techniques for the immobilization of molecular catalysts on solid or colloidal supports [188]. For example, Gröschel et al. [189], employed a catalytically active membrane based on poly(acrylic acid) networks containing palladium nanoparticles for the partial hydrogenation of propyne. In order to test the long term stability a membrane was kept under constant reaction conditions for about 6 days (reactants flow rate of 20 $mL.min^{-1}$ and temperature of 298 K) and a conversion and selectivity of about 50% and 88% were obtained, respectively (TON data not presented). Milano-Brusco et al. [190], used a different approach based on the potential of surfactant based reaction media in different homogeneous catalytic reactions. The reaction under study was the enantioselective catalytic hydrogenation of dimethyl itaconate (DMI) using two different reaction media. In the first one, the Rh catalyst is complexed with the chiral ligand (2S,4S)-1-tert-butoxycarbonyl-4-diphenylphosphino-2-(diphenylphosphinometyl) -pyrrolidine (BPPM) (T = 30 °C and P = 1.1 bar). After complete hydrogenation was achieved, micellar enhanced ultrafiltration (MEUF) with a polyethersulfone membrane (Nadir P010) was used to recycle the catalyst achieving up to 95% retention; in this configuration three repetitive batches of DMI were performed and an enantiomeric excess (ee) of up to 69% was obtained (TON data not presented). In the second reaction medium, Triton X-100 was used for the hydrogenation of DMI with a Rh catalyst complexed with the water-soluble tris(3-sulfophenyl)phosphine trisodium salt (TPPTS) at 50 °C and 1.1 bar. With this system, phase separation induced by temperature allowed for up to four repetitive batches of DMI hydrogenations, resulting in a TON of 1530. Nevertheless, anchoring the catalyst on, for instance, inorganic supports or organic polymers often results in a loss of activity and selectivity [185]. Zhan et al., 2011 [191], reported a novel type of Heck reaction catalyst, composed of hydrophilic interpenetrating polymer networks (PINs) and palladium (Pd) nanoparticles that could be recycled 20 times in DMF; however, the yields were not stable from cycle to cycle, with variations from 60 to 90 %. Seto et al. [192] reported a Pd(0)-loaded membrane reactor for the Suzuki coupling reaction between aryl halide and phenyl boronic acid in aqueous media using a membrane matrix consisting of SiO_2. The authors were able to reach a TON of 1200 in 6 days.

The recent development of organic solvent nanofiltration (OSN) provides an alternative to the classical heterogenization of homogeneous complexes. An OSN-membrane is used to separate the homogeneous catalyst from the reaction mixture and thus recycle the homogeneous complex. OSN has already been performed at laboratory scale to recycle

homogeneous catalysts and its importance and relevance has been emphasised by works such as: Nair et al., 2001 [188], who performed a semi-continuous nanofiltration-coupled catalysis for a well-known Heck coupling reaction. They permeated the post-reaction mixture through a polyimide OSN membrane achieving an overall 90 % catalyst retention after four catalyst recycles (five reaction-filtration sequences) and a TON of 1200; Datta, et al., 2003 [193], developed catalysts for the Heck, Sonogashira and Suzuki type coupling reactions, which were retained by poly(dimethylsiloxane) (PDMS) membranes (retention higher than 99.5 %) but the catalysts lost activity after a series of catalyst recycles; Aerts, et al., 2006 [185], who used silicon-based OSN-membranes to recycle the Co-Jacobsen catalyst four times in diethylether (Et_2O), achieving 98.5 % retention and a minor decrease in the conversion from one cycle to another; Vogt et. al, 2009 [194], reported the synthesis of multiple phosphine ligands attached to a dendritic support via 'click' chemistry (molecular weight enlargement – MWE – catalysts) and their application in the Pd-catalyzed Suzuki coupling as well as their recovery and reuse by means of nanofiltration. In this work the reaction performed was the Suzuki–Miyaura coupling between 4-bromotoluene and phenyl boronic acid at 60 °C for 16 h with three different ligands. A ceramic membrane (Nanofiltration inopor® nano 450 Da) with retention higher than 99 % for the three MWE catalysts was employed and four catalyst recycles were performed, achieving initial yields of 99 % but decreasing from cycle to cycle (TON data not presented).

All previous examples of OSN stated above were performed in discontinuous or semi-continuous mode but current interest in the continuous flow production of fine chemicals has motivated a re-evaluation of how synthetic transformations are performed at the laboratory, intermediary, and manufacturing scales. In terms of organic chemistry both continuous flow processing and microreactor technology are techniques that are more relevant these days [195, 196]. Although continuous operations might require more time initially to set up equipment and find the optimum conditions - concentrations, temperatures and flow rates - other parameters such as mixing and temperature can be more easily controlled when compared to batch processes [192, 197, 198]. One of the major drawbacks of the continuous flow systems is the handling of solids or precipitation during operation which can lead to clogging of the flow path. There are some approaches that can mitigate the effects of solids in the flow path such as reactor surfaces that do not promote nucleation, introduction of ultrasound transducers, sonication and flushing the system with a solvent that will dissolve the solid – this technique can lead to cross-contamination and operation stoppage [196]. Few works have been published in the literature about continuous flow production with catalyst retention using OSN. One of the very first works in continuous catalysis was performed by Kragl et al., 1999 [199]. These authors focused on the usage of diaminopropyl-type dendrimers bearing palladium phosphine complexes as catalysts for the allylic

substitution in a continuously operating chemical membrane reactor. Retention rates by ultra- or nanofiltration membranes -Nadir UF-PA-5 and SELRO MPF-50, respectively - higher than 99.9% resulted in a total TON for the Pd catalyst of circa 95. However, in the reactions of T = 25 °C and a flow rate of 20 $mL.h^{-1}$ the conversion starting at 100 % decreased to around 80 % after 40 h (80 residence times) and the experiment was stopped. van Koten, et al., 2003 [200] developed a shape-persistent nanosize dodecakis (NCN-Pd^{II}-aqua) complex [201] that was applied as a homogeneous catalyst under continuous reaction conditions in a nanofiltration membrane reactor. The reaction performed was the double Michael reaction between methyl vinyl ketone and ethyl-cyanoacetate and the membrane used was Koch MPF-50 flat-membrane (catalyst rejection of 99.5%). Under the reaction conditions of T = 23 °C and P = 20 bar a TON of 3000 and a conversion of 85 % was obtained (26 h, 65 exchanged reactor volumes). De Smet, et al., 2001 [202], have performed a continuous enantioselective hydrogenation of dimethyl itaconate with acetic acid;[1-(2-diphenylphosphanylnaphthalen-1-yl)naphthalen-2-yl]-diphenylphosphane;ruthenium (Ru-BINAP) catalyst and of methyl 2-acetamidoacrylate with (1Z,5Z)-cycloocta-1,5-diene;(2R,5R)-1-[2-[(2R,5R)-2,5-diethylphospholan-1-ium-1-yl]phenyl]-2,5-diethylphospholan-1-ium;rhodium; trifluoromethanesulfonate (Rh-EtDUPHOS) catalyst in a hybrid process composed of a CSTR followed by a NF unit (NF-coupled catalysis). For the first reaction they achieved a conversion of 100 % throughout the entire run and for the second reaction the conversion was 100 % initially but then decreased to 90 % in the later stages. The catalyst retention was above 97 % for both reactions. The TON for the hydrogenation with Ru-BINAP and Rh-EtDUPHOS was, respectively, 1950 and 930. Fang, et al., 2011 [203], reported a continuous homogeneous hydroformylation with bulky rhodium catalyst complexes retained by nanofiltration membranes (STARMEM®) but in practice those experiments were performed in a semi-continuous mode. Sequential batches of 16 to 22 hours were performed at 50 - 60 °C and at different pressures (maximum 3.0 MPa syngas) achieving high catalyst retention (> 99 %) but relatively low yields; for instance, for 1-octene hydroformylation catalysed by PBB10d at 3.0 MPa the conversion was around 50 % (TON data not presented).

More recently the use of continuous-flow reactors for multistep synthesis has gained a considerable amount of interest because they allow for integration of the individual reaction steps and subsequent separations in one single streamlined process. For instance Noel, et al., 2011 [204], used a microreactor (100 µL) for the palladium-catalyzed Suzuki-Miyaura cross-coupling reactions (synthesis of biaryls starting from substituted phenols) in flow connected to a microfluidic extraction operation with a porous fluoropolymer membrane to remove impurities and a packed-bed reactor to increase the mixing and efficiency of the biphasic Suzuki-Miyaura cross-coupling reaction. They were able to obtain, on average,

isolated yields of 95 %. O'Neal E. and Jensen K., 2004 [205] reported a ring-closing metathesis reaction in continuous-flow nanofiltration with recycle of the metathesis catalyst. In this study, the system used an amount of catalyst inferior to 2 mg during 50 h of operation which was equivalent to approximately 70 batch tests in series (70 recycle experiments). The system had a total volume of 2.9 mL and a Puramem® 280 membrane (PI based membrane) was used for separating the catalyst from the product with catalyst rejections around 99 %; consequently the Ruthenium catalyst contamination was below 1 ppm. A turnover number of 677 was obtained when accounting only for the measured permeated product. By accounting to the total product in the system after the experiment was stopped and with the product present in the samples the TON was 935. In another method recently published it was suggested the combination of thermomorphic multicomponent solvent (TMS) system with OSN [206]. TMS is the occurrence of two phases in which the product and the catalyst show different solubilities by decreasing the temperature in the reaction phase. In this study a hydroformylation is performed and experimental data for TMS and OSN are obtained separately. The authors used an ONF2 type membrane (GMT Membrantechnik GmbH) and a rejection of more than 90 % of the Rh catalyst complexed with bidentate ligands such as Biphephos and Xantphos was obtained. Performing a hypothetical combination of TMS and OSN the authors were able to obtain a product stream with less than 1 ppm of Rh catalyst.

For a more comprehensive review of recycling of homogeneous catalysts using membrane separation the author of this thesis strongly recommend the review of Vogt et al., 2011 [207]. The author of this thesis also suggests the review of Gürsel et al., 2015 [208] about catalyst separation and/or recycling in continuous flow systems.

The main hurdle towards implementing OSN in the catalytic processes has been the compatibility of the existing OSN membranes (particularly the polymeric ones) with the reaction conditions. Typically the TMC reactions are performed at high temperatures (100 °C and above) in aggressive solvents (e.g. DMF) and at high concentrations of base/acid – quite challenging conditions for the polymeric membranes. Although successful, most of the above cited catalytic reactions combined with membrane separations have been performed in a batch or semi-continuous mode and at mild conditions (non-aggressive solvents, low concentration of acids or bases, moderate temperature of 30 - 50 °C) and/or the membrane separation step has been performed separately after temperature reduction and post-reaction media workup to make it compatible with the membrane material. In addition, the catalyst loadings employed are usually high (0.5 – 2 mol %) and the reported TONs (usually varying from 50 to 2,000) are too low to be of commercial interest to the industry.

In this chapter, two different Heck coupling reactions are used to demonstrate the feasibility of a continuous process combining reaction with *in situ* separation of the TMC

using a PEEK membrane. In contrast to the previous works, the reaction and the separation are performed simultaneously in the same vessel, both performed at > 80 °C (high temperature) and in dimethylformamide (DMF) containing >0.3 mol.L^{-1} triethylamine (high base content). In addition, a high catalyst TON and low TMC contamination of the product was achieved for Heck reaction 1 by maintaining the catalyst loading at minimal levels throughout the runs. A summary of the state of the art and a comparison with the results presented in this work can be found in in the last section of the manuscript. Two reactor configurations are investigated: continuous single stirred tank reactor/membrane separator (m-CSTR); and a plug flow reactor (PFR) followed by m-CSTR (PFR-m-CSTR in series). It was demonstrated that the combined PFR-m-CSTR configuration is the most promising achieving catalyst TONs of ~20,000 for Heck reaction 1 but only ~ 81 for Heck reaction 2 (which proved to be a more challenging reaction).

9.2 Materials and methods

9.2.1 Chemicals

Analytical grade palladium (II) acetate [$Pd(OAc)_2$], 1,3-Bis(diphenylphosphino)propane (dppp), triphenylphosphine (PPh_3), iodobenzene (IB), 2-Chloro-5-bromonitrobenzene, methyl acrylate, ethyl acrylate, anhydrous *N*,*N*-dimethylformamide (DMF), triethylamine (NEt_3), ethyl acetate, diethyl ether, nitric acid (69 %) and hydrochloric acid (37 %) were all purchased from Sigma-Aldrich.

9.2.2 Membrane

The PEEK membrane used was obtained by dissolving VESTAKEEP® 4000P at a concentration of 12 wt. % and dried from water at 20 °C (for Heck reaction 1) and 120 °C (for Heck reaction 2) as described in 7.2.2.

9.2.2.1 Membrane characterization

9.2.2.1.1 Scanning electron microscopy and energy dispersive X-rays (SEM-EDX)

For cross-section imaging a membrane sample was broken in liquid nitrogen and pasted vertically onto SEM stubs covered with carbon tape. For surface imaging a membrane sample was cut and pasted horizontally onto SEM stubs covered with carbon tape. The samples were then coated with a chromium-layer in a Q150T turbo - pumped sputter coater (Quorum Technologies Ltd.). For SEM-EDX a JEOL JSM6400 SEM fitted with Oxford Instruments INCA energy dispersive analytical system (EDS) for elemental x-ray analysis and digital image capture enabling line scans and x-ray maps to be produced was used. Quantitative analysis is performed at 15 kV and under dry conditions at room temperature. For high-resolution SEM pictures the same procedure described in 485.2.5.2 was applied.

9.2.3 Heck coupling reactions

Two Heck reactions were studied in this chapter. Heck reaction 1 the reaction between iodobenzene **1** (MW 204 $g.mol^{-1}$) and methyl acrylate **2** (MW 86 $g.mol^{-1}$) to form E-methyl cinnamate **3** (MW 162 $g.mol^{-1}$) (Figure 9.1) was selected and carried out because it would proceed regioselectively and form a stable product. The by-product of this reaction is triethylamine hydroiodide **4** (MW 229 $g.mol^{-1}$).

Heck reaction 2 the reaction between 2-chloro-5-bromonitrobenzene **5** (MW 236.45 $g.mol^{-1}$) and ethyl acrylate **6** (MW 100.12 $g.mol^{-1}$) to form 3-(4-Chloro-2-nitrophenyl)acrylic Acid Ethyl Ester **7** (MW 255.65 $g.mol^{-1}$) (Figure 9.1) was selected and carried out because of the same reasons stated for reaction 1 but also because the product stream of this reaction (permeate stream) would be used to perform a solvent exchange from DMF to EtOH using a membrane cascade. The by-product of this reaction is triethylamine hydrobromide **8** (MW 182.10 $g.mol^{-1}$). This reaction has been published by Caron S. and Vazquez E. [209].

Heck reaction 1

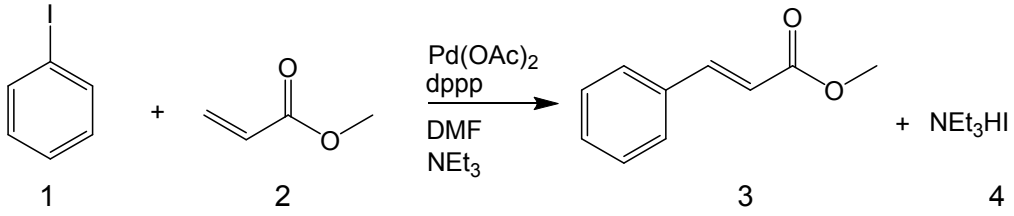

Heck reaction 2

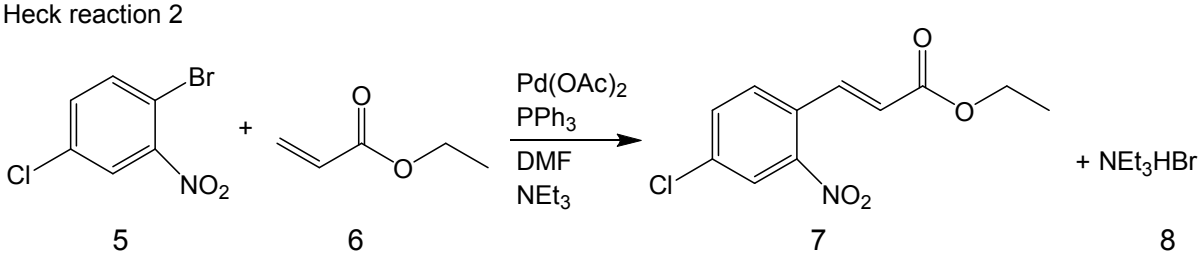

Figure 9.1 – Scheme of Heck coupling reaction 1 to form E-methyl cinnamate (3) and of Heck coupling reaction 2 to form 3-(4-Chloro-2-nitrophenyl)acrylic Acid Ethyl Ester (7).

9.2.4 Temperature studies

For Heck reaction 1 it was necessary to perform a temperature optimization. In a reaction carousel (Radleys, UK) a series of batch experiments were performed at two different temperatures: 80 °C (temperature selected as a trade-off between reaction kinetics and the boiling points of methyl acrylate, 80 °C and triethylamine, 88.8 °C) and 110 °C [210] [211]. In a carousel tube 5.4 mg (0.024 mmol) of $Pd(OAc)_2$ and 19.8 mg (0.048 mmol) of dppp were stirred for 15 minutes at room temperature in DMF (2 mL). 0.273 mL (2.45 mmol) of iodobenzene, 0.264 mL (2.93 mmol) of methyl acrylate, 0.5 mL (3.58 mmol) of triethylamine and 1 mL of DMF were then added and the solution was stirred throughout the experiment. For catalyst pre-activation the same amount of $Pd(OAc)_2$ and dppp were added to 2 mL of

DMF and the mixture was stirred for an additional 30 minutes at 80 °C. 0.273 mL (2.45 mmol) of iodobenzene, 0.264 mL (2.93 mmol) of methyl acrylate, 0.5 mL (3.58 mmol) of triethylamine and 1 mL of DMF were then added and the solution was stirred throughout the experimental run. 0.1 mL samples were taken for analysis.

9.2.5 Catalyst concentration studies

In order to determine the minimum catalyst loading that allows the reaction to achieve completion within a working day, a series of experiments were performed as batches in a reaction carousel with different catalyst, [$Pd(OAc)_2$], concentrations. For Heck reaction 1 the temperature used was 80 °C ± 2 °C and the catalyst concentrations used were: 0.002 mol %, 0.004 mol %, 0.0078 mol %, 0.0156 mol %, 0.03125 mol %, 0.0625 mol %, 0.125 mol %, 0.25 mol %, 0.5 mol % and 1 mol %. For each concentration the same procedure described in 9.2.4 for catalyst pre-activation was applied. For Heck reaction 2 the temperature used was 90 °C ± 2 °C (as reported in [209]) and the catalyst concentrations used were: 0.05 mol %, 0.1 mol %, 0.5 mol %, 1 mol %, 5 mol % and 10 mol %. No pre-activation period was required for Heck reaction 2.

9.2.6 Ethyl acrylate concentration studies

Using the same procedure used in 9.2.5 different ethyl acrylate concentrations were studied using a 1 mol % catalyst concentration: 2 equivalents, 3 equivalents, 5 equivalents and 10 equivalents.

9.2.7 Reaction kinetics

From the batch experiments it was determined that the reaction rate could be approximated by a first order reaction with respect to the limiting substrate IB (C_s) by using the isolation method. Plotting the graph $\ln(C_s/C_{s_0})$ vs. time (A, Appendix) a kinetic rate of 0.0219 min^{-1} ($T_{ref.} = 80\,°C;\ p_{ref.} = 1\,bar$) was determined for a catalyst loading of 0.031 mol % for Heck reaction 1.

$$(-r_S) = \frac{dC_S}{dt} = K.(C_S)^n \overset{n=1}{\Longleftrightarrow} (-r_S) = K.C_S \qquad \text{Equation 9.1}$$

9.2.8 Continuous Heck coupling reaction combined with OSN membrane separation

9.2.8.1 System setup: m-CSTR and PFR

The two configurations used in this study are shown in Figure 9.2. The first configuration was a single reactor system consisting of a one pot reactor/ membrane separator cell (m-

CSTR) where the reaction and catalyst separation from the reaction mixture were performed at the same time. A constant flow of feed solution was supplied to the cell via an HPLC pump. Equivalent flow of the post-reaction mixture was collected as permeate through the membrane. The cell was equipped with a pressure relief valve set to 50 bar relief pressure in order to avoid over-pressurising the system. The m-CSTR was equipped with a magnetic stirrer bar, and placed on a hotplate stirrer. The second configuration consisted of two reactors in series. A constant flow of the feed solution was first passed through a U-shaped PFR, placed in a heating chamber. The outlet of the PFR was directly connected to the inlet of the m-CSTR.

The m-CSTR (Figure 9.3) was made of 316 SS, could operate under high pressure (69 bar), and hold circular flat sheet membranes with an effective area of 51 cm^2. The m-CSTR was operated in a bottom-to-top permeation mode and contained a magnetic stirrer in the feed/retentate chamber. This is to ensure that any dissolved gas released from a feed stream which enters the cell will move to the top of the cell and exit through the membrane. The liquid capacity of the m-CSTR was ~ 60 mL for Heck reaction 1 and ~ 100 mL for Heck reaction 2. Six ports surround the bottom section of the cell, and were used as inlet ports (feed) or outlet ports (permeate), or were connected to a thermocouple or a pressure gauge for temperature control and pressure monitoring [212].

The PFR was made of 316 SS ½'' tube with a length of 0.64 m (total volume of 60 mL).

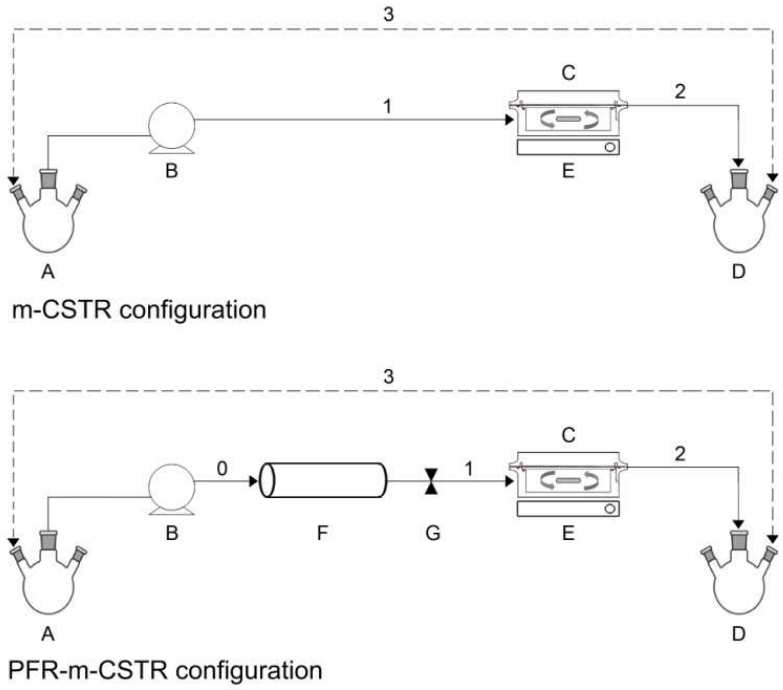

Figure 9.2 – Scheme of the single-reactor system (top). Scheme of the two reactors in series system (bottom). Legend: A - Feed solution flask; B – HPLC pump; C – m-CSTR with PEEK membrane (stirred membrane cell); D – Permeate collector flask; E – Heating/stirring plate; F – PFR; G – PFR outlet sampling valve. 0 – PFR inlet stream; 1 –m-CSTR inlet stream; 2 – m-CSTR outlet stream/ permeate; 3 – Nitrogen supply. Adapted from [117].

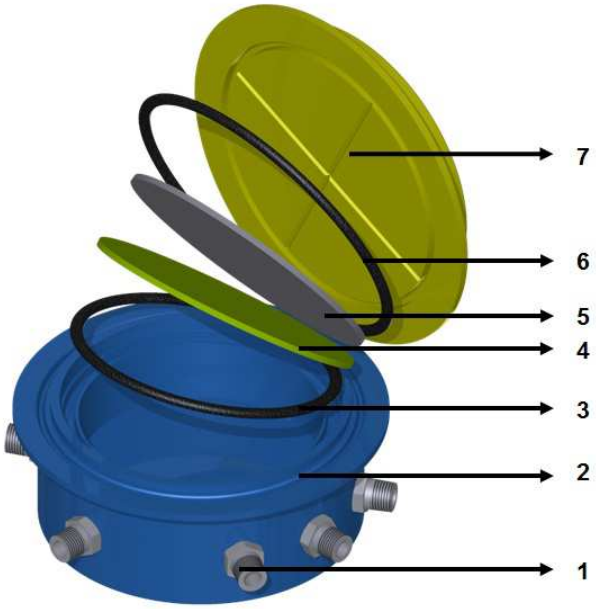

Figure 9.3 – Stirred tank reactor/membrane separator (m-CSTR) layout. Legend: 1 - Inlet/outlet ports; 2 - Feed/retentate chamber; 3 – Inner o-ring; 4 – Membrane; 5 - Sintered plate; 6 - Outer o-ring; 7 - Cover. Adapted from [117].

9.2.8.2 Operating procedure

9.2.8.2.1 Heck reaction 1

For 100 mL of the initial feed solution, 0.0044 g $Pd(OAc)_2$ (2.0×10^{-4} mol.L^{-1}, ~ 0.033 mol %) and 0.016 g dppp (4.0×10^{-4} mol.L^{-1}, ~ 0.063 mol %) were added into a 500 mL two-neck round bottom flask. The flask was vacuum degassed and then placed under an N_2 atmosphere. After that, and always under an N_2 atmosphere, 65.2 mL of anhydrous DMF were added and the solution was mixed using a magnetic stirrer. Then, 6.8 mL of iodobenzene (final concentration of 0.6 mol.L^{-1}), 10 mL of methylacrylate and 18 mL of triethylamine were added to the flask and mixed. The flask was then connected to the system as a feed solution and kept under an N_2 blanket (~ 0.5 bar overpressure). More feed solution was prepared throughout the running of the system by using the procedure described above but with 10 times lower catalyst and ligand concentrations.

Note: The single-reactor system was run initially in a batch mode. 50 mL starting solution (0.6 mol.L^{-1} iodobenzene; 3.2×10^{-4} mol.L^{-1} $Pd(OAc)_2$), were added into the m-CSTR chamber and stirred for ~ 12 hours at 80 °C (overnight). On the following day the system was started in continuous mode using a feed stream containing 0.6 mol.L^{-1} iodobenzene and 2×10^{-5} mol.L^{-1} Pd catalyst.

9.2.8.2.2 Heck reaction 2

For 300 mL of the initial feed solution, 7.2 g 2-chloro-5-bromonitrobenzene (0.1 mol.L^{-1}), 0.067 g $Pd(OAc)_2$ (1.0×10^{-3} mol.L^{-1}, ~ 1.0 mol %) and 0.16 g PPh_3 (2.0×10^{-4} mol.L^{-1}, ~ 0.2 mol %) were added into a 500 mL two-neck round bottom flask. The flask was vacuum degassed and then placed under an N_2 atmosphere. After that, and always under an N_2 atmosphere, ~ 262 mL of anhydrous DMF were added and the solution was mixed using a magnetic stirrer. Then, 32 mL of ethyl acrylate (10 equivalents, 1 mol.L^{-1}) and 5.9 mL of triethylamine (1.4 equivalents, 0.14 mol.L^{-1}) were added to the flask and mixed. The flask was then connected to the system as a feed solution and kept under an N_2 blanket (~ 0.5 bar overpressure). More feed solution was prepared throughout the running of the system by using the procedure described above but with 10 times lower catalyst and ligand concentrations. Different catalyst and ethyl acrylate loadings were changed throughout the continuous running in order to increase productivity and decrease residence time.

Note: The single-reactor system was run initially in a batch mode. 100 mL starting solution (0.1 mol.L^{-1} 2-chloro-5-bromonitrobenzene; 1.0×10^{-3} mol.L^{-1} $Pd(OAc)_2$), were added into the m-CSTR chamber and stirred for ~ 12 hours at 90 °C (overnight). On the following day the system was started in continuous mode using a feed stream containing 0.1 mol.L^{-1} 2-chloro-5-bromonitrobenzene but no Pd catalyst. For the PFR-m-CSTR the system was run initially at 0.5 mol % Pd (5×10^{-4} mol.L^{-1} $Pd(OAc)_2$) and 3 equivalents of ethyl acrylate (0.3 mol.L^{-1}). The Pd concentration as well as the ethyl acrylate concentration were changed throughout the run.

9.2.9 Analytical methods

9.2.9.1 Conversion

An Agilent 6890 Series II gas chromatograph equipped with a HP - 5 column (5 % phenyl methyl siloxane; capillary: 30m×0.530 mm×1.50 µm) and a flame ionization detector (FID) was used for determining the conversion of limiting substrate to product by comparing the area of the individual characteristic peaks [Conversion = Area product/(Area product + Area substrate)]. The programme ran from 40 °C (1 min hold) to 200 °C with a ramp of 15 °C.min^{-1}.

9.2.9.2 Product extraction

9.2.9.2.1 E-methyl cinnamate

In order to confirm that the right product has been obtained, permeate solution was mixed initially with distilled water (1:1) and ethyl acetate (1:4) and the mixture was allowed to phase-separate in a separating funnel. Brine solution (1:15) was added to facilitate phase

separation and the organic phase was then subjected to three washes with water using brine in-between. The resultant organic phase was partially evaporated in a rotary evaporator. The paste residue consisted mostly of methyl cinnamate with traces of iodobenzene and DMF. A thin layer of this was spread on a petri dish to allow evaporation of the residual DMF. An ^{1}H-NMR scan (not shown) confirmed the methyl cinnamate presence and also the traces of iodobenzene.

9.2.9.2.2 3-(4-Chloro-2-nitrophenyl)acrylic Acid Ethyl Ester

In order to isolate the product of Heck reaction 2 the same procedure used in [209] was applied. An ^{1}H-NMR scan (not shown) confirmed the presence of 3-(4-Chloro-2-nitrophenyl)acrylic Acid Ethyl Ester and also the traces of 2-chloro-5-bromonitrobenzene. Mass spectrometry of the product was also performed and confirmed its presence.

9.2.9.3 Side product extraction and analysis

9.2.9.3.1 Triethylamine hydroiodide

The retentate was subjected to vacuum filtration to separate the salt from the liquid component, consisting of DMF and the substrates. After washing with ether the cake was left at room temperature to evaporate remaining traces of ether. ^{1}H-NMR revealed it to be exclusively triethylamine hydroiodide.

The solubility of the salt in the retentate was determined at 80 °C and atmospheric pressure for two post-reaction mixture compositions of the initial iodobenzene concentration: 0.6 mol.L^{-1} and 1.2 mol.L^{-1}. Though the reactor was operated under a pressure of 20-40 bar, salt solubility is expected to change negligibly within this pressure range. The experiments were performed on the reaction carousel by adding known amounts of salt to the post-reaction mixture until the solubility limit was reached. The saturation concentrations of the salt were found to be ~ 3.35 mol.L^{-1} and ~ 2.14 mol.L^{-1} for the initial substrate concentrations of 0.6 mol.L^{-1} and 1.2 mol.L^{-1} respectively.

The membrane rejection of the salt was determined by analysing permeate and retentate samples using an Agilent 1100 HPLC equipped with ELSD detector (Varian 385-LC). A reverse-phase HPLC column (ACE C-18, 250 mm × 4.6 mm) packed with 5μm diameter silica particles with 300 Å pores size was operated at 30 °C. Water (adjusted to pH ~ 6.5 with 0.1 mol.L^{-1} ammonium acetate buffer) and methanol were used as the mobile phase, at 1 mL.min^{-1} flow rate. A ramp from 50% methanol / 50% water to 95% methanol / 5% water in 35 minutes was followed by 4 minutes at 95% methanol and then a ramp back to 50% methanol / 50% water in 1 minute. Rejection is given A (Appendix) and it was found to be 45.6 %.

9.2.9.3.2 Triethylamine hydrobromide

In order to obtain the triethylamine hydrobromide salt the same procedure used in [213] was adopted.

The solubility of the salt was determined at 90 °C and atmospheric pressure by adding known amounts of salt to DMF until visible precipitation occurs. The solubility limit of the salt was found to be ~ 0.55 mol.L^{-1}. The rejection of the salt was found to be 54 %.

9.2.9.4 Palladium analysis

0.5 mL feed, permeate and retentate samples were heated at 90 °C on a hotplate stirrer. After complete drying, 1.5 mL of aqua regia (nitric acid and hydrochloric acid 1:3 v/v) was added to each dried sample to digest the organic content (digestion within ~ 24 hours). Each sample was then diluted in 10 mL centrifuge tubes with distilled water and mixed (the small residual organic matter was found not to interfere with the analysis). The samples were analysed using *Inductively Coupled Plasma* Optical Emission Spectrometry (ICP-OES) on a Perkin-Elmer Optima 2000DV spectrometer and compared against a calibration curve of 2 ppm, 5 ppm and 10 ppm palladium standard samples.

9.3 Results and discussion for Heck reaction 1

9.3.1 Batch experiments for the Heck coupling reaction

9.3.1.1 Temperature studies

For the carousel experiments at two different temperatures the reaction reached 98% conversion after 40 minutes at 110 °C whereas for a temperature of 80 °C the reaction reached 99.5% conversion after 2 hours (Figure 9.4). Nevertheless, the conversion of starting material to product was slow at 80 °C, increasing sharply after 100 minutes of reaction time. This indicates that formation of the *in situ* catalyst complex was the rate limiting step. Hence, a complementary experiment was performed by stirring $Pd(OAc)_2$ and dppp together in DMF (2 mL) for 30 minutes at 80 °C (for pre-activation) prior to the addition of the remaining reagents. The reaction proceeded to full conversion in 50 minutes with catalyst pre-activation (Figure 9.4). As the boiling point of methyl acrylate is 80 °C and of triethylamine is 88.8 °C it was decided to investigate the kinetics and perform all membrane experiments at 80 °C in order to minimise the evaporation of these reagents. In addition, the glass transition temperature (T_g) of the PEEK polymer used for membrane preparation is ~ 140 °C and the lower operational temperature will minimise the membrane structural changes.

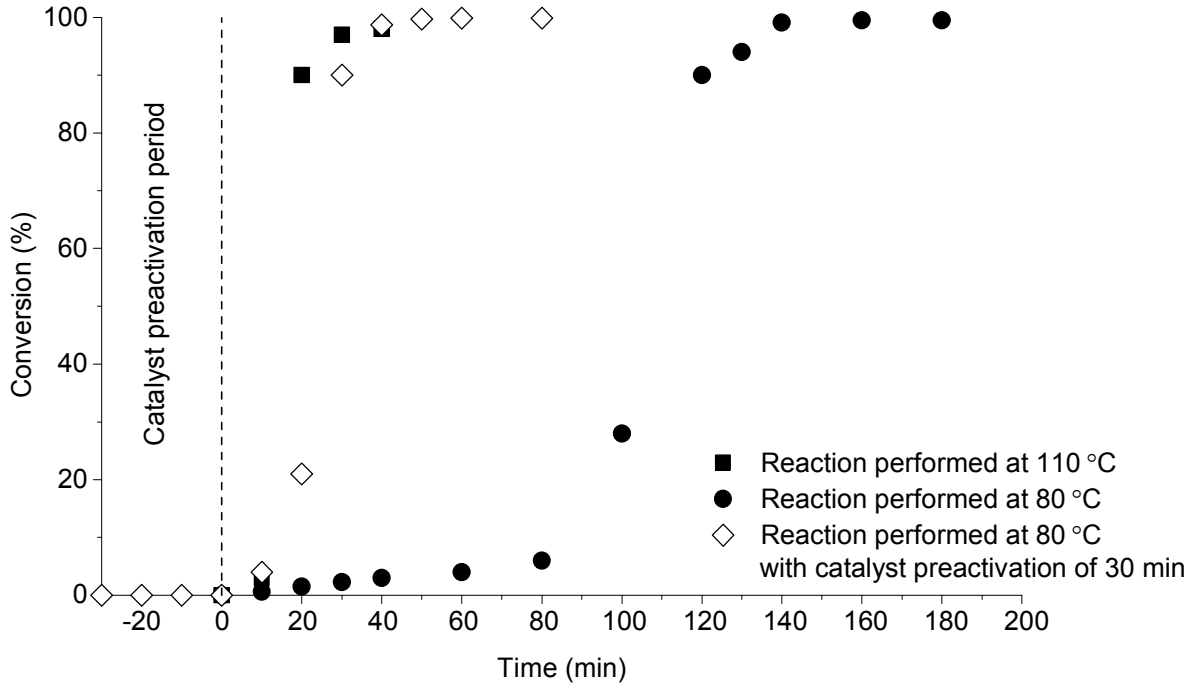

Figure 9.4 – Conversion over time of the Heck coupling reaction at 110 °C and at 80 °C with and without catalyst pre-activation. The reaction was performed as batch in a reaction carousel.

9.3.1.2 Catalyst concentration studies

As described earlier, in order to determine the minimum catalyst concentration essential for reaction completion within a workday, a series of experiments were performed on a reaction carousel at 80 °C, varying the catalyst concentrations. This experiment allows for a direct comparison between the maximum TONs achieved in a simple batch reactor and those in a continuous process combined with membrane separation. It was found that the reaction rate decrease starts somewhere between 0.0078 - 0.0156 mol % catalyst loading (Figure 9.5). From this experimental data it was established that the optimal catalyst concentration (as a trade-off between high reaction rate and catalyst loading) should be around ~ 0.03 mol %, which corresponds to a catalyst concentration of ~ 2×10^{-4} mol.L^{-1}.The former value was fixed as the limiting concentration in the continuous reactor so at any given moment the catalyst concentration in the reactor should be maintained above or equal to this value.

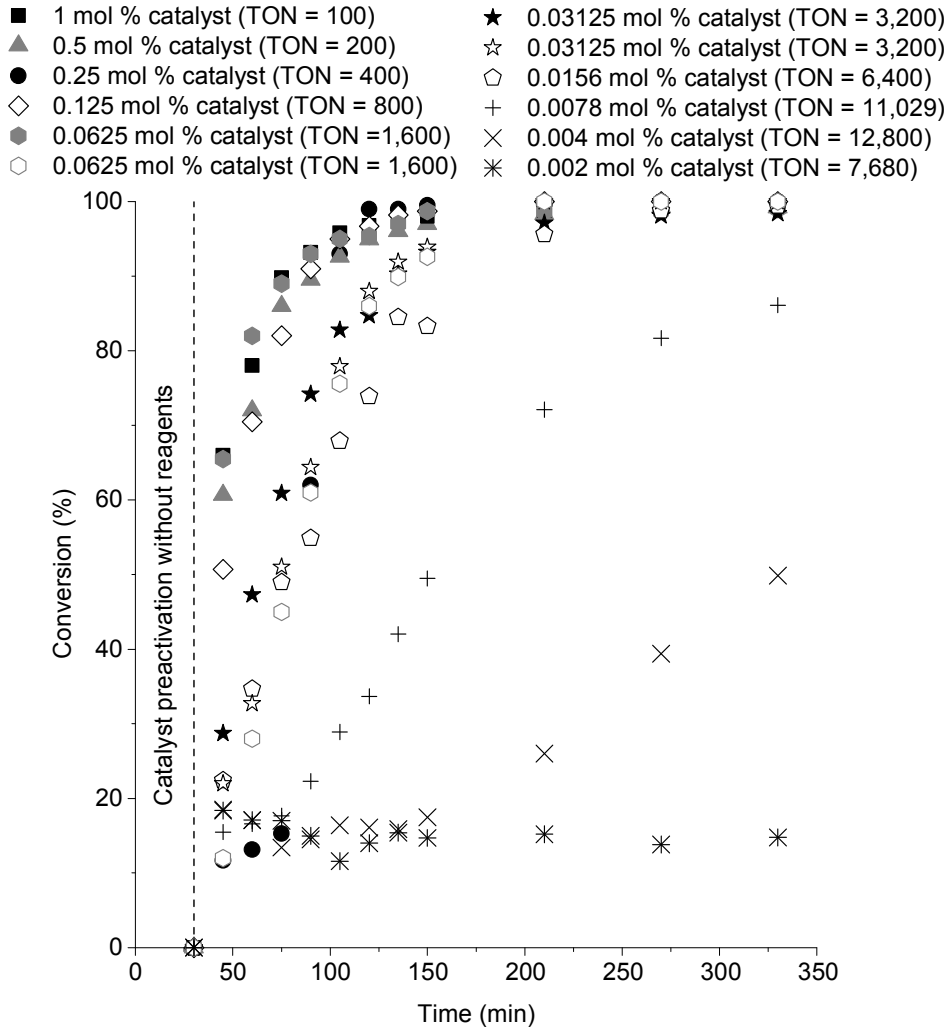

Figure 9.5 – Effect of the catalyst concentration on the Heck coupling reaction performed in batch on the reaction carousel expressed as conversion values as a function of time. For each catalyst concentration the TON is presented in brackets.

9.3.2 Continuous Heck coupling reaction combined with OSN membrane separation

9.3.2.1 Single-reactor system: m-CSTR

The first experiment was performed using only the m-CSTR. Preliminary experiments performed using the PEEK membrane have shown ~ 90 % rejection of the Pd catalyst (~ 10 % losses). From the previous chapter (Chapter 8) it was verified that PEEK membranes become more open with temperature, with a MWCO of 795 g.mol^{-1} for PS in DMF at 85 °C. The combined molecular weights of $Pd(OAc)_2$ and dppp is 636.95 g.mol^{-1} and a slightly lower rejection was expected. Nevertheless, it should be taken into account that the average kinetic diameter of this catalyst complex in DMF is slightly higher than the kinetic diameter of the corresponding PS with the same MW, ~ 1.5 nm vs. 0.99 nm (diameters calculated using BioChem3D ® Ultra). Therefore, in order to compensate the 10 % losses and to maintain and run the continuous reactor at the target concentration of 2×10^{-4} mol.L^{-1}, the feed stream

should contain 2 × 10^{-5} mol.L^{-1} catalyst. An added benefit of this strategy is that the Pd concentration in the permeate stream will remain low, 2 × 10^{-5} mol.L^{-1}, throughout the experiment. As stated in the operating procedure, the system was started initially in batch mode and then run in continuous mode. It was found that for batch mode the reaction proceeded to full conversion in approximately 5 hours (hence in Figure 9.6 at time 0 the conversion is 100 %).

The rejections of product and substrate by the membrane were assumed to be negligible. The catalyst preactivation period of 30 minutes is an order of magnitude lower than its residence time in the reactor (300-600 minutes) and it was assumed that the catalyst is fully active. According to the model predictions (Equation 9.2, Equation 9.3 and Equation 9.4) the expected conversion at 300 minutes residence time (0.2 mL.min^{-1} flow rate, operating pressure ~ 35 bar) was 86.7 %, while at a residence time of 600 minutes (0.1 mL.min^{-1} flow rate, operating pressure ~ 20 bar) the model estimation was for 92.9 % conversion. As can be seen from Figure 9.6 the experimental and theoretical results for the conversion in continuous mode correlate reasonably well, although for the residence time of 600 minutes the experimental values of conversion are higher than the predicted ones. There could be various reasons for this deviation including some changes in the rejection of product and substrate or variations in the feed flow rate. In fact the assumption for constant 0% rejection of the product and substrate may not be quite accurate. Thus for example assuming 30 % rejection of the product and the substrate will increase the apparent conversion measured in the permeate from 93 to 95 % for a residence time of 600 minutes. The conversion data are overall scattered. In general it is a rather complex system but the conversion can be described reasonably well by a relatively simple model.

$$V_{CSTR}\frac{dC_{CSTR,S}}{dt} = C_{in,S}.Q_{in} - Q_{out}.C_{CSTR,S} - \mathrm{V}_{CSTR}.\mathrm{K}.C_{CSTR,S} \qquad \text{Equation 9.2}$$

$$V_{CSTR}\frac{dC_{CSTR,P}}{dt} = C_{in,P}.Q_{in} - Q_{out}.C_{CSTR,P} - \mathrm{V}_{CSTR}.\mathrm{K}.C_{CSTR,P} \qquad \text{Equation 9.3}$$

$$x_{CSTR} = \frac{C_{CSTR,P}}{C_{CSTR,S} + C_{CSTR,P}} \qquad \text{Equation 9.4}$$

The Pd concentration in the permeate (calculated from Equation 9.5) was within the expected range of 2-3 ×10^{-5} mol.L^{-1} but on average it was slightly higher than the predicted value (2×10^{-5} mol.L^{-1}). The Pd concentration in the retentate is again within the expected range but lower than the predicted one: 1.6 × 10^{-4} mol.L^{-1} vs. 2 × 10^{-4} mol.L^{-1} . These results suggest that the Pd rejection is lower than 90 %, with the Pd mass balance closed within 10 % error. In this experiment ~ 0.97 mol (~ 157 g) of product was produced and ~ 5.4 × 10^{-5}

mol (~ 12 mg) of catalyst was utilised, resulting in a catalyst TON (Equation 9.6) of approximately 17,963. On average there was ~ 25.8 mg Pd.kg product^{-1} in the permeate stream. Although the result was rather encouraging in terms of catalyst TON the achieved conversion was still below that obtained in a batch process. One possible way to increase the conversion is to increase the residence time. Once the reactor (or reactors) already has (or have) a fixed volume this can be achieved either by decreasing the flow rate (which might not be feasible practically) or to combine several types of reactors in series. In fact, for a reaction with first order kinetics the CSTR is not the best possible reactor configuration. For such types of reaction a PFR configuration is more efficient as a smaller volume is required compared to a CSTR for substrate conversions near 99 % [214]. As a further strategy for improving conversion, a combination of PFR followed by membrane CSTR was investigated. This specific sequence of reactors was obtained using the Levenspiel plots – which are a useful tool for sequencing reactors in such a way to obtain the best overall conversion with smaller reactor volumes. An added benefit to having PFR before the m-CSTR reactor is that the Pd catalyst would be pre-activated fully before entering the m-CSTR thus eventually accelerating the reaction. In addition, reduced losses through the membrane could be expected, due to the fact that $Pd(OAc)_2$ has a molecular weight (MW) of 224.51 g.mol^{-1}, while the MWs of the Pd complexes with dppp ligand (active species) are higher than 600 g.mol^{-1} and are therefore rejected better by the membrane. It is indeed very simple to assume single rejection value for the catalyst. In fact according to the Heck reaction mechanism, the Pd can be found in various molecules, so called catalytic species, which may actually co-exist. Since these species have different sizes and molecular weights the membrane rejection may also vary. However according to the reaction mechanism proposed by Amatore et al [215] all Pd complexes co-existing during the reaction have molecular weight within the range of 600 g.mol^{-1} and above and should be well rejected by the membrane. Thus the only specie with rejection considerably lower than the others is $Pd(OAc)_2$ with MW of 224.52 g.mol^{-1}(assuming rejection similar to the marker molecules it could be expected a rejection of ~50%). On the other hand according to the same work [215] the formation of the first Pd complex $Pd(OAc)_2$dppp (MW 636.96 g.mol^{-1}) is fast, and thus the probability of free $Pd(OAc)_2$ permeating through the membrane is diminished. Literature data [215] suggest that the formation of Pd complex is a first order reaction with respect to Pd and zero order toward the ligand. Of course this is an idealised case, where the membrane performs in the same way for any type of molecules depending only on their molecular weight. In reality there are other factors also affecting the separation (e.g. membrane-catalyst species interactions) and further extensive study is necessary to elucidate this interesting topic.

$$V_{CSTR}\frac{dC_{CSTR,i}}{dt} = C_{in,i}.Q_{in} - Q_{out}(1-R)C_{CSTR,i} \quad \text{Equation 9.5}$$

$$TON = \frac{total\ moles\ of\ product\ synthesised}{total\ moles\ of\ catalyst\ added\ through\ the\ run} \quad \text{Equation 9.6}$$

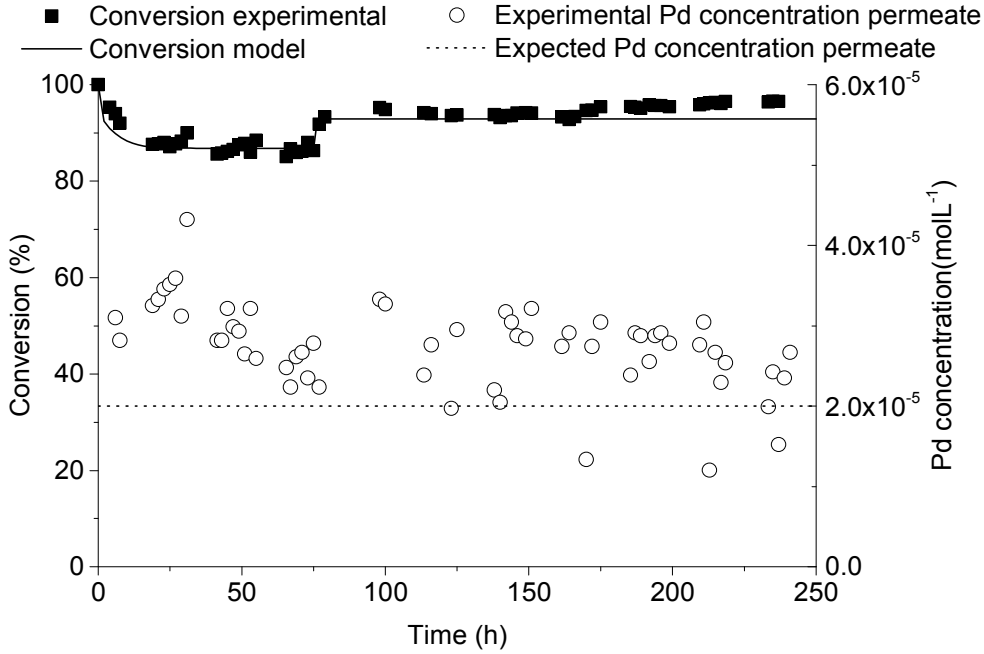

Figure 9.6 – Experimental results of conversion and Pd concentration for the continuous Heck coupling reaction in the single m-CSTR system operated close to the limiting catalyst concentration ($2x10^{-4}$ mol.L^{-1}).). Experimental points are obtained for the permeate stream. The conversion was estimated using initial conditions from the batch start-up of the reactor - 60 mL starting solution, with 100% conversion - 0.6 mol.L^{-1} initial concentration of product and 3.2×10^{-4} mol.L^{-1} $Pd(OAc)_2$. The continuous run was simulated using a feed stream containing 0.6 mol.L^{-1} iodobenzene and 2×10^{-5} mol.L^{-1} Pd catalyst at 0.2 mL.min^{-1} flow rate (residence time of 300 minutes) for the first 75 hours and 0.1 mL.min^{-1} flow rate (600 minutes residence time) thereafter. 90% rejection was assumed for the Pd catalyst and 0% for the product and substrate.

9.3.2.2 Two-reactors in series system: PFR-m-CSTR

- 1.2 mol.L^{-1} Iodobenzene with membrane

After the promising results from the first set of m-CSTR experiments it was decided to investigate further options for increasing the catalyst TON in a PFR-m-CSTR system. One option is to increase the concentration of reagents and/or the feed flow rate. In order to challenge the system, both parameters were doubled and the experiment was started using a feed of 1.2 mol.L^{-1} iodobenzene at 0.2 mL.min^{-1} flow rate (10 hours residence time, 5 in the PFR and 5 in the CSTR). To avoid delays at start-up, the m-CSTR was used as it was, already pre-filled with the post-reaction mixture from the last single m-CSTR continuous

experiment. The m-CSTR was directly connected to the empty PFR. A continuous run was started using a feed solution of 1.2 mol.L^{-1} iodobenzene and 2 x 10^{-5} mol.L^{-1} catalyst and the start-up time for the experiment was considered to be approximately 5 hours after initiating the feed supply, when the PFR-m-CSTR system was completely filled and permeation through the membrane occurred.

From the results in Figure 9.7 one can observe that the conversion was around 98 % throughout the process except for an isolated drop in the conversion (to a value around 92 %) after 5 hours (reasons unknown). The pressure in the system was constant at ~ 35 bar but after 23 hours of operation it increased to around 40 bar. Therefore, the flow rate in the system was decreased to 0.1 mL.min^{-1}, which in turn made the pressure drop to a value of ~ 26 bar. However, the pressure started to build up again, reaching 40 bar after 49 hours and still increasing, so for safety reasons the experiment was stopped. Crystalline triethylamine hydroiodide was found inside the m-CSTR after disassembling the system. This result underlined one potential problem when running the m-CSTR in a continuous process: accumulation of side products.

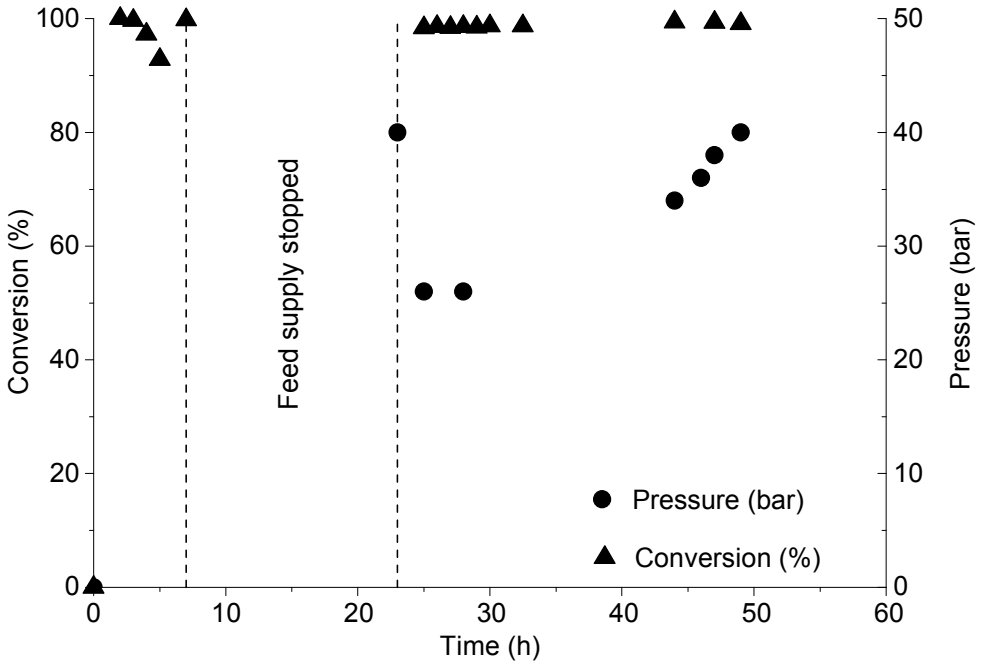

Figure 9.7 – Conversion values in the m-CSTR outlet stream/permeate (left axis) and pressure values (right axis) inside the m-CSTR as a function of time for the two-reactors in series system operated at 1.2 mol.L^{-1} iodobenzene concentration. The system was stopped after 7 hours and restarted after 22 hours.

- Salt accumulation in the m-CSTR study

The salt accumulation problem observed during the last reaction could cause a serious problem during continuous process operation and further investigation was necessary. Measurements were performed in order to obtain the salt solubility limits at different post-reaction media compositions (0.6 mol.L^{-1} and 1.2 mol.L^{-1}). As mentioned earlier the

saturation concentrations of the salt were found to be 3.35 mol.L^{-1} and 2.14 mol.L^{-1} respectively. The salt rejection by the membrane was also determined to be 45.6 %. A mathematical model was used (Equation 9.5) to determine the time after which the concentration of the salt in the m-CSTR reaches its saturation limit under the reaction conditions employed. For simplicity, the salt formation was assumed to be instantaneous, with a conversion of 100 %. This model also helps to predict whether precipitation would pose a problem for a feed having an iodobenzene concentration of 0.6 mol.L^{-1}. Estimated salt concentration in the m-CSTR as a function of time is shown in Figure 9.8.

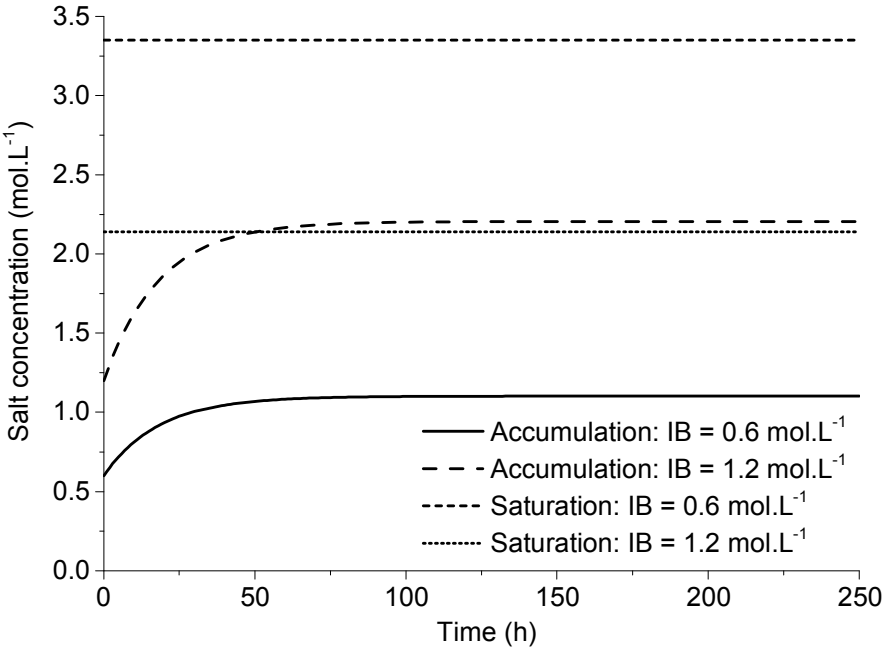

Figure 9.8 – Salt concentration with time at two different iodobenzene concentrations in the feed solution – 0.6 mol.L^{-1} and 1.2 mol.L^{-1}. IB denotes 'Initial iodobenzene concentration'. The estimation for IB = 0.6 mol.L^{-1} was performed using a flow rate of 0.1 mL.min^{-1} and an initial salt concentration of 0.6 mol. L^{-1}, as expected after starting the experiment as batch; For the IB = 1.2 mol.L^{-1} estimation, a flow rate of 0.2 mL.min^{-1} was used and an initial salt concentration of 1.1 mol. L^{-1}.

As is evident from Figure 9.8, the salt concentration never reaches its solubility limit with a feed iodobenzene concentration of 0.6 mol.L^{-1} and salt precipitation will not occur. However, doubling the initial substrate concentration causes the salt concentration to reach its saturation value of 2.14 mol.L^{-1} after approximately 44 hours (the initial salt concentration in the m-CSTR was expected to be ~ 1.1 mol.L^{-1}; the experiment was started using post-reaction mixture from the m-CSTR continuous experiment of 0.6 mol.L^{-1} IB, where the steady state concentration has already been achieved). In this process, rapid crystallisation and reactor clogging seemed to have occurred at ~ 50 hours (~ 35 hours operational time) which is in reasonable agreement with the model estimations (between 40 and 50 hours). In a membrane filtration unit operating with concentrated solutions, a concentration polarisation phenomenon often occurs [216] where next to the membrane surface, concentrations

several times higher than in the bulk solution may exist. Thus crystallisation in an m-CSTR may be initiated earlier than in a non-membrane process. At 0.6 mol.L^{-1} IB concentration salt crystallisation was not observed even though several experiments were performed with durations of more than 250 hours. Overall, this undesired phenomenon should be carefully considered and monitored in continuous membrane reactors.

- 0.6 mol.L^{-1} Iodobenzene with membrane

For this experiment with the two-reactors system, a residence time of 20 hours (10 h in the m-CSTR and 10 h in the PFR) was implemented (flow rate of 0.1 mL.min^{-1}) in order to make a direct comparison with the single m-CSTR reactor performance. The system was started in continuous mode and was fed initially with 100 mL feed solution with 2×10^{-4} mol.L^{-1} Pd concentration followed by feed solution with 2×10^{-5} mol.L^{-1} Pd concentration (all at 0.1 mL.min^{-1} flow rate). It was expected that this reactor configuration would be able to achieve and maintain continuously a ~ 100 % conversion throughout the entire run. Indeed, the results showed that for 142 h operational time the conversion was stable at ~ 100 % but after that it started to decrease slowly and by the end of the run (~ 254 h) reached values around 96 % (Figure 9.9). From the Pd concentration measurements (Figure 9.9) it may be concluded that this decrease in conversion is related to the lower Pd rejection of the membrane - 75 % rejection instead of the assumed 90 % rejection - which means that the palladium concentration of 2×10^{-5} mol.L^{-1} present in the feed was not enough to compensate the palladium loss throughout the system run (the Pd concentration in the retentate at the end of the run was ~ 5×10^{-5} mol.L^{-1}, 5 times lower than anticipated). On average the palladium concentration in the permeate was around 2.6×10^{-5} mol.L^{-1} (2.75 ppm). After the system was disassembled it was possible to verify that the membrane was swollen. Such phenomenon was not observed during the previous experiment and is probably due to the fact that the experiment was started directly in a continuous mode (not in batch, as with the single m-CSTR reactor experiment); the m-CSTR was not initially pre-filled with liquid and the dry membrane was heated for several hours at the beginning of the experiment.

In addition, samples from the PFR outlet were also taken during the run in order to verify the efficiency of the PFR and also to prove that the m-CSTR with PEEK membrane was necessary for achieving conversions near 100 %. From Figure 9.10 one can observe that the conversion in the PFR was below 80 % and that it decreased throughout the run. In fact, based on a rough estimation from the batch experiments (Figure 9.5) it was expected that the conversion in the PFR (operating at ~ 0.0033 mol % catalyst, 2×10^{-5} mol.L^{-1}) should be in the range of not more than 40 - 50 % throughout most of the run. The observed higher

efficiency of the PFR was attributed to a laminar flow with back mixing and/or existence of dead zones in the PFR (non-ideal plug flow reactor) resulting in a higher than anticipated catalyst concentration (Figure 9.10). This could be expected since with the current flow rate of 0.1 mL.min^{-1} the Re number in the PFR is <1.

$$t_r = \frac{V}{Q} \quad \text{Equation 9.7}$$

$$x_{PFR} = 1 - e^{-k.t_{r_{PFR}}} \quad \text{Equation 9.8}$$

$$x_{CSTR} = \frac{x_{PFR} + k.t_{r_{CSTR}}}{1 + k.t_{r_{CSTR}}} \quad \text{Equation 9.9}$$

$$V_{PFR} = L.\frac{\pi D^2}{4} \quad \text{Equation 9.10}$$

$$v = \frac{Q}{A} \quad \text{Equation 9.11}$$

$$Re = \frac{\rho v D}{\mu} \quad \text{Equation 9.12}$$

In this experiment ~ 0.96 mol (~ 156 g) product was obtained and ~ 4.65 × 10^{-5} mol (~ 10 mg) of catalyst was utilised, resulting in a catalyst TON of approximately 20,645. On average there was ~ 26.8 mg Pd.kg product^{-1} in the permeate stream, with Pd mass balance closing within 6 % error. Overall improved system performance in terms of conversion and catalyst TON was obtained as compared to the single m-CSTR system.

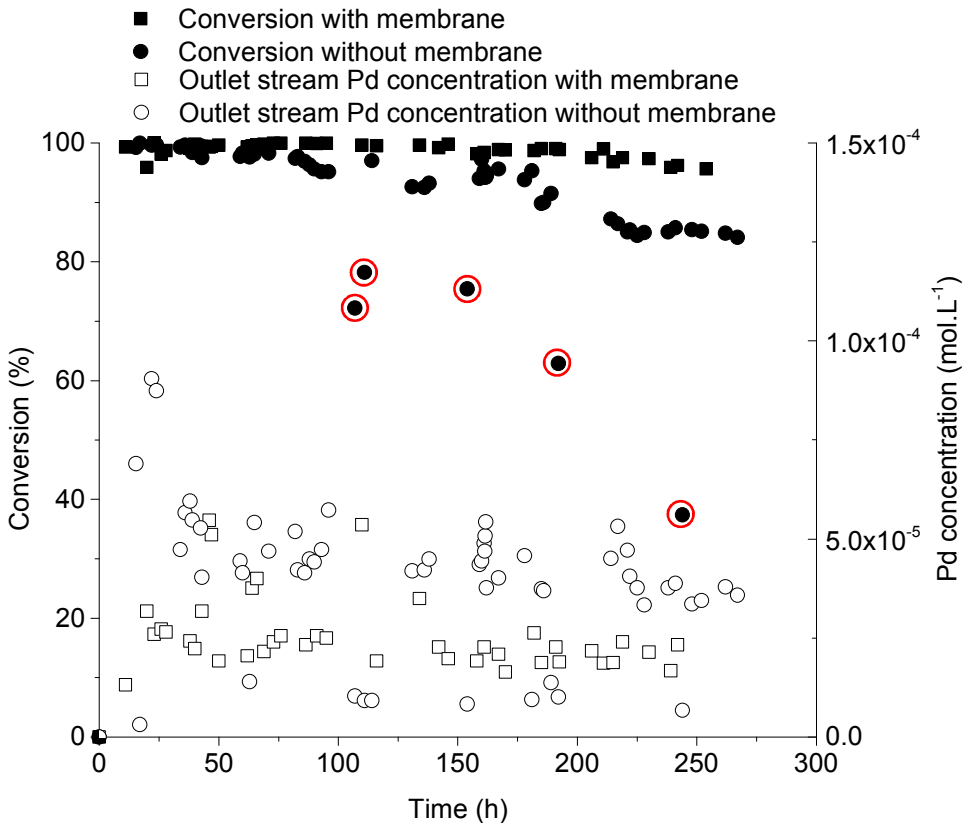

Figure 9.9 – Conversion values in the CSTR outlet stream (permeate) as a function of time for the two-reactors system operated at 0.6 mol.L-1 iodobenzene concentration for the experiments performed with and without membrane (left axis); Pd concentration in the outlet stream of the CSTR vs. time for the experiments performed with and without membrane (right axis). (Points marked with red circles denote sudden drops in the conversion of the CSTR outlet stream possibly due to by-pass streams coming directly from the PFR).

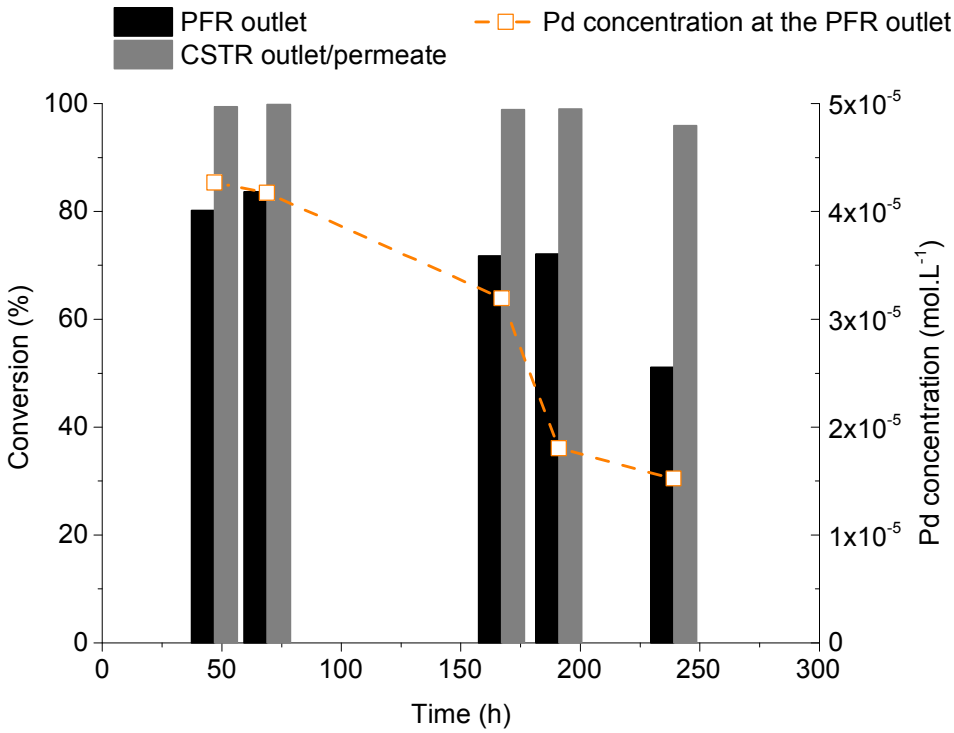

Figure 9.10 – Conversion obtained for the PFR outlet and m-CSTR outlet/permeate at the same time points in the two-reactors in series system operated at 0.6 mol.L^{-1} iodobenzene concentration (left axis); Pd concentration at the PFR outlet (right axis). Data for the experiment with membrane.

- 0.6 mol.L^{-1} Iodobenzene without membrane (blank test)

In the last experiment (0.6 mol.L^{-1} iodobenzene with membrane) the Pd rejection was around 75 % and the conversion only started to decrease after 142 h of running even though the Pd concentration in the retentate was 5 times lower than the one expected – 5 × 10^{-5} mol.L^{-1} instead of 2 × 10^{-4} mol.L^{-1}. From these results it was rather obvious to question the importance of the membrane in terms of function and whether or not the PFR-CSTR system could reach the same values of conversion without it. An experiment was therefore performed without membrane (blank experiment) in order to assess the membrane contribution. The membrane was removed from the cell and the system was fed initially with 100 mL feed solution with 2 × 10^{-4} mol.L^{-1} Pd concentration followed by feed solution with 2 × 10^{-5} mol.L^{-1} Pd concentration (all at 0.1 mL.min^{-1} flow rate) in order to closely reproduce the conditions at the experiment with membrane. Comparison between the experimental results obtained with and without membrane is also shown on Figure 9.9. Although in the beginning both experimental runs gave similar conversion the conversion started clearly to diverge after 59 hours. By the end of the run without membrane, at around 263 hours, the conversion dropped to ~ 82 % (~ 84 % at 255 hours vs. 96 % for the membrane experiment). As could be expected the Pd concentration in the outlet stream was higher for the experiment without membrane. Occasionally there were sharp drops in the conversion of the

outlet stream (red circled points); a possible cause for these sudden fluctuations could be by-pass streams coming directly from the PFR reactor. The measured conversion at the PFR reactor outlet for the experiment without membrane was also lower than the experiment with membrane, although the measured Pd concentration was within the same range (Figure 9.11).

In this experiment ~ 1.06 mol (~ 172 g) product were produced and ~ 6 × 10^{-5} mol (~ 13.5 mg) of catalyst were utilised resulting in catalyst TON of approximately 17,667. As an average there was ~ 34.3 mg Pd.kg $product^{-1}$ in the permeate stream and the Pd mass balance closed within 11 % error. Overall the membrane experiment showed higher conversion, higher catalyst TON and lower Pd content per kg product. This effect will be more pronounced for longer runs and improved membrane performance, where the catalyst will be better retained and the conversion would remain stable at ~ 100 %.

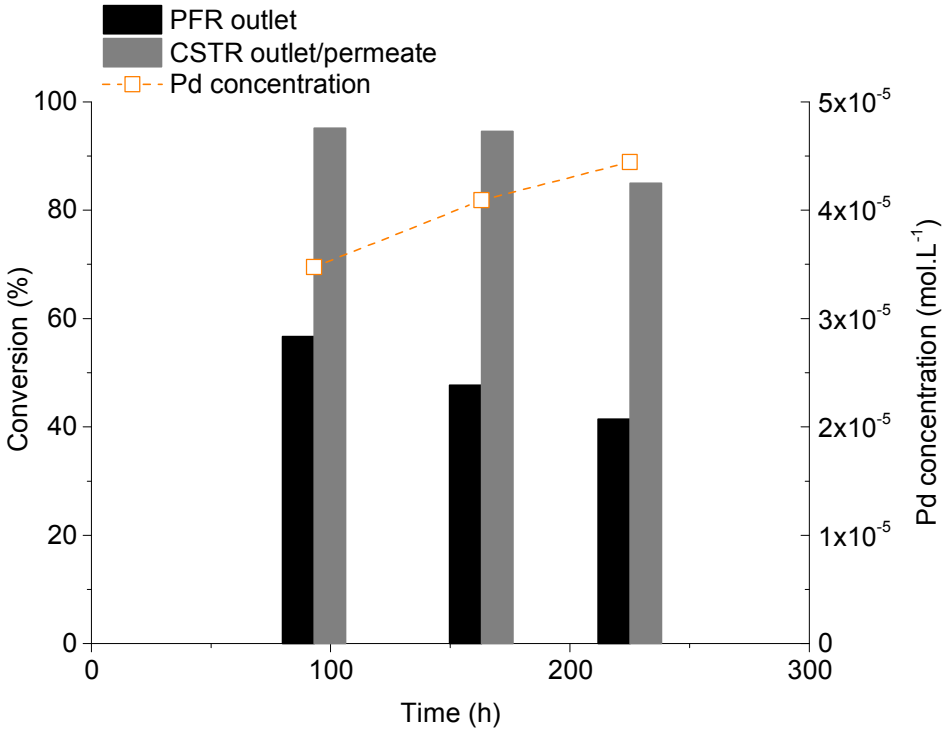

Figure 9.11 – Conversion obtained for the PFR outlet and CSTR outlet at the same time points in the two-reactors in series system operated at 0.6 mol.L^{-1} iodobenzene concentration (left axis); Pd concentration at the PFR outlet (right axis). Data for the blank experiment.

9.3.3 Process considerations and comparison with other processes and configurations

A comparison of these results with others reported in the literature for catalytic processes integrating membrane separation clearly demonstrates the superiority of this process configuration not only in terms of productivity but also in terms of downstream purification (see Table 9.1). While other processes tackle the problem of catalyst retention or catalyst

recycle, attention has been paid neither to the productivity and the overall TON nor to the optimisation of the catalyst loading. In fact, comparing the catalyst loading of different processes only the one reported in [191] uses lower catalyst loading 0.030 mol % vs. 0.032 mol % and reports higher overall TON, 46,823, and lower downstream contamination (0 mg Pd.kg product^{-1}) than the PFR-m-CSTR configuration reported in this study (see Table 9.1). However, the manufacture of Pd nanoparticles encaged in nanoporous interpenetrating polymer networks is not simple and might not be ready for immediate scale-up (see Table 9.1). In addition, the conversion reported in [191] is lower than the one obtained in this system, 70 % versus 98%. One weakness of this process is the relatively low catalyst retention obtained (most of the published works, demonstrate catalyst retention ~99%, see Table 9.1). In this aspect, further optimisation of PEEK membrane production will be essential in bringing even better efficiency to the process.

As a proof-of-concept it is interesting to compare the productivity of the continuous process with the same process performed in batch with and without a membrane. The calculations were performed using the same initial feed composition and a system volume of 1 L for batch modes and a volume of 120 mL for continuous mode. A production of 100 kg was set as the process target for this process. A summary of the calculated results is presented in Table 9.2 below. As can be seen from the table, the continuous process gave again a superior performance in terms of productivity, catalyst TON and the product purity. Although the operation time for PFR-m-CSTR is substantially higher (one order of magnitude) than for batch modes it is nevertheless important to emphasize the difference in volumes considered for both modes. This difference is related to the fact that a small continuous reactor is safer in terms of material inventory than a larger batch reactor of 1 L. Several small continuous reactors operating in parallel will reduce substantially the production time while still maintaining the production safe. This result clearly demonstrates the potential of OSN technology in continuous catalytic processes.

Table 9.1 – Comparison of different process configurations published in literature in terms of reaction type, solvent(s) employed, independence of reaction with separation, type of catalyst employed, catalyst loading (mol %), catalyst retention (mol %), conversion (%), contamination (mg Pd per kg of product) and overall TON.

Reference	Reaction	Solvent	Reaction and separation performed independently	Catalyst employed	Catalyst loading (mol %)	Catalyst retention (%)	Conversion (%)	Contamination (mg TM.kg product^{-1})	Overall TON [a,b]
[188]	Heck coupling	Ethyl acetate and acetone	Yes	$Pd(OAc)_2(PPh_3)_2$	0.275	90.0	98	141	1,779
[193]	Heck coupling	NMP and cyclohexane	Yes	$Pd(dba)_2$	0.500	99.95	55	11.9	87.80
[185]	Hydrolytic kinetic resolution (HKR) of epoxides	Et_2O	Yes	Co-Jacobsen	0.963	98.0	40	240	166.1
[185]	Hydrolytic kinetic resolution (HKR) of epoxides	IPA	Yes	Co-Jacobsen	0.985	93.0	45	764	91.35
[191]	Heck coupling	DMF	No	Pd nanoparticles in the IPNs	0.030	100	70	0	46,823
[202][c]	Enantioselective hydrogenation of dimethyl itaconate	Methanol	Yes	Ru-BINAP	0.563	98.0	98	6.47	1,963
[202][d]	Methyl 2-acetamidoacrylate	Methanol	Yes	Rh-EtDUPHOS	0.565	97.0	90	23.1	926
[203][e]	Hydroformylation of 1-octene	Toluene	No	Modified rhodium complex (PBB10d)	0.100	99.99	50	0.22	2640
[204]	Suzuki–Miyaura Cross-Coupling Reactions	Toluene	Not applicable	XPhos	2.000	Not applicable	95	Not applicable	47.75
m-CSTR	Heck coupling	DMF	No	$Pd(OAc)_2$ + dppp	0.032/0.002	90	~ 95	25.8	17,963
PFR-m-CSTR	Heck coupling	DMF	No	$Pd(OAc)_2$ + dppp	0.032/0.002	75	98 - 100	26.8	20,645

[a] Calculated taking into account all catalyst recycles (if applicable). [b] These numbers should not be compared explicitly because of different operating parameters (e.g. number of catalyst recycles, operation time, heterogeneous or homogeneous catalysis, process design, recovery, etc). [c] Calculated based on a flow-rate of 3.6 mL.h^{-1} and 40 hours of operation. [d] Calculated based on a flow-rate of 3.5 mL.h^{-1} and 22 hours of operation. [e] Calculated for the hydroformylation of 1-octene with PBB10d under 3.0MPa syngas and based on a flow-rate of 0.288 mL.min^{-1}. Note that in a continuous filtration mode rejection and retention are equivalent terms.

Table 9.2 – Comparison between batch mode and continuous process mode with PFR-m-CSTR for the Heck reaction under study in terms of total mass (g, produced/consumed), reactor productivity, catalyst loading (%), contamination (mg Pd per kg of product) and TON.

	Total mass (g)[a]					
	Palladium consumed	E-methyl cinnamate (product) formed	Productivity (g product. L^{-1} reactor.h^{-1})	Catalyst loading (mol %)	Contamination[b] (mg Pd.kg product^{-1})	TON
Batch without membrane[c]	21.0	100×10^3	14.57	0.032	210.1	3,123
Batch with membrane[d]	4.316	100×10^3	416.7	0.032/0.002	42.71	15,286
Continuous[e] PFR-m-CSTR	2.143	100×10^3	6944	0.032/0.002	21.43	30,580

[a] Total mass consumed/produced after 286 days, 391 days and 3453 days for batch without membrane, batch with membrane and continuous PFR-m-CSTR respectively. [b] Assuming 90 % rejection of Pd. [c] Assuming a reactor volume of 1 L, 3.43 batches per day (5 hours reaction and 2 hours for maintenance, filling, and emptying periods), a conversion of 100 % and catalyst and iodobenzene concentrations of 2×10^{-4} mol.L^{-1} and 0.6 mol.L^{-1}, respectively. [d] Assuming a reactor volume of 1 L, 2.95 batches per day (including 5 hours for reaction, 1.12 hours for filtering 85 % of the reactor medium and 2 hours for maintenance, filling, and emptying periods), a membrane area of 0.58 m^2 (flux = 1.3 L.m^{-2}.h^{-1}), a rejection of 90 % (in respect to palladium), a conversion of 100 %, a iodobenzene concentration of 0.6 mol.L^{-1} and a catalyst feed concentration of 2×10^{-4} mol.L^{-1} for the first batch and 2×10^{-5} mol.L^{-1} for the following batches. [e] Assuming 0.2 mL.min^{-1} flow rate, an average conversion of 98 %, a catalyst feed concentration of 2×10^{-4} mol.L^{-1} for the initial batch and 2×10^{-5} mol.L^{-1} throughout the continuous run; iodobenzene concentration of 0.6 mol.L^{-1}.

9.4 Results and discussion for Heck reaction 2

Heck reaction 2 is part of a wider research project; the reaction is part of a multi-step synthesis that requires solvent exchange [209]. The outlet stream of Heck reaction 2 was fed into a membrane cascade (after removal of triethylamine and ethyl acrylate) in order to perform a solvent exchange from DMF to EtOH (data not shown here). The subsequent reaction is performed in EtOH and a packed bed reactor filled with iron powder is used as a catalyst (Figure 9.12). Unlike Heck reaction 1 this study is not much focused on Pd removal but on the proof of concept of using a membrane cascade for solvent exchange as an intermediary step of a multi-step synthesis. Given the relevance of PEEK membranes for the first reaction of this multi-step synthesis, named Heck reaction 2, only data for this reaction is presented in this section.

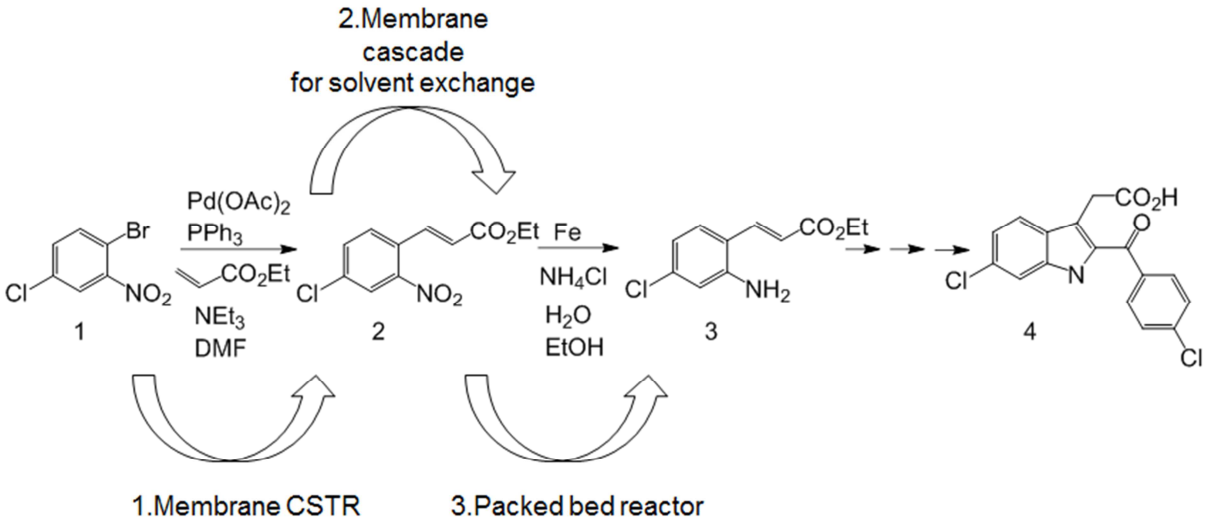

Figure 9.12 – Schematic of chemical reaction of [6-Chloro-2-(4-chlorobenzoyl)-1H-indol-3-yl]-acetic acid formation depicting the first two steps. Heck reaction 2 is the first reaction of this multistep synthesis and is part of a wider research project involving solvent exchange with membrane cascade and a subsequent reaction using a packed bed reactor.

Heck reaction 2 was performed using the same equipment as used in Heck reaction 1. The m-CSTR volume used was 100 mL instead of 60 mL. The rejections of the substrate, product and salt were determined to be 9 %, 24 % and 54 %, respectively, at 90 °C in DMF for the PEEK membrane. From the practical knowledge obtained in Heck reaction 1, the solubility of triethylamine hydrobromide (salt) was determined in order to find the optimal concentration for avoiding precipitation of the salt in the m-CSTR and have an acceptable productivity. The solubility for the salt was found to be 0.55 mol.L^{-1} at 90 °C in DMF. Using the solubility limit of the salt, two values of substrate concentration in the feed, 0.1 mol.L^{-1} and 0.2 mol.L^{-1}, were modelled in order to verify the salt concentration after reaching steady state and verify if it is below the solubility limit. A mathematical model was used (Equation 9.5) to determine the time after which the concentration of the salt in the m-CSTR reaches its saturation limit under the reaction conditions employed. For simplicity, the salt formation was assumed to be instantaneous, with a conversion of 100 %. From Figure 9.13 it was possible to verify that both initial concentrations of 2-chloro-5-bromonitrobenzene, 0.1 mol.L^{-1} and 0.2 mol.L^{-1}, generate a salt concentration in the m-CSTR below the solubility limit.

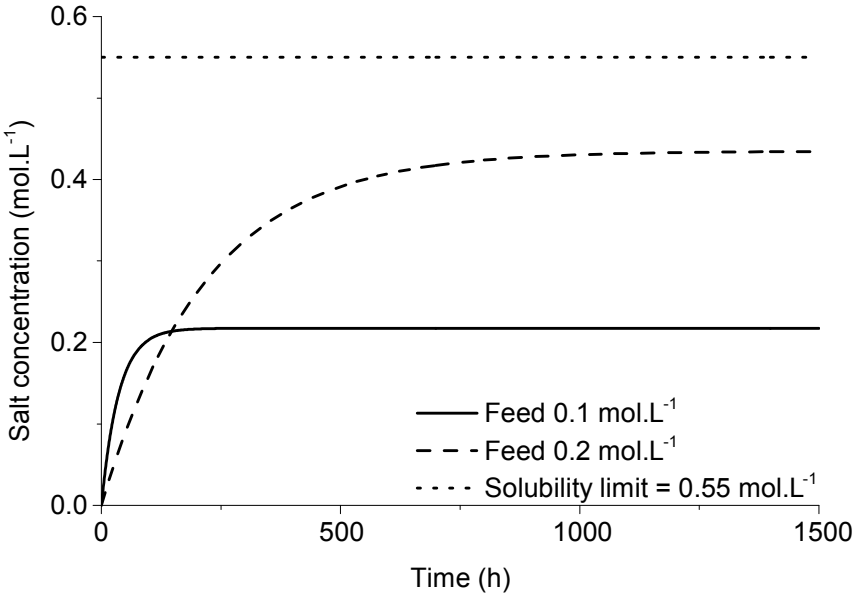

Figure 9.13 – Salt concentration with time at two different 2-chloro-5-bromonitrobenzene concentrations in the feed solution – 0.1 mol.L^{-1} and 0.2 mol.L^{-1}. CB denotes 'Initial 2-chloro-5-bromonitrobenzene concentration'. The estimation for CB = 0.1 mol.L^{-1} and CB = 0.2 mol.L^{-1} was performed using a flow rate of 0.1 mL.min^{-1} and a rejection of the salt of 54 %.

9.4.1 Continuous Heck coupling reaction combined with OSN membrane separation: Single-reactor system (m-CSTR)

The first run was performed only in the m-CSTR (without PFR) and was started in batch by loading all the reagents and catalyst with a concentration of 1 mol % (1.0×10^{-3} mol.L^{-1}) as used by Caron, S. and Vazquez E. [209]. After 24 hours, reagents were fed at 0.1 mL.min^{-1} with a concentration of 0.1 mol.L^{-1} of 2-chloro-5-bromonitrobenzene and 10 equivalents of ethyl acrylate. The results for conversion and catalyst concentration are presented in Figure 9.14. Conversion of the substrate was in average ~ 87 % which was a bit lower than expected from the batch experiments. This lower conversion could be attributed to the fact that Pd is not being fed constantly (only reagents). On average the Pd concentration in the permeate was ~ 9.9×10^{-6} mol.L^{-1}, much lower than expected from an estimation for 90 % rejection, 1.0×10^{-4} mol.L^{-1}, suggesting a rejection of ~ 99 % for the Pd catalyst. However, after opening the cell at the end of the experiment the Pd concentration in the retentate was also quite low, 3.4×10^{-5} mol.L^{-1}, and the mass-balance on Pd did not close. The TON for this continuous reaction was around 1273 and the Pd contamination in the product was ~ 33 mg Pd.kg of product^{-1}.

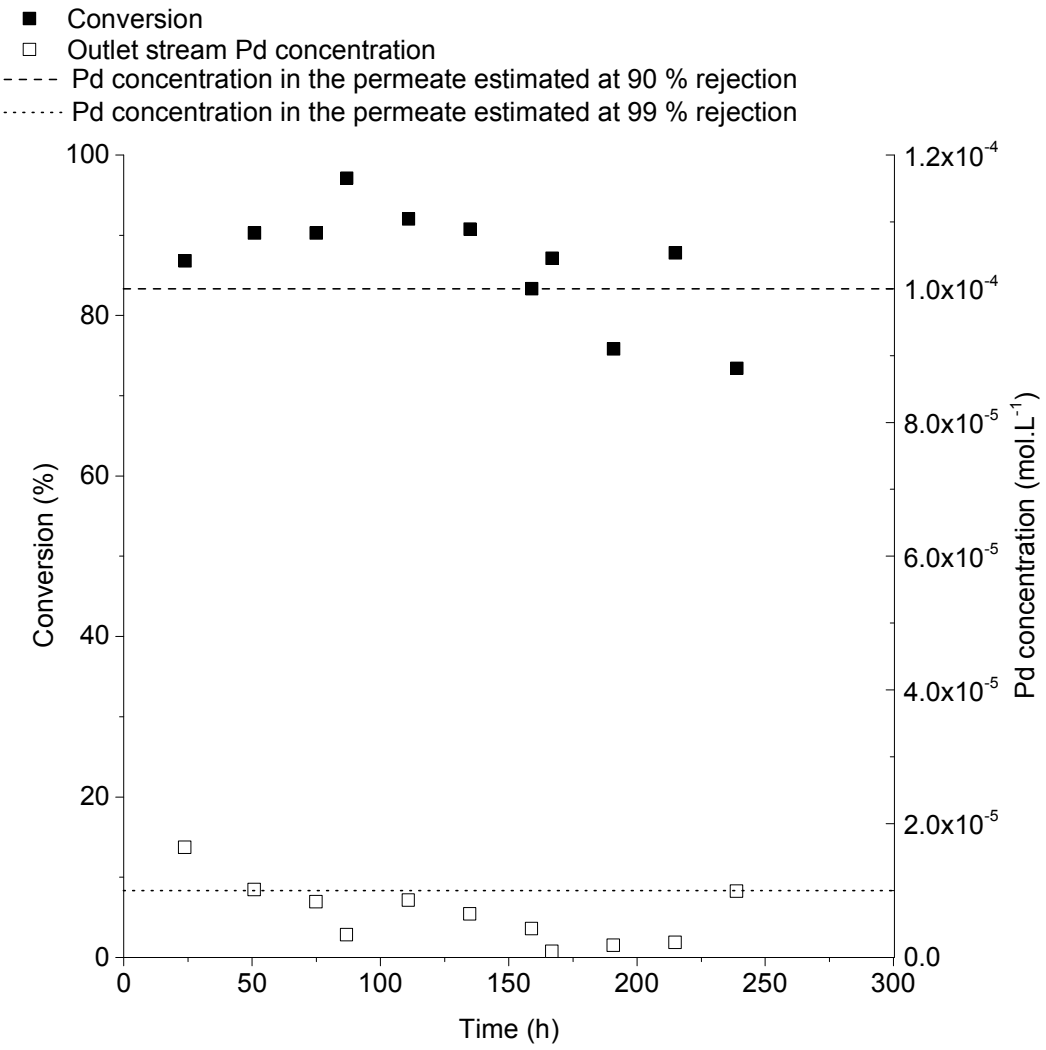

Figure 9.14 – Conversion values in the CSTR outlet stream (permeate) as a function of time for the system operated at 0.1 mol.L^{-1} 2-chloro-5-bromonitrobenzene concentration (left axis); Pd concentration in the outlet stream of the CSTR vs. time.

After opening the cell it was possible to verify that the membrane was covered in Pd. This Pd "film" on the membrane surface did not affect the permeance (there were no changes in the pressure of the system) which means it was porous and probably helped increasing the rejection of Pd over time. The rejection of the Pd was expected to be lower than the one for Heck reaction 1 given the fact that the catalyst complex has a total MW of 487.49 g.mol^{-1} which is lower than the MWCO expected at this temperature, 795 g.mol^{-1}. However, as the mass-balance of Pd did not close it is difficult to determine the cause of this higher rejection. Using SEM pictures it was possible to observe Pd particles on the membrane surface.

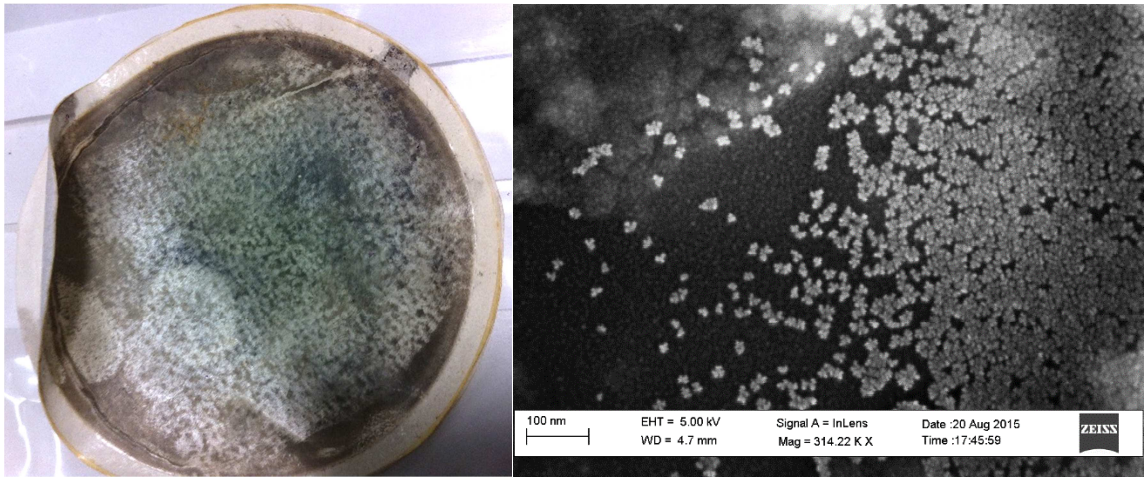

Figure 9.15 – Left: Image of PEEK membrane after being removed from the m-CSTR depicting deposition of Pd on its surface. Right: SEM image of the surface of PEEK membrane with a magnification of 314.22 k times showing Pd nanoparticles deposited on the surface.

9.4.2 Continuous Heck coupling reaction combined with OSN membrane separation: two-reactors in series system (PFR-m-CSTR)

In order to obtain better productivity and to have a good mass balance on Pd another experiment was performed using a PFR followed by the m-CSTR. The initial catalyst loading was also decreased from 1 mol % to 0.5 mol % given that after 24 hours it was possible to obtain 100 % conversion with the catalyst loading of 0.5 mol % (see Figure 9.16 a)). As can be seen in Figure 9.16 b) the ethyl acrylate concentration influences to a great extent the reaction kinetics. The reaction was reported with 10 equivalents for the ethyl acrylate [209]. Initially it was thought to decrease the amount of ethyl acrylate to two equivalents in order to decrease the excess of this reagent (closer to the stoichiometry of the reaction and similar to Heck reaction 1) and therefore diminish the exposure to the strong smell that this compound exhibits. To give a margin for excess of 50 %, 3 equivalents were used instead. The initial feed consisted of a total volume of 300 mL and the flow rate was set at 0.05 $mL.min^{-1}$ (total residence time of ~ 53 hours). Since the conversion was not as high as predicted (> 90 %) the catalyst loading was increased to 1 mol % (Figure 9.17) and since the conversion was still dropping after 200 h the ethyl acrylate concentration was increased to 10 eq. The following feed streams were prepared with 0.1 mol % (assuming 10 % Pd rejection).

After 1098 h of operation the flow rate was changed to 0.25 $mL.min^{-1}$ (total residence time of 10.6 h) and the catalyst loading was increased to 10 mol %. This change was performed to decrease the overall process residence time. As a consequence the conversion dropped because the previous feed that was inside the PFR and m-CSTR did not have time to convert due to the lower catalyst loading (0.1 mol %). After 1187 h the flow rate was further increased to 0.5 $mL.min^{-1}$ to reduce considerably the residence time to approximately 5.3 h. At the end of the experiment (~ 1200 h) the conversion was only around 60 % and the experiment had to be stopped because of time constraints. Conversion data for the CSTR

and PFR as well as Pd concentration in the permeate outlet are presented in Figure 9.17 and Figure 9.18 respectively. Fluctuations in conversion were due to technical problems with the HPLC pump given the aggressive medium of this reaction (90 °C, DMF, triethylamine and ethyl acrylate). For this continuous reaction the TON was quite low, ~ 81.4, due to low average conversion of 79 % which decreased productivity of the reactor to a value of only 0.91 $g.L^{-1}.h^{-1}$.

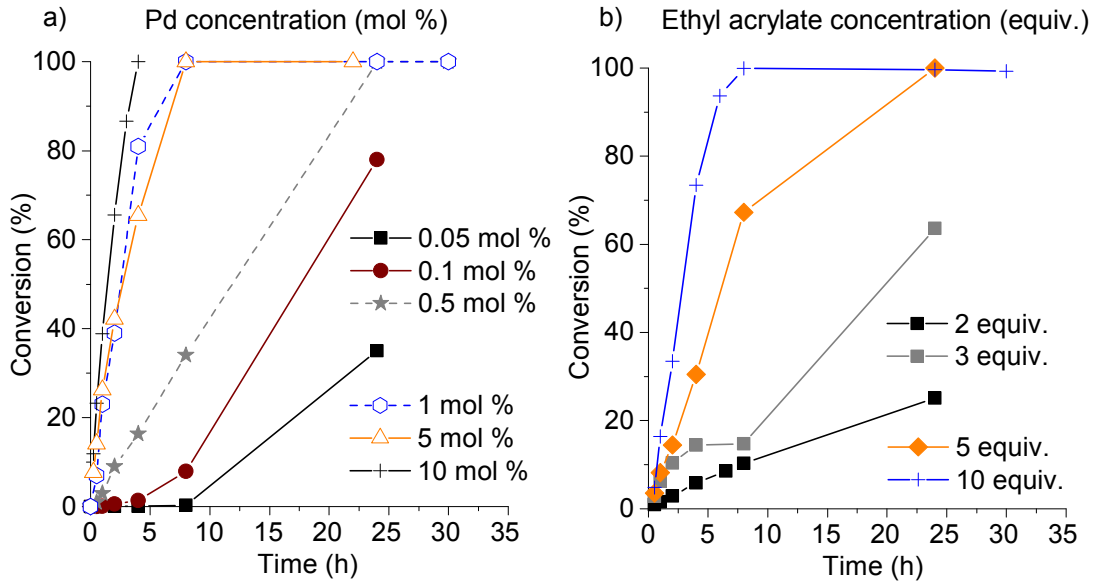

Figure 9.16 – a) Effect of the catalyst concentration on the Heck coupling reaction 2 performed in batch on the reaction carousel expressed as conversion values as a function of time. b) Effect of the ethyl acrylate concentration on the Heck coupling reaction 2 performed in batch on the reaction carousel expressed as conversion values as a function of time. The catalyst loading was 1 mol % for the ethyl acrylate concentrations studied.

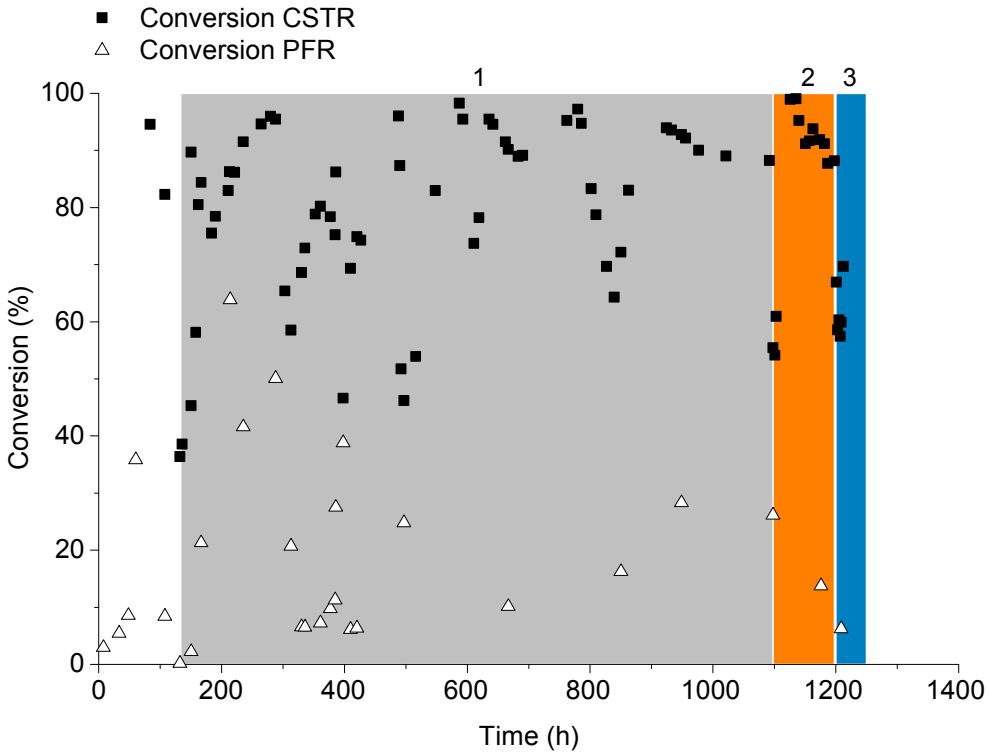

Figure 9.17 – Conversion values in the PFR outlet stream and in the CSTR outlet stream (permeate) as a function of time for the system operated at 0.1 mol.L^{-1} 2-chloro-5-bromonitrobenzene concentration. The shaded areas numbered from 1 to 3 represent different total residence times: 1 - 53 h; 2 - 10.6 h; 3 – 5.3 h.

The Pd concentration in the permeate (CSTR outlet) was in general lower than expected due to higher rejection, 95 % instead of 90 %. This lower Pd in the permeate was not directly correlated with higher active catalyst concentration in the reactor. In fact, in terms of Pd concentration, and observing the same as in the previous run, it was verified that the palladium inside the reactor was lower than expected. This was again attributed to the formation of a Pd "film" on the membrane surface as can be seen in Figure 9.19 and Figure 9.20. In Figure 9.20 (b, c and d) it was possible to observe particles on the surface of the membrane and using SEM-EDX it was possible to confirm the presence of Pd on the surface but also on the cross-section. In average, the surface had 50 % Pd (in terms of atomic percentage and comparing with the oxygen and carbon from the membrane) whereas the cross-section shows a variance of Pd content along the longitudinal axis. The Pd content was high for spectrum points s2(2) and s3(3), 47.90 % and 21.29 % respectively, which was not in agreement with the high rejection the membrane exhibited for Pd. This fact could be explained by some contamination from the membrane surface when preparing the sample for SEM. By dissolving in *aqua regia* 2 membrane pieces (average area of 0.55 cm^2) obtained from the membrane used in the reaction and applying the same procedure for Pd analysis it was possible to obtain an average value of Pd adsorbed on the membrane

surface of ~ 0.013 g. Overall, the Pd contamination in the product stream was higher than the previous run (the m-CSTR run) with a value of ~ 153 mg Pd.kg of product^{-1}.

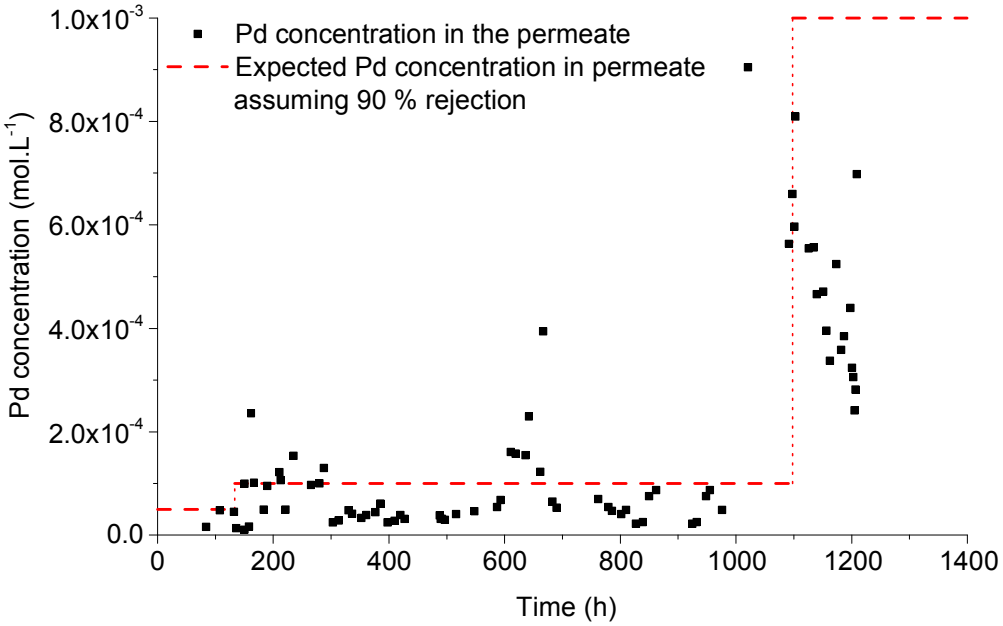

Figure 9.18 – Pd concentration (mol.L^{-1}) in the outlet stream of the CSTR (permeate) as a function of time. The red dashed line represents the expected Pd concentration in the permeate assuming 90 % rejection.

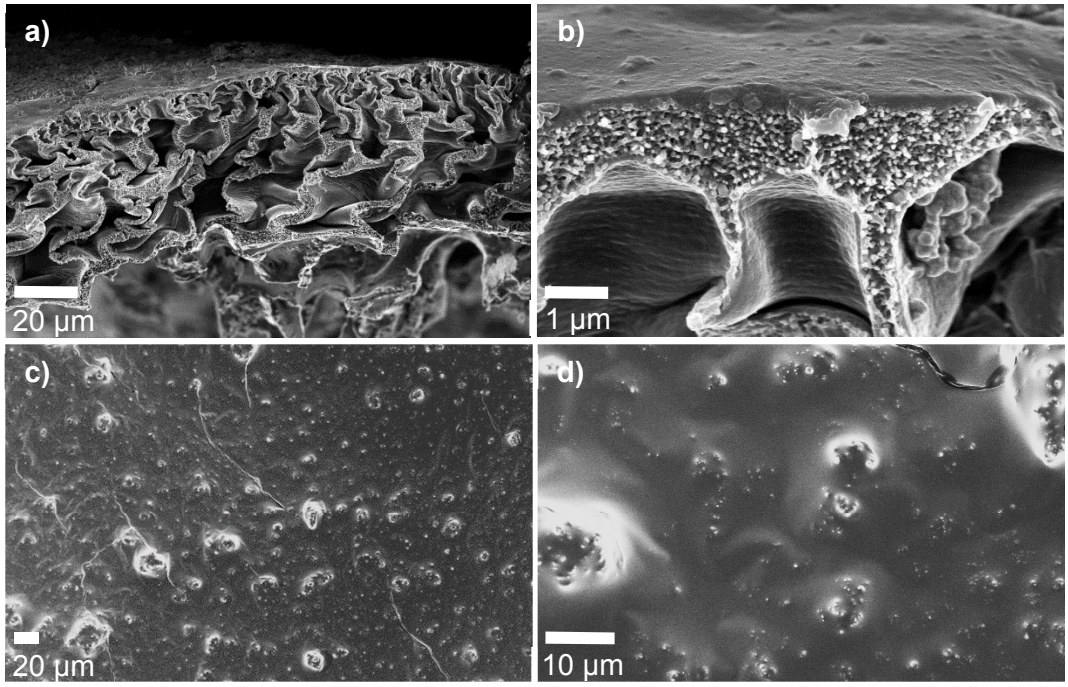

Figure 9.19 – SEM images of PEEK membrane used for Heck reaction 2 after being removed from the m-CSTR. a) and b) are images of the cross-section and c) and d) are images of the membrane surface. Magnification of the images: a) 1.91 kx; b) 34.03 kx; c) 0.74 kx and d) 4.34 kx.

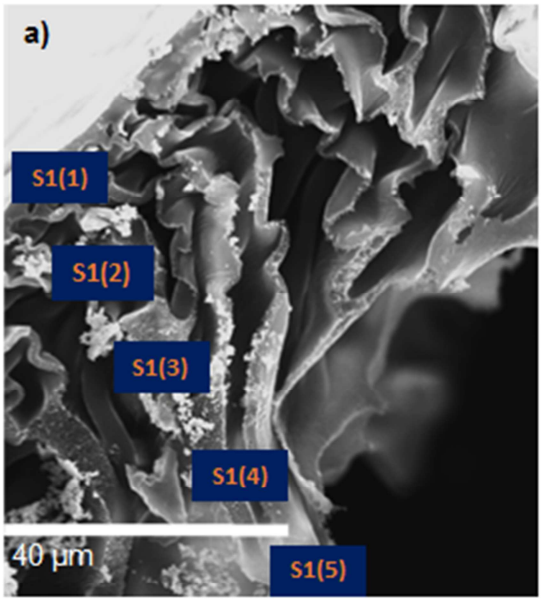

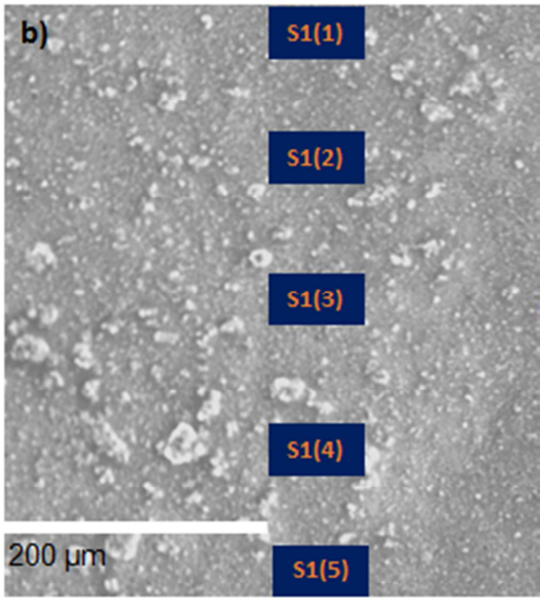

Spectrum	C (%)	O (%)	Pd (%)
s1(1)	54.99	45.35	-0.33
s2(2)	41.87	10.23	47.90
s3(3)	59.08	19.64	21.29
s4(4)	75.05	24.21	0.73
s5(5)	71.22	27.75	1.03

Spectrum	C (%)	O (%)	Pd (%)
s1(1)	19.39	30.54	50.07
s2(2)	21.75	31.46	46.79
s3(3)	19.99	28.13	51.88
s4(4)	17.49	26.73	55.78
s5(5)	20.08	34.28	45.64

Figure 9.20 – SEM-EDX of PEEK membrane used for Heck reaction 2. a) cross-section image; b) surface image. Underneath each SEM image there is the corresponding elemental analysis in atomic percent (%).

9.5 Conclusions

This chapter has shown the potential of PEEK membrane process for performing Heck catalytic reactions in continuous mode and achieving high catalyst TON, stable productivity and low Pd content per kg product. Heck reaction 1 proved to be technically challenging with the salt accumulation and consequent precipitation. The reaction itself was easy to perform and the conversion was around 98 % for the m-CSTR and PFR-m-CSTR configurations. The best system was the PFR-m-CSTR with a TON of ~ 20,000 and Pd contamination in the product stream of ~ 27 mg Pd per kg of product. In this reaction, when the PEEK membrane was removed there was no visible deposit of Pd film on its surface. The second Heck reaction (Heck reaction 2) was had an overall conversion lower than 90 %. The reason for this was attributed to technical problems arising from the HPLC pump given the harshness of ethyl acrylate and DMF that damaged the pump seals and check valves. The initial residence time was set at 53 h (flow rate of 0.05 $mL.min^{-1}$). In order to decrease the

residence time of Heck reaction 2 to 10.6 h, and increase productivity, the flow rate was set at 0.25 mL.min^{-1}. The conversion dropped as the previous feed had a low catalyst loading (0.1 mol %). After 1187 h the flow rate was further increased to 0.5 mL.min^{-1} (residence time of 5.3 h) and the conversion was around 60 % until ~ 1200 h of operation (when the experiment was terminated). In this reaction, the Pd rejection was above 98 % which was unexpected given the fact that the Pd complex of Heck reaction 2 has a lower MW, 487.49 g.mol^{-1}, than the Pd complex of Heck reaction 1, 795 g.mol^{-1}. This could be explained by the formation of a Pd "film" on the membrane surface that functioned as an additional "separating layer" without compromising the permeance of the membrane. The formation of this "film" could also explain the poor mass balance and the lower Pd concentration inside the m-CSTR.

Overall this chapter demonstrated that coupling the continuous process with a membrane separation step improves the continuous process performance, the catalyst productivity (TON) even further and reduces undesired metal content in the product stream. It also revealed the potential adverse effect of side product accumulation in the combined continuous reactor-membrane separation units, which may lead to serious process disruptions or decrease in substrate conversion and therefore lower productivity. Finally the excellent potential of PEEK membranes in high temperature catalytic processes has been demonstrated as it was the goal of this thesis.

Chapter 10. Final conclusions and future directions

10.1 Conclusions

This work demonstrated for the first time that it is possible to produce nanofiltration membranes from highly resistant native PEEK material. Without modifying the PEEK membranes (for example by changing the monomers or by sulphonating the polymer), the membranes were developed and an understanding of the post-phase inversion parameters was attempted. Although a theoretical and phenomenological model was not developed regarding the drying mechanism and the solvents filling the pores prior to drying, this thesis opens the way to explain such phenomena using a statistical model. The transport mechanism was also studied at temperatures above 30 °C and this was performed for the first time for polymeric membranes with organic solvents. These results shed some light in terms of changes in the active layer when increasing the filtration temperature. Given the stability of PEEK NF membranes at high temperatures, it was possible to perform reaction and separation of Pd catalyst in reactions operated at temperatures around 90 °C (a 2-in-1 process).

To investigate the preparation conditions, four different PEEK powders from two different brands were investigated, VESTAKEEP® (2000P and 4000P) and VICTREX® (150P and 450P). The membranes had a low degree of sulfonation and exhibited excellent resistance toward polar aprotic solvents, acids and bases. Membrane separation performance was tested in THF and DMF. The permeance of DMF was lower, as expected from the increase in solvent viscosity (DMF is 1.7 times more viscous than THF). The post-phase inversion drying process of the membranes was shown to be the reason for the change in the separation performance from the ultra to the nanofiltration range. Some correlation between MW of the PEEK polymer and membrane performance was also established: higher MW PEEK polymer produces tighter membranes with lower permeances. The selected brand and grade for all subsequent studies in this thesis was VESTAKEEP® 4000P. The PEEK membranes produced from this grade were shown to be resistant to acids and bases for a period of 2880 h (by performing a solubility test) and to have a DC of ~ 45 %.

After establishing a procedure for producing the PEEK membranes at bench scale, the membranes were successfully scaled-up to spiral-wound modules and it was verified that the casting speed influenced the final membrane performance in terms of permeance. The two SW modules produced from the continuous casting of PEEK membranes had a permeance of 0.47 $L.h^{-1}.m^{-2}.bar^{-1}$ and 0.26 $L.h^{-1}.m^{-2}.bar^{-1}$ for casting speeds of 0.01 $m.s^{-1}$ and 0.06 $m.s^{-1}$ respectively. Under SEM, the membranes cast at different speeds showed differences in the thicknesses of the separating layer, with the lower casting speed originating thinner

separating layers, 176 nm at 0.01 $m.s^{-1}$ vs. 230 nm at 0.06 $m.s^{-1}$. However, these were very preliminary results and more scaling-up studies should be performed in terms of casting speed to understand better the continuous casting but also to establish a procedure that produces reproducible membranes.

Whether PEEK membranes are produced at bench scale or industrially, it was verified that their manufacturing process and waste-treatment cost are an environmentally friendly choice when compared with other common OSN membranes such as polyimide based membranes. Calculating the solvent intensity (common green metric) and the waste cost (£. kg^{-1} polymer) in order to compare the different membrane production it was possible to conclude that PEEK membrane manufacturing has a much lower environmental burden. The solvent intensity of PEEK was 8.3 (both bench and industrial scale) whereas the P84 PI production methods at bench and industrial scales range from 35 to 224. In terms of waste cost, PEEK membrane production had a cost of 45 £. kg^{-1} polymer at both bench and industrial scales whereas P84 PI production methods had an average cost of 1019 £. kg^{-1} polymer at bench scale and an average cost of 189 £. kg^{-1} polymer at industrial scale.

Even though PEEK membranes were stable in DMF and THF without crosslinking, the permeance of the membranes was low when compared with commercial OSN membranes, 0.2 $L.h^{-1}.m^{-2}.bar^{-1}$ vs. 1-4 $L.h^{-1}.m^{-2}.bar^{-1}$. In order to manipulate the performance of PEEK membranes, two factors were investigated: the concentration of polymer in the dope solution and the solvent filling the pores prior to drying. When varying the polymer dope concentration from 8 wt. % to 12 wt. % a shift from more open membranes (8 wt. %) to tighter membranes (10 wt. % and 12 wt. %) was observed. The type of solvent filling the membrane pores prior to drying had a pronounced effect on the separation performance. It was possible to vary the MWCO from 295 $g.mol^{-1}$ to 1400 $g.mol^{-1}$ (in terms of nanofiltration range). This result was encouraging because it proved that it was possible to change the performance of a phase inverted membrane by simply replacing the solvent filling the membrane pores. However, it was not possible to increase the permeance while maintaining the MWCO constant. Another parameter studied for both factors (polymer concentration and solvent filling prior to drying) was the effect of drying temperature. When comparing the membranes dried at 120 °C from different solvents (drying temperatures were 20 °C, 40 °C, 80 °C and 120 °C) the following trend was observed (from lower MWCO to higher MWCO membrane): water < IPA < MeOH < n-hexane < EtOH < acetone < THF. The tightest membrane, dried from water at 120 °C, had a MWCO of 395 $g.mol^{-1}$ and a permeance of 0.2 $L.h^{-1}.m^{-2}.bar^{-1}$ whereas the THF dried membrane (the loosest membrane) did not have a MWCO in the NF range and had a permeance of ~ 2.5 $L.h^{-1}.m^{-2}.bar^{-1}$. When comparing the different drying temperatures for the same solvent, it was observed that the effect of drying temperature was negligible for membranes dried from water whereas for membranes dried

from other solvents the effect was more pronounced (e.g. acetone and THF). In summary, by increasing the temperature from 20 °C to 120 °C it was possible to further manipulate the MWCO when drying from the same solvent. A summary of the results obtained in Chapter 7 is presented in Figure 10.1 By performing a statistical analysis of the presented data an attempt was made to understand the relevant solvent properties involved in the drying treatment. The Hansen solubility parameter, polarity and their interactions with molar volume were found to be the most important parameters influencing membrane MWCO. Nevertheless, this was just an initial study of a very complex phenomenon that needs to be further investigated in order to understand how ISA membranes can still be manipulated after phase inversion.

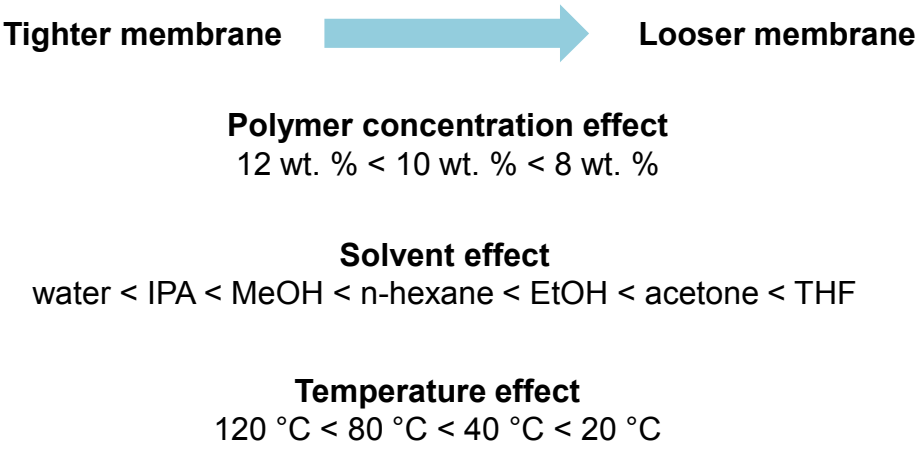

Figure 10.1 – Summary of the results obtained in Chapter 7. Controlling molecular weight cut-off of PEEK nanofiltration membranes using membrane drying

Another study in this thesis was the fact that PEEK NF membranes did not age under drying conditions. The change in performance over time for most ISA membranes has been a major drawback due to loss in permeance (known as physical aging). In this study, the tensile strength was measured for PEEK membranes air-dried at 20 °C and 120 °C and for PEEK membranes vacuum dried at 190 °C. The results showed an increase of the Young's Modulus of elasticity with the temperature for PEEK membranes and values of 61 MPa, 108 MPa and 170 MPa were obtained for 20 °C, 120 °C and 190 °C respectively. However, the maximum strain attained at 190 °C, 7.5 %, was much lower than at 20 °C and 120 °C, 65 % and 75 % respectively. This result showed the membrane was less elastic at 190 °C. PBI and PI membranes were also compared with PEEK membranes but after annealing these membranes became brittle and it was not possible to measure tensile strength. The reason for this structural change of PBI and PI membranes was attributed to a molecular rearrangement on a surface level because these membranes presented no permeance after 6 h and 24 h of annealing. PEEK maintained its permeance after 6 h and 24 h of annealing

at 120 °C, 0.2 $L.h^{-1}.m^{-2}.bar^{-1}$, due to inefficient polymer packing that prevents major polymer rearrangements (negligible aging). As mentioned before, the PEEK membranes were postulated to be suitable for high temperature filtrations. PEEK membranes were stable over a period of 4 weeks in DMF, reaching temperatures up to 140 °C (around the glass transition temperature of PEEK). PI membranes could not resist one cycle of high temperature, and even though PBI membranes were robust for the first two filtration cycles their performance changed with a decrease in rejection for cycles 3 and 4. With the increase of temperature, the membranes presented a higher pore size, which was inferred from the lower rejection observed experimentally.

As a final assessment, PEEK membranes were used in continuous Heck catalytic reactions. Two reactor configurations are investigated: a continuous single stirred tank reactor/membrane separator (m-CSTR); and a plug flow reactor (PFR) followed by m-CSTR (PFR-m-CSTR). It was proved that the catalyst productivity (TON) could be further increased and that the Pd contamination in the product stream could be reduced. For Heck reaction 1, a TON of ~ 20,000 was obtained for the PFR-m-CSTR configuration and a Pd contamination of ~ 27 mg Pd per kg of product was present in the outlet stream. In terms of Heck reaction 2 (a more challenging reaction), the TON obtained for the PFR-m-CSTR configuration was ~ 81 and the Pd contamination in the outlet stream was around 153 mg Pd. kg of $product^{-1}$. It also revealed the potential adverse effect of side product accumulation in the combined continuous reactor-membrane separation units, which may lead to serious process disruptions or decrease in substrate conversion and therefore lower productivity. The excellent potential of PEEK membranes in high temperature catalytic reactions has been demonstrated as hypothesized in the beginning of this thesis.

10.2 Future directions

Non-modified and non-sulphonated PEEK NF membranes were first developed during the research project leading to this PhD thesis. Consequently, there is still a lot of room for improvement in terms of membrane performance and understanding of transport mechanism. One of the major issues, and unsolved problem, with PEEK membranes is the low permeance. However, if performing a Heck reaction it would not be so problematic due to the high residence time required to achieve full conversion. Assuming a productivity of 6.944 kg $product.L^{-1}$ $reactor.h^{-1}$ (from 9.3.3) and a desired production of 100 kg of product per day, then a reactor volume of 0.6 L would be required. Knowing the residence time of the reaction to be 10 h (Heck reaction 1), the required flow rate would be 0.06 $L.h^{-1}$. Since PEEK membrane has a permeance of 0.2 $L.h^{-1}.m^{-2}.bar^{-1}$ this means that only an area of 0.01 m^2 would be required to perform the reaction at 30 bar (less than the module area obtained in Chapter 5, ~ 0.2 m^2). Modifying the dope preparation is the starting point for manipulating

the properties of the membrane. The solvents used for dissolving PEEK, methane sulphonic acid and sulphuric acid, could be used in other concentrations to further manipulate the properties of the membrane. Another strategy for dope preparation is the usage of other solvents that can dissolve PEEK at temperatures above room temperature such as high boiling point esters, benzophenone or diphenyl sulphone. In addition, pore fillers, such as graphite or titanium oxide, could be added to the dope in order to increase the mechanical properties of the formed membrane and help decreasing compaction.

The phase inversion process can also be further studied by changing the composition of the water bath with solvents that could delay the coagulation of the polymer and decrease the macrovoid structure of PEEK membranes to a more spongy structure. On the other hand the separating layer should be formed instantly to be as thin as possible to increase the permeance. Changing the coagulation bath temperature could also help to further manipulate the membrane properties.

Another way to increase the permeance could be via spin coating a thin film of PEEK using a looser PEEK membrane as support. By doing so, the swelling of the support and membrane itself would be equal thus avoiding the appearance of creases during filtration that could lead to a decrease in performance. The spin coating would also help in understanding better the transport mechanism in PEEK membranes as it would be possible to establish a relationship between thickness and permeance. With this technique, thinner PEEK films may be obtained as opposed with the 'phase inversion' technique where an asymmetric structure with pore size distribution is obtained. This technique was carried out briefly and it was not possible to achieve solid and reproducible results or even uniform thin films in the nanometre range due to time constraints. However, some advice for future work was possible to be gathered. It seems that a good range for spin coating PEEK films lays between 5 wt.% and 9 wt.% (polymer concentration) while maintaining the same ratio of MSA to SA. Lower concentrations such as 2 wt.% and 3 wt.% were too dilute and did not enable the formation of a film; higher concentrations like 12 wt. % were to viscous to be spread and very thick films were formed. Another consideration to take into account is the substrate where the film is coated. Glass substrates have less adhesion to the PEEK film than polystyrene ones which makes the detachment of the film easier. Using polymeric UF substrates could also be a possibility for spin coating PEEK (ideally PEEK UF support due to compatibility issues). Although most of the acid is removed from the film while spinning, some of it remains and it is necessary to add water to the film surface; this can be done while spin coating but introduces non-uniformity on the film or by dipping the film in water after spin coating which is similar to phase inversion.

Although post-fabrication methods such as drying from different solvents at different temperatures have been extensively studied in this thesis, a model to predict the final

membrane performance is required. A mathematical formulation that connects the theory behind the drying process with the experimental data could be performed for PEEK membranes by incorporating mass and heat transfer elements as well as the mechanical properties of the membrane matrix.

The high temperature filtrations performed in this study helped to understand the changes that occur in the separating layer with the increase of temperature, i.e., the increase of pore size in the active layer. Although not ideal to have a molecular rearrangement and changes in the membrane performance, the increase in pore size with temperature can be used as a self-cleaning function when there is deposition of molecules on the membrane surface. Further studies of membrane fouling and its subsequent removal using this technique could be performed. The development of PEEK membranes or PEEK composite membranes that do not undergo molecular rearrangement under high temperature filtrations would be a relevant topic to be investigated. Another aspect of the high temperature filtration is to choose carefully the materials used as backing (or support) for the membrane and the sealing materials (the o-rings) because these should be high temperature resistant and can in fact become the bottleneck in high temperature filtrations.

References

References

1. Karan, S., Z. Jiang, and A.G. Livingston, *Sub–10 nm polyamide nanofilms with ultrafast solvent transport for molecular separation.* Science, 2015. **348**(6241): p. 1347-1351.
2. Marchetti, P., et al., *Molecular Separation with Organic Solvent Nanofiltration: A Critical Review.* Chemical Reviews, 2014. **114**(21): p. 10735-10806.
3. Tsuru, T., et al., *Temperature effect on transport performance by inorganic nanofiltration membranes.* AIChE Journal, 2000. **46**(3): p. 565-574.
4. Vanherck, K., G. Koeckelberghs, and I.F.J. Vankelecom, *Crosslinking polyimides for membrane applications: A review.* Progress in Polymer Science, 2013. **38**(6): p. 874-896.
5. See Toh, Y.H., et al., *In search of a standard method for the characterisation of organic solvent nanofiltration membranes.* Journal of Membrane Science, 2007. **291**(1–2): p. 120-125.
6. See Toh, Y.H., F.W. Lim, and A.G. Livingston, *Polymeric membranes for nanofiltration in polar aprotic solvents.* Journal of Membrane Science, 2007. **301**(1–2): p. 3-10.
7. Saidani, H., et al., *Interplay between the Transport of Solutes Across Nanofiltration Membranes and the Thermal Properties of the Thin Active Layer.* Langmuir, 2009. **26**(4): p. 2574-2583.
8. Siddique, H., et al., *Mixed matrix membranes for organic solvent nanofiltration.* Journal of Membrane Science, 2014. **452**: p. 354-366.
9. Peeva, L., J. Arbour, and A. Livingston, *On the Potential of Organic Solvent Nanofiltration in Continuous Heck Coupling Reactions.* Organic Process Research & Development, 2013. **17**(7): p. 967-975.
10. da Silva Burgal, J., et al., *Organic solvent resistant poly(ether-ether-ketone) nanofiltration membranes.* Journal of Membrane Science, 2015. **479**(0): p. 105-116.
11. Mulder, M., *Characterisitation of membranes*, in *Basic Principles of Membrane Technology*, Springer, Editor. 1996, Springer. p. 157-201.
12. Baker, R.W., *Overview of membrane science and technology*, in *Membrane Technology and Applications*. 2004, John Wiley & Sons, Ltd. p. 1-7.
13. W. J.KOROS, Y.H. MA, and T. SHIMIDZU, *TERMINOLOGY FOR MEMBRANES AND MEMBRANE PROCESSES* 1996. **68**(MACROMOLECULAR DIVISION COMMISSION ON FUNCTIONAL POLYMERS): p. 1479-1489.
14. Athayde, D.D., et al., *Review of perovskite ceramic synthesis and membrane preparation methods.* Ceramics International, 2016. **42**(6): p. 6555-6571.
15. Li, K., *Ceramic Membranes and Membrane Processes*, in *Ceramic Membranes for Separation and Reaction*. 2007, John Wiley & Sons, Ltd. p. 1-20.
16. Ismail, A.F. and L.I.B. David, *A review on the latest development of carbon membranes for gas separation.* Journal of Membrane Science, 2001. **193**(1): p. 1-18.
17. Vandezande, P., L.E.M. Gevers, and I.F.J. Vankelecom, *Solvent resistant nanofiltration: separating on a molecular level.* Chemical Society Reviews, 2008. **37**(2): p. 365-405.
18. Van der Bruggen, B., *Fundamentals of Membrane Solvent Separation and Pervaporation*, in *Membrane Operations*. 2009, Wiley-VCH Verlag GmbH & Co. KGaA. p. 45-61.
19. Loeb, S. and S. Sourirajan, *Sea Water Demineralization by Means of an Osmotic Membrane*, in *Saline Water Conversion II*. 1963, AMERICAN CHEMICAL SOCIETY. p. 117-132.
20. Vankelecom, I.F.J., et al., *Nanofiltration membrane materials and preparation*, in *Nanofiltration - Principles and Applications*, A.I. Schäfer, A.G. Fane, and T.D. Waite, Editors. 2006, Elsevier. p. 33-42.

21. Lau, W.J., et al., *A recent progress in thin film composite membrane: A review.* Desalination, 2012. **287**(0): p. 190-199.
22. Marchetti, P., et al., *Molecular Separations via Organic Solvent Nanofiltration - A Review.* 2013.
23. Aroon, M.A., et al., *Performance studies of mixed matrix membranes for gas separation: A review.* Separation and Purification Technology, 2010. **75**(3): p. 229-242.
24. Shimoda, T. and H. Hachiya, *Process for preparing a polyether ether ketone membrane*, U.S. Patent, Editor. 1999, Asahi Kasei Kogyo Kabushiki Kaika: USA.
25. Soroko, I., et al., *The effect of membrane formation parameters on performance of polyimide membranes for organic solvent nanofiltration (OSN). Part B: Analysis of evaporation step and the role of a co-solvent.* Journal of Membrane Science, 2011. **381**(1–2): p. 163-171.
26. See-Toh, Y.H., F.C. Ferreira, and A.G. Livingston, *The influence of membrane formation parameters on the functional performance of organic solvent nanofiltration membranes.* Journal of Membrane Science, 2007. **299**(1–2): p. 236-250.
27. Young, T.-H., J.-H. Huang, and W.-Y. Chuang, *Effect of evaporation temperature on the formation of particulate membranes from crystalline polymers by dry-cast process.* European Polymer Journal, 2002. **38**(1): p. 63-72.
28. See-Toh, Y.H., M. Silva, and A. Livingston, *Controlling molecular weight cut-off curves for highly solvent stable organic solvent nanofiltration (OSN) membranes.* Journal of Membrane Science, 2008. **324**(1–2): p. 220-232.
29. Vandezande, P., et al., *Solidification of Emulsified Polymer Solutions via Phase Inversion (SEPPI): A Generic Way To Prepare Polymers with Controlled Porosity.* Chemistry of Materials, 2008. **20**(10): p. 3457-3465.
30. Vandezande, P., K. Vanherck, and I. Vankelecom, *Cross-linked polyimide membranes*, U.P. Office, Editor. 2008, Evonik Fibres Gmbh: USA.
31. Linder, et al., *Solvent-stable semipermeable composite membranes* U.P. Office, Editor. 1991 Aligena AG (Basel, CH) USA.
32. Linder, et al., *Solvent stable membranes* U.P. Office, Editor. 1991, Aligena AG (Basel, CH) USA.
33. Kumbharkar, S.C., P.B. Karadkar, and U.K. Kharul, *Enhancement of gas permeation properties of polybenzimidazoles by systematic structure architecture.* Journal of Membrane Science, 2006. **286**(1–2): p. 161-169.
34. Wang, K.Y., Y. Xiao, and T.-S. Chung, *Chemically modified polybenzimidazole nanofiltration membrane for the separation of electrolytes and cephalexin.* Chemical Engineering Science, 2006. **61**(17): p. 5807-5817.
35. Livingston, A.G. and Y.S. Bhole, *Asymmetric membranes for use in nanofiltration*. 2012, Imperial Innovations Limited.
36. Valtcheva, I., et al., *Organic solvent nanofiltration (OSN) membranes for application in extreme pH conditions*. 2013, Imperial College London.
37. Beerlage, M.A.M., *Polyimide ultrafiltration membranes for non-aqueous systems*. 1994: Enschede. p. 211.
38. Manos, P., *Gas separation membrane drying with water replacement liquid*. 1978, E. I. Du Pont De Nemours And Company.
39. MacDonald, W. and C.-Y. Pan, *Method for drying water-wet membranes*. 1974.
40. King, W.M., M.-W. Tang, and C.G. Wensley, *Air dried cellulose acetate membranes*. 1989.
41. Brown, G.L., *Formation of films from polymer dispersions.* Journal of Polymer Science, 1956. **22**(102): p. 423-434.
42. Manos, P., *Membrane drying process*. 1978, E. I. Du Pont De Nemours And Company.
43. Rose, J.B., *Discovery and development of the "VICTREX" polyaryletherketone PEEK*, in *High performance polymers: their origin and development*, R.B. Seymour and G.S. Kirshenbaum, Editors. 1986, Elsevier: New York. p. 187-193.

44. Rae, P.J., E.N. Brown, and E.B. Orler, *The mechanical properties of poly(ether-ether-ketone) (PEEK) with emphasis on the large compressive strain response.* Polymer, 2007. **48**(2): p. 598-615.
45. Díez-Pascual, A.M., G. Martínez, and M.n.A. Gómez, *Synthesis and Characterization of Poly(ether ether ketone) Derivatives Obtained by Carbonyl Reduction.* Macromolecules, 2009. **42**(18): p. 6885-6892.
46. Fibers, P. *Performance Fibers PEEK* 2013 [cited 2013; Available from: http://www.performancefibers.com/PDFs/Europe/PF-PEEK-E.pdf.
47. *PEEK White Paper*. 2013; Available from: http://www.performancefibers.com/PDFs/Europe/PF%20PEEK%20White%20Paper,%20Feb%202011.pdf.
48. Jin, X., et al., *A sulphonated poly(aryl ether ketone).* British Polymer Journal, 1985. **17**(1): p. 4-10.
49. Devaux, J., et al., *On the molecular weight determination of a poly(aryl-ether-ether-ketone) (PEEK).* Polymer, 1985. **26**(13): p. 1994-2000.
50. Bailly, C., et al., *The sodium salts of sulphonated poly(aryl-ether-ether-ketone) (PEEK): Preparation and characterization.* Polymer, 1987. **28**(6): p. 1009-1016.
51. Jansen, J. and E. Drioli, *Poly(ether ether ketone) derivative membranes—a review of their preparation, properties and potential.* Polymer Science Series A, 2009. **51**(11-12): p. 1355-1366.
52. Bishop, M.T., et al., *Microporous peek membranes and the preparation thereof*, in *US Patent Office*, U.P. Office, Editor. 1991, Filmtec Corporation, The Dow Chemical Company: USA.
53. Yuan, Y., *Porous poly(aryl ether ketone) membranes, processes for their preparation and use thereof*, U.P. Office, Editor. 2005, Porogen Llc: USA.
54. Costa, L.C., *Asymmetric semipermeable poly(aryletherketone) membranes and method of producing same*, in *US Patent Office*, U.P. Office, Editor. 1992, Ionics, Incorporated: USA.
55. ANNELIESE, G., et al., *Process for making polymeric membranes based on polyether ether ketone*, E.P. Office, Editor. 1996, REHAU AG & CO.
56. Khan, A.L., X. Li, and I.F.J. Vankelecom, *Mixed-gas CO2/CH4 and CO2/N2 separation with sulfonated PEEK membranes.* Journal of Membrane Science, 2011. **372**(1–2): p. 87-96.
57. Khan, A.L., X. Li, and I.F.J. Vankelecom, *SPEEK/Matrimid blend membranes for CO2 separation.* Journal of Membrane Science, 2011. **380**(1–2): p. 55-62.
58. Li, H., et al., *A novel sulfonated poly(ether ether ketone) and cross-linked membranes for fuel cells.* Journal of Power Sources, 2010. **195**(19): p. 6443-6449.
59. Fontananova, E., et al., *Preparation and characterization of new non-fluorinated polymeric and composite membranes for PEMFCs.* Journal of Membrane Science, 2010. **348**(1–2): p. 326-336.
60. Hendrix, K., et al., *Crosslinking of modified poly (ether ether ketone) membranes for use in solvent resistant nanofiltration.* Journal of Membrane Science, (0).
61. Hendrix, K., et al., *Synthesis of modified poly (ether ether ketone) polymer for the preparation of ultrafiltration and nanofiltration membranes via phase inversion.* Journal of Membrane Science, (0).
62. Tsuru, T., et al., *Permeation Characteristics of Electrolytes and Neutral Solutes through Titania Nanofiltration Membranes at High Temperatures.* Langmuir, 2010. **26**(13): p. 10897-10905.
63. Ben Amar, N., et al., *Effect of Temperature on the Transport of Water and Neutral Solutes across Nanofiltration Membranes.* Langmuir, 2007. **23**(6): p. 2937-2952.
64. Snow, M.J.H., et al., *New techniques for extreme conditions: high temperature reverse osmosis and nanofiltration.* Desalination, 1996. **105**(1–2): p. 57-61.
65. Qi, H., et al., *Enhanced performance of a macroporous ceramic support for nanofiltration by using α-Al2O3 with narrow size distribution.* Ceramics International, 2013. **39**(3): p. 2463-2471.

66. Valtcheva, I.B., et al., *Beyond polyimide: Crosslinked polybenzimidazole membranes for organic solvent nanofiltration (OSN) in harsh environments.* Journal of Membrane Science, 2014. **457**: p. 62-72.
67. Shibuya, N. and R.S. Porter, *A kinetic study of PEEK sulfonation in concentrated sulfuric acid by ultraviolet-visible spectroscopy.* Polymer, 1994. **35**(15): p. 3237-3242.
68. Blundell, D.J. and B.N. Osborn, *The morphology of poly(aryl-ether-ether-ketone).* Polymer, 1983. **24**(8): p. 953-958.
69. Semenov, A.N., *II. The effect of polymer density fluctuations on dynamics of high-molecular-weight polymers*, in *Theoretical Challenges in the Dynamics of Complex Fluids*, T. McLeish, Editor. 1997. p. 82-84.
70. Manos, P., *Membrane drying process*. 1978, E. I. Du Pont De Nemours And Company.
71. King, W.M., M.-W. Tang, and C.G. Wensley, *Air dried cellulose acetate membranes*. 1989.
72. Daoust, D., et al., *Chemical modification of poly(ether ether ketone) for size exclusion chromatography at room temperature: 1. Absolute molecular-mass determination for sulfonated PEEK.* Polymer, 1994. **35**(25): p. 5491-5497.
73. Daoust, D., et al., *Chemical modification of poly(ether ether ketone) for size exclusion chromatography at room temperature: 2. On the reliability of the derivatization procedure for PEEK molecular-mass determination—application to PEEK-carbon fibre composite.* Polymer, 1994. **35**(25): p. 5498-5503.
74. Wypych, G., *Knovel Solvents - A Properties Database*. ChemTec Publishing.
75. Bowen, W.R. and J.S. Welfoot, *Modelling of membrane nanofiltration—pore size distribution effects.* Chemical Engineering Science, 2002. **57**(8): p. 1393-1407.
76. Bowen, W.R. and J.S. Welfoot, *Modelling the performance of membrane nanofiltration—critical assessment and model development.* Chemical Engineering Science, 2002. **57**(7): p. 1121-1137.
77. Wilke, C.R. and P. Chang, *Correlation of diffusion coefficients in dilute solutions.* AIChE Journal, 1955. **1**(2): p. 264-270.
78. Perry, R.H. and D.W. Green, *Heat and Mass Transfer*, in *Perry's Chemical Engineers' Handbook*, D.W. Green, Editor. 1999, McGraw-Hill.
79. Muthu Lakshmi, R.T.S., V. Choudhary, and I.K. Varma, *Sulphonated poly(ether ether ketone): Synthesis and characterisation.* Journal of Materials Science, 2005. **40**(3): p. 629-636.
80. Shibuya, N. and R.S. Porter, *Kinetics of PEEK sulfonation in concentrated sulfuric acid.* Macromolecules, 1992. **25**(24): p. 6495-6499.
81. Hay, J.N., J.I. Langford, and J.R. Lloyd, *Variation in unit cell parameters of aromatic polymers with crystallization temperature.* Polymer, 1989. **30**(3): p. 489-493.
82. Lai, Y.H., et al., *On the PEEK composites reinforced by surface-modified nano-silica.* Materials Science and Engineering: A, 2007. **458**(1–2): p. 158-169.
83. Loy, X.Z.K. and S.K. Sinha, *Lubrication of polyether ether ketone (PEEK) surface by liquid ultrathin films for high wear durability.* Wear, 2012. **296**(1–2): p. 681-692.
84. Schwinge, J., et al., *Spiral wound modules and spacers: Review and analysis.* Journal of Membrane Science, 2004. **242**(1–2): p. 129-153.
85. Baker, R.W., *3 MEMBRANES AND MODULES*, in *Membrane Technology and Applications*. 2004, John Wiley & Sons, Ltd. p. 139-150.
86. *SelRO® MPS-34 - pH Stable Membrane Nanofiltration Spiral Module Series – 2540, 4040* [cited 2016 23-01-2016]; Available from: http://www.kochmembrane.com/PDFs/Data-Sheets/Spiral/NF/KMS_SelRO_MPS_34_2540_4040_Datasheet.aspx.
87. *SolSep BV Robust Membrane Technologies*. [cited 2016 23/01/2016]; Available from: http://www.solsep.com/.
88. *About DuraMem® & PuraMem®: Membrane Properties* [cited 2016 23-01-2016]; Available from: http://duramem.evonik.com/product/duramem-puramem/en/about/membrane-properties/pages/default.aspx.

89. *DuraMem® and PuraMem®: Integrate solvent-stable membrane technology to increase the value in your production process.* [cited 2016 23-01-2016]; Available from: http://duramem.evonik.com/sites/lists/PP-HP/Documents/DuraMem-PuraMem-EN.pdf.
90. Stern, S.A., et al., *HELIUM RECOVERY BY PERMEATION.* Industrial & Engineering Chemistry, 1965. **57**(2): p. 49-60.
91. Hofstetter, T.B., C. Capello, and K. Hungerbühler, *Environmentally Preferable Treatment Options for Industrial Waste Solvent Management: A Case Study of a Toluene Containing Waste Solvent.* Process Safety and Environmental Protection, 2003. **81**(3): p. 189-202.
92. Amelio, A., et al., *Guidelines based on life cycle assessment for solvent selection during the process design and evaluation of treatment alternatives.* Green Chemistry, 2014. **16**(6): p. 3045-3063.
93. Figoli, A., et al., *Towards non-toxic solvents for membrane preparation: a review.* Green Chemistry, 2014. **16**(9): p. 4034-4059.
94. Anastas, P.T.W., J. C., *Green Chemistry: Theory and Practice*. Oxford University Press: New York. 1998.
95. Drioli, E., et al., *Process intensification strategies and membrane engineering.* Green Chemistry, 2012. **14**(6): p. 1561-1572.
96. Szekely, G., et al., *Sustainability assessment of organic solvent nanofiltration: from fabrication to application.* Green Chemistry, 2014. **16**(10): p. 4440-4473.
97. Kim, J.F., et al., *Increasing the sustainability of membrane processes through cascade approach and solvent recovery-pharmaceutical purification case study.* Green Chemistry, 2014. **16**(1): p. 133-145.
98. Peeva, L., et al., *Continuous purification of active pharmaceutical ingredients using multistage organic solvent nanofiltration membrane cascade.* Chemical Engineering Science, 2014. **116**(0): p. 183-194.
99. Van der Bruggen, B., M. Mänttäri, and M. Nyström, *Drawbacks of applying nanofiltration and how to avoid them: A review.* Separation and Purification Technology, 2008. **63**(2): p. 251-263.
100. Benmouhoub, N., et al., *Aqueous sol-gel routes to bio-composite capsules and gels.* Green Chemistry, 2008. **10**(9): p. 957-964.
101. Sanchez, C., H. Arribart, and M.M. Giraud Guille, *Biomimetism and bioinspiration as tools for the design of innovative materials and systems.* Nat Mater, 2005. **4**(4): p. 277-288.
102. Darder, M., P. Aranda, and E. Ruiz-Hitzky, *Bionanocomposites: A New Concept of Ecological, Bioinspired, and Functional Hybrid Materials.* Advanced Materials, 2007. **19**(10): p. 1309-1319.
103. Valtcheva, I.B., et al., *Beyond polyimide: Crosslinked polybenzimidazole membranes for organic solvent nanofiltration (OSN) in harsh environments.* Journal of Membrane Science, 2014. **457**(0): p. 62-72.
104. Jimenez-Gonzalez, C., D.J.C. Constable, and C.S. Ponder, *Evaluating the "Greenness" of chemical processes and products in the pharmaceutical industry-a green metrics primer.* Chemical Society Reviews, 2012. **41**(4): p. 1485-1498.
105. Henderson, R.K., et al., *Expanding GSK's solvent selection guide - embedding sustainability into solvent selection starting at medicinal chemistry.* Green Chemistry, 2011. **13**(4): p. 854-862.
106. Freger, V. and S. Srebnik, *Mathematical model of charge and density distributions in interfacial polymerization of thin films.* Journal of Applied Polymer Science, 2003. **88**(5): p. 1162-1169.
107. E., C.J., *Interfacially synthesized reverse osmosis membrane* 1981 FilmTec Corporation.
108. Soroko, I., Y. Bhole, and A.G. Livingston, *Environmentally friendly route for the preparation of solvent resistant polyimide nanofiltration membranes.* Green Chemistry, 2011. **13**(1): p. 162-168.

109. Vanherck, K., et al., *A simplified diamine crosslinking method for PI nanofiltration membranes.* Journal of Membrane Science, 2010. **353**(1–2): p. 135-143.
110. Hendrix, K., K. Vanherck, and I.F.J. Vankelecom, *Optimization of solvent resistant nanofiltration membranes prepared by the in-situ diamine crosslinking method.* Journal of Membrane Science, 2012. **421–422**: p. 15-24.
111. Medina-Gonzalez, Y., et al., *Towards green membranes: preparation of cellulose acetate ultrafiltration membranes using methyl lactate as a biosolvent.* International Journal of Sustainable Engineering, 2010. **4**(1): p. 75-83.
112. Cannon, C.R., *Cellulose acetate membranes*, A.-G. Corporation, Editor. 1969, Aerojet-General Corporation,.
113. Tao, M.-m., et al., *Effect of solvent power on PVDF membrane polymorphism during phase inversion.* Desalination, 2013. **316**(0): p. 137-145.
114. Xing, D.Y., S.Y. Chan, and T.-S. Chung, *The ionic liquid [EMIM]OAc as a solvent to fabricate stable polybenzimidazole membranes for organic solvent nanofiltration.* Green Chemistry, 2014. **16**(3): p. 1383-1392.
115. Capello, C., S. Hellweg, and K. Hungerbühler, *Environmental Assessment of Waste-Solvent Treatment Options.* Journal of Industrial Ecology, 2008. **12**(1): p. 111-127.
116. Sereewatthanawut, I., et al., *Demonstration of Molecular Purification in Polar Aprotic Solvents by Organic Solvent Nanofiltration.* Organic Process Research & Development, 2010. **14**(3): p. 600-611.
117. Peeva, L., et al., *Experimental strategies for increasing the catalyst turnover number in a continuous Heck coupling reaction.* Journal of Catalysis, 2013. **306**(0): p. 190-201.
118. Strathmann, H. and K. Kock, *The formation mechanism of phase inversion membranes.* Desalination, 1977. **21**(3): p. 241-255.
119. Lazic, Z.R., *Design of Experiments in Chemical Engineering: A Practical Guide*. 2004: Wiley-VHC Verlag GmbH & Co. KGaA.
120. Smallwood, I.M., *Handbook of Organic Solvent Properties*. Elsevier.
121. Gevers, L.E.M., et al., *Optimisation of a lab-scale method for preparation of composite membranes with a filled dense top-layer.* Journal of Membrane Science, 2006. **281**(1–2): p. 741-746.
122. Matsuyama, H., M.-m. Kim, and D.R. Lloyd, *Effect of extraction and drying on the structure of microporous polyethylene membranes prepared via thermally induced phase separation.* Journal of Membrane Science, 2002. **204**(1–2): p. 413-419.
123. Jie, X., et al., *Influence of drying method on morphology and properties of asymmetric cellulose hollow fiber membrane.* Journal of Membrane Science, 2005. **246**(2): p. 157-165.
124. Matsuyama, H., et al., *Effect of organic solvents on membrane formation by phase separation with supercritical CO2.* Journal of Membrane Science, 2002. **204**(1–2): p. 81-87.
125. Scheirs, J., *Surface-Tension and Solubility-Parameter Effects*, in *Compositional and Failure Analysis of Polymers: A Practical Approach*
2000, WILEY.
126. Flick, E.W., *Industrial Solvents Handbook (5th Edition)*. William Andrew Publishing/Noyes.
127. VICTREX. *Material properties guide*. 2013 21/11/2013; Available from: http://www.victrex.com/docs/literature-docs/Victrex_Material%20Properties%20Guide%20%20%203_7_US.pdf.
128. Gardner, E.S., *Forecasting: Methods and applications (Second Edition), Makridakis, S., Wheelwright, S. C. and McGee, V. E., New York: Wiley, 1983.*, in *Journal of Forecasting*. 1984, John Wiley & Sons, Ltd. p. 457-460.
129. Székely, G., et al., *Molecularly imprinted organic solvent nanofiltration membranes – Revealing molecular recognition and solute rejection behaviour.* Reactive and Functional Polymers, 2015. **86**: p. 215-224.

130. Tang, Q., W. Hu, and S. Napolitano, *Slowing Down of Accelerated Structural Relaxation in Ultrathin Polymer Films.* Physical Review Letters, 2014. **112**(14): p. 148306.
131. Song, Q., et al., *Controlled thermal oxidative crosslinking of polymers of intrinsic microporosity towards tunable molecular sieve membranes.* Nat Commun, 2014. **5**.
132. Hutchinson, J.M., *Physical aging of polymers.* Progress in Polymer Science, 1995. **20**(4): p. 703-760.
133. Hodge, I.M., *Physical Aging in Polymer Glasses.* Science, 1995. **267**(5206): p. 1945-1947.
134. Murphy, T.M., et al., *Physical aging of layered glassy polymer films via gas permeability tracking.* Polymer, 2011. **52**(26): p. 6117-6125.
135. Cangialosi, D., et al., *Physical aging in polymers and polymer nanocomposites: recent results and open questions.* Soft Matter, 2013. **9**(36): p. 8619-8630.
136. McKeown, N.B. and P.M. Budd, *Polymers of intrinsic microporosity (PIMs): organic materials for membrane separations, heterogeneous catalysis and hydrogen storage.* Chemical Society Reviews, 2006. **35**(8): p. 675-683.
137. Volkov, A.V., et al., *Poly[1-(trimethylsilyl)-1-propyne] as a solvent resistance nanofiltration membrane material.* Journal of Membrane Science, 2006. **281**(1–2): p. 351-357.
138. Volkov, A.V., et al., *High permeable PTMSP/PAN composite membranes for solvent nanofiltration.* Journal of Membrane Science, 2009. **333**(1–2): p. 88-93.
139. Fritsch, D., et al., *High performance organic solvent nanofiltration membranes: Development and thorough testing of thin film composite membranes made of polymers of intrinsic microporosity (PIMs).* Journal of Membrane Science, 2012. **401–402**: p. 222-231.
140. Tsarkov, S., et al., *Solvent nanofiltration through high permeability glassy polymers: Effect of polymer and solute nature.* Journal of Membrane Science, 2012. **423–424**: p. 65-72.
141. Neil B Mckeown, P.M.B., Detlev Fritsch, *Thin layer composite membrane*. 2005.
142. Gorgojo, P., et al., *Ultrathin Polymer Films with Intrinsic Microporosity: Anomalous Solvent Permeation and High Flux Membranes.* Advanced Functional Materials, 2014. **24**(30): p. 4729-4737.
143. McKeown, N.B., *Polymers of Intrinsic Microporosity.* ISRN Materials Science, 2012. **2012**: p. 16.
144. Lonsdale, H.K., U. Merten, and R.L. Riley, *Transport properties of cellulose acetate osmotic membranes.* Journal of Applied Polymer Science, 1965. **9**(4): p. 1341-1362.
145. Sharma, R.R., R. Agrawal, and S. Chellam, *Temperature effects on sieving characteristics of thin-film composite nanofiltration membranes: pore size distributions and transport parameters.* Journal of Membrane Science, 2003. **223**(1–2): p. 69-87.
146. Sharma, R.R. and S. Chellam, *Temperature Effects on the Morphology of Porous Thin Film Composite Nanofiltration Membranes.* Environmental Science & Technology, 2005. **39**(13): p. 5022-5030.
147. Sharma, R.R. and S. Chellam, *Temperature and concentration effects on electrolyte transport across porous thin-film composite nanofiltration membranes: Pore transport mechanisms and energetics of permeation.* Journal of Colloid and Interface Science, 2006. **298**(1): p. 327-340.
148. Jin, X., et al., *Effects of feed water temperature on separation performance and organic fouling of brackish water RO membranes.* Desalination, 2009. **239**(1–3): p. 346-359.
149. Lianchao, L., et al., *A novel nanofiltration membrane prepared with PAMAM and TMC by in situ interfacial polymerization on PEK-C ultrafiltration membrane.* Journal of Membrane Science, 2006. **269**(1–2): p. 84-93.

150. Dang, H.Q., W.E. Price, and L.D. Nghiem, *The effects of feed solution temperature on pore size and trace organic contaminant rejection by the nanofiltration membrane NF270.* Separation and Purification Technology, 2014. **125**(0): p. 43-51.
151. Liang, C.H., *Separation properties of high temperature reverse osmosis membranes for silica removal and boric acid recovery.* Journal of Membrane Science, 2005. **246**(2): p. 127-135.
152. Goosen, M.F.A., et al., *Effect of feed temperature on permeate flux and mass transfer coefficient in spiral-wound reverse osmosis systems.* Desalination, 2002. **144**(1–3): p. 367-372.
153. Schaep, J., et al., *Removal of hardness from groundwater by nanofiltration.* Desalination, 1998. **119**(1–3): p. 295-301.
154. Mänttäri, M., et al., *Effect of temperature and membrane pre-treatment by pressure on the filtration properties of nanofiltration membranes.* Desalination, 2002. **145**(1–3): p. 81-86.
155. Jian, X., et al., *Preparation of UF and NF poly (phthalazine ether sulfone ketone) membranes for high temperature application.* Journal of Membrane Science, 1999. **161**(1–2): p. 185-191.
156. Han, J., et al., *Preparation and performance of SPPES/PPES hollow fiber composite nanofiltration membrane with high temperature resistance.* Desalination, 2014. **350**(0): p. 95-101.
157. da Silva Burgal, J., et al., *Controlling molecular weight cut-off of PEEK nanofiltration membranes using a drying method.* Journal of Membrane Science, 2015. **493**: p. 524-538.
158. Fibers, P. *Performance Fibers PEEK* 2013 [cited 2013; Available from: http://www.performancefibers.com/PDFs/Europe/PF-PEEK-E.pdf.
159. Belfort, G., et al., *Diagnosis of membrane fouling using a rotating annular filter. 1. Cell culture media.* Journal of Membrane Science, 1993. **77**(1): p. 1-22.
160. Zydney, A.L., et al., *Use of the log-normal probability density function to analyze membrane pore size distributions: functional forms and discrepancies.* Journal of Membrane Science, 1994. **91**(3): p. 293-298.
161. Otero, J.A., et al., *Three independent ways to obtain information on pore size distributions of nanofiltration membranes.* Journal of Membrane Science, 2008. **309**(1–2): p. 17-27.
162. Deen, W.M., *Hindered transport of large molecules in liquid-filled pores.* AIChE Journal, 1987. **33**(9): p. 1409-1425.
163. Bowen, W.R. and A.O. Sharif, *Transport through Microfiltration Membranes—Particle Hydrodynamics and Flux Reduction.* Journal of Colloid and Interface Science, 1994. **168**(2): p. 414-421.
164. Bowen, W.R., A.W. Mohammad, and N. Hilal, *Characterisation of nanofiltration membranes for predictive purposes — use of salts, uncharged solutes and atomic force microscopy.* Journal of Membrane Science, 1997. **126**(1): p. 91-105.
165. Zhao, Y.H., M.H. Abraham, and A.M. Zissimos, *Fast Calculation of van der Waals Volume as a Sum of Atomic and Bond Contributions and Its Application to Drug Compounds.* The Journal of Organic Chemistry, 2003. **68**(19): p. 7368-7373.
166. Murphy, T.M., et al., *Enthalpy recovery and structural relaxation in layered glassy polymer films.* Polymer, 2012. **53**(18): p. 4002-4009.
167. Cheng, S.Z.D., M.Y. Cao, and B. Wunderlich, *Glass transition and melting behavior of poly(oxy-1,4-phenyleneoxy-1,4-phenylenecarbonyl-1,4-phenylene) (PEEK).* Macromolecules, 1986. **19**(7): p. 1868-1876.
168. Farrow, G., *Crystallinity, 'crystallite size' and melting point of polypropylene.* Polymer, 1963. **4**: p. 191-197.
169. Boucher, V.M., et al., *Enthalpy Recovery in Nanometer to Micrometer Thick Polystyrene Films.* Macromolecules, 2012. **45**(12): p. 5296-5306.
170. Cebe, P., *Annealing study of poly(etheretherketone).* Journal of Materials Science. **23**(10): p. 3721-3731.

171. *Thermoplastic polymeric adhesive for structural bonding applications for orthopaedic devices*, in *American Society for Composites - Ninth technical conference*, A.S.f. Composites, Editor. 1994, Technomic Publishing Company, Inc. p. 29.
172. Lovinger, A.J. and D.D. Davis, *Electron-microscopic investigation of the morphology of a melt-crystallized polyaryletherketone.* Journal of Applied Physics, 1985. **58**(8): p. 2843-2853.
173. Tsuji, M., et al., *TEM Studies on Solution-Grown Crystals of Poly (aryl-ether-ether-ketone) (PEEK).* Bulletin of the Institute for Chemical Research, Kyoto University, 1989. **67**(2): p. 77-88.
174. Ivanov, D.A., R. Legras, and A.M. Jonas, *Interdependencies between the Evolution of Amorphous and Crystalline Regions during Isothermal Cold Crystallization of Poly(ether−ether−ketone).* Macromolecules, 1999. **32**(5): p. 1582-1592.
175. Nakanishi, H., et al., *Positronium formation at free-volume sites in the amorphous regions of semicrystalline PEEK.* Journal of Polymer Science Part B: Polymer Physics, 1989. **27**(7): p. 1419-1424.
176. Ramani, R. and S. Alam, *Influence of poly(ether imide) on the free volume hole size and distributions in poly(ether ether ketone).* Journal of Applied Polymer Science, 2012. **125**(4): p. 3200-3210.
177. Shi, G.M., et al., *Sorption, swelling, and free volume of polybenzimidazole (PBI) and PBI/zeolitic imidazolate framework (ZIF-8) nano-composite membranes for pervaporation.* Polymer, 2013. **54**(2): p. 774-783.
178. Kumbharkar, S.C., et al., *Variation in acid moiety of polybenzimidazoles: Investigation of physico-chemical properties towards their applicability as proton exchange and gas separation membrane materials.* Polymer, 2009. **50**(6): p. 1403-1413.
179. van Zanten, J.H., W.E. Wallace, and W.-l. Wu, *Effect of strongly favorable substrate interactions on the thermal properties of ultrathin polymer films.* Physical Review E, 1996. **53**(3): p. R2053-R2056.
180. Forrest, J.A. and K. Dalnoki-Veress, *The glass transition in thin polymer films.* Advances in Colloid and Interface Science, 2001. **94**(1–3): p. 167-195.
181. Monson, L., S.I. Moon, and C.W. Extrand, *Permeation resistance of poly(ether ether ketone) to hydrogen, nitrogen, and oxygen gases.* Journal of Applied Polymer Science, 2013. **127**(3): p. 1637-1642.
182. Rickman, M., R.H. Davis, and J. Pellegrino, *Temperature-variation study of neutral solute and electrolyte fractionation through cellulose acetate and polyamide membranes.* Journal of Membrane Science, 2014. **461**: p. 114-122.
183. Wolf, C.J., J.A. Bornmann, and M.A. Grayson, *Absorption of toluene in poly(aryl-ether-ether-ketone).* Journal of Polymer Science Part B: Polymer Physics, 1992. **30**(2): p. 113-126.
184. Wolf, C.J., et al., *Solvent-induced crystallinity in poly(aryl-ether-ether-ketone) [PEEK].* Journal of Polymer Science Part B: Polymer Physics, 1992. **30**(3): p. 251-257.
185. Aerts, S., et al., *The use of solvent resistant nanofiltration in the recycling of the Co-Jacobsen catalyst in the hydrolytic kinetic resolution (HKR) of epoxides.* Journal of Membrance Science, 2006. **280**: p. 245–252.
186. Dijkstra, H.P., G.P.M. van Klink, and G. van Koten, *The Use of Ultra- and Nanofiltration Techniques in Homogeneous Catalyst Recycling.* Accounts of Chemical Research, 2002. **35**(9): p. 798-810.
187. Cole-Hamilton, D.J., *Homogeneous Catalysis--New Approaches to Catalyst Separation, Recovery, and Recycling.* Science, 2003. **299**(5613): p. 1702-1706.
188. Nair, D., et al., *Semi-continuous nanofiltration-coupled Heck reactions as a new approach to improve productivity of homogeneous catalysts.* Tetrahedron Letters, 2001. **42**: p. 8219–8222.
189. Gröschel, L., et al., *Hydrogenation of Propyne in Palladium-Containing Polyacrylic Acid Membranes and Its Characterization.* Industrial & Engineering Chemistry Research, 2005. **44**(24): p. 9064-9070.

190. Milano-Brusco, J.S., et al., *Catalytic Reactions in Surfactant Systems:Product Isolation and Catalyst Recycling.* Industrial & Engineering Chemistry Research, 2009. **49**(3): p. 1098-1104.
191. Zhan, K., et al., *Pd nanoparticles encaged in nanoporous interpenetrating polymer networks: A robust recyclable catalyst for Heck reactions.* Reactive and Functional Polymers, 2011. **71**: p. 756–765.
192. Seto, H., et al., *Membrane reactor immobilized with palladium-loaded polymer nanogel for continuous-flow Suzuki coupling reaction.* AIChE Journal, 2015. **61**(2): p. 582-589.
193. Datta, A., K. Ebert, and H. Plenio, *Nanofiltration for Homogeneous Catalysis Separation:Soluble Polymer-Supported Palladium Catalysts for Heck, Sonogashira, and Suzuki Coupling of Aryl Halides.* Organometallics, 2003. **22**: p. 4685-4691.
194. Janssen, M., C. Müller, and D. Vogt, *'Click' Dendritic Phosphines: Design, Synthesis, Application in Suzuki Coupling, and Recycling by Nanofiltration.* Advanced Synthesis & Catalysis, 2009. **351**(3): p. 313-318.
195. Cantillo, D. and C.O. Kappe, *Immobilized Transition Metals as Catalysts for Cross-Couplings in Continuous Flow—A Critical Assessment of the Reaction Mechanism and Metal Leaching.* ChemCatChem, 2014. **6**(12): p. 3286-3305.
196. Jensen, K.F., B.J. Reizman, and S.G. Newman, *Tools for chemical synthesis in microsystems.* Lab on a Chip, 2014. **14**(17): p. 3206-3212.
197. Jensen, K.F., R.L. Hartman, and J.P. McMullen, *Deciding Whether To Go with the Flow: Evaluating the Merits of Flow Reactors for Synthesis.* Angewandte Chemie International Edition, 2011. **50**: p. 7502 – 7519.
198. Anderson, N.G., *Using Continuous Processes to Increase Production.* Organic Process Research and Development, 2012. **16**: p. 852−869.
199. Brinkmann, N., et al., *Allylic Substitution with Dendritic Palladium Catalysts in a Continuously Operating Membrane Reactor.* Journal of Catalysis, 1999. **183**(2): p. 163-168.
200. Dijkstra, H.P., et al., *Application of a Homogeneous Dodecakis(NCN-PdII) Catalyst in a Nanofiltration Membrane Reactor under Continuous Reaction Conditions.* Advanced Synthesis & Catalysis, 2003. **345**(3): p. 364-369.
201. Dijkstra, H.P., et al., *Shape-Persistent Nanosize Organometallic Complexes: Synthesis and Application in a Nanofiltration Membrane Reactor.* The Journal of Organic Chemistry, 2002. **68**(3): p. 675-685.
202. Smet, K.D., et al., *Nanofiltration-coupled catalysis to combine the advantages of homogeneous and heterogeneous catalysis.* Chemical Communications (Cambridge), 2001: p. 597–598.
203. Fang, J., et al., *Continuous homogeneous hydroformylation with bulky rhodium catalyst complexes retained by nano-filtration membranes.* Applied Catalysis A: General, 2011. **393**: p. 294–301.
204. Noel, T., et al., *Suzuki–Miyaura Cross-Coupling Reactions in Flow: Multistep Synthesis Enabled by a Microfluidic Extraction.* Angewandte Chemie International Edition, 2011. **50**: p. 5943 –5946.
205. O'Neal, E.J. and K.F. Jensen, *Continuous Nanofiltration and Recycle of a Metathesis Catalyst in a Microflow System.* ChemCatChem, 2014. **6**(10): p. 3004-3011.
206. Dreimann, J., et al., *Highly integrated reactor–separator systems for the recycling of homogeneous catalysts.* Chemical Engineering and Processing: Process Intensification, 2016. **99**: p. 124-131.
207. Janssen, M., C. Muller, and D. Vogt, *Recent advances in the recycling of homogeneous catalysts using membrane separation.* Green Chemistry, 2011. **13**(9): p. 2247-2257.
208. Vural Gursel, I., et al., *Separation/recycling methods for homogeneous transition metal catalysts in continuous flow.* Green Chemistry, 2015. **17**(4): p. 2012-2026.

209. Caron, S., et al., *Efficient Synthesis of [6-Chloro-2-(4-chlorobenzoyl)-1H-indol-3-yl]-acetic Acid, a Novel COX-2 Inhibitor.* The Journal of Organic Chemistry, 2003. **68**(10): p. 4104-4107.
210. Alonso, D.A., C. Najera, and M.C. Pacheco, *Oxime Palladacycles: Stable and Efficient Catalysts for Carbon-Carbon Coupling Reactions.* Organic letters, 2000. **2**(13): p. 1823-1826.
211. Alonso, D.A., C. Najera, and M.C. Pacheco, *Oxime-Derived Palladium Complexes as Very Efficient Catalysts for the Heck-Mizoroki Reaction.* Advanced Synthesis & Catalysis, 2002. **344**: p. 172-183.
212. Lin, J.C.-T. and A.G. Livingston, *Nanofiltration membrane cascade for continuous solvent exchange.* Chemical Engineering Science, 2007. **62**: p. 2728 – 2736.
213. Odinokov, S.E., V.P. Glazunov, and A.A. Nabiullin, *Infrared spectroscopic studies of hydrogen bonding in triethylammonium salts. Part 3.-Strong hydrogen bonding.* Journal of the Chemical Society, Faraday Transactions 2: Molecular and Chemical Physics, 1984. **80**(8): p. 899-908.
214. Levenspiel, O., *Design for Single Reactions*, in *Chemical Reaction Engineering*. 1999, John Wiley & Sons: Hoboken. p. 120-139.
215. Amatore, C. and A. Jutand, *Mechanistic and kinetic studies of palladium catalytic systems.* Journal of Organometallic Chemistry, 1999. **576**(1–2): p. 254-278.
216. Peeva, L.G., et al., *Effect of concentration polarisation and osmotic pressure on flux in organic solvent nanofiltration.* Journal of Membrance Science, 2004. **236**: p. 121–136

Appendix

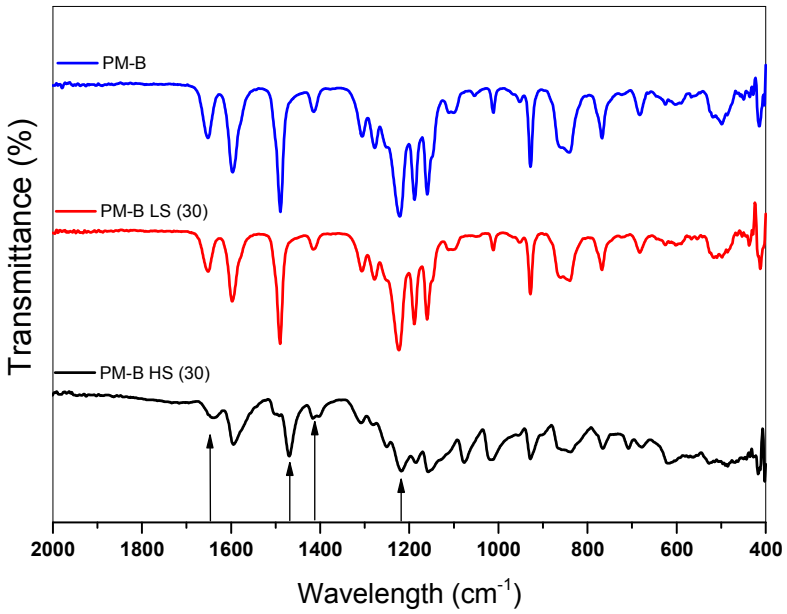

Figure A1 – ATR-FTIR spectra of PEEK membranes: PM-B, PM-B LS (30) and PM-B HS (30). The arrows show the peaks related to the backbone carbonyl stretching at 1649.5 cm^{-1}, the aromatic C-C stretching at 1488 cm^{-1}, the asymmetric stretching vibration of the O=S=O at 1412 cm^{-1}, the symmetric stretching vibration of O=S=O at 1220 cm^{-1}.

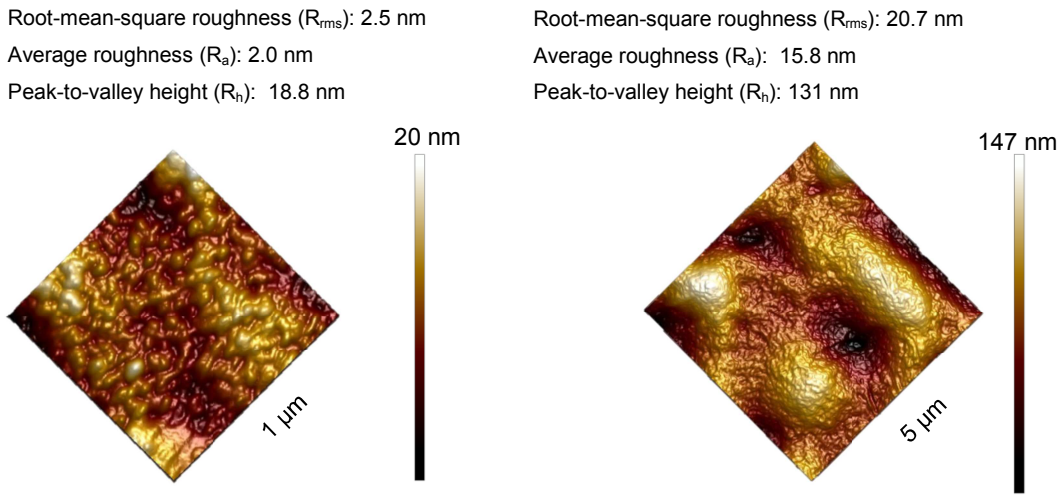

Figure A2 – AFM topographical image of PM-B.

Table A1 – Solubility of PM-B (at 20 °C) in different acid/basic solutions

		Membrane mass		
Acid/Base	Concentration (M)	Initial mass (mg)	Final mass (mg)	Mass loss (%)
H2SO4	2	247.3	245.7	0.65
HCl	2	246.0	245.3	0.28
KOH	2	205.6	204.2	0.68
NaOH	25	47.2	47.1	0.21
MEA	16.4	55.8	55.8	0.00

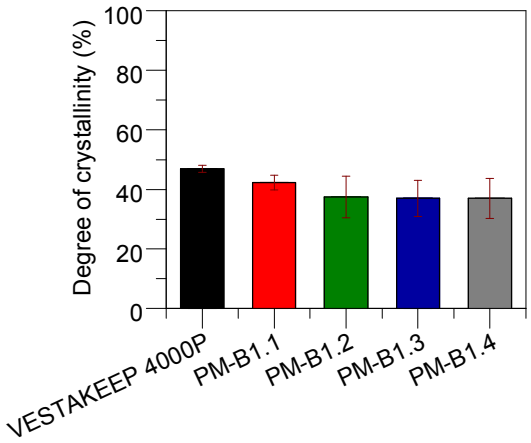

Figure A3 – Degree of crystallinity (%) obtained from DSC (7.2.3.3) for VESTAKEEP® 4000P and membranes PM-B dried from water at different temperatures: PM-B1.1, PM-B1.2, PM-B1.3 and PM-B1.4. The error bars represent the standard deviation from two sequential heating cycles.

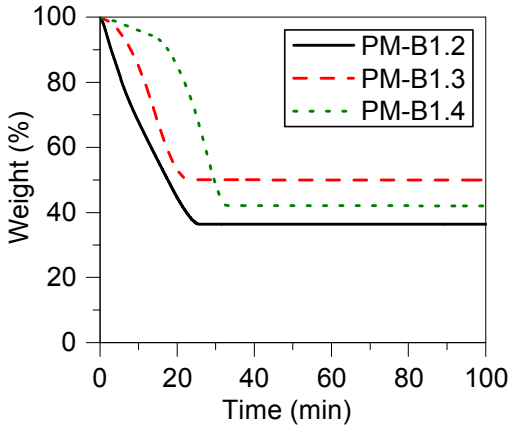

Figure A4 – Weight loss (%) as a function of time (min) obtained from TGA analysis for membranes PM-B dried at different temperatures (40 °C, 80 °C and 120 °C).

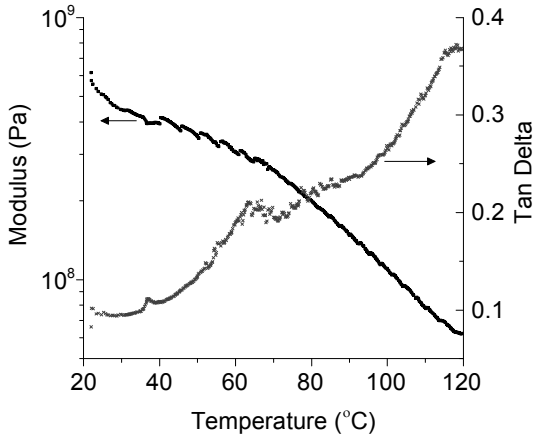

Figure A5 – Values of dynamic modulus (stiffness, Pa) and mechanical damping (tan delta) for membrane PM-B 12 wt%. The membrane was inserted while water "wet" at a heating rate of 2 K.min^{-1}. The tests were carried out at 1 Hz with a displacement of 0.05 mm.

Table A2 – Properties of the solvents used for the solvent exchange: vapour pressure (kPa), surface tension ($mN.m^{-1}$), Hansen solubility parameter $(cal.cm^{-3})^{0.5}$, polarity parameter (kcal.mol-1), molar volume ($cm^3.mol^{-1}$) and viscosity (cP). All properties listed were obtained from [34] at 20 °C and 1 bar. In addition, rejection values (%) for the dimer (MW = 236 g.mol-1) and permeance values ($L.h^{-1}.m^{-2}.bar^{-1}$) for PEEK membranes 12 wt.% dried at 120 °C from the corresponding solvent, and used for the modelling, are presented.

	Vapour pressure (kPa)	Surface tension ($mN.m^{-1}$)	Hansen solubility parameter $(cal.cm^{-3})^{0.5}$	Polarity parameter ($kcal.mol^{-1}$)	Molar volume ($cm^3.mol^{-1}$)	Viscosity (cP)	Rejection (%)	Permeance ($L.h^{-1}.m^{-2}.bar^{-1}$)
Water	2.33	72.75	25.5	63.1	18	1	88.05	0.36
MeOH	16.933	22.6	14.5	55.4	40.6	0.6	71.9268	1.07
EtOH	5.9466	22.3	13.4	51.9	58.6	1.08	66.13	1.13
IPA	4.1	21.7	11.5	48.4	76.9	2	81.5211	0.86
Acetone	30.8	23.3	10	42.2	73.8	0.33	53.85	2.15
THF	21.6	26.4	9.1	37.4	81.9	0.46	48.44	2.72
Hexane	20.17	18.4	6.9	31	131.4	0.31	73.06	1.49
Acetonitrile	9.6	29.1	11.9	45.6	52.9	0.38	56.57	1.94
Heptane	6.093	19.3	7.5	31.1	147	0.41	62.69	0.92

Table A3 - Design of experiments considering five different factors – molecular weight (MW), PEG concentration (% w/w), time of impregnation (h), drying temperature (°C) and solvent (water or IPA).

Run	Factor A MW ($g.mol^{-1}$)	Factor B Concentration (% w/w)	Factor C Time (h)	Factor D Temperature (°C)	Factor E Solvent
1	200	100	24	20	Water
7	200	2	24	20	IPA
12	200	100	6	20	IPA
13	200	2	6	20	Water
2	200	2	24	100	Water
5	200	100	24	100	IPA
14	200	100	6	100	Water
17	200	2	6	100	IPA
4	400	51	15	60	Water
6	400	51	15	60	IPA
16	400	51	15	60	Water
18	400	51	15	60	Water
20	400	51	15	60	IPA
21	400	51	15	60	IPA
3	600	2	6	20	IPA
9	600	100	6	20	Water
10	600	2	24	20	Water
22	600	100	24	20	IPA
8	600	2	6	100	Water
11	600	100	24	100	Water
15	600	2	24	100	IPA
19	600	100	6	100	IPA

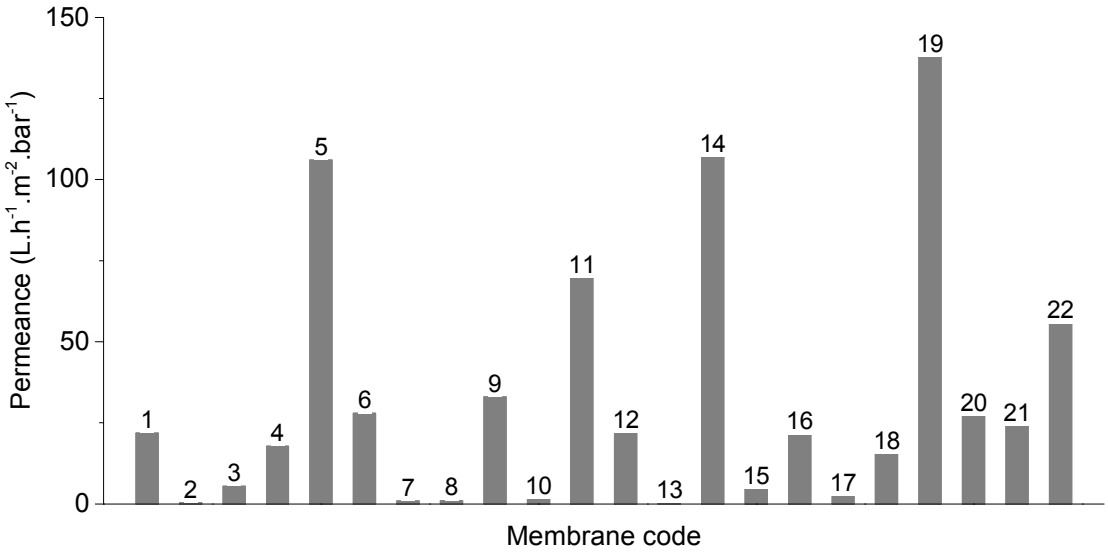

Figure A6 – Results expressed as permeance of acetone and PS ($L.h^{-1}.m^{-2}.bar^{-1}$) for each of the runs of the DoE.

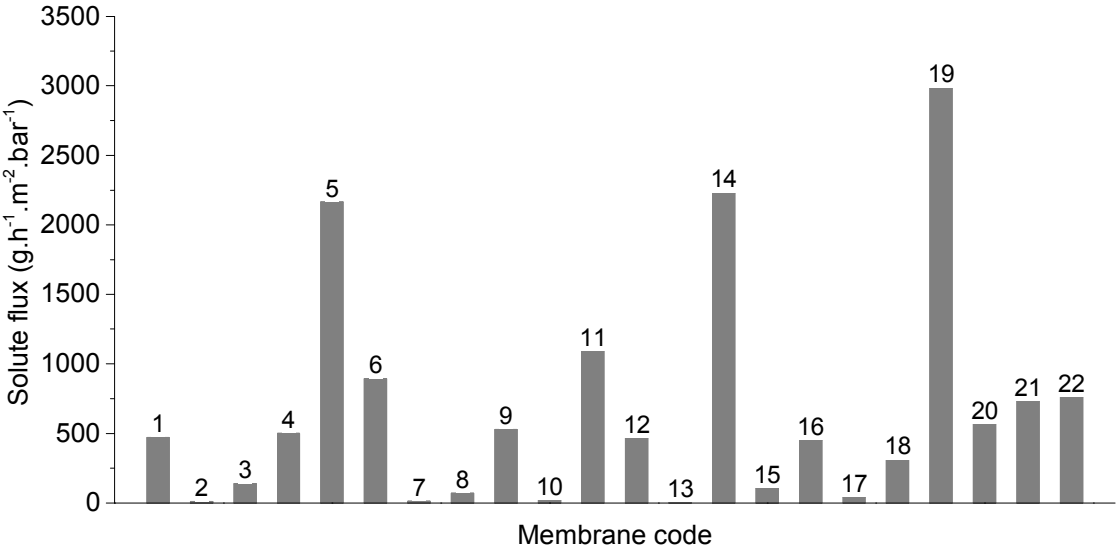

Figure A7 – Results expressed as solute flux ($g.h^{-1}.m^{-2}$) of the styrene dimer for each of the runs of the DoE.

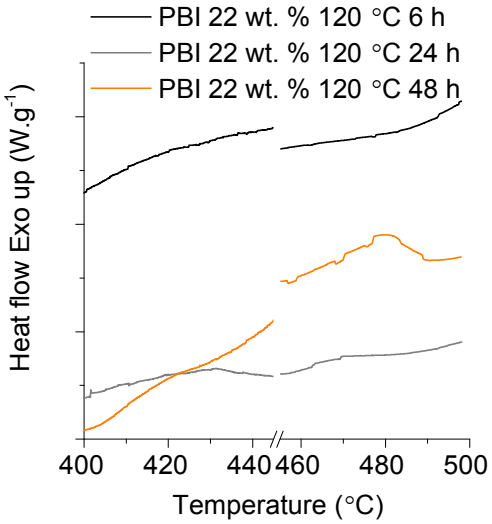

Figure A8 – DSC thermograms around the Tg of PBI (427 °C) showing the PBI membranes annealed at 120 °C for 6 h, 24 h and 48 h (air dried). The thermograms shown were acquired at a scan rate of 10 $°C.min^{-1}$ before 450 °C and after at a scan rate of 2 $°C.min^{-1}$.

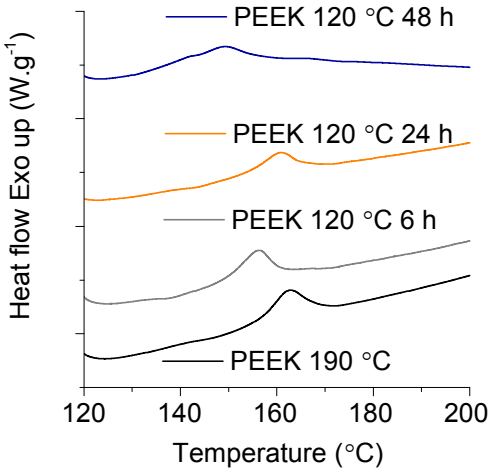

Figure A9 – DSC thermograms around the Tg of PEEK (143 °C) showing the PEEK membranes annealed at 120 °C for 6 h, 24 h and 48 h (air dried) and at 190 °C for 24 h under vacuum conditions. The thermograms shown were acquired at a scan rate of 2 °C.min^{-1}.

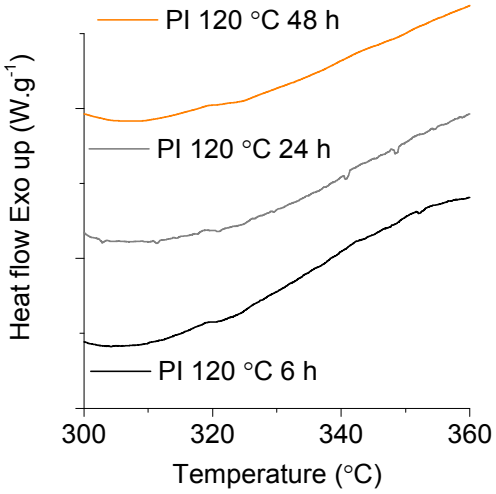

Figure A10 – DSC thermograms around the Tg of PI (315 °C) showing the PI membranes annealed at 120 °C for 6 h, 24 h and 48 h (air dried) and at 190 °C for 24 h under vacuum conditions. The thermograms shown were acquired at a scan rate of 2 °C.min^{-1}.

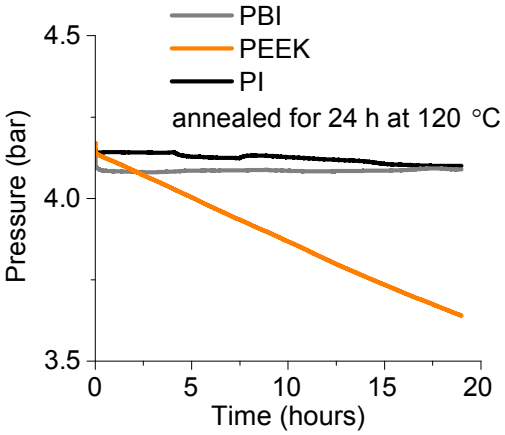

Figure A11 – Pressure drop (bar) for the different membranes under study, PBI, PEEK and PI, after annealing for 24 hours at 120 °C from water. The system was pressurized to approximately 4 bar (60 psi) using oxygen and the pressure was recorded automatically for a period of 18 hours.

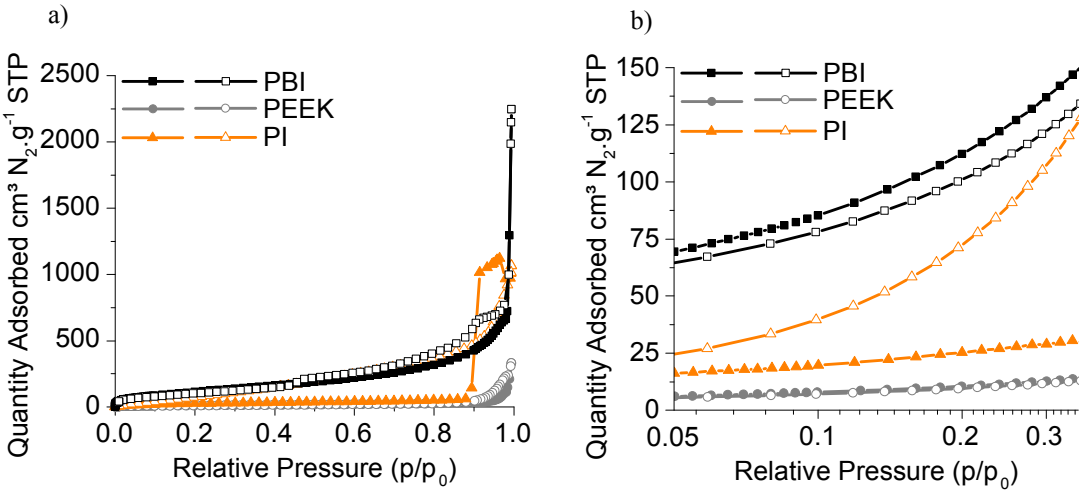

Figure A12 – a) N_2 adsorption desorption isotherms PBI, PEEK and PI membranes at 77 K for partial pressures between 0 and 1 (samples were degassed at 120 °C). b) Detail of isotherms plotted in a) for partial pressures between 0.05 and 0.35 (samples were degassed at 120 °C). The closed points refer to the adsorption isotherm and the open points refer to the desorption isotherm.

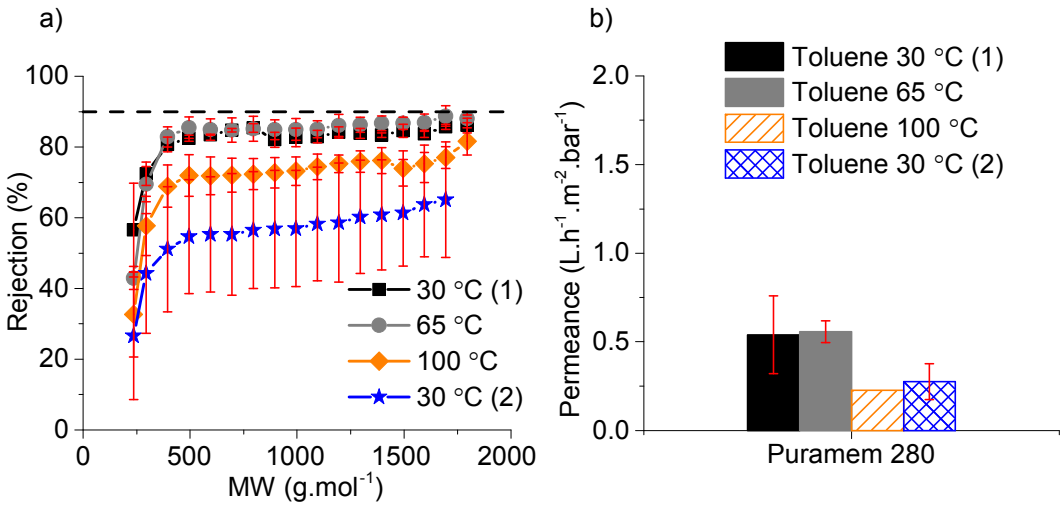

Figure A13 – a) Rejection values (%) for Puramem 280 membranes after 24h at 30 °C, 65 °C, 100 °C and cooling down to 30 °C. b) Permeance values ($L.h^{-1}.m^{-2}.bar^{-1}$) for Puramem 280 membranes after 24h at 30 °C, 65 °C, 100 °C and cooling down to 30 °C. The membranes were used to filter with a solution of toluene and PS (1 $g.L^{-1}$).

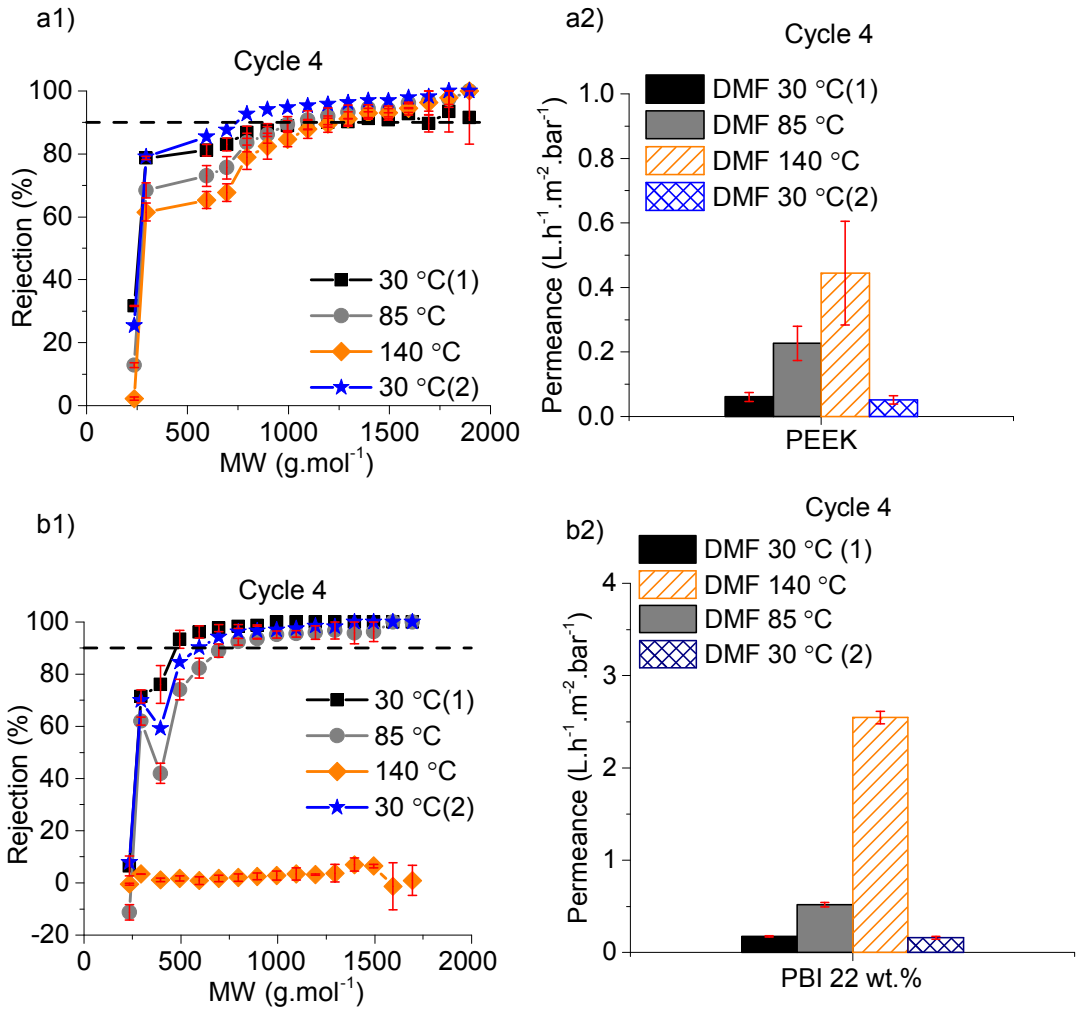

Figure A14 – a1) Rejection values (%) of cycle 4 for PEEK membranes after 24h at 30 °C, 85 °C, 140 °C and cooling down to 30 °C. a2) Permeance values ($L.h^{-1}.m^{-2}.bar^{-1}$) of cycle 4 for PEEK membranes after 24h at 30 °C, 85 °C, 140 °C and cooling down to 30 °C. The membranes were used to filter with a solution of DMF and PS (1 $g.L^{-1}$). b1) Rejection values (%) of cycle 4 for PBI 22 wt.% crosslinked with DBX membranes after 24h at 30 °C, 85 °C, 140 °C and cooling down to 30 °C. c2) Permeance values ($L.h^{-1}.m^{-2}.bar^{-1}$) of cycle 4 for PBI 22 wt.% crosslinked with DBX membranes after 24h at 30 °C, 85 °C, 140 °C and cooling down to 30 °C. The membranes were used to filter with a solution of DMF and PS (1 $g.L^{-1}$).

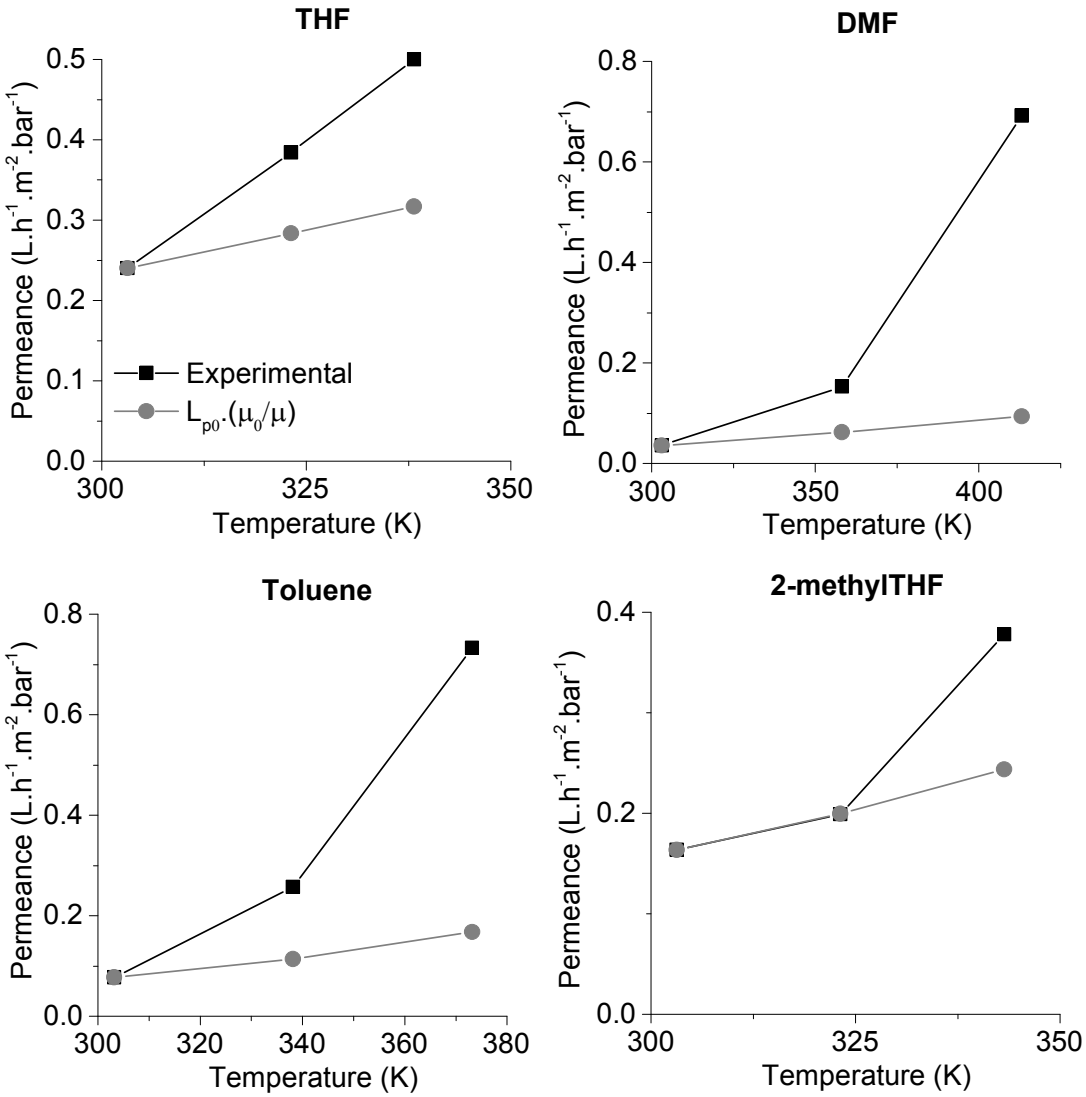

Figure A15 – Experimental values of permeance ($L.h^{-1}.m^{-2}.bar^{-1}$) for the different solvents tested.

MatLab script to calculate the mean pore size and standard deviation using the pore flow model with a log probability function.

```
clc
close all
clear
global x nu0 deltaP dsol d_vec Rej_vec_exp Dif_vec dp_mean s res R
T v Rej_vec b x y nu0 deltaP dsol d Dif fr int_fr int_num int_denom
f_num f_denom d_vec Dif_vec lambda fi nu R T Kc Kd Pe Y Rej v
Rej_vec_calc b

%% Process Description

% This script is to calculate average pore diameter and density
function.
```

```
  %% Constants

  nu0 =0.000755377;
  deltaP = 30*10^5;
  dsol = 5.2*10^-10;
  Dif_vec = [2.83535, 2.13124, 1.79931, 1.57698, 1.41546, 1.29165,
1.19305, 1.11227, 1.0446, 0.986902, 0.936987, 0.893282, 0.854621,
0.820123]*10^-9;
  v = 77.4*10^-6; % molar volume of the solvent
  R=8.314;
  T=30+273;
  d_vec = [0.466340826,0.620409908, 0.734858975, 0.838462045,
0.93414182, 1.023684869,    1.108281453,    1.188773544,
1.265783719,    1.339788306,    1.411161764,    1.480205047,
1.54716451, 1.612244968]*10^-9;
  Rej_vec = [0.198    0.327   0.537   0.759   0.831   0.906   0.929
0.938   0.953   0.958   0.950   0.968   1.000   1.000];

  %% Equations

  OPTIONS = optimset('TolFun',10^-60,'TolX',10^-
60,'MaxFunEvals',10000,'MaxIter',10000);

  [res,RESNORM,RESIDUAL,EXITFLAG,OUTPUT,LAMBDA] =
lsqcurvefit(@fit_dp,[1.5,0.1],d_vec,Rej_vec,0,5,OPTIONS);

  EXITFLAG

  dp_mean = res(1)*10^-9
  s = res(2)*10^-9
  Rej_vec_calc


  x = 5*10^-12:5*10^-12:5*10^-9;
  y = exp(-(log(x./dp_mean) + log(s.^2./dp_mean.^2 +
1)./2).^2./(2.*log(s.^2./dp_mean.^2 +
1))./(x.*(2.*pi.*log(s.^2./dp_mean.^2 + 1)).^(1./2));

  figure(1)

  plot(x,y)

  figure(2)
  plot(d_vec,Rej_vec,d_vec,Rej_vec_calc)

  function f = fit_dp(X0,varargin)

  global x nu0 deltaP dsol dp_mean d s Dif fr int_fr int_num
int_denom f_num f_denom d_vec Dif_vec lambda fi nu R T Kc Kd Pe Y
Rej v Rej_vec_calc b

  dp_mean = X0(1)*10^-9;
  s = X0(2)*10^-9;

  if s>0
```

```
  for i = 1:length(d_vec)

      d=d_vec(i);
      Dif=Dif_vec(i);

      x = 2*dp_mean/1000:2*dp_mean/1000:2*dp_mean;

      for j=1:length(x)

      if x(j)<=0.46*10^-9

          nu(j) = 10*nu0;

      else

          nu(j) = (nu0*(1+18.*(dsol./x(j))- 9.*((dsol./x(j)).^2)));

      end

      end


      for j=1:length(x)

          lambda(j) = (d./x(j));
           fi(j)= (1-lambda(j)).^2;

      if lambda(j)>=0 & lambda(j)<=0.8

          Kd (j)= 1.0 - 2.30.*lambda(j) + 1.154.*(lambda(j)).^2 +
0.224.*(lambda(j)).^3;
          Kc (j)= (2-fi(j)).*(1.0+0.054.*lambda(j)-
0.988.*(lambda(j)).^2+0.441.*(lambda(j)).^3);
          Y(j)=(32.*nu(j).*Kd(j).*Dif.*v)./(R.*T.*(x(j).^2));
          Pe(j) =((Kc(j)-
Y(j)).*(x(j).^2).*deltaP)./(32.*nu(j).*Kd(j).*Dif);
          Rej(j)= 1-((fi(j).*(Kc(j)-Y(j)))./(1-(1-(fi(j).*(Kc(j)-
Y(j)))).*exp(-Pe(j))));

      end

      if lambda(j)>0.8 & lambda(j)<=1

          Kd (j)= -6.830 + 19.348.*lambda(j) -
12.518.*(lambda(j)).^2;
          Kc(j) = (2-fi(j)).*(-0.105+0.318.*lambda(j)-
0.213.*(lambda(j)).^2);
          Y(j)=(32.*nu(j).*Kd(j).*Dif.*v)./(R.*T.*(x(j).^2));
          Pe(j) =((Kc(j)-
Y(j)).*(x(j).^2).*deltaP)./(32.*nu(j).*Kd(j).*Dif);
          Rej(j)= 1-((fi(j).*(Kc(j)-Y(j)))./(1-(1-(fi(j).*(Kc(j)-
Y(j)))).*exp(-Pe(j))));

      end
```

```
      if lambda(j) > 1

          Rej(j)=1;

      end


      fr(j) =
((1./(x(j).*(2.*pi().*log(1.0+(s./dp_mean).^2)).^(1./2))).*exp(-
(((log(x(j)./dp_mean))+0.5*log(1.0+(s./dp_mean).^2)).^2)./(2.*log(1.
0+(s./dp_mean).^2))));

      end

      int_fr = trapz (fr);


      for j=1:length(x)

      f_num (j)= (((fr(j)./int_fr).*x(j).^4.*Rej(j))./nu(j));
      f_denom (j)= (((fr(j)./int_fr).*x(j).^4.)./nu(j));

      end

      Rej;

      f_num;
      int_num(i)=trapz(f_num);
      int_denom(i)=trapz(f_denom);
      Rej_vec_calc(i)=int_num(i)./int_denom(i);

  end
  end

  f = Rej_vec_calc;
```